# APPROACHES FOR ASSESSING THE PRESENCE AND IMPACT OF THYROID HORMONE DISRUPTING CHEMICALS IN DELPHINID CETACEANS

By

Eric Wilson Montie

B.S. Zoology, University of Rhode Island, 1993
M.S. Environmental Toxicology, Clemson University, 1999

Submitted in partial fulfillment of the requirements for the degree of

Doctor of Philosophy

at the

MASSACHUSETTS INSTITUTE OF TECHNOLOGY

and the

WOODS HOLE OCEANOGRAPHIC INSTITUTION

September, 2006



Signature of Author 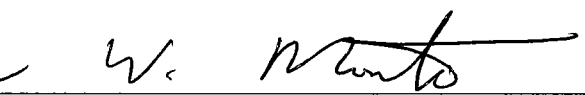

Joint Program in Oceanography/Applied Ocean Science and Engineering
Massachusetts Institute of Technology and Woods Hole Oceanographic Institution
September 2006

Certified by 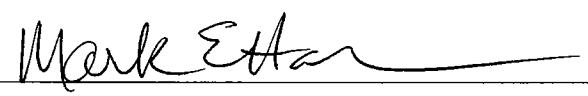

Mark E. Hahn
Thesis Supervisor

Accepted by 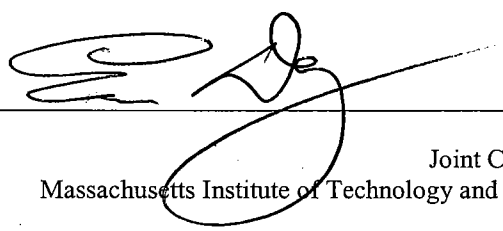

Edward F. DeLong, Chair
Joint Committee for Biological Oceanography
Massachusetts Institute of Technology and Woods Hole Oceanographic Institution

**APPROACHES FOR ASSESSING THE PRESENCE AND IMPACT OF THYROID HORMONE DISRUPTING CHEMICALS IN DELPHINID CETACEANS**

by
Eric Wilson Montie

Submitted in partial fulfillment of the requirements for the degree of
Doctor of Philosophy

## ABSTRACT

Cetacean blubber is a primary site for lipid storage, which the animal utilizes during periods of energetic stress. It is important to understand how the blubber responds to factors such as ontogeny, water temperature, reproductive status, and nutritional state because blubber is also the primary bioaccumulation site for persistent organic pollutants (POPs) such as polychlorinated biphenyls (PCBs). During periods of lipid mobilization such as lactation, PCBs from the blubber are mobilized into the circulatory system and may cause toxic effects. One particular toxic mechanism may include the induction of cytochrome P450 enzymes in the integument and liver, which could enhance the biotransformation of PCBs to hydroxylated metabolites (OH-PCBs). OH-PCBs may then interfere with thyroid hormone dependent neurodevelopment. The goals of these studies were to investigate the relationships between lipid dynamics and PCB effects and to devise a quantitative approach to assess neurodevelopment in delphinid cetaceans. Blubber morphology, cytochrome P450 1A1 (CYP1A1) expression in the skin-blubber biopsy, blubber and plasma PCBs, and plasma OH-PCBs were assessed in bottlenose dolphins (*Tursiops truncatus*). In addition, magnetic resonance (MR) images of the post-mortem brain *in situ* were obtained from Atlantic white-sided dolphin (*Lagenorhynchus acutus*) specimens.

These results showed that: 1) Factors such as ontogeny, water temperature, and reproductive status affected blubber morphology in bottlenose dolphins. In response to warmer water, the lipid content of the blubber decreased and this appeared to involve loss of lipids from adipocytes in the middle blubber layer. Similar to the effects of starvation on blubber morphology, lactation decreased adipocyte size predominantly in the deeper blubber, 2) CYP1A1 levels in the deep blubber were significantly related to the total plasma $TEQ_{98}$ concentrations, adipocyte shrinkage, and plasma OH-PCB levels, 3) Through *in situ* MR imaging of stranded, Atlantic white-sided dolphin specimens, the size of brain structures that depend on thyroid hormones for maturation could be measured accurately. Future studies can use this technique, coupled with chemical analysis of brain regions, to determine if thyroid hormone disrupting chemicals in delphinid cetaceans are associated with changes in the size of brain structures.

Thesis Supervisor: Mark E. Hahn
Title: Senior Scientist, Biology Department, WHOI

## ACKNOWLEDGEMENTS

I would like to thank Dr. Patricia Fair and Dr. Gregory Bossart for initiating The Bottlenose Dolphin Health and Risk Assessment (HERA) Project, a collaborative effort between the National Ocean Service, Center for Coastal Environmental and Biomolecular Research, National Oceanic and Atmospheric Administration (NOAA) and Harbor Branch Oceanographic Institution. The HERA Project was conducted under National Marine Fisheries Permit No. 998-1678-00, issued to Dr. Gregory Bossart, of Harbor Branch Oceanographic Institution in March 2003. I would like to thank the numerous researchers who participated in the capture and release field study of bottlenose dolphins in South Carolina and Florida. I am especially thankful to Larry Hansen, Eric Zolman, Dr. Forrest Townsend, Mr. Larry Fulford, Steven McCulloch, the NOAA and HBOI staff and all of the veterinarians who provided their expertise, and all the volunteers whose help made the health assessment studies possible. In addition, I am greatly indebted to the hard work of Greg Mitchum who graciously provided the blubber lipid content and PCB data; Dr. Magali Houde and Dr. Derek Muir who provided the plasma PCB and OH-PCB concentrations; Wayne McFee who provided the age data; Todd Speakman and Eric Zolman who through their valiant efforts provided important life history data; Dr. Vicke Starczak and Dr. Andy Solow for all their statistical expertise. I would like to thank Scott Garvin (my intern), Dr. Joanna Wilson, Dr. Jim Staruk, and Bruce Woodin for assistance in histology and immunohistochemistry. I would also like to thank Jeff Adams, Dr. Carolyn Angell, Dr. Julie Goldstein, Maggie Holbrook, Dr. Matt Jenny, Dr. Tin Klanjscek, Elizabeth Murdoch, Melissa Recks, Asha Samuels, and Dr. Gloria Seaborn for helpful discussions. I would also like to thank Dr. Ross Norstrom for insightful discussions on PCB toxicokinetics.

I would like to thank Katie Touhey and the following past and present members of the Cape Cod Stranding Network for coordination and collection of Atlantic white-sided dolphin, common dolphin, harbor seal, and grey seal specimens: Kristen Patchett, Andrea Bogomolni, Betty Lentell, Brian Sharp, Kate Swails, Sarah Herzig, and Trish O'Callaghan. The possession of marine mammal parts was allowed under an authorization letter from Dana Hartley and the National Marine Fisheries Service Northeast Region. I would like to thank Dr. David Rotstein and Dr. Roger Williams for their assistance in histopathology and parasite identifications. I would like to thank Dr. Lori Marino for cetacean neuro-anatomy consultation. I am especially thankful to Scott Garvin, Rick Rupan, Dr. Tin Klanjscek, Dr. Gareth Lawson, Regina Campbell-Malone, Joy Lapseritis, Paul Ryan Craddock, Tim Cole, Brendan Hurley, Misty Nelson, Brenda Rone, and Misty Niemeyer for assistance during specimen preparation and necropsies. I am indebted to Julie Arruda, Scott Cramer, Iris Fischer, Bill Perrault, Dr. Steven Sweriduk, Terri Plifka, Cheryl Loring, and Rose Pearson for assistance during MR imaging of specimens and data processing. I would also like to thank Greg Early and Dr. Mark Baumgartner for helpful discussions. I would like to thank all the individuals who assisted in preliminary chemical analysis of brain samples including Wouter Gebbink, Dr. Chris Reddy's lab, and Dr. Robert Letcher's lab.

I would especially like to thank my committee members. First and foremost, I would like to thank my advisor Dr. Mark Hahn for giving me the freedom to pursue my research interests. I admire him as a brilliant scientist and a family man, and look forward to having him as a lifelong friend and colleague. I am so thankful to Dr. Gerald Schneider for his expertise in neuro-anatomy and driving down to the Cape from MIT to help in segmentation of MR images. I would like to thank Dr. Michael Moore for his encouragement, passion, and necropsy expertise. To Dr. Darlene Ketten, I am so thankful to you for making a large portion of this thesis possible by making things happen. I thank Dr. Robert Letcher for inviting me to Ottawa to learn chemical analyses and all his patience. To Dr. John Stegeman, I am thankful for your constructive comments on my work and inspirational discussions in pursuing a career in science. I would like to thank Dr. Chris Reddy for all your encouragement and taking me into your lab to perform chemical analyses. I thank Dr. Peter Tyack for chairing both my thesis proposal defense and thesis defense.

Support networks were vital in finishing this thesis. The MIT/WHOI Joint Program offers incredible support to their students. In particular, I would like to thank Julie Westwater, Marsha Gomes, Laishona Vitelli, and Ronnie Schwartz. Marsha, I thank you for all the talks. I thank the Hahn lab for good science and good times: Dr. Sibel Karchner, Diana Franks, Dr. Maria Hansson, Dr. Matthew Jenny, Dr. Ann Tarrant, Dr. Rebeka Merson, Dr. Brad Evans, Joy Lapseritis, and Kristen Whalen. To WHOI Class 2000: Amanda McDonald, Dr. Welkin Pope, Dr. Tin Klanjscek, Dr. Sheri Simmons, Dr. Gareth Lawson, Dr. Kristen Gribble, and Joy Lapseritis. I thank you for all the good times and support, even though sometimes it was not all that fun. Joy thanks for helping out so much in the end – I owe you one. To my housemates and good friends, I would like to thank Rick, Paulie, and Scott for your friendship and listening to my problems. It means a lot. I would especially like to thank Scott Garvin – my intern and friend.

I would like to thank surfing and my bros Tim, Murro, Phil, John, Ryan, Kerry, Juan, Guillermo, Duncan, and Steven. We've shared a lot of waves and incredible times together – experiencing the fury and calm of the ocean, learning about passion, fear, humility, anger, frustration, joy, friendship, and dedication. We have a bond that will keep us together throughout our lives.

To Rewa and Misty, thank you for the love you offered. I wish you the best in life. Misty, I thank you for sticking around this past year, helping with the edits, and supporting me through a difficult time period in life.

I thank God for my family. Pickens and Liberty, the best and most devoted dogs a man could have. Thank you Liberty for holding on so long – I know you tried sweetie. Mom and Dad, thanks for always being there and believing in me. Mom, your strength in life is an inspiration to me. I only hope I can be as strong as you. Dad, thank you for instilling in me a love for the earth and all the critters in it. I love you both so much.

To the dolphins and the earth, I hope that the human race, for its sake, will realize the value of the forest, the oceans, the rivers, and all the wild creatures and lands. Thank you for sharing yourself with me. In life, I will try my best to be a steward of the land and sea.

Funding for this research was provided by an Environmental Protection Agency STAR fellowship (U-91616101-2) awarded to Eric Montie, NOAA contract #WC1330-02SE0257, NOAA contract #JHT04P1226, NOAA Fisheries Marine Mammal Health and Stranding Response Program, the Florida Protect Wild Dolphins License Plate Fund, the National Woman's Farm and Garden Association Scholarship awarded to Eric Montie, Shields MRI and CT of Cape Cod, the Quebec Labrador Fund/Atlantic Center for the Environment, Woods Hole Oceanographic Institution Academic Programs Office, Office of Naval Research, and NOAA Fisheries Marine Mammal Health and Stranding Response Program.

## TABLE OF CONTENTS

## LIST OF FIGURES

Chapter 3:

## LIST OF TABLES

# CHAPTER I:
# INTRODUCTION

**POPs and Emerging Contaminants in Marine Mammals**

Marine mammals bioaccumulate persistent organic pollutants (POPs) such as organochlorine pesticides like dichlorodiphenylethanes (i.e. DDTs), dieldrin, chlordanes, and hexachlorocyclohexanes (HCHs), as well as industrial solvents and their byproducts such as chlorinated dibenzo-*p*-dioxins, dibenzofurans, and polychlorinated biphenyls (PCBs) (Blomkvist et al., 1992; DeLong et al., 1973; Hansen et al., 2004; Kannan et al., 1993; Muir et al., 1996; Ross et al., 2000; Tuerk et al., 2005). In some populations of marine mammals, the levels of POPs in blubber are extremely high (Table 1.). Exposure of marine mammals to these compounds has been associated with mass mortalities and health effects, including reproductive abnormalities and immune dysfunction (DeLong et al., 1973; Kannan et al., 1993; Ross et al., 1996).

Emerging environmental contaminants may pose a new threat to the health of marine mammals. The flame-retardants are one class of emerging contaminants (Birnbaum and Staskal, 2004; de Boer et al., 1998; Hooper and McDonald, 2000). These compounds include polybrominated biphenyls (PBBs), polybrominated diphenyl ethers (PBDEs), tetra-bromobisphenol A (TBBPA), and hexabromocyclododecane (HBCD). Although these compounds are similar in structure and behavior to well-known environmental contaminants such as PCBs, they have not been banned domestically or internationally, except for a voluntary phase-out of pentabromodiphenyl ether (pentaBDE) by the sole manufacturer on December 31, 2004. These chemicals are produced globally at an estimated 150,000 tonnes a year (de Boer et al., 1998). Like PCBs and DDT, PBDEs have lipophilic and metabolically resistant properties that make them long-lived, bioaccumulating environmental pollutants (de Boer et al., 1998). In a study that has alarmed both the scientific and political community, Meironyte et al. (1999) showed that the sum of the concentrations of PBDE congeners in Swedish human milk from 1972 to 1997 had increased from 0.07 to 4.02 ng/g lipids; over the same time period, the total toxic equivalents (TEQ) from PCBs in human milk in Sweden decreased. PBDEs and other brominated flame-retardants may be the “new PCB problem”.

Halogenated phenolics have also emerged as important environmental contaminants in wildlife and humans (Letcher et al., 2000; Sandau, 2000). These include such pollutants as the hydroxylated metabolites of PCBs (OH-PCBs), the hydroxylated metabolites of PBDEs (OH-PBDEs), and pentachlorophenol. These compounds interact with the thyroid hormone system and have been recently recognized as a group of contaminants that may pose a threat to human and marine mammal health (Brouwer et al., 1998; Letcher et al., 2000). Research has shown that these compounds are retained in the plasma of humans and marine mammals (Houde et al., 2006; Letcher et al., 2000; McKinney et al., 2006; Sandala et al., 2004). Most species have plasma OH-PCB concentrations ranging from 5-30% of the total PCBs (Sandau, 2000). However, in some marine mammals like polar bears, OH-PCB levels are generally higher than PCB concentrations (Sandau, 2000).

Marine mammals accumulate and retain a mixture of PCB and PBDE congeners, as well as OH-PCB and OH-PBDE congeners. The mixture of these chemicals in marine mammals and their additive impacts on the thyroid hormone system are a cause for concern, particularly for the fetus and neonate that depend on a functional thyroid hormone system for proper neuro-development (Figure 1).

**Induction of Xenobiotic Metabolizing Enzymes and Formation of Hydroxylated Metabolites**

PCBs induce cytochrome P450 monooxygenases (CYP) and are metabolized by these enzymes. These enzymes biotransform PCBs to OH-PCB metabolites. To better understand hydroxylated metabolites of PCBs and their effects, it is important to explain the processes that lead to their formation. CYP enzymes biotransform PCBs by inserting an oxygen into these compounds. Oxygen insertion can eventually lead to the formation of hydroxylated metabolites. One mechanism involves epoxidation followed by epoxide ring opening. In the epoxide ring intermediate, a chlorine atom can shift its position to another carbon. This shift has been given the name National Institute of Health Shift or "NIH Shift" (Guroff et al., 1967). PCB metabolism studies have shown that several

isomers of hydroxylated metabolites can be formed from one PCB congener through an NIH Shift mechanism (Ishida et al., 1991).

The superfamilies of CYPs exist in a wide range of species from bacteria to mammals, exhibiting an enormous diversity in genetic structure. According to their amino acid sequences, the CYP genes are classified into over 74 families. OH-PCBs are derived from phase I metabolism of parent PCB congeners by enzymes belonging to the CYP1A and CYP2B (and possibly CYP isoforms) enzyme families (Letcher et al., 2000; Yoshimura et al., 1987). The hydroxylation of PCBs by either CYP1A or CYP2B isozymes is dependent upon the chlorine substitution pattern of the PCB congener on each of the biphenyl rings. In rat liver, CYP1A is important in phase I oxidative metabolism of PCB congeners with chlorine substituents at one or both *para* positions, and with adjacent non-halogenated *ortho* and *meta* carbons on at least one ring (Kaminsky et al., 1981; Mills et al., 1985). CYP2B is important in phase I oxidative metabolism of PCB congeners that have two *ortho*-chlorines and *meta*-, *para*-vicinal hydrogens.

Historically, PCBs have been divided into three different groups based on their induction of CYPs (Safe, 1984). PCB congeners that cause CYP1A induction contain chlorines in both *para* and at least two *meta* positions with no substitution in the *ortho* position. These congeners are termed the coplanar PCBs because the rings can achieve a planar configuration. The induction mechanism of CYP1A type enzymes involves the activation of the aryl hydrocarbon receptor (AHR) signaling pathway (Hahn, 1998). AHR ligands include planar halogenated aromatic hydrocarbons (PHAHs) (i.e. non-ortho and some mono-ortho substituted PCBs and 2,3,7,8-tetrachlorodibenzo-p-dioxin (TCDD or dioxin)) and polycyclic aromatic hydrocarbons (PAHs).

PCBs that contain at least one chlorine in the *ortho* position of the biphenyl ring cause CYP2B induction (Honkakoski and Negishi, 1998). However, the most active phenobarbitol-type inducers are PCBs that contain at least two *ortho* and two *para* chlorine substituents (Denomme et al., 1983). This chlorine pattern reduces free rotation of the biphenyl rings, which hinders a planar biphenyl configuration. The induction

mechanism of CYP2B type enzymes involves the constitutive androstane receptor (CAR) (reviewed by Waxman (1999)). "Mixed" inducers are chemicals that can induce both CYP1A and CYP2B enzymes.

In summary, these enzymes (and possibly other CYPs) are induced by PCB substrates and act on the substrate, introducing a hydroxyl group into the aromatic ring. At this point, the hydroxylated metabolite can be converted into a more water-soluble product and excreted, or retained in plasma or perhaps other tissues.

**CYP1A1 Induction as a Biomarker in Delphinid Cetaceans**

CYP1A1 induction is a valuable biomarker of exposure to PHAHs and has been used extensively in fish, birds, and marine mammals (Stegeman and Hahn, 1994). Its advantages include the extensive database demonstrating its relationship to PHAH exposure (Moore et al., 1998). In delphinid cetaceans, CYP1A1 has been shown to be a valuable biomarker of exposure to PHAHs (White et al., 1994; Wilson et al., 2005). Its advantages include the relatively robust methods that exist for its detection (formalin preservation followed by immunohistochemistry) and the fact that it can be measured in skin-blubber biopsy samples (Angell et al., 2004). In vitro assays have demonstrated CYP1A1 induction in sperm whale (*Physeter macrocephalus*) skin biopsy slices exposed to β-napthoflavone (BNF), a prototypical CYP1A1 inducer (Godard et al., 2004).

In the integument, CYP1A1 expression is strongest and most frequent in vascular endothelial cells of the arterial system and capillaries within the blubber of cetaceans (Angell et al., 2004). This is consistent with earlier observations that CYP1A is highly inducible in vertebrate endothelial cells (Stegeman et al., 1989). It has been suggested that the movement of AHR agonists from the blubber across the endothelial cells and into the bloodstream (i.e. as occurs during blubber lipid mobilization) could induce CYP1A1 in vascular endothelial cells (Angell et al., 2004). In other vertebrate species, PCBs and DDTs have been shown to move out of adipose tissue during lipid mobilization (Dale et al., 1962; Findlay and De Freitas, 1971; Sodergren and Ulfstrand, 1972). Hence, understanding blubber morphology and lipid dynamics may be important factors in

understanding CYP1A1 expression in the blubber biopsy, its relationship to AHR agonists (e.g. non-ortho and mono-ortho PCBs), and its involvement in the production of HO-PCBs. Understanding these processes in delphinids is a major goal of this thesis.

**Blubber Morphology and Dynamics**

Blubber is dynamic and multifunctional, serving many roles: it functions biomechanically to provide support during locomotion and increases efficiency by streamlining the body surface (Hamilton et al., 2004; Pabst, 2000); it contributes to buoyancy (Dearolf et al., 2000; Kipps et al., 2002; McLellan et al., 2002); it is a primary site for lipid storage, which the animal utilizes during periods of energetic stress (Aguilar and Borrel, 1991; Koopman et al., 1996; Koopman et al., 2002; Struntz et al., 2004). The high lipid content also provides insulation, decreasing the heat loss from the body core to the external environment (Dunkin et al., 2005; Worthy and Edwards, 1990).

Histological and biochemical evidence from stranded specimens suggest that cetacean blubber is stratified (Aguilar and Borrell, 1990; Koopman et al., 1996; Koopman et al., 2002; Struntz et al., 2004). For example, in bottlenose dolphins (*Tursiops truncatus*) that either stranded or were killed incidentally in fishing operations in North Carolina and Virginia, Struntz et al. (2004) showed dramatic blubber stratification based in adipocyte number, adipocyte area, and structural fiber density. At the mid-thoracic site, adipocyte areas and numbers varied significantly across the blubber depth, with smaller and fewer adipocytes near the epidermis or "superficial" layer. Adipocyte numbers and size increased in the "middle" blubber and then decreased again in the "deep" layer near the border of the sub-dermal connective tissue sheath and muscle layer. These data, as well as the impacts of emaciation on blubber morphology, have brought forth the hypothesis that the "inner" or "middle" and "deep" blubber layers are more dynamic with regards to lipid mobilization, while the "outer" or "superficial" blubber is more static (Aguilar and Borrell, 1990; Koopman et al., 2002; Struntz et al., 2004)

Blubber is the primary bioaccumulation site for POPs such as organochlorine pesticides and PCBs (Marsili and Focardi, 1997; Schantz et al., 1993; Tirpenou et al., 1998). During periods of lipid mobilization such as lactation, POPs are mobilized into the circulatory system (Norstrom and Muir, 1994; Ridgway and Reddy, 1995; Wolkers et al., 2004). Thus, knowledge of the structure and dynamics of blubber is important in marine mammal toxicology because this information is essential for understanding the mobilization of pollutants from the blubber into the bloodstream and investigating associated health effects on the animal and its offspring.

**Maternal Transfer of POPs and Halogenated Phenolics**

In many marine mammal species, there is a strong correlation between increasing POP blubber residue levels and age, until animals reach sexual maturity (Borrell et al., 1995; Cockcroft et al., 1989; Ross et al., 2000). At this time and thereafter, females experience a pronounced decrease in contaminant burdens in the blubber, while males continue to accumulate POPs throughout their lives. This reduction in contaminant burdens in sexually mature females has been best explained by the transfer of these burdens from the maternal blubber to offspring during pregnancy and lactation. It has been predicted that first-born dolphin calves receive a fourfold higher initial burden of PCBs than subsequent calves, with 90% of this load being transferred through lactation (Cockcroft et al., 1989). It was estimated that almost 80% of the contaminant burden of a lactating female is passed to a first-born calf and that this transfer would take approximately seven weeks after birth (Cockcroft et al., 1989).

Researchers conducting a thirty-year study in Sarasota Bay, Florida have discovered that first-born bottlenose dolphin calves rarely survive (Wells, 2000). In the same population of bottlenose dolphins (i.e. from Sarasota, Florida), first-born calves also have higher PCB concentrations than subsequent calves of similar age (Wells et al., 2005). The mechanism for this high mortality is unknown and could involve mother inexperience or possibly contaminant transfer to the calf. The relative high and acute exposure of the first-born calf to environmental chemicals is a subject of concern.

There is no information about the maternal transfer of halogenated phenolics in marine mammals. In rat studies, maternal exposure to Aroclor 1254 from gestation days (GD) 10 to 16 resulted in accumulation of the metabolite 4-OH-2,3,3',4',5-pentachlorobiphenyl (4-OH-CB107) in fetal plasma and brain (Morse et al., 1996). Recent work has shown that prenatal exposure of radiolabeled 4-OH-CB107 resulted in the accumulation of this compound in the fetus (Meerts et al., 2002). In fact, the fetal/maternal ratios at GD 20 in liver, cerebellum, and plasma were all greater than 1 (11.0, 2.6, and 1.2, respectively). Transthyretin (TTR), a thyroid hormone binding protein, is thought to be responsible for maternal to fetal transport of thyroxine (T4) across the placenta (Achen et al., 1992). The high binding affinity of xenobiotics such as OH-PCBs and other halogenated phenolics to TTR has been hypothesized to result in facilitated transport of these compounds across the placenta to the fetus (Meerts et al., 2002).

**Contaminants in the Brain**

Many POPs that are found at high levels in milk and that are maternally transferred in marine mammals are neurotoxic (Vedder, 1996). These include such organochlorine insecticides as the dichlorodiphenylethanes (i.e. DDTs), the cyclodienes (i.e dieldrin, chlordanes), and the cyclohexanes (i.e. hexachlorocyclohexane or HCH) (reviewed by Ecobichon (1996)). DDT poisoning is associated with effects on the central nervous system (CNS) in humans. DDT elicits its effects at the level of the neuronal membrane by reducing potassium transport across the membrane. The cyclodienes are potent neurotoxicants that block the λ-aminobutyric acid (GABA) receptor found in the CNS. The blocking of this ion channel impedes the uptake of chloride ions by neurons and causes a state of uncontrolled excitation. Technical grade HCH used in insecticides contains a mixture of isomers: the λ- and α-isomers are convulsant poisons; the β- and δ-isomers are CNS depressants. PCBs are also neurotoxic but the exact mechanism is unclear and most likely involves multiple mechanisms (Seegal, 2000).

POP distribution in the brain has been studied in rats and humans (Table 2) but there is limited information about the distribution of halogenated phenolics in the brain. Meerts et al., (2002) have shown the accumulation of [$^{14}$C]-labeled 4-OH-CB107 in fetal rat cerebellum and forebrain. More detailed regional analysis has not yet been completed. An important point to consider when hypothesizing the distribution of halogenated phenolics in the brain is the ability of TTR to bind to these compounds and alter their distribution. In humans, the three thyroxine transport proteins (albumin, thyroid binding globulin, and TTR) are synthesized by the liver, but only TTR is synthesized in the brain in the epithelial cells of the choroid plexus (Dickson et al., 1987). All the newly synthesized TTR is transported towards the brain into the cerebrospinal fluid (CSF). In fact, the ratio of transthyretin to albumin concentration is 30-fold higher in the CSF than in blood plasma. TTR in CSF serves as the main thyroxine transport protein (Schreiber et al., 2001). Since TTR is synthesized in the choroid plexus and is secreted into the CSF, it is possible that these tissues retain higher levels of OH-PCBs, OH-PBDEs, and other halogenated phenolics, specifically compounds that have a high affinity for TTR. Consistent with this, Takasuga et al. (2004) observed that the levels of OH-PCBs in human CSF were higher than the levels of PCBs, opposite of what was found in the serum.

Chemical analysis has been limited in marine mammal brains (Table 3). Studies have not addressed whether contaminants bioaccumulate in specific brain regions. Furthermore, our understanding of the distribution and bioaccumulation of halogenated phenolics in the brain of delphinid cetaceans is non-existent. Above all, there is very limited knowledge on exposure of the brain to environmental chemicals during the fetal and neonatal stage, which is especially important because in the fetus and neonate, the blood-brain barrier is incomplete and the brain is still developing (Eriksson, 1997).

**POPs and Halogenated Phenolics Decrease Thyroid Hormone Levels**

There is much evidence that POPs, including the brominated flame retardants and the halogenated phenolics, can interfere with the thyroid hormone system in rats, humans, and seals. Decreased serum levels of T4 have been correlated with exposure to PCBs

both in rats and in humans (reviewed by Brouwer et al. (1998)). Furthermore, Brouwer et al. (1989) showed that consumption of PCB-contaminated fish caused vitamin A and thyroid hormone deficiencies in the common seal, *Phoca vitulina*. New classes of halogenated pollutants - the brominated flame retardants – have recently been identified as thyroid hormone disrupters (Birnbaum and Staskal, 2004). Of particular interest are the PBDEs, which have been shown to drastically reduce circulating T4 concentrations (Zhou et al., 2002).

To date, there are at least three independent, but possibly interacting, mechanisms that may explain the ability of PCBs (and other related compounds) to reduce circulating and tissue levels of thyroid hormones. First, PCBs have been shown to change thyroid gland structure, perhaps directly interfering with thyroid gland function (Collins et al., 1977). These findings are consistent with the report of Byrne et al. (1987) that PCB exposure reduces the ability of thyroid stimulating hormone (TSH) to increase serum T4 *in vivo*. Recently, Pocar et al. (2006) used a primary porcine thyrocyte culture (derived from pigs) as an experimental model to show that TCDD and PCB126 significantly down-regulate the sodium iodide symporter (NIS) and the cathepsins (Cat B and L). NIS is an important enzyme in thyroid epithelial cells, where it catalyzes the active accumulation of iodide. Cat B and L help in the proteolysis of thyroglobulin, which allows controlled liberation of T4 and 3,3',5-triiodothyronine (T3) from the thyroid follicle into the circulatory system. Both NIS and Cat B & L are important in thyroid hormone production. Thus, PCBs may directly interfere with the ability of the thyroid gland to respond to TSH.

Second, PCBs can increase the metabolism of thyroid hormones. Research in the past has shown that PCB exposure increased the bile flow rate, as well as biliary excretion of $^{125}$I-T4 (Bastomsky et al., 1976). PCB exposure also induces the expression and activity of UDP-glucuronosyltransferase (UDP-GT) (Kolaja and Klaassen, 1998) and increases T4 glucuronidation (Visser et al., 1993). UDP-GT induction could explain the increased bile flow rate and excretion of T4. Thus, these actions may facilitate serum T4 clearance by hepatic metabolism, reducing the half-life of T4 in the blood. Finally, as

previously stated, OH-PCBs bind to TTR in the blood, and can potentially displace T4 *in vivo* (Cheek et al., 1999). These three mechanisms of toxicity may combine to interfere with the ability of the thyroid gland to respond to TSH and produce thyroid hormones, reduce the half-life of T4 in the serum, and lessen the carrying capacity of the blood for T4.

**Thyroid Hormone Action**

T4 is the main product released from the normal thyroid. It is considered the inactive prohormone because T3 is the ligand that modulates the thyroid hormone receptor (TR). T4 is transported to target tissues via three transport proteins exhibiting different T4 affinities – thyroid binding globulin (TBG), TTR, and albumin. The distribution of these binding proteins is not universal in the animal kingdom (Schreiber and Richardson, 1997). Currently, there are limited data on how T4 traverses the vascular barrier and reaches the target cell.

*Activation of Thyroxine.* Type I and Type II 5'-deiodinases (D1 and D2, respectively) activate the prohormone T4 to form the active hormone T3 (reviewed by Kohrle (1999)). D1 can also inactivate the active hormone T3 to form 3, 5-diiodothyronine (T2) or iodothyronine sulfates. Another deiodinase isoenzyme, the 5-deiodinase (D3), inactivates the prohormone T4 by eliminating iodine to form the inactive product rT3 (reverse T3) or T2. T3 homeostasis in tissues is maintained by these three enzymes (D1, D2, and D3). The presence and activity of these enzymes are tissue specific.

D2 is especially important because of its apparent role in the development of the central nervous system and the cochlea, and its reaction to hypothyroidism. D2 is expressed in the brain, inner ear, the severely hypothyroid anterior pituitary, the placenta, the skin, and brown adipose tissue in rodents (Bates et al., 1999; Campos-Barros et al., 2000; Kohrle, 1999; Schroder-van der Elst et al., 1998; Tu et al., 1997). During hypothyroidism, D2 activity increases because the protein is stabilized and the half-life is prolonged (as cited in (Kohrle, 1999)). These observations have led to the theory that D2

produces T3 for local cellular demands independent of circulating T3 (Kohrle, 1999). For example, Schroder-van der Elst et al. (1998) investigated deiodinase activities in fetal rat tissues at several levels of iodine deficiency. One of the more important findings was that D2 activity increased in the fetal skin, brain, and placenta as a result of iodine deficiency. Even more interesting was the higher level of D2 in fetal skin compared to the brain and the increased skin D2 activity in even mild iodine deficiency. Based on these findings, the authors concluded that skin D2 is physiologically important in fetal thyroid hormone economy. Skin D2 contributes to the intracellular T3 content of the skin and, possibly, to the plasma T3.

Campos-Barros et al. (2000) investigated deiodinase expression in the mouse cochlea before the onset of hearing. D2 activity increased rapidly in the mouse cochlea to peak around postnatal day 7, after which activity decreased by P10. The peak in activity a few days before the onset of hearing suggests an important role for D2 in increasing local levels of T3. Such a role for D2 activity has been further supported in rats made mildly hypothyroidic by an antithyroid chemical propylthiouracil (PTU) or PCBs (Crofton et al., 2000; Goldey, 1995a; Goldey and Crofton, 1998; Herr et al., 1996). Both of these treatments reduced serum levels of T4 but not T3 because protective measures maintained serum T3 levels. Nonetheless, auditory deficits were seen. These studies support the view that circulating T3 levels are inadequate for the developing cochlea and increased D2 activity is necessary to convert T4 to T3, in order to increase local T3 levels for normal cochlear development.

*Thyroid Hormone Receptor.* T3 acts primarily at the nuclear level by regulating the transcription of thyroid-hormone-responsive genes, as reviewed in Anderson (2001). Thyroid hormones enter the cell, move to the nucleus, and bind to the thyroid hormone receptor (TR), a receptor belonging to the larger family of nuclear receptors. Two isoforms of TR exist, known as TR$\alpha$ and TR$\beta$. T3 binds to the TR with much higher affinity than T4 and is thought to be the active hormone in the nucleus. TR interacts with specific DNA sequences known as thyroid hormone response elements (TREs). TR binds to the TRE as a heterodimer with the retinoid X receptor (RXR). These TREs are

located in the proximal promoter regions of thyroid hormone-responsive genes. The genes give rise to proteins that are very important in development of the inner ear, retina, cerebellum, hippocampus, and cerebral cortex.

*Thyroid Hormone Responsive Genes in the CNS*. Numerous T3-regulated genes have been identified in the rodent CNS (reviewed by Anderson (2001)), but roles for these gene products in the brain are not well established. Recently, it has been found that many of these genes encode transcriptional regulatory proteins, one of which is the mammalian basic transcription element-binding protein (BTEB) (Denver et al., 1999). Overexpression of BTEB in neuro-2a cells has been shown to dramatically increase the number and length of neurites, suggesting an important role of BTEB in dendritic growth (Denver et al., 1999). Furthermore, T3 administration was shown to increase BTEB mRNA levels in primary neurons, astrocytes, and oligodendrocytes prepared from E16 (for neurons) and P2 (for astrocytes and oligodendrocytes) rat brain.

It is known that oligodendrocytes express active forms of thyroid hormone receptors and that thyroid hormones are important in myelination, as reviewed by Anderson (2001). In fact, the most striking effect of neonatal hypothyroidism is the delay in myelinogenesis and a decrease in the number of myelinated axons, without any effect on the total number of axons. It has been shown that thyroid hormones regulate the expression of several key enzymes and proteins of the myelin sheath (Barradas et al., 2001). These include 2'3'-cyclic nucleotide 3'-phosphodiesterase (CNPase), myelin basic protein (MBP), proteolipidic protein (PLP), as well as myelin-associated/oligodendrocytic basic protein (MOBP). The expression of these genes is reduced in rats made hypothyroid as neonates (Barradas et al, 2001). Interestingly, deficiency of thyroid hormone during the neonate stage induced a permanent down-regulation of MOBP 22 kDa isoform and PLP expression in adulthood.

**Hypothyroidism, Environmental Chemicals, and Neurodevelopment**

If thyroid hormone deficiencies (hypothyroidism) occur during fetal or neonatal development, severe pathological situations can occur. Hypothyroid effects include

disorders of process outgrowth, synaptogenesis, and myelination in neuron development, as reviewed by Anderson (2001) (Table 4). These disorders manifest themselves as smaller and more tightly packed peripheral and central neuronal cell bodies. The affected areas can be related to the various deficits in learning and motor skills of hypothyroid animals. This is revealed in the disorders known as cretinism (in the case of fetal development) and congenital hypothyroidism (in the case of neonatal development). Cretinism occurs when there is a severe iodine deficieny in the diet of pregnant women and is characterized in the fetus by extreme mental retardation, deaf-mutism, impaired voluntary motor activity and hypertonia (Delange, 2000). Congenital hypothyroidism, if untreated, results in severe intellectual deficits in children (Song et al., 2001).

Hypothyroidism has been shown to cause decreases in brain volume and weight in both clinical and experimental cases. Brain magnetic resonance (MR) imaging in patients with hypothyroidism before and after treatment showed a significant increase in brain size with thyroid hormone supplement (Oatridge et al., 2002). Furthermore, surgical thyroidectomy of sheep fetus at 98 days causes a significant reduction in brain weight at birth (McLntosh et al., 1982). In rats dosed with propylthiouracil to induce neonatal hypothyroidism, there was a significant decrease in brain and cerebellar weights (Nathaniel et al., 1988). This condition was alleviated with T4 replacement therapy.

PCB exposure in humans is associated with cognitive and behavioral retardation (Gilbert et al., 2000; Schantz, 1996a; Schantz et al., 2001; Schantz et al., 1991; Schantz et al., 1995; Schantz et al., 1996b; Wong et al., 1997). This may be partly explained by the ability of these compounds to affect brain development by interfering with the thyroid hormone system. This hypothesis is supported by a series of significant findings. First, neurological deficits observed in humans associated with PCB exposure are similar to those deficits observed in the offspring born from hypothyroxinemic women (Gilbert et al., 2000; Goldey and Crofton, 1998). Second, exposure of pregnant rats to OH-PCBs (specifically 4-OH-CB107) results in the transfer of this compound to the fetal brain, a decrease in total T4 (TT4) in fetal plasma and brain samples, and concomitant increase of D2 activity in fetal forebrain (Meerts et al., 2002). Third, it has been shown that

exposure of rat offspring to PCBs results in severe hearing loss and motor deficits (Goldey and Crofton, 1998). These deficits are accompanied by a drastic decrease in circulating T4, and the deficits are attenuated by T4 replacement therapy. Cochlear pathologies in these rats reveal outer hair cell losses similar to lesions common in severe hypothyroidism (Crofton et al., 2000; Goldey et al., 1995). Fourth, in mouse cerebellar culture assays, HO-PCBs inhibit thyroid-hormone-dependent arborization of Purkinje cell dendrites (Kimura-Kuroda et al., 2005). Fifth, in fetal rats, Aroclor 1254 (a PCB mixture) decreases the density of oligodendroglial cells of the corpus callosum (Sharlin et al., 2006).

**Brain Development in Marine Mammals**

Considering that thyroid hormone is especially important in development and neurological outcome in offspring, environmental pollutants like PCBs, PBDEs, and halogenated phenolics that are maternally transferred and affect thyroid function may affect the development of the brain. Delphinid cetaceans (especially first-borns) may be particularly sensitive to these effects because of the high degree of bioaccumulation and maternal transfer of chemicals during a critical period of brain development.

Odontocetes (toothed whales, dolphins, and porpoises) have undergone unique evolutionary adaptations to live constantly in an aquatic environment. One of the most prominent modifications has been in relative brain size. In fact, several odontocete species have encephalization quotients (a measure of relative brain size) that are second only to modern humans (Marino, 1998b; Ridgway and Brownson, 1984). Several studies have been completed on odontocete neuroanatomy, as reviewed by Morgane et al. (1986) and Ridgway (1990). However, few studies have focused on quantitative measurements of odontocete brain structures (Marino et al., 2000; Tarpley and Ridgway, 1994). Fewer studies have focused on odontocete prenatal neuroanatomy or provided quantitative data on prenatal brain structures (Marino et al., 2001b).

Table 5 lists neonatal brain weights as a percentage of total adult brain weight for a variety of odontocete species (Marino, 1998a, 1999). These values fall between the

rhesus monkey, which has a very high brain weight at birth, and the human, which has a very low brain weight at birth. Compared to any other primate or cetacean, humans are born with the least developed brain (i.e. in terms of percent adult brain weight at birth). The harbor porpoise (*Phocoena phocoena*) and the La Plata river dolphin (*Pontoporia blainvillei*) are born with very mature brains, 85-90% of adult size at birth (Marino, 1998a, 1999). Dolphins belonging to the family Delphinidae (e.g. *T. truncatus*, *D. delphis*, and *O. orca*) are born with brains between 42% and 60% of adult size. In delphinid cetaceans, the brain will grow 40% to 60% more with some of that development occurring during nursing, when exposure to neurodevelopmental toxicants is extremely high.

**Rationale and Approach for Thesis Research**

Cetacean blubber is a primary site for lipid storage, which the animal utilizes during periods of energetic stress. This process affects the structure of blubber. It is likely that multiple factors affect blubber morphology in delphinid cetaceans. These factors may include ontogeny, geographic location, water temperature, sex, reproductive status, and nutritional state. It is important to understand how the blubber responds to these factors because blubber is also the primary storage site for persistent organic pollutants (POPs). During periods of lipid mobilization such as lactation, POPs from the blubber are mobilized into the circulatory system and may cause toxic effects. One particular toxic mechanism may include the induction of cytochrome P450 enzymes (e.g. CYP1A and CYP2B enzymes) in the integument and liver, which could enhance the production of OH-PCBs. OH-PCBs (as well as parent PCBs that are not hydroxylated) may then interfere with the thyroid hormone system and affect neurodevelopment. The goal of this thesis is to investigate some of these hypotheses and devise a quantitative approach to assess neurodevelopment in delphinid cetaceans.

In delphinid cetaceans, POPs accumulate in the blubber in high quantities. In other vertebrate species, PCBs and DDTs have been shown to move out of adipose tissue during lipid mobilization. Hence, knowledge of the structure and dynamics of blubber is

important because this information is essential for understanding the mobilization of pollutants from the blubber into the bloodstream and investigating associated health effects to the animal and its offspring. **Chapter 2** describes an investigation of the factors that influence blubber morphology and blubber dynamics in bottlenose dolphins (*Tursiops truncatus*) captured and released from the coastal waters of Charleston, SC (CHS) and Indian River Lagoon, FL (IRL). The specific objectives of Chapter 2 are to:

- Determine if the blubber was stratified in these live-captured bottlenose dolphins;
- Compare the blubber morphology of dolphins captured at two geographic locations (CHS vs. IRL);
- Investigate the influence of age class and sex on blubber morphology, while controlling for differences in geographic location;
- Examine how blubber morphology varies with reproductive state.

CYP1A1 has been shown to be a valuable biomarker of exposure and effect to halogenated aromatic hydrocarbons (e.g. non-*ortho* and mono-*ortho* PCBs). In the integument, CYP1A1 expression is strongest and most frequent in vascular endothelial cells of the arterial system and capillaries within the blubber of delphinids. It has been suggested that the movement of AHR agonists (e.g. non-*ortho* and mono-*ortho* PCBs) from the blubber across the endothelial cells and into the bloodstream (i.e. as occurs during blubber lipid mobilization) could induce CYP1A1 in vascular endothelial cells. Hence, understanding blubber morphology and lipid dynamics may be important factors in understanding CYP1A1 expression in the blubber biopsy, its relationship to AHR agonists, and its involvement in the production of HO-PCBs. In **Chapter 3**, I report an investigation of the interrelationships among CYP1A1 expression, PCBs and OH-PCBs, and blubber dynamics of the bottlenose dolphins studied in Chapter 2. Specifically, the objectives of Chapter 3 are to:

- Quantitatively test the hypothesis that CYP1A1 expression is stratified in the blubber of these dolphins;
- Compare depth-specific expression in CHS and IRL dolphins;

- Determine if there is a relationship between depth-specific expression and total blubber and plasma 2,3,7,8-TCDD Toxic Equivalents (TEQ);
- Explore the role of blubber dynamics in CYP1A1 induction;
- Investigate the relationship between depth-specific CYP1A1 expression and plasma HO-PCB concentrations.

PCBs and their hydroxylated metabolites (OH-PCBs) can interfere with the thyroid hormone system and normal brain development. Delphinid cetaceans (especially first-borns) may be particularly sensitive to these effects because of the high degree of bioaccumulation and maternal transfer of chemicals during a sensitive time period of brain maturation. It is important to develop approaches to assess the effects of environmental chemicals on neurodevelopment in odontocetes. Presently, suitable methods do not exist. Magnetic resonance imaging (MRI), a common diagnostic tool in human medicine, has recently been used to study the comparative neuroanatomy of the beluga whale (Marino et al., 2001a), the fetal common dolphin (*Delphinus delphis*)(Marino et al., 2001b), the bottlenose dolphin (Marino et al., 2001c), the harbor porpoise (*Phocoena phocoena*) (Marino et al., 2003b), the dwarf sperm whale (*Kogia simus*) (Marino et al., 2003a), the spinner dolphin (*Stenella longirostris orientalis*) (Marino et al., 2004b), and the killer whale (Marino et al., 2004a). MR imaging offers a non-invasive and non-destructive method of acquiring a permanent archive of external and internal brain structure data. In addition, MR imaging, coupled with advanced software image analysis, can accurately determine regional brain volumes, while traditional dissection and photography can introduce more error in performing quantitative measurements.

**Chapter 4** illustrates a novel, quantitative approach to assess neurodevelopment in a delphinid cetacean, the Atlantic white-sided dolphin (*Lagenorhynchus acutus*), by determining the volumes of brain structures from MR images of the post-mortem brain intact within the skull with the head still attached to the body (i.e. *in situ* imaging). In future studies, this approach might be used to understand the potential impacts of anthropogenic chemicals (such as PCBs, PBDEs, and their hydroxylated metabolites) on

the size of brain regions that depend on thyroid hormones for maturation (such as cerebellum grey matter, corpus callosum, and hippocampus). Specifically, the objectives of Chapter 4 are to:

- Validate techniques by determining if MR imaging coupled with advanced software image processing and segmentation could accurately determine volumes;
- Provide an anatomically labeled MRI-based atlas of the fetal and subadult Atlantic white-sided dolphin brain;
- Determine the white matter and grey matter volumes of the total brain and cerebellum along an ontogenetic series from fetus to adult using MR images;
- From MR images, determine the mid-sagittal area of the corpus callosum and the volumes of the left and right hippocampal formation.

**REFERENCES**


Achen MG, Harms PJ, Thomas T, Richardson SJ, Wettenhall REH, Schreiber G. 1992. Protein synthesis at the blood-brain barrier. The major protein secreted by amphibian choroid plexus is a lipocalin. Journal of Biological Chemistry 267(32):23170-23174.

Aguilar A. 1983. Organochlorine pollution in sperm whales, *Physeter macrocephalus*, from the temperate waters of the eastern North Atlantic. Marine Pollution Bulletin 14(9):349-352.

Aguilar A, Borrel A. 1991. Heterogeneous distribution of organochlorine contaminants in the blubber of baleen whales: implications for sampling procedures. Marine Environmental Research 31:275-286.

Aguilar A, Borrell A. 1990. Patterns of lipid content and stratification in the blubber of fin whales (*Balaenoptera physalus*). Journal of Mammalogy 71:544-554.

Anderson G. 2001. Thyroid hormones and the brain. Frontiers in Neuroendocrinology 22(1):1-17.

Angell C, Wilson J, Moore M, Stegeman J. 2004. Cytochrome P4501A1 expression in cetacean integument: implications for detecting contaminant exposure and effects. Marine Mammal Science 20:554-566.

Barradas PC, Vieira RS, De Freitas MS. 2001. Selective effect of hypothyroidism on expression of myelin markers during development. Journal of Neuroscience Research 66(2):254-261.

Bastomsky C, Murthy P, Banovac K. 1976. Alterations in thyroxine metabolism produced by cutaneous application of microscope immersion oil: effects due to polychlorinated biphenyls. Endocrinology 98:1309-1314.

Bates JM, St Germain DL, Galton VA. 1999. Expression profiles of the three iodothyronine deiodinases, D1, D2, and D3, in the developing rat. Endocrinology 140(2):844-851.

Bernhoft A, Skaare JU. 1994. Levels of selected individual polychlorinated biphenyls in different tissues of harbour seals (*Phoca vitulina*) from the southern coast of Norway. Environmental Pollution 86(1):99-107.

Birnbaum LS, Staskal DF. 2004. Brominated Flame Retardents: Cause for Concern? Environmental Health Perspectives 112(1):9-17.

Blomkvist G, Roos A, Jensen S, Bignert A, Olsson M. 1992. Concentrations of sDDT and PCB in seals from Swedish and Scottish waters. Ambio 21(8):539-545.

Borrell A, Bloch D, Desportes G. 1995. Age trends and reproductive transfer of organochlorine compounds in long-finned pilot whales from the Faroe Islands. Environmental Pollution 88:283-292.

Brouwer A, Morse DC, Lans MC, Schuur AG, Murk AJ, Klasson-Wehler E, Bergman A, Visser TJ. 1998. Interactions of persistent environmental organohalogens with the thyroid hormone system: mechanisms and possible consequences for animal and human health. Toxicology and Industrial Health 14(1-2):59-84.

Brouwer A, Reijnders PJH, Koeman JH. 1989. Polychlorinated biphenyl (PCB)-contaminated fish induces vitamin A and thyroid hormone deficiency in the common seal (*Phoca vitulina*). Aquatic Toxicology 15(1):99-106.

Byrne JJ, Carbone JP, Hanson EA. 1987. Hypothyroidism and abnormalities in the kinetics of thyroid hormone metabolism in rats treated chronically with polychlorinated biphenyl and polybrominated biphenyl. Endocrinology 121(2):520-527.

Campos-Barros A, Amma LL, Faris JS, Shailam R, Kelley MW, Forrest D. 2000. Type 2 iodothyronine deiodinase expression in the cochlea before the onset of hearing. Proceedings of the National Academy of Sciences, USA 97(3):1287-1292.

Cheek AO, Kow K, Chen J, McLachlan JA. 1999. Potential mechanisms of thyroid disruption in humans: interaction of organochlorine compounds with thyroid receptor, transthyretin, and thyroid-binding globulin. Environmental Health Perspectives 107(4):273-278.

Cockcroft VG, De Kock AC, Lord DA, Ross GJB. 1989. Organochlorines in bottlenose dolphins (*Tursiops truncatus*) from the East coast of South Africa. South African Journal of Marine Science 8:207-217.

Collins W, Capen C, Kasza L, Carter C, Dailey R. 1977. Effect of polychlorinated biphenyl (PCB) on the thyroid gland of rats. Ultrastructural and biochemical investigations. American Journal of Pathology 89:119-130.

Corrigan FM, Murray L, Wyatt CL, Shore RF. 1998. Diorthosubstituted polychlorinated biphenyls in caudate nucleus in Parkinson's disease. Experimental Neurology 150:339-342.

Corrigan FM, Wienburg CL, Shore RF, Daniel SE, Mann D. 2000. Organochlorine insecticides in substantia nigra in Parkinson's disease. Journal of Toxicology and Environmental Health 59(4):229-234.

Crofton K, Ding D, Padich R, Taylor M, Henderson D. 2000. Hearing loss following exposure during development to polychlorinated biphenyls: a cochlear site of action. Hearing Research 144(1-2):196-204.

Dale EW, Gaines TB, Hayes WJ. 1962. Storage and excretion of DDT in starved rats. Toxicology and Applied Pharmacology 4:89-106.

de Boer J, Wester PG, Klamer HJ, Lewis WE, Boon JP. 1998. Do flame retardants threaten ocean life? Nature 394:28-29.

Dearolf JL, McLellan WA, Dillaman RM, Frierson D, Jr., Pabst DA. 2000. Precocial development of axial locomotor muscle in bottlenose dolphins (*Tursiops truncatus*). Journal of Morphology 244:203-215.

Delange F. 2000. Endemic Cretinism. Braverman L, Utiger R, editors. Philadelphia: Lippincott Williams and Wilkins. 743-754 p.

DeLong RL, Gilmartin WG, Simpson JG. 1973. Premature births in California sea lions: association with high organochlorine pollutant residue levels. Science 181(4105):1168-1170.

Denomme M, Bandiera SM, Lambert I, Copp L, Safe L, Safe S. 1983. Polychlorinated biphenyls as phenobarbitone-type inducers of microsomal enzymes. Structure-activity relationships for a series of 2,4-dichloro-substituted congeners. Biochemical Pharmacology 32(19):2955-2963.

Denver RJ, Ouellet L, Furling D, Kobayashi A, Fujii-Kuriyama Y, Puymirat J. 1999. Basic transcription element-binding protein (BTEB) is a thyroid hormone-regulated gene in the developing central nervous system. Evidence for a role in neurite outgrowth. The Journal of Biological Chemistry 274(33):23128-23134.

Dickson PW, Aldred AR, Menting JGT, Marley PD, Sawyer WH, Schreiber G. 1987. Thyroxine transport in choroid plexus. Journal of Biological Chemistry 262(29):13907-13915.

Dunkin RC, McLellan WA, Blum JE, Pabst D. 2005. The ontogenetic changes in the thermal properties of blubber from Atlantic bottlenose dolphin *Tursiops truncatus*. The Journal of Experimental Biology 208:1469-1480.

Ecobichon D. 1996. Toxic Effects of Pesticides. In: Klaassen CD, editor. Casarett & Doull's Toxicology - The Basic Science of Poisons. 5th ed. New York: The McGraw-Hill Companies, Inc. p 643-689.

Eriksson P. 1997. Developmental neurotoxicity of environmental agents in the neonate. Neurotoxicology 18(3):719-726.

Findlay GM, De Freitas ASW. 1971. DDT movement from adipocyte to muscle cell during lipid utilization. Nature 229(63-65):63-65.

Fleming L, Mann JB, Bean J, Briggle T, Sanchez-Ramos JR. 1994. Parkinson's disease and brain levels of organochlorine pesticides. Annals of Neurology 36(1):100-103.

Gauthier JM, Pelletier E, Brochu C, Moore S, Metcalfe CD, Beland P. 1998. Environmental contaminants in tissues of a neonate St Lawrence beluga whale (*Delphinapterus leucas*). Marine Pollution Bulletin 36(1):102-108.

Gilbert ME, Mundy WR, Crofton KM. 2000. Spatial learning and long-term potentiation in the dentate gyrus of the hippocampus in animals developmentally exposed to Aroclor 1254. Toxicological Sciences 57(1):102-111.

Godard CAJ, Smolowitz RM, Wilson JY, Payne RS, Stegeman JJ. 2004. Induction of cetacean cytochrome P4501A1 by B-napthoflavone exposure of skin biopsy slices. Toxicological Sciences 80:268-275.

Goldey EK, LS; Lau,C; Rehnberg,GL; Crofton,KM. 1995a. Developmental exposure to polychlorinated biphenyls (Aroclor 1254) reduces circulating thyroid hormone concentrations and causes hearing deficits in rats. Toxicology and Applied Pharmacology 135(1):77-88.

Goldey ES, Crofton KM. 1998. Thyroxine replacement attenuates hypothyroxinemia, hearing loss, and motor deficits following developmental exposure to Aroclor 1254 in rats. Toxicological Sciences 45(1):94-105.

Goldey ES, Kehn LS, Rehnberg GL, Crofton KM. 1995. Effects of developmental hypothyroidism on auditory and motor function in the rat. Toxicology and Applied Pharmacology 135(1):67-76.

Guroff G, Daly J, Jerina D, Renson J, Witkop B, Udenfriend S. 1967. Hydroxylation-induced migration: the NIH shift. Science 157:1524-1530.

Hahn ME. 1998. The aryl hydrocarbon receptor: a comparative perspective. Comparative Biochemistry and Physiology C: Comparative Pharmacology and Toxicology 121(1-3):23-53.

Hamilton JL, McLellan WA, Pabst DA. 2004. Functional morphology of tailstock blubber of the harbor porpoise (*Phocoena phocoena*). Journal of Morphology 261:105-117.

Hansen LJ, Schwacke LH, Mitchum GB, Hohn AA, Wells RS, Zolman ES, Fair PA. 2004. Geographic variation in polychorinated biphenyl and organochlorine

pesticide concentrations in the blubber of bottlenose dolphins from the US Atlantic coast. The Science of the Total Environment 319:147-172.

Herr DW, Goldey ES, Crofton KM. 1996. Developmental exposure to Aroclor 1254 produces low-frequency alterations in adult rat brainstem auditory evoked responses. Fundamental and Applied Toxicology 33:129-128.

Holden AV. 1978. Pollutants and seals - A review. Mammal Review 8(1-2):53-66.

Honkakoski P, Negishi M. 1998. Regulatory DNA elements of phenobarbital-responsive cytochrome P450 CYP2B genes. Journal of Biochemical and Molecular Toxicology 12(1):3-9.

Hooper K, McDonald TA. 2000. The PBDEs: an emerging environmental challenge and another reason for breast-milk monitoring programs. Environmental Health Perspectives 108(5):387-392.

Houde M, Pacepavicius G, Wells RS, Fair PA, Letcher RJ, Alaee M, Bossart GD, Hohn AA, Sweeney J, Solomon KR, Muir DCG. 2006. Polychlorinated biphenyls (PCBs) and hydroxylated polychlorinated biphenyls (OH-PCBs) in plasma of botlenose dolphins (*Tursiops truncatus*) from the Western Atlantic and the Gulf of Mexico.

Ishaq R, Karlson K, Naef C. 2000. Tissue distribution of polychlorinated naphthalenes (PCNs) and non-ortho chlorinated biphenyls (non-ortho CBs) in harbour porpoises (*Phocoena phocoena*) from Swedish waters. Chemosphere 41(12):1913-1925.

Ishida C, Koga N, Hanioka N, Saeki HK, Yoshimura H. 1991. Metabolism in vitro of 3,4,3',4'- and 2,5,2',5'-tetrachlorobiphenyl by rat liver microsomes and highly purified cytochrome P-450. Journal of Pharmacobio-Dynamics 14:276-284.

Jenssen BM, Skaare J, Ekker M, Vongraven D, Lorentsen SH. 1996. Organochlorine compounds in blubber, liver and brain in neonatal grey seal pups. Chemosphere 32(11):2115-2125.

Kaminsky LS, Kennedy MW, Adams SM, Guengerich FP. 1981. Metabolism of dichlorobiphenyls by highly purified isozymes of rat liver cytochrome P-450. Biochemistry 20:7379-7384.

Kannan K, Tanabe S, Borrell A, Aguilar A, Focardi S, Tatsukawa R. 1993. Isomer-specific analysis and toxic evaluation of polychlorinated biphenyls in striped dolphins affected by an epizootic in the western Mediterranean Sea. Archives of Environmental Contamination and Toxicology 25(2):227-233.

Karlson K, Ishaq R, Becker G, Berggren P, Broman D, Colmsjoe A. 2000. PCBs, DDTs and methyl sulphone metabolites in various tissues of harbour porpoises from Swedish waters. Environmental Pollution 110(1):29-46.

Kimura-Kuroda J, Nagata I, Kuroda Y. 2005. Hydroxylated metabolites of polychlorinated biphenyls inhibit thyroid-hormone-dependent extension of cerebellar purkinje cell dendrites. Developmental Brain Research 154:259-263.

Kipps EK, McLellan WA, Rommel SA, Pabst DA. 2002. Skin density and its influence on buoyancy in the manatee (*Trichechus manatus latirostris*), harbor porpoise (*Phocoena phocoena*), and bottlenose dolphin (*Tursiops truncatus*). Marine Mammal Science 18:765-778.

Kodavanti PR, Ward TR, Derr-Yellin EC, Mundy WR, Casey AC, Bush B, Tilson HA. 1998. Congener-specific distribution of polychlorinated biphenyls in brain regions, blood, liver, and fat of adult rats following repeated exposure to Aroclor 1254. Toxicology and Applied Pharmacology 153:199-210.

Kohrle J. 1999. Local activation and inactivation of thyroid hormones: the deiodinase family. Molecular and Cellular Endocrinology 151(1-2):103-119.

Kolaja KL, Klaassen CD. 1998. Dose-response examination of UDP-glucuronosyltransferase inducers and their ability to increase both TGF- beta expression and thyroid follicular cell apoptosis. Toxicological Sciences 46(1):31-37.

Koopman HN, Iverson S, Gaskin D. 1996. Stratification and age-related differences in blubber fatty acids of the male harbour porpoise (*Phocoena phocoena*). Journal of Comparative Physiology, B 135:628-639.

Koopman HN, Pabst DA, McLellan WA, Dillaman RM, Read AJ. 2002. Changes in blubber Distribution and morphology associated with starvation in the harbour porpoise(*Phocoena phocoena*):Evidence for Regional differences in blubber structure and function. Physiological and Biological Zoology 75(5):498-512.

Letcher RJ, Klasson Wehler E, Bergman A. 2000. Methyl Sulfone and Hydroxylated Metabolites of Polychlorinated biphenyls. In: Paasivinta J, editor. The Handbook of Environmental Chemistry: New types of Persistent Halogenated Compounds. Heidelberg: Springer-Verlaq. p 314-359.

Marino L. 1998a. Brain growth patterns in the La Plata River dolphin (*Pontoporia blainvillei*). Aquatic Mammals 24(3):111-116.

Marino L. 1998b. A comparison of encephalization between odontocete cetaceans and anthropoid primates. Brain, Behavior and Evolution 51(4):230-238.

Marino L. 1999. Brain growth in the harbor porpoise and Pacific white-sided dolphin. Journal of Mammalogy 80(4):1353-1360.

Marino L, Murphy TL, Deweerd AL, Morris JA, Fobbs AJ, Humblot N, Ridgway SH, Johnson JI. 2001a. Anatomy and three-dimensional reconstructions of the brain of the white whale (*Delphinapterus leucas*) from magnetic resonance images. The Anatomical Record 262(4):429-439.

Marino L, Murphy TL, Gozal L, Johnson JI. 2001b. Magnetic resonance imaging and three-dimensional reconstructions of the brain of a fetal common dolphin, Delphinus delphis. Anatomy and Embryology 203:393-402.

Marino L, Rilling JK, Lin SK, Ridgway SH. 2000. Relative volume of the cerebellum in dolphins and comparison with anthropoid primates. Brain, Behavior and Evolution 56(4):204-211.

Marino L, Sherwood CC, Delman BN, Tang CY, Naidich TP, Hof PR. 2004a. Neuroanatomy of the killer whale (*Orcinus orca*) from magnetic resonance images. The Anatomical Record A:1-7.

Marino L, Sudheimer K, McLellan WA, Johnson JI. 2004b. Neuroanatomical structures of the spinner dolphin (*Stenella longirostris orientalis*) brain from magnetic resonance images. The Anatomical Record Part A 279A:601-610.

Marino L, Sudheimer K, Pabst DA, McLellan WA, Johnson JI. 2003a. Magnetic resonance images of the brain of a dwarf sperm whale (*Kogia simus*). Journal of Anatomy 203:57-76.

Marino L, Sudheimer K, Sarko D, Sirpenski G, Johnson JI. 2003b. Neuroanatomy of the harbor porpoise (*Phocoena phocoena*) from magnetic resonance images. Journal of Morphology 257:308-347.

Marino L, Sudheimer KD, Murphy TL, Davis KK, Pabst DA, McLellan WA, Rilling JK, Johnson JI. 2001c. Anatomy and three-dimensional reconstructions of the brain of a bottlenose dolphin (*Tursiops truncatus*) from magnetic resonance images. The Anatomical Record 264(4):397-414.

Marsili L, Focardi S. 1997. Chlorinated hydrocarbon (HCB, DDTs and PCBs) levels in cetaceans stranded along the Italian coasts: An overview. Environmental Monitoring and Assessment 45(2):129-180.

McKinney MA, De Guise S, Martineau D, Beland P, Lebeuf M, Letcher RJ. 2006. Organohalogen contaminants and metabolites in beluga whale (*Delphinapterus leucas*) liver from two Canadian populations. Environmental Toxicology and Chemistry 25(5):30-41.

McLellan WA, Koopman HN, Rommel SA, Read AJ, Potter CW, Nicolas JR, Westgate AJ, Pabst DA. 2002. Ontogenetic allometry and body composition of harbour porpoises (*Phocoena phocoena, L.*) from the western North Atlantic. Journal of Zoology 257:457-471.

McLntosh GH, Potter BJ, Hetzel BS, Hua CH, Cragg BG. 1982. The effects of 98 day foetal thyroidectomy on brain development in the sheep. Journal of Comparative Pathology 92(4):599-608.

Meerts IA, Assink Y, Cenijn PH, Van Den Berg JH, Weijers BM, Bergman A, Koeman JH, Brouwer A. 2002. Placental transfer of a hydroxylated polychlorinated biphenyl and effects on fetal and maternal thyroid hormone homeostasis in the rat. Toxicological Sciences 68(2):361-371.

Meironyte D, Noren K, Bergman A. 1999. Analysis of polybrominated diphenyl ethers in Swedish human milk. A time-related trend study, 1972-1997. Journal of Toxicology and Environmental Health 58:329-341.

Metcalfe C, Metcalfe T, Ray S, Paterson G, Koenig B. 1999. Polychlorintated biphenyls and organochlorine compounds in brain, liver and muscle of beluga whales (*Delphinapterus leucas*) from the Arctic and St Lawrence Estuary. Marine Environmental Research no 1:1-15.

Mills RA, Millis CD, Dannan GA, Guengerich FP, Aust SD. 1985. Studies on the structure-activity relationships for the metabolism of polybrominated biphenyls by rat liver microsomes. Toxicology and Applied Pharmacology 78:96-104.

Moore, MJ, Miller CA, Weisbrod AV, Shea D, Hamilton PK, Kraus SD, Rowntree VJ, Patenaude N, and Stegeman JJ. 1998. In: International Whaling Commission Workshop.

Morse DC, Wehler EK, Wesseling W, Koeman JH, Brouwer A. 1996. Alterations in rat brain thyroid hormone status following pre- and postnatal exposure to polychlorinated biphenyls (Aroclor 1254). Toxicology and Applied Pharmacology 136(2):269-279.

Morgane PJ, Jacobs MS, Galaburda A. 1986. Evolutionary morphology of the dolphin brain. Dolphin cognition and behavior: 5-29.

Mossner S, Barudio I, Spraker TS, Antonelis G, Early G, Geraci JR, Becker PR, Ballschmiter K. 1994. Determination of HCHs, PCBs, and DDTs in brain tissues of marine mammals off different age. Fresenius Journal of Analytical Chemistry 349:708-716.

Muir DCG, Koczanski K, Rosenberg B, Beland P. 1996. Persistent organochlorines in beluga whales (*Delphinapterus leucas*) from the St. Lawrence River Estuary. 2. Temporal trends, 1982-1994. Environmental Pollution 93(2):235-245.

Nathaniel EJH, Nathaniel DR, Nathaniel LM, Burt S, Panfili F. 1988. Effect of thyroxine replacement therapy on the growth patterns of body, brain, and cerebellum in the neonatal hypothyroid rat. Experimental Neurology 101(1):1-16.

Ness DK, Schantz SL, Hansen LG. 1994. PCB congeners in the rat brain: selective accumulation and lack of regionalization. Journal of Toxicology and Environmental Health 43(4):453-468.

Norstrom RJ, Muir DCG. 1994. Chlorinated hydrocarbon contaminants in Arctic marine mammals. The Science of the Total Environment 154:107-128.

Oatridge A, Barnard ML, Puri BK, Taylor-Robinson SD, Hajnal JV, Saeed N, Bydder GM. 2002. Changes in brain size with treatment in patients with hyper- or hypothyroidism. American Journal of Neuroradiology 23(9):1539-1544.

Oehme M, Schlabach M, Hummert K, Luckas B, Nordoy ES. 1995. Determination of levels of polychlorinated dibenzo-p-dioxins, dibenzofurans, biphenyls and pesticides in harp seals from the Greenland Sea. Science of the Total Environment 162(2-3):75-91.

Pabst DA. 2000. To bend a dolphin: Convergence of force transmission designs in cetaceans and scombrid fishes. American Zoologist 40:146-155.

Pocar P, Klonisch T, Brandsch C, Eder K, Frohlich C, Hoang-Vu C, Hombach-Klonisch S. 2006. AhR-agonist-induced transcriptional changes of genes involved in thyroid function in primary porcine thyrocytes. Toxicologial Sciences 89(2):408-414.

Ridgway S, Reddy M. 1995. Residue levels of several organochlorines in Tursiops truncatus milk collected at varied stages of lactation. Marine Pollution Bulletin 30(9):609-614.

Ridgway SH, Brownson RH. 1984. Relative brain sizes and cortical surface areas in odontocetes. Acta Zoologica Fennica 172:149-152.

Ridgway SH. 1990. The Bottlenose Dolphin. The Central Nervous System of the Bottlenose Dolphin. p 69-97.

Ross P, De Swart R, Addison R, Van Loveren H, Vos J, Osterhaus A. 1996. Contaminant-induced immunotoxicity in harbour seals: Wildlife at risk? Toxicology 112(2):157-169.

Ross PS, Ellis GM, Ikonomou MG, Barrett-Lennard LG, Addison RF. 2000. High PCB concentrations in free-ranging Pacific killer whales, *Orcinus orca*: effects of age, sex and dietary preference. Marine Pollution Bulletin 40(6):504-515.

Safe S. 1984. Polychlorinated biphenyls (PCBs) and polybrominated biphenyls (PBBs): biochemistry, toxicology, and mechanism of action. Critical Reviews in Toxicology 13(4):319-395.

Saghir SA, Hansen LG, Holmes KR, Kodavanti PRS. 2000. Differential and non-uniform tissue and brain distribution of two distinct super(14)C-hexachlorobiphenyls in weanling rats. Toxicological Sciences 54:60-70.

Sandala GM, Sonne-Hansen C, Dietz R, Muir DCG, Valters K, Bennett ER, Born EW, Letcher RJ. 2004. Hydroxylated and methyl suflone PCB metabolites in adipose and whole blood of polar bear (*Ursus maritimus*) from East Greenland. Science of the Total Environment 331:125-141.

Sandau CD. 2000. Analytical chemistry of hydroxylated metabolites of PCBs and other halogenated phenolic compounds in blood and their relationship to thyroid hormone and retinol homeostasis in humans and polar bears. Ottawa, Ontario: Carleton University. 202 p.

Schantz MM, Koster BJ, Wise SA, Becker PR. 1993. Determination of PCBs and chlorinated hydrocarbons in marine mammal tissues. Stoeppler M, Zeisler R, editors. 323-345 p.

Schantz SL. 1996a. Developmental neurotoxicity of PCBs in humans: What do we know and where do we go from here? Neurotoxicology and Teratology 18(3):217-227.

Schantz SL, Gardiner JG, Polverejan E, Gasior DM, Sweeney AM, Humphrey HEB, McCaffrey RJ. 2001. Thyroid function in older adults exposed to PCBs via consumption of contaminated Great Lakes fish. 2205 Commonwealth Boulevard Ann Arbor MI 48105, [URL http //iaglr.org/]: International Association for Great Lakes Research.

Schantz SL, Levin ED, Bowman RE. 1991. Long-term neurobehavioral effects of perinatal polychlorinated biphenyl (PCB) exposure in monkeys. Environmental Toxicology and Chemistry 10(6):747-756.

Schantz SL, Moshtaghian J, Ness DK. 1995. Spatial learning deficits in adult rats exposed to ortho-substituted PCB congeners during gestation and lactation. Fundamental and Applied Toxicology 26(1):117-126.

Schantz SL, Seo B-W, Moshtaghian J, Peterson RE, Moore RW. 1996b. Effects of gestational and lactational exposure to TCDD or coplanar PCBs on spatial learning. Neurotoxicology and Teratology 18(3):305-313.

Schreiber G, Richardson SJ. 1997. The evolution of gene expression, structure, and function of transthyretin. Comparative Biochemistry and Physiology, B 116(2):137-160.

Schreiber G, Richardson SJ, Prapunpoj P. 2001. Structure and expression of the transthyretin gene in the choroid plexus: a model for the study of the mechanism of evolution. Microscopy Research and Technique 52(1):21-30.

Schroder-van der Elst JP, van der Heide D, Morreale de Escobar G, Obregon MJ. 1998. Iodothyronine deiodinase activities in fetal rat tissues at several levels of iodine deficiency: a role for the skin in 3,5,3'-triiodothyronine economy? Endocrinology 139(5):2229-2234.

Seegal RF. 2000. The neurotoxicological consequences of developmental exposure to PCBs. Toxicological Sciences 57(1):1-3.

Sharlin DS, Bansal R, Zoeller RT. 2006. Polychlorinated biphenyls exert selective effects on cellular composition of white matter in a manner inconsistent with thyroid hormone insufficiency. Endocrinology 147(2):846-858.

Sodergren A, Ulfstrand S. 1972. DDT and PCB relocate when caged robins use fat reserves. Ambio 1:36-40.

Song SI, Daneman D, Rovet J. 2001. The influence of etiology and treatment factors on intellectual outcome in congenital hypothyroidism. Journal of Developmental and Behavioral Pediatrics 22(6):376-384.

Stegeman JJ, Miller MR, Hinton DE. 1989. Cytochrome P450IA1 induction and localization in endothelium of vertebrate (teleost) heart. Molecular Pharmacology 36:723-729.

Stegeman JJ and Hahn ME. 1994. Biochemistry and molecular biology of monooxygenases: Current perspectives on forms, functions, and regulation of cytochrome P450 in aquatic species. In Aquatic Toxicology: Molecular, Biochemical and Cellular Perspectives (Malins, D.C., and Ostrander, G.K., eds), pp. 87-206,CRC/Lewis, Boca Raton

Struntz DJ, McLellan WA, Dillaman R, Blum J, Kucklick J, Pabst D. 2004. Blubber development in bottlenose dolphins (*Tursiops truncatus*). Journal of Morphology 259:7-20.

Takasuga T, Senthilkumar K, Watanabe K, Takemori H, Shoda T, Kuroda Y. 2004. Ultratrace analysis of polychlorinated biphenyls (PCBs) and their hydroxylated metabolites (OH-PCBs) in human serum and cerebrospinal fluid (CSF) samples. Organohalogen Compounds 66:2529-2534.

Tanabe S, Tatsukawa R, Tanaka H, Maruyama K, Miyazaki N, Fujiyama T. 1981. Distribution and total burdens of chlorinated hydrocarbons in bodies of striped dolphins (*Stenella coeruleoalba*). Agricultural and Biological Chemistry 45(11):2569-2578.

Tarpley RL, Ridgway SH. 1994. Corpus callosum size in delphinid cetaceans. Brain Behavior and Evolution 44:156-165.

Tirpenou AE, Tsigouri AD, Gouta EH. 1998. Residues of organohalogen compounds in various dolphin tissues. Bulletin of Environmental Contamination and Toxicology 60(2):216-224.

Tu HM, Kim S, Salvatore D, Bartha T, Legradi G, Larsen PR, Lechan RM. 1997. Regional distribution of type 2 thyroxine deiodinase messenger ribonucleic acid in rat hypothalamus and pituitary and its regulation by thyroid hormone. Endocrinology 138(8):3359-3368.

Tuerk KJ, Kucklick JR, McFee WE, Pugh RS, Becker PR. 2005. Factors influencing persistent organic pollutant concentrations in the Atlantic white-sided dolphin (*Lagenorhynchus acutus*). Environmental Toxicology and Chemistry 24(5):1079-1087.

Vedder JM. 1996. Levels of organochlorine contaminants in milk relative to health of bottlenose dolphins from Sarasota, Florida. Santa Cruz: University of California Santa Cruz. 35 p.

Visser T, Kaptein E, vanToor H, van Raay J, Van de Berg KJ, Joe C, van Engelen J, Brouwer A. 1993. Glucoronidation of thyroid hormone in rat liver: effects of in vivo treatment with microsomal enzyme inducers and in vitro assay conditions. Endocrinology 133:2177-2186.

Waxman DJ. 1999. P450 gene induction by structurally diverse xenochemicals: central role of nuclear receptors CAR, PXR, and PPAR. Archives of Biochemistry and Biophysics 369(1):11-23.

Wells RS, editor. 2000. Reproduction in wild bottlenose dolphins: overview of patterns observed during a long-term study. Silver Spring, MD. 57-74 p.

Wells RS, Tornero V, Borrell A, Aguilar A, Rowles TK, Rhinehart HL, Hofmann S, Jarman WM, Hohn AA, Sweeney JC. 2005. Integrating life-history and reproductive success data to examine potential relationships with organochlorine compounds for bottlenose dolphins (*Tursiops truncatus*) in Sarasota Bay, Florida. Science of the Total Environment 349(1-3):106.

White RD, Hahn ME, Lockhart WL, Stegeman JJ. 1994. Catalytic and immunochemical characterization of hepatic microsomal cytochromes P450 in beluga whale (*Delphinapterus leucas*). Toxicology and Applied Pharmacology 126(1):45-57.

Wilson JY, Cooke SR, Moore MJ, Martineau D, Mikaelian I, Metner DA, Lockhart WL, Stegeman JJ. 2005. Systemic effects of Arctic pollutants in beluga whales indicated by CYP1A1 expression. Environmental Health Perspectives 113:1594-1599.

Wolkers H, Lydersen C, Kovacs KM. 2004. Accumulation and lactational transfer of PCBs and pesticides in harbor seals (*Phoca vitulina*) from Svalbard, Norway. Science of the Total Environment 319(1-3):137.

Wong PW, Joy RM, Albertson TE, Schantz SL, Pessah IN. 1997. Ortho-substituted 2,2',3,5',6-pentachlorobiphenyl (PCB 95) alters rat hippocampal ryanodine receptors and neuroplasticity in vitro: Evidence for altered hippocampal function. Neurotoxicology 18(2):443-456.

Worthy G, Edwards E. 1990. Morphometric and biochemical factors affecting heat loss in a small temperate cetacean (*Phocoena phocoena*) and a small tropical cetacean (*Stenella attenuata*). Physiol Zool 60:432-442.

Yoshimura H, Yonemoto Y, Yamada H, Koga N, Oguri K, Saeki S. 1987. Metabolism in vivo of 3,4,3',4'-tetrachlorobiphenyl and toxicological assesment of the metabolites in rats. Xenobiotica 17:897-910.

Zhou T, Taylor MM, DeVito MJ, Crofton KM. 2002. Developmental exposure to brominated diphenyl ethers results in thyroid hormone disruption. Toxicological Sciences 66(1):105-116.

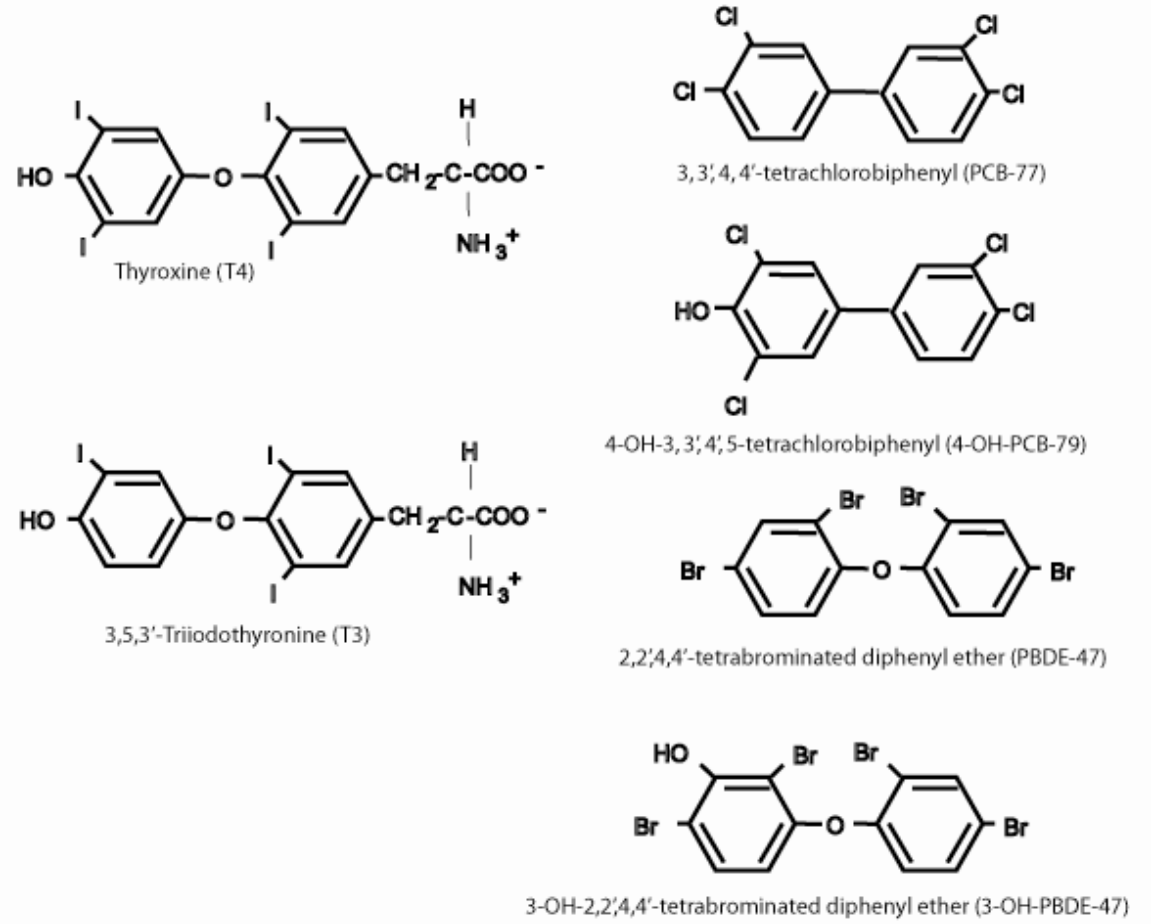


**Figure 1. A comparison of thyroid hormones, polychlorinated biphenyls (e.g. PCB-77), and emerging contaminants such as the polybrominated diphenyl ethers (e.g. PBDE-47) and halogenated phenolics (e.g. 4-OH-PCB-79 and 3-OH-PBDE-47).**

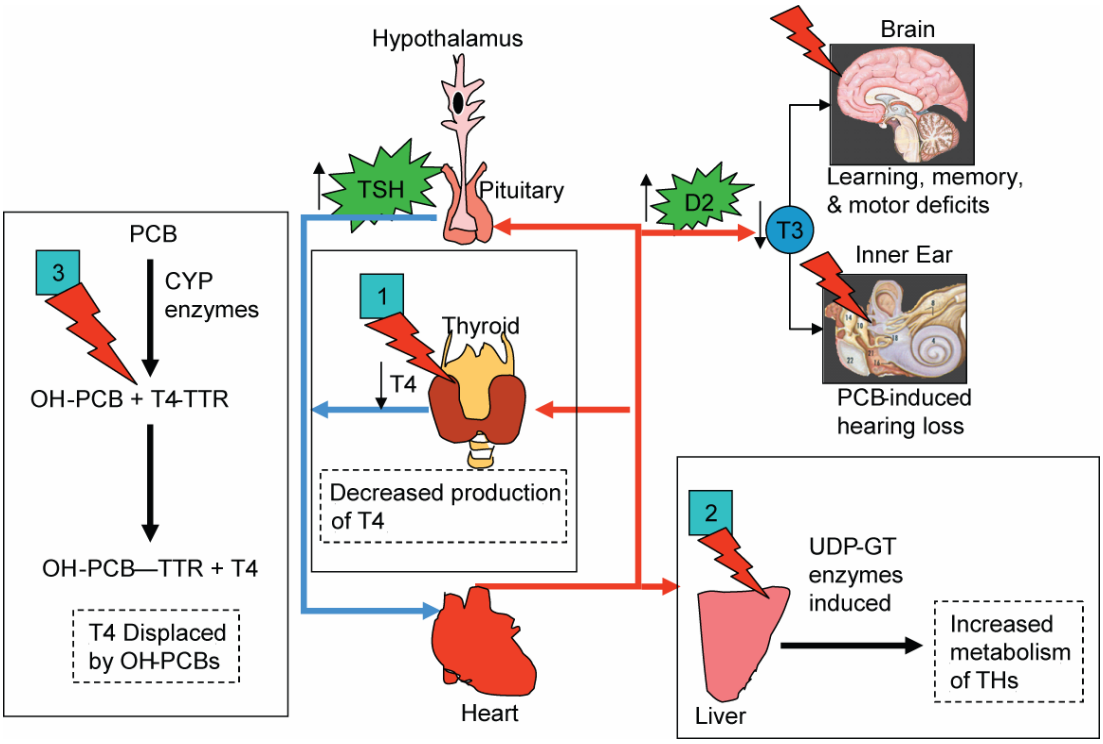


**Figure 2. Interacting mechanisms that may explain the ability of PCBs (and other related compounds) to reduce circulating and tissue levels of thyroid hormones.** PCBs can decrease the production of thyroxine (T4), increase the metabolism of thyroid hormones, or the metabolites of PCBs (OH-PCBs) may bind to transthyretin (TTR), a thyroid hormone transport protein. These mechanisms may decrease the supply of thyroid hormone (T3) necessary for the developing brain and inner ear. The organism may increase thyroid stimulating hormone (TSH) or type II 5'-deiodinase (D2), as a mechanism to increase thyroid hormones.

Table 1. Examples of PCB concentrations found in the blubber of marine mammals. Calculations based on (a) lipid weight or (b) wet weight of blubber. Nm = not mentioned.

| Common Name | Region | Number of Animals | Sample Period | Sex | Mean Age | Sum PCB Blubber Residues (ppm) | Reference |
|---|---|---|---|---|---|---|---|
| California sea lion | San Miguel Island | 6 | 1970 | F | 8 | 85 - 145 (b) | Delong, 1973 |
| Grey seal | Baltic Sea | 5 | 1981-1988 | F | Nm | 930 - 5300 (a) | Blomkvist et al, 1992 |
| Beluga whale | St. Lawrence Estuary | 15 | 1987-1990 | M | 20 | 8 - 412 (a) | Muir et al., 1996 |
| Striped dolphin | Western Mediterranean | 9 | 1990 | M | 12 | 140 - 670 (b) | Kannan et al., 1996 |
| Killer whale | British Columbia | 5 | 1993-1996 | M | 24 | 251 - 306 (a) | Ross et al., 2000 |
| Bottlenose dolphin | Charleston, SC, USA | 4 | 1999 | M | >10 | 24 – 85 (a) | Hansen et al., 2004 |
| Atlantic white-sided dolphin | Cape Cod, MA, USA | 15 | 1993-2000 | M/F | juvenile | 13 – 63 (b) | Tuerk et al., 2005 |

Table 2. Research studies that have focused on distribution of POPs in rat and human brains.

| Species | Study | Findings | Reference |
|---|---|---|---|
| rat | 1) Weaned rats were dosed with Aroclor 1242. PCBs were measured in the frontal cortex, hippocampus, and caudate putamen.<br>2) Weaned rats were exposed to radiolabeled PCB77 (planar congener) or PCB47 (nonplanar congener). | 1) There were no differences among brain regions or sexes.<br>2) PCB 77 treated pups showed higher activity in areas with blood vessels present, while pups treated with PCB47 showed higher activity in the brain (no regionalization). This was consistent with blood-brain ratios for PCB47 and 77 which were 16.8 and 0.44, respectively. | (Ness et al., 1994) |
| rat | Adults were exposed to Aroclor 1254. PCB congeners were measured in the cerebellum, frontal cortex, and striatum. | PCBs accumulated in the frontal cortex, cerebellum, and striatum. Heavily chlorinated congeners accumulated in the brain, including PCBs 163, 138, 153, 132, 156, 171, 118, 99, 105. | (Kodavanti et al., 1998) |
| rat | Rats were exposed to a single intra-peritoneal dose of 8 mg/kg radio-labeled PCB169 (coplanar congener) or PCB153 (nonplanar congener). | CB 169 did not accumulate to high levels in the brain. However, PCB153 was 4 to 9 fold higher than that of 169. PCB153 was detected in fiber tracts throughout the brain. These white matter tracts included the corpus callosum, internal and external capsules, medial lemniscus, tegmentum of the mesencephalon and metencephalon, and cerebellar peduncles. PCB153 was not found in the ventricular system and vascular spaces. | (Saghir et al., 2000) |
| humans | OC pesticides were measured in postmortem brain samples from 20 Parkinson's disease (PD), 7 Alzheimer's disease (AD), and 14 non-neurological control cases. | Dieldrin was detected in 6 of 20 PD brains, 1 of 7 AD, and in none of 14 control samples. | (Fleming et al., 1994) |

Table 2. (*Continued*).

| | | | |
|---|---|---|---|
| humans | OCs and PCBs were measured in the caudate nucleus obtained from patients with Parkinsons disease and from normal patients. | Significantly higher concentrations of dieldrin and PCB 153 were found in the PD tissue. | (Corrigan et al., 1998) |
| humans | Pesticide levels in the substantia nigra were correlated from patients who were diagnosed with Parkinsons disease (PD), cortical Lewy body dementia, Alzheimers disease (AD), or were healthy. | Gamma HCH was significantly higher in PD tissues than in the other 3 groups. Dieldrin was higher in PD tissues than in AD or control samples, while DDE and total PCBs were only higher in PD substantia nigra samples. | (Corrigan et al., 2000) |

Table 3. Chemical analysis performed on brains of marine mammals. Note the lack of regional studies and the absence of data on halogenated phenolics in brain regions.

| Region | Species | Analytes | Reference |
|---|---|---|---|
| "brain" | grey seal, harbour porpoise | DDTs, dieldrin, PCBs | (Holden, 1978) |
| cerebrum, cerebellum, medulla | striped dolphin | DDTs, PCBs, pesticides | (Tanabe et al., 1981) |
| "brain" | sperm whale | DDTs, PCBs | (Aguilar, 1983) |
| "brain" | harbour seal | PCBs | (Bernhoft and Skaare, 1994) |
| "brain" | harp seal | DDTs, PCDD/PCDFs, PCBs | (Oehme et al., 1995) |
| cerebrum, cerebellum, hypothalamus | common dolphin | PCBs, HCHs | (Mossner et al., 1994) |
| "brain" | neonatal grey seal | DDTs, PCBs | (Jenssen et al., 1996) |
| "brain" | striped dolphin | DDTs, PCBs, HCB | (Marsili and Focardi, 1997) |
| "brain" | neonate beluga whale | DDTs, pesticides, PCBs | (Gauthier et al., 1998) |
| "brain" | beluga whale | DDTs, PCBs, pesticides | (Metcalfe et al., 1999) |
| "brain" | harbour porpoise | DDTs, MeSO2-DDE, PCBs, MeSO2-PCBs | (Karlson et al., 2000) |
| "brain" | harbour porpoise | PCNs, non-ortho PCBs | (Ishaq et al., 2000) |

Table 4. Pathologies in the brain, inner ear, and thyroid gland in fetal and neonatal hypothyroidism.

| Cell or Region | Developmental Abnormalities |
|---|---|
| | |
| Oligodendrocyte | Decreased myelin around nerves. |
| | |
| Astrocyte | Impaired maturation of radial glial cells in CA1 region of hippocampus and Bergmann astrocyes of cerebellum. |
| | |
| Cerebellum | Reduction in Purkinje cell dendritic arborization.<br>Reduction in parallel fiber outgrowth.<br>Reduction in ultimate number of granule cells.<br>Abnormal proportions of basket cells, stellate cells, and astrocytes.<br>Reduction of dendritic spread. |
| | |
| Hippocampus | Reduction in number of dentate gyrus granule cells.<br>Reduction of mossy fiber system and number of moss fiber-CA3 pyramidal synapses. |
| | |
| Cerebral cortex | Reduction of dendritic growth and synaptogenesis.<br>Cells packed closer together.<br>Spine number along apical shaft of visual cortex pyramidal cells is reduced.<br>Abnormal topography of projection fields in corpus callosum. |
| | |
| Inner ear | Enlargement of tectorial membrane, inner hair cell hypertrophy, regional loss of outer hair cells, outer hair cell stereocilia absence. |
| | |
| Thyroid gland | Increased hypertrophy, hyperplasia, and follicle size. |

Table 5. Percent adult brain weight at birth.

| Species | Common Name | % Adult Brain Weight at Birth |
|---|---|---|
| *Tursiops truncatus* | bottlenose dolphin | 42% |
| *Delphinus delphis* | common dolphin | 57% |
| *Orcinus orca* | killer whale | 53% |
| *Homo sapiens* | human | 25% |
| *Macaca mulatta* | rhesus monkey | 60% |
| *Pan troglodytes* | chimpanzee | 33% |

# CHAPTER II:

# BLUBBER MORPHOLOGY IN WILD BOTTLENOSE DOLPHINS (*TURSIOPS TRUNCATUS)* FROM THE SOUTHEAST UNITED STATES: INFLUENCE OF GEOGRAPHIC LOCATION, AGE CLASS, AND REPRODUCTIVE STATE

**ABSTRACT**

This study investigated blubber stratification, as well as the effects of geographic location, age class, sex, and reproductive state on blubber morphology of bottlenose dolphins (*Tursiops truncatus*) captured and released in the Southeast United States. Seventy-four skin-blubber biopsies at sites 5-10 cm caudal to the dorsal fin and 10 cm ventral to the dorsal ridge were collected from captured and released bottlenose dolphins from two geographic locations: i) Charleston, SC (n=38) and ii) Indian River Lagoon, FL (n=36). Lipid content was measured from subsections of each biopsy. Histological slides were prepared using hematoxylin and eosin stains, viewed by light microscopy, and contiguous images were captured along the biopsy vertical axis from the epidermis to the subdermal sheath. Images were analyzed for morphological features including structural fiber densities and adipocyte numbers and sizes. Histological analysis of blubber revealed stratification into a superficial, middle, and deep layer, similar to previous studies on stranded specimens. CHS dolphins contained higher levels of total blubber lipids than IRL dolphins, and this difference was reflected in larger adipocytes of the middle blubber layer in CHS animals, possibly reflecting the colder mean yearly water temperatures in Charleston, SC. Subadult dolphins contained higher levels of total blubber lipids than adult animals, and this difference was reflected in more adipocytes in the middle blubber layer. Reproductive state affected the blubber morphology of CHS females. Both subadults and pregnant females contained larger adipocyte cross-sectional areas of the entire blubber than simultaneously pregnant and lactating dolphins. The smaller adipocyte size of the entire blubber in pregnant-lactating dolphins suggests that the combination of pregnancy and lactation increased the energetic demands, and blubber lipids were used as energy currency. Adipocytes in the deep blubber layer were significantly smaller in lactating and simultaneously pregnant & lactating animals compared to pregnant dolphins, further supporting the hypothesis that the deep blubber is more dynamic during periods of energetic stress. Total blubber lipid content and adipocyte size in the deep blubber of mothers with calves linearly decreased with calf

length. This provided evidence that the energetic demands of lactation cause mobilization of lipid that affects blubber morphology in bottlenose dolphins. This study demonstrates that bottlenose dolphin blubber may respond in a distinctive manner to different factors such as ontogeny, water temperature, and reproductive state. In conclusion, the ontogenetic decrease in blubber lipid from subadult to adult occurs via a decrease in the number of adipocytes in the middle blubber layer. In response to warmer water, the lipid content of the blubber also decreases, but the mechanism may involve lipid loss of adipocytes (i.e. cells shrink) in the middle layer. Similar to the effects of starvation on blubber morphology, lactation decreases adipocyte size predominantly in the deeper blubber. Future research should focus on the hormonal and molecular control of blubber dynamics.

**KEYWORDS:** Blubber; adipocyte; pregnancy; lactation; thermoregulation; bottlenose dolphin

## INTRODUCTION

Cetaceans (whales, dolphins, and porpoises) contain a specialized hypodermis, referred to as blubber (Parry, 1949). It is defined as the layer of fatty tissue between the epidermis and the underlying muscle. Blubber is dynamic and multifunctional: it functions biomechanically to provide support during locomotion, increases efficiency by streamlining the body surface (Hamilton et al., 2004; Pabst, 2000); it contributes to buoyancy (Dearolf et al., 2000; Kipps et al., 2002; McLellan et al., 2002); it is a primary site for lipid storage, which the animal utilizes during periods of energetic stress (Aguilar and Borrel, 1991; Koopman et al., 1996; Koopman et al., 2002; Struntz et al., 2004). The high lipid content also provides insulation, decreasing the heat flow from the body core to the external environment (Dunkin et al., 2005; Worthy and Edwards, 1990).

Blubber is also important toxicologically in cetaceans. It is the primary bioaccumulation site for persistent organic pollutants (POPs) such as organochlorine pesticides and polychlorinated biphenyls (PCBs) (Marsili et al., 1997; Schantz et al.,

1993; Tirpenou et al., 1998). During periods of lipid mobilization such as in lactation, POPs are mobilized into the circulatory system, reaching target sites and possibly affecting health and survival (Chapter 3; Norstrom and Muir, 1994; Ridgway and Reddy, 1995; Wolkers et al., 2004). Understanding the detailed structure and dynamics of blubber is important not only because it is a critical component in mammalian adaptation to the aquatic environment, but also because it is essential for understanding the mobilization of pollutants from the blubber into the bloodstream and investigating associated health effects (Chapter 3).

Histological and biochemical evidence from stranded specimens suggest that blubber is stratified in cetaceans (Ackman et al., 1965, 1975a; Lockyer et al., 1984; Aguilar and Borrell, 1990; Koopman et al., 1996; Koopman et al., 2002; Struntz et al., 2004). For example, in fin whales (*Balaenoptera physalus*), Aguilar and Borrell (1990) described the vertical stratification of lipid content. The external blubber layer of fin whales did not show any variation in lipid content with age or reproductive status. In contrast, the inner blubber was more variable suggesting the importance of this layer in the dynamics of fat storage. In odontocetes, Koopman et al. (1996) noted vertical stratification of fatty acid composition between the "inner" and "outer" blubber layers in male harbor porpoises (*Phocoena phocoena*). Shorter chain length fatty acids (< 18 carbons) were found to be significantly more abundant in the "outer" layer, while the long-chain unsaturated fatty acids (>18 carbons) were more common in the "inner" blubber layer. In bottlenose dolphins (*Tursiops truncatus*) that had either stranded or been incidentally killed in fishing operations in North Carolina and Virginia, Struntz et al. (2004) showed dramatic blubber stratification based on the number of adipocytes, adipocyte area, and structural fiber density. At the mid-thoracic site, adipocyte areas and numbers varied significantly across the blubber depth, with smaller and fewer adipocytes near the epidermis or "superficial" layer. Adipocyte numbers and size increased in the "middle" blubber and then decreased again in the "deep" layer near the border of the sub-dermal connective tissue sheath and muscle layer. These observations, as well as the impacts of emaciation on blubber morphology, have brought forth the hypothesis that the

"inner" or "middle" and "deep" blubber layers have a more dynamic role in lipid mobilization, while the "outer" or "superficial" blubber is more static (Ackman et al., 1965, 1975a; Lockyer et al., 1984; Aguilar and Borrell, 1990; Koopman et al., 2002; Struntz et al., 2004).

Surprisingly little is known about the variability of blubber composition and histological structure between dolphins that inhabit different geographic locations, which differ in mean yearly water temperatures, or among females of varying reproductive states. It is likely that multiple factors affect blubber structure in bottlenose dolphins; these may include age class, geographic location, water temperature, sex, reproductive status, and nutritional state. For example, Struntz et al. (2004) showed that the blubber from bottlenose dolphins of different life history categories varied in histological structure. Blubber from adult and juvenile animals had significantly higher lipid content and mean adipocyte size than that of fetuses. Pregnant dolphins were shown to have the highest blubber lipid content and adipocyte size of all life history categories. Emaciated adults (n = 2) had total blubber lipid content equivalent to fetuses and adipocyte size much smaller than robust adults. However, that study utilized stranded specimens from multiple geographic locations and ontogeny was investigated without controlling for sex. How do differences in mean yearly water temperatures, such as those found in different geographic locations, affect blubber structure? Does lactation affect blubber morphology? To our knowledge, a thorough study addressing these questions has yet to be investigated for any cetacean species.

The goals of the current study were two-fold. The first objective was to describe and measure the variability of blubber morphology of wild, bottlenose dolphins captured and released at two different coastal locations in the Southeast United States. Those results are described in this chapter. The second objective was to obtain data for use in the Bottlenose Dolphin Health and Risk Assessment (HERA) Project, the goal of which is to better understand the effects of contaminants (i.e. POPs) on dolphin health. One aspect of the HERA project involved assessing the response of cytochrome P4501A1 (CYP1A1) in the blubber to environmental chemicals. CYP1A1 induction is a valuable

biomarker of exposure to and effects of polyhalogenated aromatic hydrocarbons (PHAHs), as has been demonstrated in marine mammal studies (Bandiera et al, 1997; McKinney et al, 2004; White et al., 1994; Wilson, 2003; Wilson et al., 2005). Microscopic inspection of the blubber, prior to analysis of CYP1A1, allowed us to understand the biology and multiple roles of the blubber layers and to incorporate this knowledge in interpreting CYP1A1 expression in the integument of bottlenose dolphins (see Chapter 3).

The specific objectives of the present study were to: 1) determine if the blubber was stratified in these live-captured bottlenose dolphins; (2) compare the blubber morphology of dolphins captured at two geographic locations, which have different water temperature regimes; and (3) investigate the influence of age class and sex on blubber morphology, while controlling for differences in geographic location. Additionally, samples from pregnant and lactating females were available to examine how blubber morphology varies with reproductive state.

## METHODS

### *Specimens*

The HERA Project, a collaboration between the National Ocean Service Center for Coastal Environmental Health & Biomolecular Research and Harbor Branch Oceanographic Institution, was initiated in 2003, as a comprehensive, integrated, multi-disciplinary research project designed to assess the health of Atlantic bottlenose dolphins in two southeast coastal regions, Charleston, SC and the Indian River Lagoon, FL. The objectives of the project are to develop tools and techniques to better assess the health of bottlenose dolphins and to develop links between dolphin health and possible environmental stressors. These research goals are aimed at understanding the cumulative effects of multiple stressors (including the impacts of environmental contaminants) and will ultimately provide information critical to the preparation of effective management plans.

As part of this project, blubber samples were collected from seventy-four bottlenose dolphins that were captured and released in estuarine waters from these two geographic locations: (i) Charleston (CHS), SC in August 2003 (n = 38); and (ii) Indian River Lagoon (IRL), FL in July 2003 (n = 36) (Figure 1). The CHS study location was in the estuarine waters of Charleston, SC (32º54'0"N, 80º1'47"W), situated in the central region of the state's coastal zone. This includes Charleston Harbor, as well as portions of the main channels and creeks of the Ashley River, Cooper River, Wando River, and the Stono River Estuary. The IRL study location extends from the north near Merritt Island, FL 80° 47′46 W south to the St. Lucie Inlet 27°47′ 41 N. Within the IRL, capture-release activities were conducted in two separate areas. The northern capture area included Mosquito Lagoon, and portions of the Indian and Banana Rivers north of latitude 28$^{o}$ 15'0"N. The southern capture area included the St. Lucie inlet, the north and south forks of the St. Lucie River, and the Indian River south of latitude 27 $^{o}$ 25'0"N. These two areas were collectively termed the IRL geographic location.

All animal capture and sampling procedures involving dolphins were approved by the National Marine Fisheries Service as part of the permitting process, and were approved by the HBOI Institutional Animal Care and Use Committee (IACUC). Capture and release programs followed methods previously described by Scott et al. (1990). Briefly, dolphins were encircled with a large mesh seine net (366 m in length and 6 m strike depth) in water depths of approximately 2 m or less. Once the dolphins were encircled, small boats with experienced animal handlers surrounded the net circumference to restrain and support the animal(s) once they struck the net perimeter. Once the dolphins were restrained, blood samples were collected from the captured dolphins. Then, the animals were placed in a stretcher and transported to a processing boat for a detailed health examination and further sample collection. Heart rate and respirations were monitored at five-minute intervals. Animals were sponged intermittently with sea water and kept under a shaded canopy until released. A comprehensive, standardized protocol included the following: a complete physical and ultrasound examination; morphological measurements including weight, length, and

girths; and collection of blood, urine, and various tissues for hematology, serum chemistry, microbiology, immune function, and biomarker research. Dolphins were evaluated for body and skin condition, external signs of disease, and overall health. Pregnancy status, blubber depth, testes length, and an internal organ exam were determined and evaluated by ultrasound (SonoSite 180plus, Bothell, WA). Age was determined by examination of the post-natal dentine layers from an extracted tooth (Hohn et al., 1989). For dolphins in which a tooth was not extracted (n=2; FB846 and FB923), age was estimated from length measurements using relevant Gompertz growth equations (Fair and Bossart, 2005).

Male dolphins were divided into two life history categories. Males less than 10 years old were classified as reproductively immature sub-adults, while older males (greater than 10 years) were classified as adults. This age cutoff comes from the examination of male testosterone data, which indicate low concentrations until the age of 10, followed by a spike in concentration for older male dolphins (Fair and Bossart, 2005). Female dolphins were divided into five life history categories (reproductively immature sub-adult; adults; pregnant; lactating; and simultaneously pregnant & lactating). Reproductively immature sub-adult females were characterized as females less than 7 years of age (Fair and Bossart, 2005). Adult females were characterized as females greater than 7 years but not pregnant and not lactating. Pregnancy was determined by ultrasound and lactating females were identified by palpation of mammary glands and presence of milk. Adult, pregnant, lactating, and pregnant-lactating females were also divided into two different classes based on whether the female had a calf at the time of capture. For the females with calves, the calf length was recorded and used as a proxy for lactation day.

***Blubber Biopsy Collection***

Biopsies measuring approximately 2 x 3 centimeters (cm) were surgically removed from the left side at a site 5-10 cm caudal to the dorsal fin and 10 cm ventral to the dorsal ridge, which is the standard surgical site for bottlenose dolphin health

assessments (Figure 2A; (Hansen et al., 2004; Wells et al., 2005)). The biopsy site (i.e the caudal insertion of the dorsal fin) was chosen because prior studies with small cetaceans have shown that this blubber is dynamic with regards to lipid deposition and mobilization (Koopman et al., 1996; 2002). The surgical site was cleaned with an antiseptic scrub and lidocaine was injected in an L-block configuration approximately 4 cm anterior to the biopsy region. For each biopsy sample, the veterinarian attempted to collect a representation of the deep blubber. However, in some cases, biopsy samples removed did not encompass the entire deep blubber layer in order to avoid penetration into the muscle and potential risk of infection for the animal. The wound was left un-sutured to enhance healing and avoid foci for infection.

Immediately after collection, the biopsy wedge was trimmed and then subdivided into five full-depth subsections. A 1.5 x 3.0 cm blubber sub-sample with skin removed was stored in a pre-cleaned Teflon container and frozen at -80$^{o}$C until environmental contaminants and lipid content could be measured. The detached skin was split in half and placed in two separate cryovials. One vial was archived at -80$^{o}$C for metal analysis. The other vial, containing 20% dimethyl sulfoxide, was stored at room temperature for genetic analysis. A 0.5 x 1.5 cm skin-blubber slice was fixed in 10% neutral buffered formalin (NBF) for histological analysis and cytochrome P4501A immunohistochemistry (Figure 2B). Three 0.5 x 1.5 cm skin-blubber slices were placed into 3 separate cryovials, flash frozen in liquid nitrogen, and archived at -80$^{o}$C for enzyme and molecular studies, fatty acid measurements, and perfluorinated chemical analyses.

***Lipid Content***

Blubber lipid content data were provided by Greg Mitchum (NOAA). The 1.5 x 3.0 cm frozen sub-sample was used to measure non-volatile and solvent extractable lipid. The sub-samples were cut into thin slices with a hexane-rinsed scalpel blade, mixed with 30 g $Na_2SO_4$ (heated at 700$^{o}$C for 24 h, then cooled in a dessicator before use), and then homogenized with a hexane-cleaned mortar and pestle. The mixture was then placed into a 33-mL pressurized fluid extractor cell (Dionex, Salt Lake City, UT). After extraction,

the total non-volatile and solvent extractable lipid was measured gravimetrically by reducing the volume of solvent with a Turbovap (Zymark, Hopkinton, MA) and then allowing the remaining solvent to evaporate at room temperature overnight. The mass of the remaining material divided by the total wet weight extracted represented the fraction of total non-volatile and solvent extractable lipid.

***Histological Analysis***

Several methods have been used to measure the size of adipocytes, each with advantages and disadvantages. A widely used technique for measuring adipocyte size involves fixing samples in osmium tetroxide and counting the cells electronically (Hirsch and Gallian, 1968). The mean adipocyte size is then estimated by dividing the lipid weight by the number of cells counted. Disadvantages of this technique include cell swelling artifacts associated with osmium and the lack of information on the size distribution of adipocytes in the fat sample. Another method used to estimate adipocyte size involves measuring triglyceride levels and DNA contents, with the estimated adipocyte size expressed as triglyceride levels per DNA content (Chen and Farese, 2002). Similar to the previous technique, this method does not provide details on the size distribution of adipocytes in the fat sample. A third technique involves measuring the size of freshly prepared adipocytes by collagenase digestion (Di Girolamo et al., 1971). This method involves digestion of the adipose tissue sample, separation of adipocytes by centrifugation, staining with methylene blue to identify the nuclei, and microscopic inspection to measure adipocyte diameter. However, the disadvantage of this technique is the lysis of large adipocytes, as observed by Hirsch and Gallian (1968).

Recently, Chen and Farese (2002) report a method for determining adipocyte size by measuring the cross-sectional area of adipocytes with computer image analysis. The adipocyte measurements were completed by fixing tissue samples in paraformaldehyde, embedding the tissue in paraffin, cutting the embedded blocks into 5 μm sections, and staining with hematoxylin and eosin (H&E). This technique produced accurate results, showing an increase in mean adipocyt-size in mice fed a high-fat diet. This method has

been used to investigate molecular markers of adipocyte size (Takahashi et al., 2005), to determine the effect of retinoic acid on white adipose tissue remodeling in mice (Mercader et al., 2006), to understand the development of blubber in bottlenose dolphins (Struntz et al., 2004), and to examine the effect of starvation on blubber morphology in harbor porpoises (Koopman et al., 2002). For the measurements described in this chapter, we used this technique to measure adipocyte size because this method allowed a large number of adipocytes to be measured rapidly and allowed the examination of the size distribution of adipocytes from the epidermis to the deep blubber.

Samples were removed from the 10% NBF solution and routinely processed through an ascending series of alcohol dips (70%, 80%, 95%, and 100%), cleared with xylene, then infiltrated with 100% paraffin. The samples were embedded in paraffin and oriented with either the transverse or tangential body plane parallel to the sectioning face, following previous research studies which showed no significant differences in adipocyte morphometrics between these two body planes (Struntz et al., 2004). The embedded sample was sectioned at 5 um using a rotary microtome (Leitz Model 1512, GMI, Ramsey, MN) and mounted on glass microscope slides. The embedded sample was cut with the blade perpendicular to the depth of the blubber. Orienting the samples in this direction minimized shrinkage artifacts to ±1.5% (compared to ±4% in the longitudinal and transverse planes), as previously described by Struntz et al. (2004). Slides were then rehydrated, stained with hematoxylin- and eosin, dehydrated with CitroSolv (Fisher Scientific, St. Louis, MO), and cover-slipped using Permount (Fisher Scientific, St. Louis, MO).

Previous studies of bottlenose dolphin blubber revealed stratification into three layers: a “superficial” layer (very high density of structural fibers and few adipocytes), a “middle” layer (more and larger adipocytes, and fewer structural fibers), and a “deep” layer (increased structural fiber densities and smaller adipocytes) (Struntz et al., 2004). For all blubber samples, the divisions of these three layers were visible on the H&E slide without magnification and the boundaries between these layers were identified and marked (Figure 2C). The superficial blubber layer extended from the ventral borders of

the dermal papillae to the boundary where the red eosin stain decreased in intensity (due to an increase in size and number of adipocytes). The middle blubber layer extended from the ventral border of the superficial blubber layer to the boundary where the eosin stain increased in intensity (due to a decrease in adipocyte size and an increased density of structural fibers). The deep layer extended from the ventral border of the middle blubber layer to the subdermal sheath that separates the blubber from the underlying muscle. In most cases, the ventral boundary of the deep blubber layer could not be determined.

Slides were viewed with a Zeiss AxioVert S100 microscope and color images were acquired with a Hamamatsu C4742-95 digital camera (Hamamatsu Corporation, Hamamatsu City, Japan). Contiguous images were captured along the entire blubber depth (from the epidermis to the deep blubber layer) (Figure 2C). Each image was captured at 50x magnification. Landmarks in the blubber were used for orientation and to avoid overlap of adjacent images.

Images were analyzed using Scion Image Beta 4.02 software (2000 Scion Corporation, National Institutes of Health, USA). Images were consistently acquired every 2.35 mm. Hence, the number of blubber depth intervals varied between individuals and ranged from 6 (1.4 cm from the dorsal border of the epidermis) to 9 (2.1 cm from the dorsal border of the epidermis). Total blubber thickness at the biopsy site was not measured because some biopsy samples collected did not encompass the entire deep blubber layer.

***Cellular Measurements***

Within each blubber depth interval, a 1 mm x 1mm box was positioned approximately in the center of the 2.35 mm x 1.76 mm image (Figure 2D). To calculate the percent area of blubber composed of extracellular, structural fibers, each image was converted to a standard value grey scale. A threshold function was used to calculate structural fiber areas per $mm^2$, since the fibers appear black. Adipocyte cell counts were estimated by determining the average number of cells that intersected the two diagonals

of a 1 $mm^2$ grid (Figure 2E). Adipocyte cell cross-sectional areas were calculated using an area tool in Scion Image and estimated for that specific blubber depth interval by averaging areas of the cells that intersected the upper left diagonal. These cellular measurements (structural fiber areas, adipocyte cell counts, and mean adipocyte cell size) were calculated for each blubber depth interval (i.e. at midpoint of each interval) and reported as 1.2, 3.5, 5.9, 8.2, 10.6, 12.9, 15.3, 17.6, and 20.0 mm distance from the dorsal surface of the epidermis. For statistical analyses, the cellular measurements for each blubber depth interval were combined based on the categorization of each interval as superficial, middle, or deep layer (as previously discussed) and averaged for a layer specific measurement. The blubber depth interval was not included in the analysis if it overlapped two layers. If a dolphin biopsy sample did not contain a representation of the deep blubber layer, that individual was not included in the data or statistical analyses. All measurements were performed blindly without knowing the animal's identification.

***Statistical Analyses***

Statistical analyses of the data were performed using SYSTAT Version No. 11.00.01 (Systat Software Inc., Richmond, CA). To investigate the effects of location, sex, and age class on blubber lipid content, a three-factor ANOVA was used with a predetermined alpha value of 0.05. This alpha value was used for all statistical analyses. Reproductively active females (lactating or pregnant) were excluded from this statistical analysis to avoid the confounding effects of lactation and pregnancy when comparing males and females.

Since multiple measurements were taken across the blubber of each animal for cellular characteristics (structural fiber areas, adipocyte cell counts, and adipocyte areas), a three-factor ANOVA with layer as a repeated measure was used to investigate the effects of location, sex, and age class on these dependent variables. Reproductively active females were also excluded from the statistical analysis. The layers evaluated included the superficial, middle, and deep blubber layers.

To investigate the effects of reproductive state on blubber lipid content, a single-factor ANOVA was used. Only Charleston females were investigated because subsets of dolphins captured from this geographical location were lactating, pregnant, or simultaneously pregnant and lactating. To investigate the effects of reproductive status on blubber cellular characteristics, a two-factor ANOVA with layer as a repeated measure was used.

Linear and non-linear regression was used to explore the relationship between total blubber lipid content and depth-specific adipocyte area versus age for CHS females. The effects of lactation day on blubber lipid content and cellular characteristics were also explored. For Charleston females that were captured with calves, the calf length was used as a proxy for lactation day. Linear regression analysis was performed with calf length as the independent variable and blubber lipid content and cellular characteristics (for superficial, middle, and deep layers) as the dependent variables. A pre-determined alpha of 0.05 was used to determine if the linear regression was statistically significant.

ANOVA assumptions were examined. The data were transformed to fulfill the assumption of homogeneity of variances for the ANOVAs. If a significant effect was discovered, pair-wise comparisons were conducted using the Tukey-Kramer test. Because age class often had a significant effect on blubber morphology, age was plotted against residuals to verify that all variability due to age was accounted for by division into the two age class categories (sub-adult and adult). Residuals between layers were also examined to verify independence.

## RESULTS

### *Blubber Stratification*

Histological analysis revealed that the blubber of CHS and IRL dolphins was morphologically stratified into three layers, similar to previous studies in stranded bottlenose dolphins (Struntz et al., 2004)(N = 60; males and non-pregnant, non-lactating females; Table 1; Figs. 3-4). These layers are referred to as the “superficial”, “middle”, and “deep” blubber layers, following the terminology published by previous investigators

(Struntz et al., 2004). The density of structural fibers in the superficial, middle, and deep blubber layers were significantly different from each other and were highest in the superficial layer, lower in the middle layer, and intermediate in the deep layer (0.80 ± 0.01, 0.33 ± 0.01, and 0.54 ± 0.01 $mm^2$, respectively; P = 0.0000106). Adipocyte cell counts in the superficial, middle, and deep blubber were significantly different from each other and were lowest in the superficial layer, higher in the middle layer, and intermediate in the deep layer (2.47 ± 0.20, 14.83 ± 0.45, and 9.68 ± 0.47 $mm^2$; P = 0.0000107). Adipocyte size in the superficial blubber layer was significantly smaller than adipocyte size in the middle blubber layer (942 ± 46 compared to 3618 ± 112 $um^2$; P = 0.0000106). Middle blubber layer adipocytes were significantly larger than deep blubber adipocytes (3618 ± 112 compared to 1089 ± 68 $um^2$; P = 0.0000106).

***The Influence of Geographic Location, Age Class, and Sex on Blubber Morphology***

*CHS vs. IRL.* One of the goals of this study was to compare the blubber morphology of dolphins captured and released in CHS and IRL locations, while including age class and sex as factors (CHS N = 30; IRL N = 29; males and non-pregnant, non-lactating females; see Statistical Analyses in Methods). Blubber stratification, lipid content, and cellular measurements (including structural fiber areas, adipocyte cell counts and mean adipocyte per-cell areas) were compared (Table 1; Figs. 3-4). Visual inspection of the blubber revealed more distinct stratification of blubber in CHS versus IRL dolphins (Fig. 3). Average and depth-specific structural fiber areas and adipocyte cell counts of the superficial, middle, and deep layers were not significantly different between CHS and IRL dolphins (Table 1; P = 0.41). However, average adipocyte cell size of the entire blubber was significantly greater in CHS (Table 1). The higher total blubber lipid content in CHS dolphins was consistent with these results (Table 1). Furthermore, the difference in adipocyte size between CHS and IRL dolphins was in the middle blubber and not the superficial or deep layers (Table 1). These findings indicate that the higher total blubber lipid content in CHS dolphins was a result of more lipids per cell rather than more adipocytes. In addition, the average adipocyte cell size of the entire

blubber was significantly greater in CHS subadults compared to IRL subadults (Table 1; Fig. 4). This difference was not seen in adults. The adipocyte size difference between CHS and IRL subadults was attributed to the middle blubber and not the superficial or deep layers (Table 1; Figs. 4E-4F).

*Subadults vs. Adults.* Another goal of this study was to compare the blubber morphology of reproductively immature subadult and adult dolphins, while including geographic location and sex as factors (Table 1; subadults N = 12; adults N = 47; males and non-lactating, non-pregnant females; see Statistical Analyses in Methods). Subadults had significantly lower average structural fiber areas of the entire blubber layer compared to adults but no differences in depth-specific fiber areas. Furthermore, subadults had more adipocytes on average than adults; the number of adipocytes was higher in the middle blubber but not the superficial or deep layers. In addition, reproductively immature sub-adults had significantly higher total blubber lipid content than adults.

Distinct differences in blubber morphology existed between reproductively immature subadult and adult dolphins from the two locations (Table 1; Fig. 4). CHS subadults had significantly higher numbers of adipocytes of the entire blubber than CHS adults. This difference was associated with more adipocytes in the middle blubber but not the superficial or deep layers. In addition, CHS subadults had significantly higher total blubber lipid content than CHS adults. However, dolphins from IRL did not exhibit this pattern, and adipocyte cell counts in IRL subadults were approximately equal to those of IRL adults. Furthermore, IRL subadults had significantly smaller adipocytes in the middle layer of the blubber than IRL adults but no differences in the superficial and deep layers.

*Sex.* The blubber morphology of males versus females (non-pregnant, non-lactating) was also compared. Males and females did not significantly differ in structural fiber areas, adipocyte cell counts, adipocyte cell size, and blubber lipid content (data not shown).

***The Influence of Female Reproductive State on Blubber Morphology***

Pregnancy and lactation are conditions that may affect the dynamics of blubber lipids in bottlenose dolphins. Deposition of lipids (i.e. higher lipid content and swelling of adipocytes) may be associated with the onset of pregnancy, while mobilization of lipids (i.e. lower lipid content and shrinkage of adipocytes) may be associated with lactation. The samples from CHS were sufficient to test the hypothesis that reproductive state affects blubber morphology in bottlenose dolphins. The females captured at CHS included reproductively immature subadults (N = 3), adults captured with calves (N =2), pregnant (N = 2), lactating (N = 3), and simultaneously pregnant & lactating (N = 2) dolphins. The IRL females did not contain any lactating females and were not used to test this hypothesis.

Total blubber lipid content and cellular measurements (including structural fiber areas, adipocyte cell counts and adipocyte size) were compared among the CHS females of varying reproductive states (Table 2; Figs. 5-7). Mean adipocyte size (i.e. cross-sectional area) of the entire blubber was significantly different between females of various life history categories (Table 2). Mean adipocyte areas in simultaneously pregnant & lactating dolphins were significantly smaller than in pregnant or subadult dolphins. Furthermore, deep blubber adipocytes were significantly smaller in lactating and simultaneously pregnant & lactating animals compared to pregnant dolphins (Table 2; Figs. 5E-F). Although blubber lipid content did not significantly differ between the female life history categories, it followed similar patterns as adipocyte cell counts and areas (Table 2). Subadult females had the highest blubber lipid content and the most numerous and largest adipocytes in the middle blubber. Simultaneously pregnant & lactating females had the lowest blubber lipid content and smallest adipocytes.

The stratification pattern of structural fiber areas, adipocyte cell counts, and adipocyte cell size showed different patterns for females of varying reproductive states (Table 2; Fig.5). First, in pregnant females, adipocyte size did not differ between the middle and deep blubber layers. The boundary between the middle and deep layer was

not distinct, which gave the blubber a bi-layer rather than a tri-layer appearance. Second, all females that were captured with calves (including the adults) had adipocyte cell count and area depth profiles that differed from those of reproductively immature subadult and pregnant females (Figs. 5C & 5E).

Lipid content of the entire blubber and depth-specific adipocyte areas were plotted versus age with the integration of important life history characteristics of individual females (Fig. 6). Lipid content displayed a non-linear reduction with age (Fig. 6A; $Y = \beta_o x^{\beta 1}$; $\beta_o = 88.2$; $\beta_1 = -0.31$; $R^2 = 0.74$). Deep blubber adipocyte areas linearly decreased with age, while no significant relationships existed for the superficial or middle layers (Figs. 6B-D; $\beta_S = -15.54$, $R^2 = 0.08$, $P = 0.35$; $\beta_M = -33.99$, $R^2 = 0.22$, $P = 0.12$; $\beta_D = -64.47$, $R^2 = 0.52$, $P = 0.008$). FB819 was pregnant at the time of capture, presumably with her first calf. The total blubber lipid content in this dolphin was equivalent to that of sub-adult females, and the deep blubber mean adipocyte area exceeded those of all female dolphins. FB801, at the time of capture, was pregnant with at least her second calf. The total blubber lipid content in this dolphin was the lowest of all CHS females.

Seven females were captured with calves (Fig. 6). The females consisted of two non-lactating, three lactating, and two simultaneously pregnant & lactating females. We hypothesized that females with larger calves would have a greater energetic demand and would increase the mobilization of blubber lipids. This hypothesis predicts that females with larger calves would have lower total blubber lipid content and smaller adipocytes. For CHS females captured with calves, blubber lipid content linearly decreased with calf length (Fig. 7A; $\beta_1 = -0.11$, $R^2 = 0.66$, $P = 0.027$). Superficial and middle adipocyte areas of the mother did not exhibit a significant relationship with calf length, while mean adipocyte areas in the deep blubber significantly decreased with increasing calf length (Fig. 7B; $\beta_S = 3.62$, $R^2 = 0.02$, $P = 0.75$; $\beta_M = -19.22$, $R^2 = 0.29$, $P = 0.21$; $\beta_D = -16.98$; $R^2 = 0.73$; $P = 0.014$).

## DISCUSSION

The goal of this study was to quantitatively measure blubber morphology (total blubber lipid content and cellular characteristics) of wild bottlenose dolphins captured and released at two different coastal locations in the Southeast United States, and to investigate factors that contribute to blubber morphology variability. We hypothesized that: (1) the blubber would be morphologically stratified into three layers, as observed in stranded bottlenose dolphins; (2) CHS dolphins would have different blubber morphology than IRL dolphins, exhibiting characteristics that would provide better insulation (more and/or larger adipocytes), since CHS water temperatures are lower than IRL in the winter and spring months; (3) subadults would have different blubber morphology than adults; and (4) reproductive state would affect blubber morphology in females.

### *Blubber Stratification*

Histological analysis revealed that the blubber was morphologically stratified into three layers, as observed in stranded bottlenose dolphins (Struntz et al., 2004) (Fig. 3). In all bottlenose dolphins, the superficial blubber layer was characterized by few and small adipocytes and high density of structural fibers (Table 1-2; Figs. 3-4, 7). The middle blubber layer contained more and larger adipocytes and fewer structural fibers. In the deep blubber layer, adipocytes increased in number but decreased in size.

These data support the hypothesis that the "outer blubber" or superficial layer is inert, while the "inner blubber" or middle and deep layers are dynamic in cetaceans. The high density of structural fibers in the superficial blubber anchors the dermal papillae, giving structural support to the skin. The large adipocytes in the middle blubber are storage depots for lipids. The smaller adipocytes in the deeper blubber indicate more lipid loss in this layer compared to the middle blubber layer. This hypothesis is supported by the observations of Koopman et al. (2002), who examined the loss of blubber in starved harbor porpoises. From the insertion of the pectoral fin to the anus,

blubber loss was substantial in starved harbor porpoises. Caudal to the anus, blubber loss was almost negligible. In these porpoises, examination of adipocyte size across different blubber sites on the body revealed that thorax adipocytes closer to the body core (i.e. the deeper blubber) shrank and disappeared during starvation. In contrast, starvation had little or no effect on adipocyte size in tailstock blubber.

The layering hypothesis is further supported by fatty acid analysis of juvenile starved harbor porpoises (Koopman et al., 2001). In these porpoises, the fatty acid composition of the inner blubber of the thorax underwent significant changes, but not the outer thorax or the tailstock blubber. In addition and contrast to the metabolically active lipids in the deep blubber of the thorax, diet has no effect on the composition of odontocete acoustic lipids in the melon (as reviewed by Koopman et al. (2006)). In bottlenose dolphins, it is most likely the case that the metabolically dynamic blubber extends from the insertion of the pectoral fin to the anus, following the stratification patterns described herein (i.e. at the caudal insertion of the dorsal fin blubber site).

***Differences in Blubber Morphology between CHS and IRL Dolphins***

CHS and IRL dolphins (males and non-pregnant, non-lactating females) exhibited differences in blubber morphology (i.e. adipocyte cross-sectional area and total blubber lipid content) (Table 1; Figs. 3-4). Mean adipocyte cross-sectional areas of the superficial, middle, and deep layers in CHS dolphins were 24% larger than those in IRL animals. The geographic location differences in adipocyte area were in the middle blubber layer of the reproductively immature subadults (Table 1; Figs. 4E-F). Adipocyte areas in the middle blubber of subadult CHS dolphins were 62% larger than subadult IRL animals. The total blubber lipid content for CHS dolphins was 12% greater than IRL dolphins (Table 1; Figure 3A). The depth-specific pattern of adipocyte cross-sectional area (small adipocytes in the superficial blubber layer, larger adipocytes in the middle layer, and smaller adipocytes in the deep layer) was more dramatic in CHS dolphins compared to IRL animals. This contributed to the blubber appearing less stratified in IRL dolphins compared to CHS dolphins (Fig. 3).

There are at least four possible explanations for the higher total blubber lipid content and larger adipocyte size in CHS dolphins compared to IRL animals: (1) CHS water temperature was significantly lower than IRL water temperature in the months leading to the live captures; (2) the food supply in CHS was more abundant and/or of higher quality compared to the food supply in IRL; (3) CHS dolphins were more efficient in foraging than IRL dolphins; and/or (4) the IRL dolphins were subjected to greater energetic demands than the CHS dolphins.

It is possible that CHS dolphins contained higher total blubber lipid content and larger adipocytes than IRL dolphins because of differences in mean yearly water temperature between the two geographic locations. A primary function of blubber is to provide insulation from a water medium that conducts heat away from the core at a rate 25 times faster than air at the same temperature (Dunkin et al., 2005; Parry, 1949; Scholander et al., 1950). Between January and August 2003, the water was consistently colder in Charleston Harbor, SC compared to St. Lucie, FL based on data obtained from the Center for Operational Oceanographic Products and Services (CO-OPS), National Oceanic Atmospheric Administration and the South Florida Water Management District (Fig. 8). At the start of captures, the Charleston Harbor water temperature was 27.3$^{o}$C, while IRL, St. Lucie was approximately 30.3$^{o}$C. The lower lipid content and smaller adipocytes in IRL dolphins would increase the thermal conductivity k (W m$^{-1}$ deg.$^{-1}$) (a quantitative measure of how well heat moves through a material) of bottlenose dolphin blubber, as described by Dunkin et al. (2005). This would allow more heat to dissipate from the body core in IRL dolphins. In fact, it has been shown that bottlenose dolphins in Sarasota, Florida drastically thin their blubber during summer months, when estuarine water temperature can reach 32$^{o}$C (~ 90$^{o}$F) (R. Wells, unpublished data). Perhaps, both CHS and IRL dolphin blubber had acclimated to the higher seasonal water temperature, but IRL thinning was more dramatic because of the warmer water in IRL compared to CHS in the months prior to the time of capture (i.e. April through July) (Fig. 8).

It has been shown that the blubber of cetaceans distributed in more northern latitudes has lower thermal conductivities compared to that of cetaceans inhabiting more

southern latitudes (Worthy and Edwards, 1990). For example, harbor porpoise blubber has a thermal conductivity of 0.1, while pan-tropical spotted dolphin *Stenella attenuata* blubber has a thermal conductivity of 0.2 (Worthy and Edwards, 1990). In bottlenose dolphins, we hypothesized that animals occupying more northern latitudes (i.e. colder water) would have larger adipocytes and higher lipid content (i.e. lower thermal conductivities). This hypothesis was supported by our data and was strengthened by lipid and adipocyte measurments of mid-thoracic blubber of male subadult bottlenose dolphins that had either stranded or been incidentally killed in fishing operations in North Carolina and Virginia (Struntz et al, 2004). In these dolphins, mean blubber lipid content was 57%, with a mean adipocyte cross-sectional area of 4416 $um^2$ (Struntz et al., 2004). In our study, CHS and IRL subadult males had an average blubber lipid content of 47% (mean adipocyte area of 2356 $um^2$) and 38% (mean adipocyte area of 1817 $um^2$), respectively. This provides some circumstantial evidence that bottlenose dolphins inhabiting more northern latitudes (i.e. colder waters) have higher blubber lipid contents. However, a more rigorous test of this hypothesis would involve a longitudinal study and collection of blubber biopsies from the same individual and body region during the summer and winter at a geographic location that experiences drastic seasonal differences in water temperature.

The other three options are all reasonable explanations for higher blubber lipid content and larger mean adipocyte size in CHS dolphins compared to IRL animals. These possibilities focus on the impacts of nutritional stress on blubber lipid content and subsequent effects on adipocyte areas. Previous research has shown that starvation decreases thickness and adipocyte volume of thorax blubber in harbor porpoises, and that these effects are most dramatic in the "inner" blubber (Koopman et al., 2002). Struntz et al. (2002) have shown in a limited sample set (n = 2) that emaciated bottlenose dolphins displayed a dramatic decrease in blubber thickness, lipid content, and adipocyte size across the entire depth of the blubber, with the most marked reduction in the deep adipocytes. Thus, it is possible that IRL dolphins have lower blubber lipid content and smaller adipocyte size because these dolphins have less energy intake and/or experience

additional energy expenditures that CHS dolphins do not. However, because evidence indicates that nutritional stress affects adipocyte size predominantly in the more metabolically dynamic deep blubber, and the CHS and IRL dolphins exhibited differences in adipocyte size of the middle blubber layer only, we favor the water temperature hypothesis over the other possible explanations (Table 1; Figs. 4E-F).

Presently, there is concern for the overall health of the IRL ecosystem due to population growth, destruction of sea grass habitat, alteration of water flow, and declining water quality. Human population growth adjacent to the Indian River Lagoon increased from 1970-1990 by 124% and is projected to reach 1.1 million by 2010 (IRLNEP, 1996). Whether the decline of the IRL ecosystem has caused the quantity and/or quality of the food supply for the bottlenose dolphin to decrease is unknown, and at the present time, it is not known whether the food supply is more abundant and/or of higher quality in CHS compared to IRL. This should be a priority for future health assessment studies.

***Sex and Age Class Differences***

Overall, male and non-pregnant, non-lactating females did not differ in blubber morphology despite the larger asymptotic lengths in males (CHS = 267.4 cm; IRL = 276.3 cm) compared to females (CHS = 247.0 cm; IRL = 251.0 cm) (Fair and Bossart, 2005). However, reproductively immature subadults and adults (males and non-pregnant, non-lactating females) did exhibit differences in blubber measurements. Subadults displayed significantly higher total blubber lipid content, lower structural fiber areas, and higher adipocyte numbers than adults (Table 1; Fig. 4). The results of the present study differ from those of Struntz et al. (2004). In that study, lipid content was the lowest in fetal blubber and dramatically increased from neonate to juvenile life history stages, decreased in subadults, and increased in adults. Mean adipocyte cross-sectional areas increased from fetus to adult, while structural fiber areas were the highest in fetal blubber and equivalent in all other life history categories. Mean cell numbers were not significantly different among life history categories.

Struntz et al. (2004) did not separate sexes and grouped pregnant females in the adult age class (5 of the 6 adults were pregnant females). However, in the current study, sex was included as a factor in the statistical model and pregnant or lactating females were not included in the adult female age class category. In Struntz et al. (2004), including pregnant females in the adult life history category may have increased the blubber lipid content and adipocyte areas of adults, since it has been shown that pregnant cetaceans have the highest blubber mass, thickness, and lipid content of all life history categories (Lockyer, 1993). By separating pregnancy as a factor in adults, we show that reproductively immature subadults have higher total blubber lipid content, lower structural fiber areas, and higher adipocyte numbers than non-pregnant adults. These results are consistent with those of Dunkin et al. (2005), who found that blubber lipid content of stranded specimens decreased steadily from juvenile to adult stages, and that pregnant females were equivalent to juveniles in lipid content.

It has been hypothesized that adults display significantly lower total blubber lipid content, smaller adipocyte areas, higher structural fiber areas, and lower adipocyte numbers compared to subadults because as the dolphin's surface-area-to-volume ratio decreases with growth, there is less demand for insulation but greater demand for energy to support growth (Dunkin et al., 2005; McLellan et al., 2002; Struntz et al., 2004). These changes in blubber structure would increase the amount of heat loss from the body. In fact, Dunkin et al. (2005) showed that the thermal conductivity was higher for adults compared to subadults. In addition, both male and female adults expend energy for reproduction, and this decreases the lipid content and subsequent adipocyte size of blubber.

The effect of age class on blubber morphology displayed different patterns in CHS and IRL dolphins. Unlike IRL dolphins, CHS subadults contained more adipocytes than adults, and this difference occurred in the middle blubber layer (Table 1; Figs. 4C-D). IRL subadults had significantly lower middle blubber adipocyte areas than IRL adults, while CHS dolphins showed an opposite pattern (Table 1; Figs. 4E-F). One possible explanation is that reproductively immature subadults require more insulation

(Dunkin et al., 2005; McLellan et al., 2002; Struntz et al., 2004). CHS subadults may require higher blubber lipid content and larger adipocytes in the middle blubber because of lower water temperatures. By contrast, IRL subadults inhabiting warmer environments may not require this added insulation, which would explain why there is no difference in adipocyte areas and numbers between IRL subadults and adults.

***Influence of Reproductive State on Female Blubber Morphology***

Reproductive state affected the blubber morphology of CHS females. The mean adipocyte areas in all blubber layers were greater in subadults and pregnant females compared to simultaneously pregnant and lactating dolphins (Table 2; Fig. 5). Subadults and pregnant females also showed a trend toward higher total blubber lipid content compared to pregnant-lactating dolphins, although these results were not statistically significant. This suggests that the combination of pregnancy and lactation increased the energetic demands beyond what was supported solely by their diet. The larger mean adipocyte size and lipid content in subadults can be best explained by the necessity for greater insulation, and the lack of energetic costs involved in reproduction (see previous section). The larger mean adipocyte size and higher lipid content in pregnant females may be best explained as preparation for the high energetic costs involved in lactation.

Examination of adipocyte size across different blubber layers provided evidence that lactation (whether pregnant or not) affected adipocyte size predominantly in the deeper blubber (Table 2; Figs. 5E-F). Adipocyte areas in the superficial blubber layer of the five female life history categories were similar. In the middle blubber layer, adipocytes were the largest in subadults, followed by pregnant, lactating, adult, and then simultaneously pregnant & lactating females. In the deep blubber layer, adipocytes in pregnant females were significantly larger than those in lactating and simultaneously pregnant & lactating dolphins. Furthermore, all females that were captured with calves (including the adults) had a similar adipocyte area depth profile with predominant lipid loss in deep blubber adipocytes, quite different from the reproductively immature subadult and pregnant females. These results further support the hypothesis that the

deeper blubber is preferentially used as energy currency during costly events such as lactation.

When blubber lipid content and depth-specific adipoctye size were plotted against age, interesting aspects of female blubber morphology were found relative to specific life history characteristics (Fig. 6). For example, FB819 was presumably pregnant for the first time. Her total blubber lipid content and adipocyte size in the superficial and middle blubber layers were approximately equal to those of subadults. However, deep blubber adipocyte size for FB819 was approximately 1500 $\mu m^2$ larger than that of subadults, illustrating the depth-specific effects of pregnancy on adipocyte size. FB801 was pregnant with at least her second calf, and her total blubber lipid content was approximately 30% lower than that of FB819. Superficial and deep adipocytes in FB801 were approximately 1000 $um^2$ less than those of FB819, while the middle blubber adipocyte size was approximately equivalent in both dolphins. It is possible that successive pregnancies and subsequent offspring care impede the replenishment of blubber lipids.

The two non-reproductively active adult females were captured with calves but were not lactating. It is presumed that the calves recently weaned. It is possible that these two adults, at the time of their capture, had not yet replenished the blubber lipids lost during lactation. The total blubber lipid content of females captured with calves was less than that of all subadults and FB819 but not FB801 (Fig. 6). However, the deep blubber adipocyte size of mothers captured with calves was smaller than that of both pregnant females (FB819 and FB801). This illustrates how the energetic demands of lactation may lead to the preferential utilization of lipids in the deep layer, while in pregnancy lipids are deposited in the deep blubber. Additionally, total blubber lipid content and adipocyte size in the deep blubber linearly decreased with calf length (Figs. 7A-B). Because the energetic demands of lactation and offspring care are greater for a larger calf compared to a smaller calf, it is likely that more blubber lipids are utilized to support a larger calf. These findings highlight the importance of longitudinal studies and tracking changes in female blubber morphology from subadult to adult stages and during

major reproductive events (i.e. first pregnancy, weaning of first calf, second pregnancy, weaning of second calf, etc.).

## CONCLUSION

In summary, factors such as ontogeny, water temperature, reproductive status, and nutritional state affect blubber morphology in bottlenose dolphins (Figure 9). However, the data presented here and elsewhere suggest that the blubber responds differently to these factors. The ontogenetic decrease in blubber lipid from subadult to adult occurs via a decrease in the number of adipocytes in the middle blubber layer. In response to warmer water, the lipid content of the blubber also decreases, but the mechanism appears to involve lipid loss of adipocytes (i.e. cells shrink) in the middle layer. Similar to the effects of starvation on blubber morphology, lactation decreases adipocyte size predominantly in the deeper blubber. Future research should focus on the hormonal and molecular control of blubber dynamics. These dynamic processes are not only important in understanding the structure, function, and physiology of blubber, but are also extremely valuable in understanding the nutritional state of the animal and the mobilization of persistent chemicals into the bloodstream and their affects on the health of wild, bottlenose dolphins.

## REFERENCES

Ackman RG, Eaton CA, Jangaard PM. 1965. Lipids of the fin whale (*Balaenoptera physalus*)from North Atlantic waters. Canadian Journal of Biochemistry 43: 1513-1520.

Ackman RG, Hingley JH, Eaton CA, Sipos JC, Mitchell ED. 1975a. Blubber fat deposition in Mysticeti whales. Canadian Journal of Zoology 53: 1332-1339.

Aguilar A, Borrel A. 1991. Heterogeneous distribution of organochlorine contaminants in the blubber of baleen whales: implications for sampling procedures. Marine Environmental Research 31:275-286.

Aguilar A, Borrell A. 1990. Patterns of lipid content and stratification in the blubber of fin whales (*Balaenoptera physalus*). Journal of Mammalogy 71:544-554.

Bandiera SM, Torok SM, Letcher RJ, Norstrom RJ. 1997. Immunoquatitation of cytochromes P4501A and P4502B and comparison with chlorinated hydorcarbon levels in archived polar bear samples. Chemosphere 34: 1469-79.

Chen HC, Farese RV. 2002. Determination of adipocyte size by computer image analysis. Journal of Lipid Research 43: 986-989.

Dearolf JL, McLellan WA, Dillaman RM, Frierson D, Jr., Pabst DA. 2000. Precocial development of axial locomotor muscle in bottlenose dolphins (*Tursiops truncatus*). Journal of Morphology 244:203-215.

Di Girolamo M, Mendlinger S, Fertig JW. 1971. A simple method to determine fat cell size and number in four mammalian species. American Journal of Physiology 221: 850-858.

Dunkin RC, McLellan WA, Blum JE, Pabst D. 2005. The ontogenetic changes in the thermal properties of blubber from Atlantic bottlenose dolphin *Tursiops truncatus*. The Journal of Experimental Biology 208:1469-1480.

Fair PA, Bossart GD. 2005. Synopsis of Researcher Meeting - Bottlenose Dolphin Health and Risk Assessment Project February 22-24, 2005. NOAA Technical Memorandum. Report nr NOS NCCOS 10. 93 p.

Hamilton JL, McLellan WA, Pabst DA. 2004. Functional morphology of tailstock blubber of the harbor porpoise (*Phocoena phocoena*). Journal of Morphology 261:105-117.

Hansen LJ, Schwacke LH, Mitchum GB, Hohn AA, Wells RS, Zolman ES, Fair PA. 2004. Geographic variation in polychorinated biphenyl and organochlorine pesticide concentrations in the blubber of bottlenose dolphins from the US Atlantic coast. The Science of the Total Environment 319:147-172.

Hirsch J, Gallian E. 1968. Methods for the determination of adipose cell size in man and animals. Journal of Lipid Research 9: 110-119.

Hohn AA, Scott MD, Wells RS, Sweeney JC, Irvine AB. 1989. Growth layers in teeth from known-age, free-ranging bottlenose dolphins. Marine Mammal Science 5(4):315-342.

IRLNEP IRLNEP. 1996. The Indian River Lagoon: our heritage at risk. Melbourne, Florida: St. Johns and South Florida Water Management Districts in cooperation with the U.S. Environmental Protection Agency.

Kipps EK, McLellan WA, Rommel SA, Pabst DA. 2002. Skin density and its influence on buoyancy in the manatee (*Trichechus manatus latirostris*), harbor porpoise (*Phocoena phocoena*), and bottlenose dolphin (*Tursiops truncatus*). Marine Mammal Science 18:765-778.

Koopman HN, Iverson S, Gaskin D. 1996. Stratification and age-related differences in blubber fatty acids of the male harbour porpoise (*Phocoena phocoena*). Journal of Comparative Physiology, B 135:628-639.

Koopman HN, Pabst DA, McLellan WA, Dillaman RM, Read AJ. 2002. Changes in blubber distribution and morphology associated with starvation in the harbour porpoise (*Phocoena phocoena*): evidence for regional differences in blubber structure and function. Physiological and Biological Zoology 75(5):498-512.

Koopman HN, Budge SM, Ketten DR, Iverson SJ. 2006. Topographical distribution of lipids inside the mandibular fat bodies of odontocetes: remarkable complexity and consistency. IEEE Journal of Oceanic Engineering 31(1): 95-106.

Lockyer CH, McConnell LC, Waters TD. 1984. The biochemical composition of fin whale blubber. Canadian Journal of Zoology 62; 2553-2562.

Lockyer CH. 1993. Seasonal changes in body fat condition of Northeast Atlantic pilot whales and their biological significance. Report of the International Whaling Commission 14:325-349.

Marsili L, Casini C, Marini L, Regoli A, Focardi S. 1997. Age, growth and organochlorines (HCB, DDTs and PCBs) in Mediterranean striped dolphins *Stenella coeruleoalba* stranded in 1988-1994 on the coasts of Italy. Marine Ecology Progress Series 151:1-3.

McKinney MA, Arukwe A, DeGuise S, Martineau D, Beland P, Dallaire A, Lair S, LeBeuf M, Letcher RJ. 2004. Characterization and profiling of hepatic cytochromes P450 and phase II xenobiotic-metabolizing enzymes in beluga whales (*Delphinapterus leucas*) from the St. Lawrence estuary and the Canadian Arctic. Aquatic Toxicology 69(1): 35-49.

McLellan WA, Koopman HN, Rommel SA, Read AJ, Potter CW, Nicolas JR, Westgate AJ, Pabst DA. 2002. Ontogenetic allometry and body composition of harbour porpoises (*Phocoena phocoena*) from the western North Atlantic. Journal of Zoology 257:457-471.

Mercader J, Ribot J, Murano I, Felipe F, Cinti S, Bonet ML, Palou A. 2006. Remodeling of white adipose tissue after retinoic acid administration in mice. Endocrinology.

Norstrom RJ, Muir DCG. 1994. Chlorinated hydrocarbon contaminants in Arctic marine mammals. The Science of the Total Environment 154:107-128.

Pabst DA. 2000. To bend a dolphin: Convergence of force transmission designs in cetaceans and scombrid fishes. American Zoologist 40:146-155.

Parry DA. 1949. The structure of whale blubber, and a discussion of its thermal properties. Quart Jour Microscop Sci 90(1):13-25, 11 pl.

Ridgway S, Reddy M. 1995. Residue levels of several organochlorines in *Tursiops truncatus* milk collected at varied stages of lactation. Marine Pollution Bulletin 30(9):609-614.

Schantz MM, Koster BJ, Wise SA, Becker PR. 1993. Determination of PCBs and Chlorinated Hydrocarbons in marine mammal tissues. Science of the Total Environment 140:323-345.

Scholander PF, Walters V, Hock R, Irving L. 1950. Body insulation of some arctic and tropical mammals and birds. Biological Bulletin 99:259-269.

Struntz DJ, McLellan WA, Dillaman R, Blum J, Kucklick J, Pabst D. 2004. Blubber development in bottlenose dolphins (*Tursiops truncatus*). Journal of Morphology 259:7-20.

Takahashi M, Kamei Y, Ezaki O. 2005. Mest/Peg1 imprinted gene enlarges adipocytes and is a marker of adipocyte size. American Journal of Physiology - Endocrinology and Metabolism 288: 117-124.

Tirpenou AE, Tsigouri AD, Gouta EH. 1998. Residues of organohalogen compounds in various dolphin tissues. Bulletin of Environmental Contamination and Toxicology 60(2):216-224.

Wells RS, Tornero V, Borrell A, Aguilar A, Rowles TK, Rhinehart HL, Hofmann S, Jarman WM, Hohn AA, Sweeney JC. 2005. Integrating life-history and reproductive success data to examine potential relationships with organochlorine compounds for bottlenose dolphins (*Tursiops truncatus*) in Sarasota Bay, Florida. Science of the Total Environment 349(1-3):106.

White RD, Hahn ME, Lockhart WL, Stegeman JJ. 1994. Catalytic and immunochemical characterization of hepatic microsomal cytochromes P450 in beluga whale (*Delphinapterus leucas*). Toxicology and Applied Pharmacology 126(1):45-57.

Wilson JY. 2003. Cytochrome P4501A1 and aromatase (CYP19) in cetaceans: enzyme expression and relationship to contaminant exposure. Woods Hole, MA:

Massachusetts Institute of Technology / Woods Hole Oceanographic Institution. 260 p.

Wilson JY, Cooke SR, Moore MJ, Martineau D, Mikaelian I, Metner DA, Lockhart WL, Stegeman JJ. 2005. Systemic effects of Arctic pollutants in beluga whales indicated by CYP1A1 expression. Environmental Health Perspectives 113:1594-1599.

Wolkers H, Lydersen C, Kovacs KM. 2004. Accumulation and lactational transfer of PCBs and pesticides in harbor seals (*Phoca vitulina*) from Svalbard, Norway. Science of the Total Environment 319(1-3):137.

Worthy G, Edwards E. 1990. Morphometric and biochemical factors affecting heat loss in a small temperate cetacean (*Phocoena phocoena*) and a small tropical cetacean (*Stenella attenuata*). Physiol Zool 60:432-442.

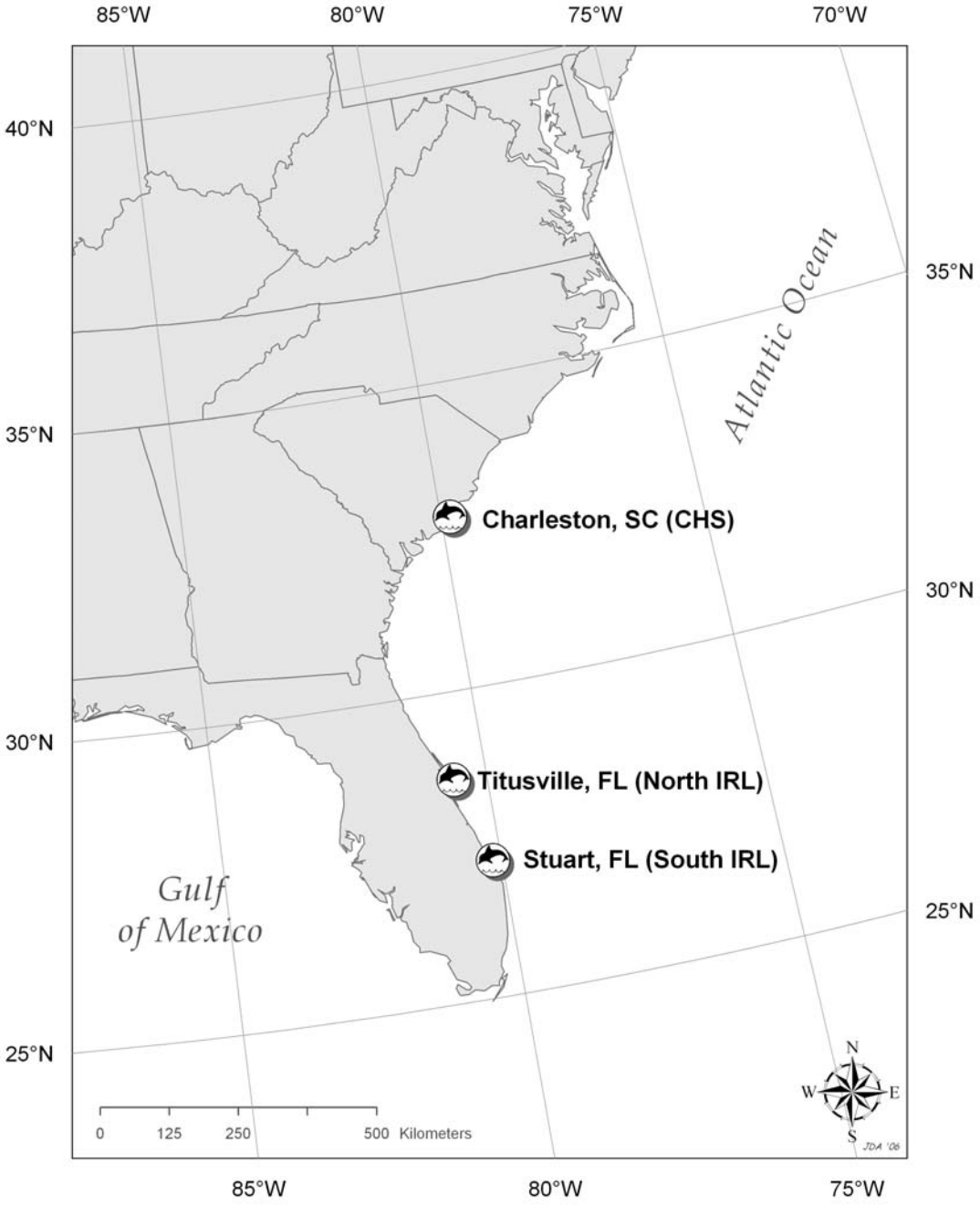


**Figure 1. Map showing the sampling locations of bottlenose dolphins along the Southeast United States Atlantic Coast.**

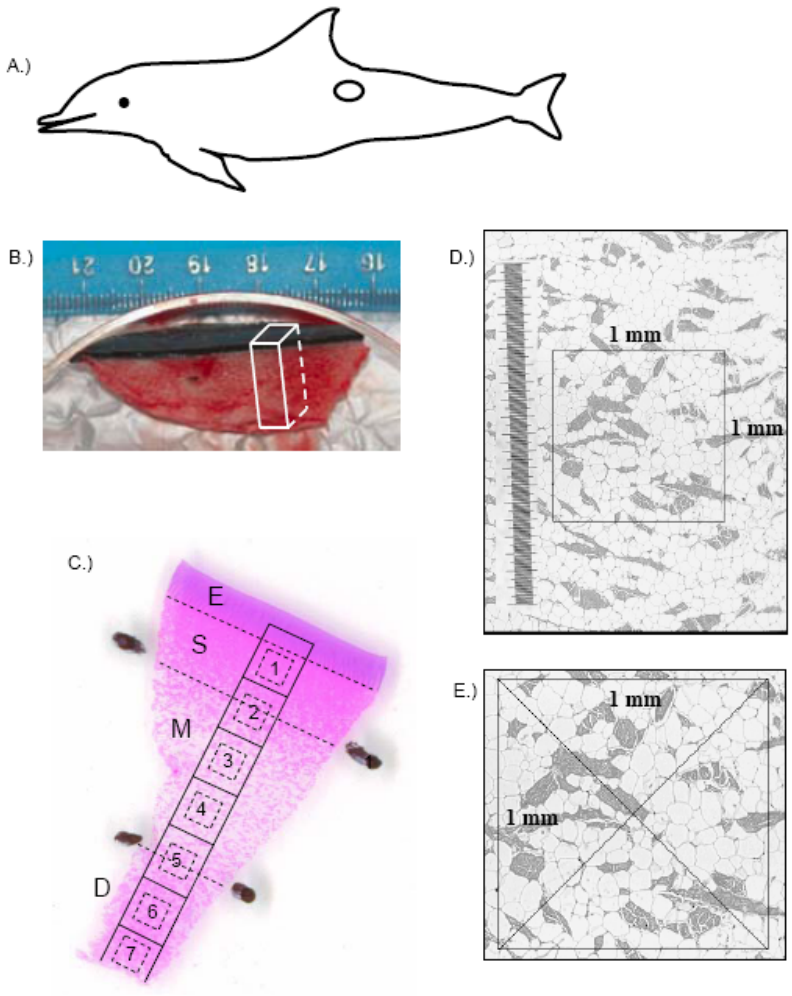


**Figure 2. Skin-blubber biopsy sampling site and histological subsampling for analysis of blubber cellular characteristics in bottlenose dolphins.** A.) Sampling site on body. B.) Representative photo of skin-blubber biopsy. The white rectangle represents the subsampling site used for histology. C.) Representative image of a hematoxylin and eosin (H&E) slide. Dotted lines across the H&E slide represent boundaries of the superficial (S), middle (M), and deep (D) blubber layers. Solid rectangles represent the contiguous images captured throughout the blubber depth. Dotted squares represent the 1mm x 1mm box used for quantitative histological analysis. D.) Representative image of the 2.35 mm x 1.76 mm contiguous image with 1 mm x 1mm box positioned approximately in the center. Scale bar = 2 mm. E.) Zoom of 1mm x 1mm box with diagonals. A threshold function was used to calculate structural fiber areas per $mm^2$, since the fibers appear black. Adipocyte cell counts were estimated by determining the average number of cells that intersected the two diagonals of the 1 $mm^2$ grid. Adipocyte cell cross-sectional areas were estimated by averaging areas of the cells that intersected the upper left diagonal.

**Figure 3. Light micrograph images of the blubber from bottlenose dolphins. Black scale bars represent 2 mm.** Solid arrows indicate adipocytes, while dotted arrows indicate structural fibers. In all images, the top is closest to the surface of the epidermis. E = epidermis; S = superficial blubber layer; M = middle blubber layer; D = deep blubber layer. A.) Contiguous images from the epidermis to the deep blubber of an adult CHS male (age 12). B.) Contiguous images from the epidermis to the deep blubber of an adult IRL male (age 12.5). C.) Representative image of the middle blubber layer, approximately 6.9 mm from the dorsal border of the epidermis, of the adult CHS male. D) Representative image of the middle blubber layer, approximately 6.9 mm from the dorsal border of the epidermis, of the adult IRL male.

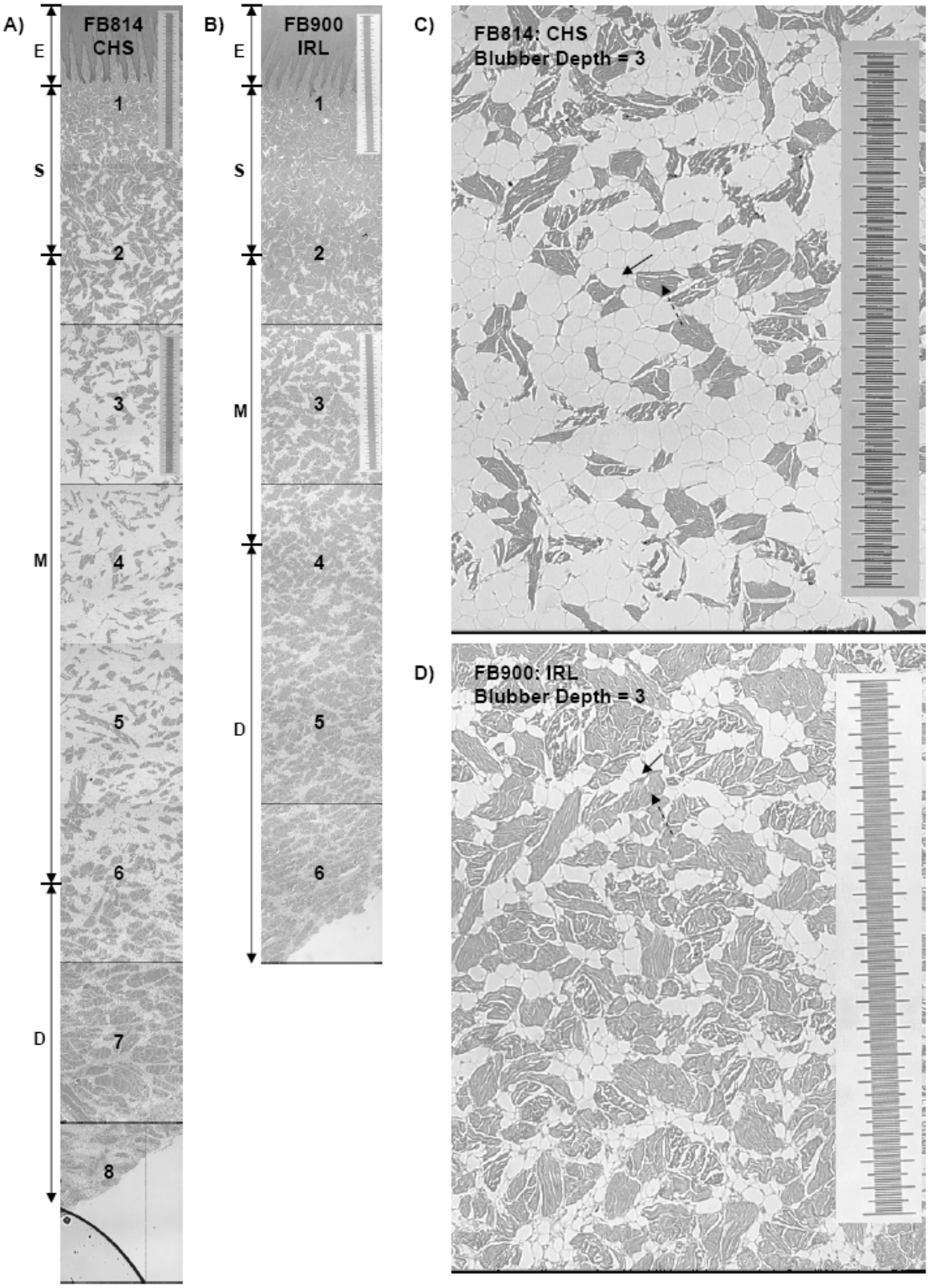
A)
FB814
CHS
E
S
M
D
1
2
3
4
5
6
7
8
B)
FB900
IRL
E
S
M
D
1
2
3
4
5
6
C)
FB814: CHS
Blubber Depth = 3
D)
FB900: IRL
Blubber Depth = 3

**Figure 4. Structural fiber areas ($mm^2$), adipocyte cell counts, and adipocyte cross-sectional areas ($um^2$) in CHS subadult, CHS adult, IRL subadult, and IRL adult dolphins.** A.) Structural fiber area means and standard errors versus approximate distance from epidermis surface. B.) Structural fiber area means and standards errors in the superficial, middle, and deep blubber layers. C.) Adipocyte cell count means and standard errors versus approximate distance from epidermis surface. D.) Adipocyte cell count means and standards errors in the superficial, middle, and deep blubber layers. E.) Adipocyte area means and standard errors versus approximate distance from epidermis surface. F.) Adipocyte area means and standards errors in the superficial, middle, and deep blubber layers. Statistical results are summarized in Table 1.

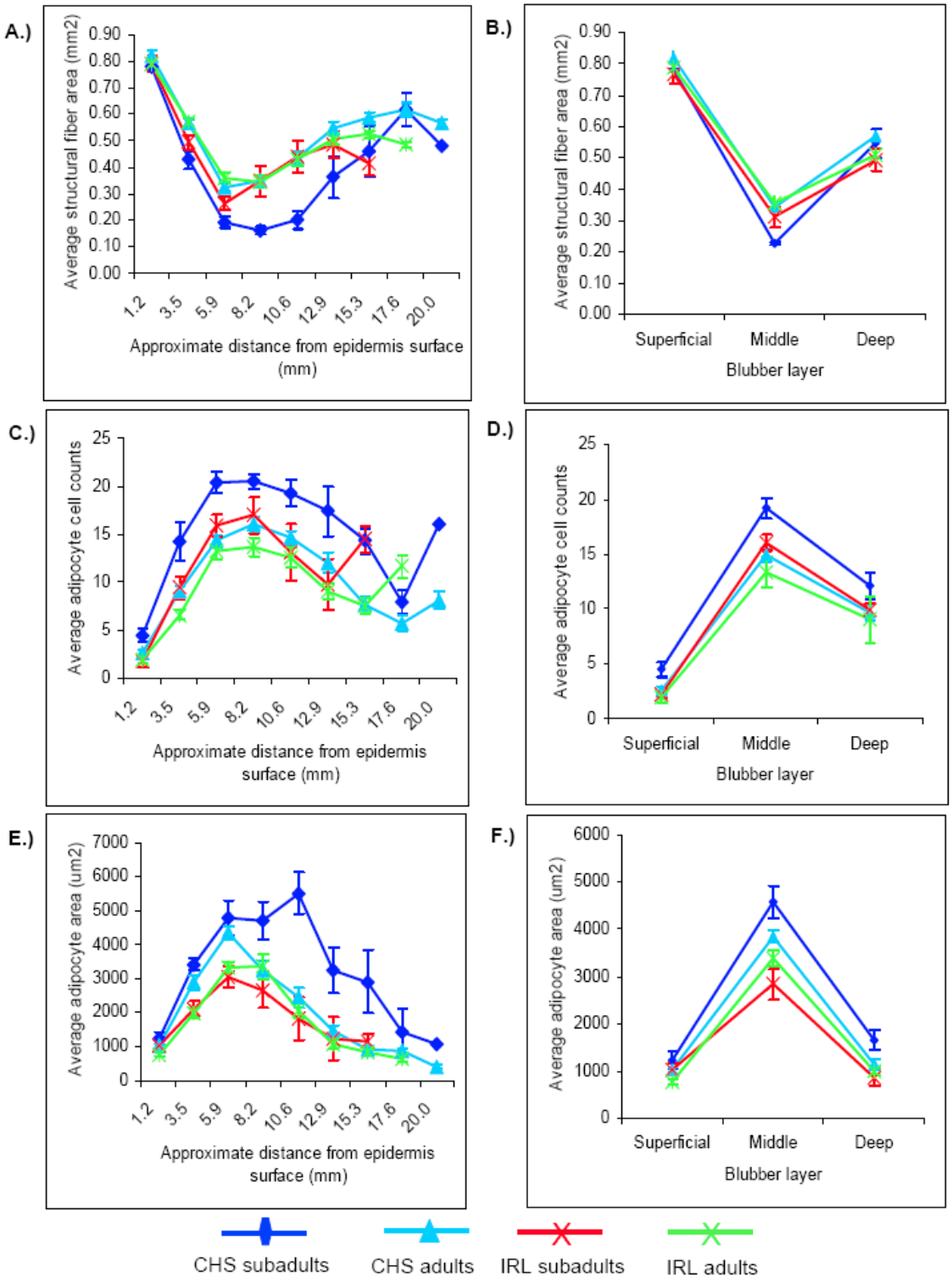
A.)
Average structural fiber area (mm2)
0.90
0.80
0.70
0.60
0.50
0.40
0.30
0.20
0.10
0.00
1.2
3.5
5.9
8.2
10.6
12.9
15.3
17.6
20.0
Approximate distance from epidermis surface (mm)
B.)
Average structural fiber area (mm2)
Superficial
Middle
Deep
Blubber layer
C.)
Average adipocyte cell counts
25
20
15
10
5
0
Approximate distance from epidermis surface (mm)
D.)
Average adipocyte cell counts
Superficial
Middle
Deep
Blubber layer
E.)
Average adipocyte area (um2)
7000
6000
5000
4000
3000
2000
1000
0
Approximate distance from epidermis surface (mm)
F.)
Average adipocyte area (um2)
6000
5000
4000
3000
2000
1000
0
Superficial
Middle
Deep
Blubber layer
CHS subadults
CHS adults
IRL subadults
IRL adults

**Figure 5. Structural fiber areas ($mm^2$), adipocyte cell counts, and adipocyte cross-sectional areas ($um^2$) in CHS females.** The female life history categories include reproductively immature subadults (N = 3), adults captured with calves (N =2), pregnant (N = 2), lactating (N = 3), and simultaneously pregnant & lactating (N = 2) dolphins. A.) Structural fiber area means and standard errors versus approximate distance from epidermis surface. B.) Structural fiber area means and standards errors in the superficial, middle, and deep blubber layers. C.) Adipocyte cell count means and standard errors versus approximate distance from epidermis surface. D.) Adipocyte cell count means and standards errors in the superficial, middle, and deep blubber layers. E.) Adipocyte area means and standard errors versus approximate distance from epidermis surface. F.) Adipocyte area means and standards errors in the superficial, middle, and deep blubber layers. Statistical results are summarized in Table 2.

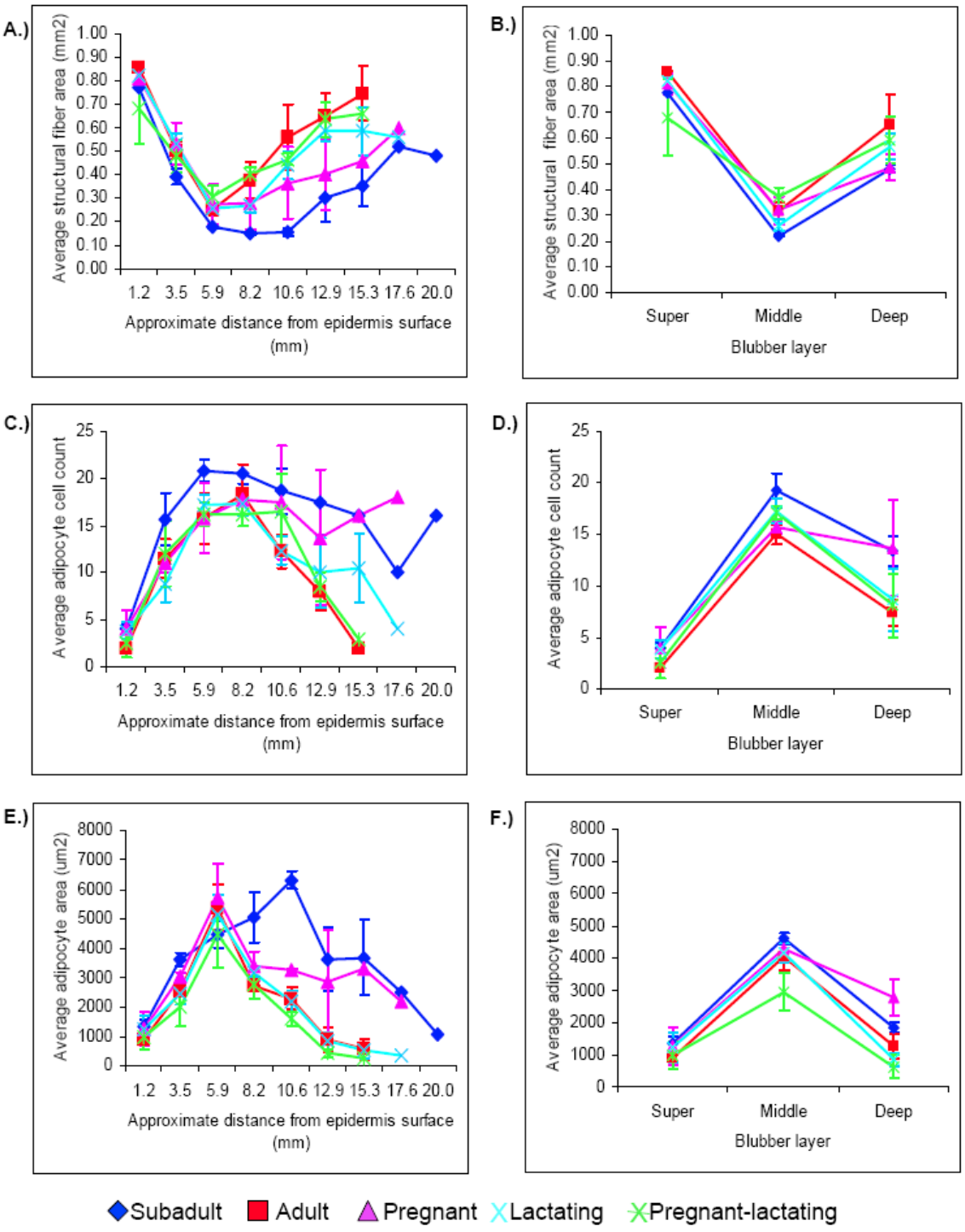
A.)
Average structural fiber area (mm2)
1.00
0.90
0.80
0.70
0.60
0.50
0.40
0.30
0.20
0.10
0.00
1.2 3.5 5.9 8.2 10.6 12.9 15.3 17.6 20.0
Approximate distance from epidermis surface (mm)
B.)
Average structural fiber area (mm2)
Super
Middle
Deep
Blubber layer
C.)
Average adipocyte cell count
25
20
15
10
5
0
Approximate distance from epidermis surface (mm)
D.)
Average adipocyte cell count
Blubber layer
E.)
Average adipocyte area (um2)
8000
7000
6000
5000
4000
3000
2000
1000
0
F.)
Subadult
Adult
Pregnant
Lactating
Pregnant-lactating

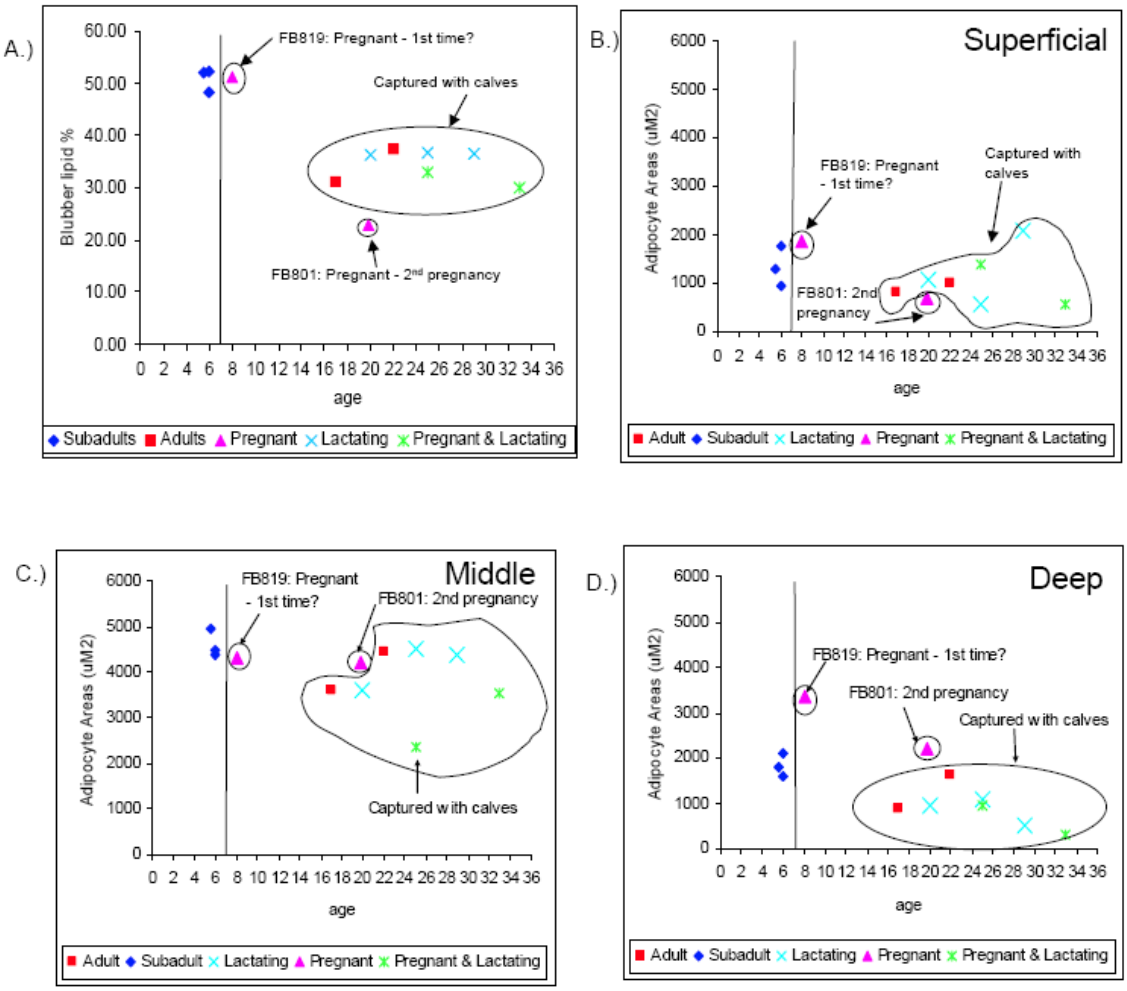


**Figure 6. Total blubber lipid % and adipocyte cross-sectional areas versus age in CHS females.** The vertical line separates reproductively immature sub-adults and adults. Certain individuals are encircled and more detailed explanations of reproductive category are given. A.) Blubber lipid % versus age. B.) Adipocyte cell areas of the superficial blubber layer versus age. C.) Adipocyte cell aress of the middle blubber layer versus age. D.) Adipocyte cell aress of the deep blubber layer versus age. Blubber lipid content data were provided by Greg Mitchum. Age data were provided by Wayne McFee.

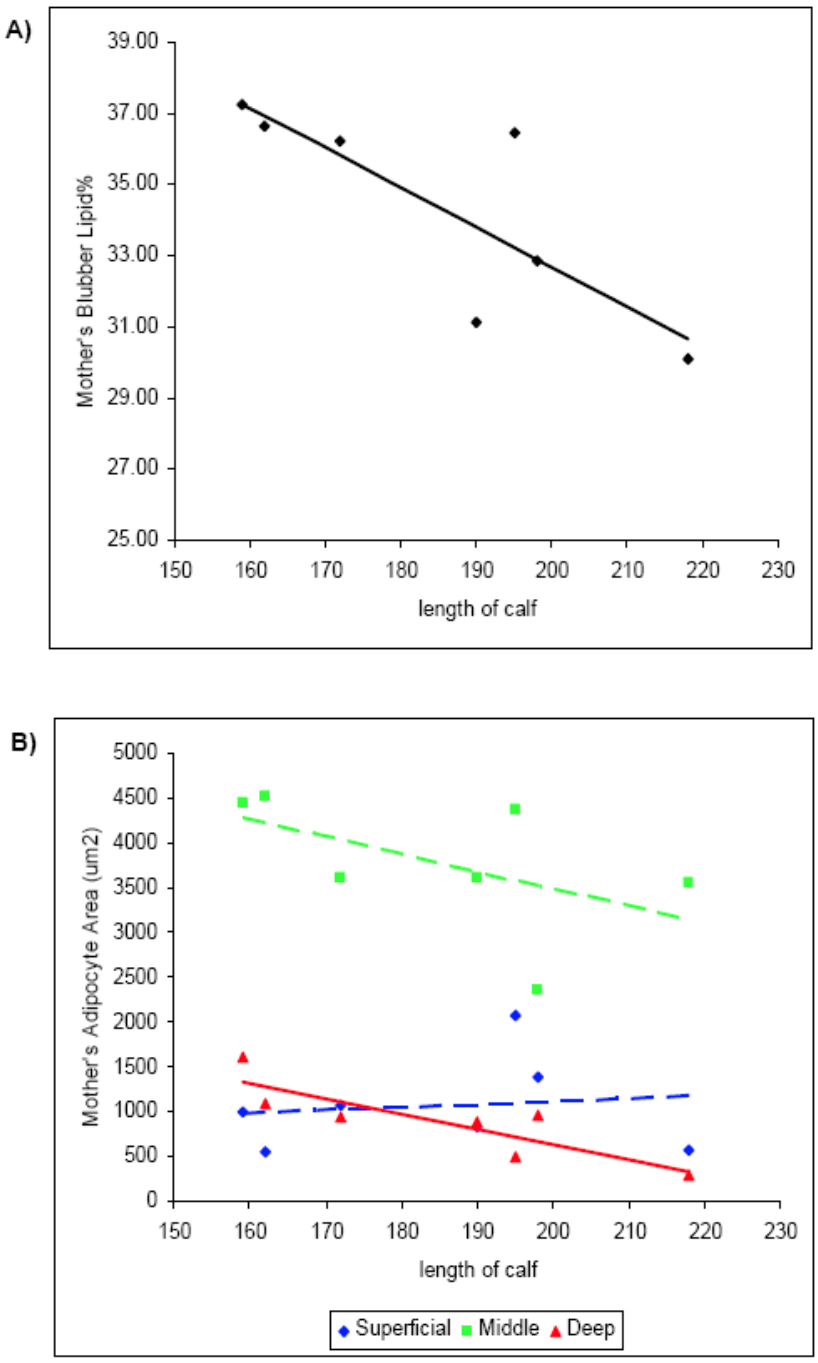


**Figure 7. Total blubber lipid % and adipocyte areas in CHS females captured with calves.** A solid line indicates a significant relationship ($p < 0.05$). A.) Blubber lipid% versus calf length. B.) Adipocyte cross sectional areas of the superficial, middle, and deep blubber layers versus calf length. Blubber lipid content data were provided by Greg Mitchum.

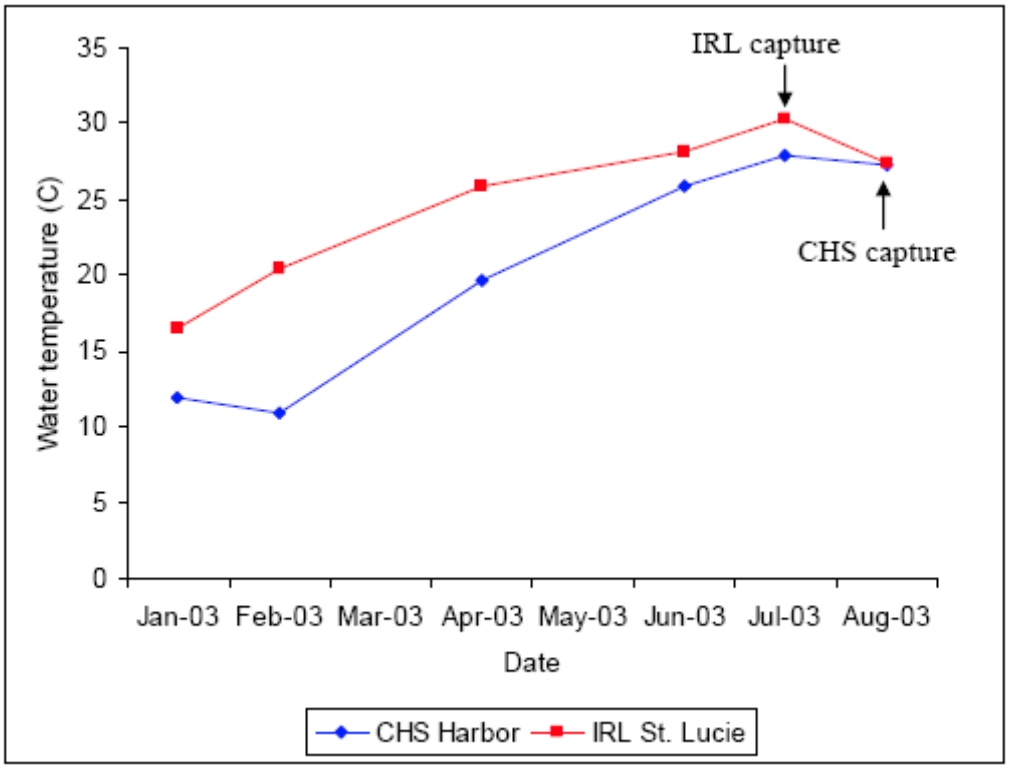


**Figure 8. Water temperature ($^{o}$C) at CHS (Charleston Harbor) and IRL (St. Lucie) locations from January through August 2003.** The historical data was obtained from the Center for Operational Oceanographic Products and Services (CO-OPS), National Oceanic Atmospheric Administration and the South Florida Water Management District. The CHS water temperature data was obtained from CO-OPS station 8665530 (Charleston Harbor, SC), while the IRL water temperature data was an average of a series of stations located in St. Lucie, FL. The arrows depict the CHS and IRL capture dates.

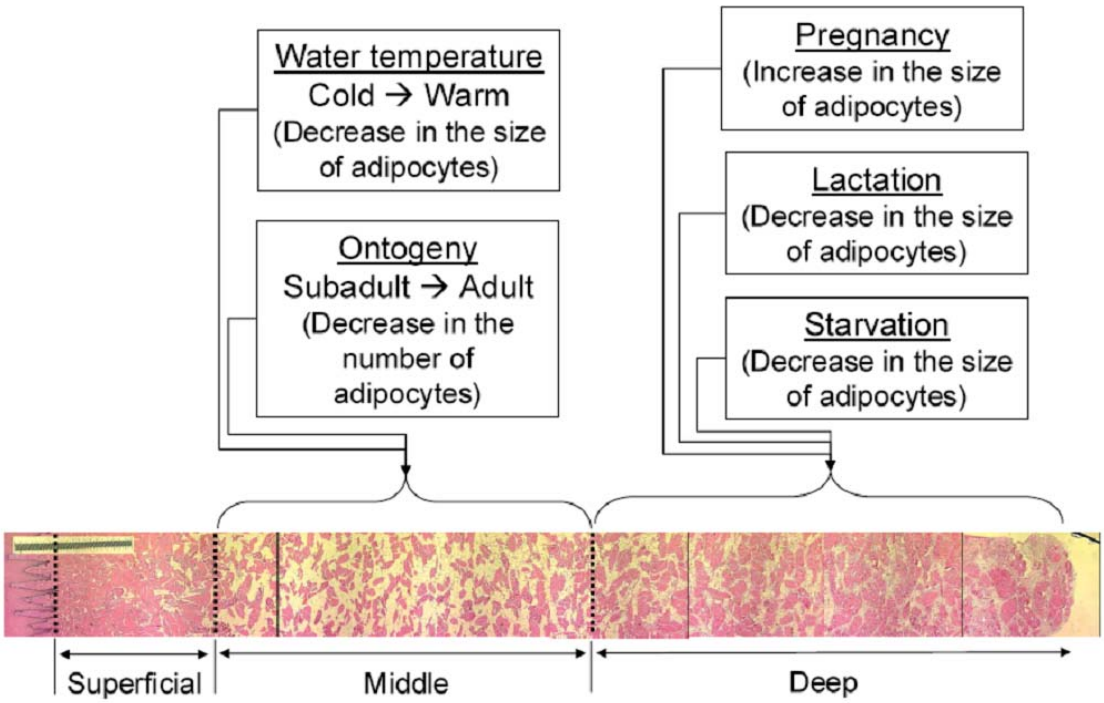


**Figure 9. A schematic illustration depicting how the blubber may respond to different factors such as water temperature, ontogeny, reproductive status, and nutritional state in bottlenose dolphins.**

Table 1. Blubber Morphological Data Reported as Means and Standard Errors for Each Location and Ageclass Category for Bottlenose Dolphins Captured and Released in Charleston, SC and Indian River Lagoon, FL during July and August 2003.[1]

| | | | | Structural Fiber Area (per $mm^2$) | | | | Adipocyte Cell Counts | | | | Mean Adipocyte Cell Area ($um^2$ per cell) | | | |
|---|---|---|---|---|---|---|---|---|---|---|---|---|---|---|---|
| Category[2] | | Age (years) | Blubber lipid % | Superficial | Middle | Deep | Average | Superficial | Middle | Deep | Average | Superficial | Middle | Deep | Average |
| CHS dolphins | N of cases | 31 | 31 | 30 | 30 | 30 | 30 | 30 | 30 | 30 | 30 | 30 | 30 | 30 | 30 |
| | Mean | 14.9 | 36.7 | 0.81 | 0.32 | 0.57 | 0.57 | 2.9 | 15.6 | 10.1 | 9.5 | 1050 | 3973 | 1219 | 2081 |
| | Std error | 1.2 | 1.8 | 0.02 | 0.02 | 0.01 | 0.02 | 0.3 | 0.6 | 0.7 | 0.6 | 65 | 133 | 106 | 154 |
| | | A[3] | A | A, a[4] | A, b | A, c | A | A, a | A, b | A, c | A | A, a | A, b | A, a | A |
| IRL dolphins | N of cases | 29 | 29 | 29 | 29 | 29 | 29 | 29 | 29 | 29 | 29 | 29 | 29 | 29 | 29 |
| | Mean | 12.4 | 33.0 | 0.78 | 0.35 | 0.51 | 0.55 | 2.0 | 14.0 | 9.2 | 8.4 | 830 | 3252 | 956 | 1679 |
| | Std error | 0.9 | 1.8 | 0.01 | 0.02 | 0.01 | 0.02 | 0.2 | 0.7 | 0.7 | 0.6 | 61 | 157 | 78 | 135 |
| | | A | B | A, a | A, b | A, c | A | A, a | A, b | A, c | A | A, a | B, b | A, a | B |
| Subadult | N of cases | 31 | 13 | 12 | 12 | 12 | 12 | 12 | 12 | 12 | 12 | 12 | 12 | 12 | 12 |
| | Mean | 5.9 | 42.4 | 0.77 | 0.28 | 0.52 | 0.52 | 3.2 | 17.4 | 10.8 | 10.5 | 1119 | 3565 | 1193 | 1959 |
| | Std error | 0.4 | 2.9 | 0.02 | 0.02 | 0.03 | 0.04 | 0.5 | 1.0 | 1.3 | 1.1 | 107 | 348 | 178 | 233 |
| | | A | A | A, a | A, b | A, c | A | A, a | A, b | A, c | A | A, a | A, b | A, a | A |
| Adult | N of cases | 29 | 47 | 47 | 47 | 47 | 47 | 47 | 47 | 47 | 47 | 47 | 47 | 47 | 47 |
| | Mean | 15.9 | 32.8 | 0.80 | 0.35 | 0.54 | 0.56 | 2.3 | 14.2 | 9.4 | 8.6 | 897 | 3632 | 1063 | 1864 |
| | Std error | 0.7 | 1.3 | 0.01 | 0.01 | 0.01 | 0.02 | 0.2 | 0.5 | 0.5 | 0.5 | 50 | 112 | 73 | 116 |
| | | B | B | A, a | A, b | A, c | B | A, a | B, b | A, c | B | A, a | A, b | A, a | A |

Table 1. (*Continued*)

| | | | | | | | | | | | | | | | |
|---|---|---|---|---|---|---|---|---|---|---|---|---|---|---|---|
| CHS subadult | N of cases | 5 | 5 | 5 | 5 | 5 | 5 | 5 | 5 | 5 | 5 | 5 | 5 | 5 | 5 |
| | Mean | 5.5 | 49.3 | 0.78 | 0.23 | 0.55 | 0.52 | 4.5 | 19.2 | 12.1 | 11.9 | 1236 | 4590 | 1661 | 2496 |
| | Std error | 0.5 | 1.9 | 0.01 | 0.00 | 0.04 | 0.06 | 0.7 | 0.9 | 1.2 | 1.7 | 173 | 340 | 218 | 421 |
| | | A | A | A, a | A, b | A, c | A | A, a | A, b | A, c | A | A, a | C, b | A, a | A |
| CHS adult | N of cases | 26 | 26 | 25 | 25 | 25 | 25 | 25 | 25 | 25 | 25 | 25 | 25 | 25 | 25 |
| | Mean | 16.8 | 34.2 | 0.82 | 0.34 | 0.57 | 0.58 | 2.6 | 14.9 | 9.7 | 9.1 | 1013 | 3850 | 1130 | 1998 |
| | Std error | 1.1 | 1.7 | 0.02 | 0.02 | 0.02 | 0.02 | 0.3 | 0.5 | 0.7 | 0.7 | 69 | 134 | 113 | 164 |
| | | B | B | A, a | A, b | A, c | A | A, a | B, b | A, c | B | A, a | BC, b | A, a | AB |
| IRL subadult | N of cases | 8 | 8 | 7 | 7 | 7 | 7 | 7 | 7 | 7 | 7 | 7 | 7 | 7 | 7 |
| | Mean | 6.2 | 38.1 | 0.77 | 0.31 | 0.49 | 0.52 | 2.2 | 16.0 | 9.9 | 9.4 | 1035 | 2833 | 859 | 1576 |
| | Std error | 0.6 | 3.8 | 0.03 | 0.03 | 0.04 | 0.05 | 0.5 | 1.4 | 2.2 | 1.5 | 137 | 335 | 179 | 237 |
| | | A | AB | A, a | A, b | A, c | A | A, a | AB, b | A, c | AB | A, a | A, b | A, a | B |
| IRL adult | N of cases | 21 | 21 | 22 | 22 | 22 | 22 | 22 | 22 | 22 | 22 | 22 | 22 | 22 | 22 |
| | Mean | 14.8 | 31.0 | 0.79 | 0.36 | 0.51 | 0.55 | 2.0 | 13.4 | 9.0 | 8.1 | 765 | 3385 | 986 | 1712 |
| | Std error | 0.9 | 1.9 | 0.01 | 0.02 | 0.01 | 0.02 | 0.3 | 0.8 | 0.6 | 0.7 | 63 | 173 | 87 | 162 |
| | | B | B | A, a | A, b | A, c | A | A, a | B, b | A, c | B | A, a | B, b | A, a | B |

[1] The data include males and non-pregnant, non-lactating females.

[2] Comparisons represented are between CHS versus IRL dolphins, subadults vs. adults, and CHS subadults vs. CHS adults vs. IRL subadults vs. IRL adults.

[3] Between categories, blubber layers that share a similar capital letter are not significantly different from each other ($P > 0.05$).

[4] Within categories, blubber layers that share a similar lower case letter are not significantly different from each other ($P > 0.05$).
Male vs. female comparisons were not significant. These data are not shown.

Table 2. Blubber Morphological Data Reported as Means and Standard Errors for Female Bottlenose Dolphins Captured and Released in Charleston, SC during August 2003.

| | | | | | Structural Fiber Area (per $mm^2$) | | | | Adipocyte Cell Counts | | | | Mean Adipocyte Cell Area ($um^2$ per cell) | | | |
|---|---|---|---|---|---|---|---|---|---|---|---|---|---|---|---|---|
| Female Life History Category | No. of animals | Age Range (yrs) | | Blubber lipid % | Superficial | Middle | Deep | Average | Superficial | Middle | Deep | Average | Superficial | Middle | Deep | Average |
| subadult | 3 | 5.5 - 6 | mean | 50.9 | 0.77 | 0.22 | 0.48 | 0.49 | 4.0 | 19.2 | 13.3 | 12.2 | 1327 | 4607 | 1834 | 2589 |
| | | | std err | 1.3 | 0.00 | 0.00 | 0.02 | 0.08 | 0.50 | 1.63 | 1.45 | 2.31 | 237 | 181 | 150 | 519 |
| | | | | A[1] | A, a[2] | A, b | A, c | A | A, a | A, b | A, b | A | A, a | A, b | AB, a | A |
| adult[3] | 2 | 17 - 22 | mean | 34.2 | 0.86 | 0.32 | 0.65 | 0.61 | 2.0 | 15.0 | 7.4 | 8.1 | 915 | 4031 | 1250 | 2065 |
| | | | std err | 3.1 | 0.01 | 0.03 | 0.12 | 0.10 | 0.00 | 1.00 | 1.25 | 2.42 | 84 | 415 | 365 | 641 |
| | | | | A | A, a | A, b | A, a | A | A, a | A, b | A, ab | A | A, a | A, b | AB, a | ABC |
| pregnant | 2 | 8 - 19.8 | mean | 37.0 | 0.81 | 0.32 | 0.49 | 0.54 | 4.0 | 15.7 | 13.7 | 11.1 | 1272 | 4271 | 2786 | 2776 |
| | | | std err | 14.1 | 0.04 | 0.05 | 0.05 | 0.09 | 2.00 | 0.67 | 4.67 | 2.63 | 576 | 51 | 571 | 586 |
| | | | | A | A, a | A, b | A, b | A | A, a | A, b | A, ab | A | A, a | A, b | A, ab | AC |
| lactating | 3 | 20 - 29 | mean | 36.5 | 0.82 | 0.26 | 0.57 | 0.55 | 3.8 | 17.3 | 8.6 | 9.9 | 1233 | 4162 | 840 | 2079 |
| | | | std err | 0.1 | 0.02 | 0.02 | 0.05 | 0.08 | 0.93 | 1.18 | 3.00 | 2.19 | 444 | 280 | 179 | 548 |
| | | | | A | A, a | A, b | A, a | A | A, a | A, b | A, ab | A | A, ab | A, a | B, b | B |
| pregnant & lactating | 2 | 25 - 33 | mean | 31.5 | 0.68 | 0.37 | 0.59 | 0.55 | 2.5 | 17.1 | 8.1 | 9.2 | 979 | 2953 | 627 | 1520 |
| | | | std err | 1.4 | 0.15 | 0.04 | 0.09 | 0.07 | 1.50 | 0.58 | 3.13 | 2.83 | 411 | 599 | 333 | 502 |
| | | | | A | A, a | A, b | A, c | A | A, a | A, b | A, ab | A | A, a | A, b | B, a | ABC |

[1] Between categories, blubber layers that share a similar capital letter are not significantly different from each other ($P > 0.05$).

[2] Within categories, blubber layers that share a similar lower case letter are not significantly different from each other ($P > 0.05$).

[3] Adult females were not lactating but were captured with calves.

# CHAPTER III:
# THE INTERRELATIONSHIPS AMONG CYTOCHROME P4501A1 EXPRESSION, PCBS AND HYDROXYLATED METABOLITES, AND BLUBBER DYNAMICS OF BOTTLENOSE DOLPHINS (*TURSIOPS TRUNCATUS*) FROM THE SOUTHEAST UNITED STATES

**ABSTRACT**

Persistent organic pollutants (POPs) bioaccumulate in the blubber of marine mammals. Therefore, it is important to understand the structure and dynamics of blubber layers and how they affect POPs and subsequent biochemical responses. Of particular interest is the response of cytochrome P4501A1 (CYP1A1) to non-ortho and mono-ortho polychlorinated biphenyls (PCBs) and the production of hydroxylated metabolites of PCBs (OH-PCBs) by CYP1A1 and other cytochrome P450 enzymes. As part of a larger study to determine the effects of anthropogenic stressors (including chemical contamination) on the health status of bottlenose dolphins (*Tursiops truncatus*) from the Southeast United States, this study used established histological and immunohistochemical methods to document the structure of blubber and to assess the expression of CYP1A1 in skin-blubber biopsies of dolphins captured in the waters of Charleston, SC (n=38), and Indian River Lagoon, FL (n=36). CYP1A1 expression was strongest and most frequent in capillary endothelial cells within the blubber, similar to findings in other studies of cetacean CYP1A1. CYP1A1 expression differed among the blubber layers: deep > middle > superficial. CYP1A1 expression in the deep blubber was significantly higher in dolphins from CHS as compared to those from IRL. CYP1A1 expression in the deep blubber increased with total plasma 2,3,7,8-TCDD Toxic Equivalents (TEQ), while no such relationship was found for the superficial or middle layers. We tested the hypothesis that blubber dynamics was an important factor in CYP1A1 induction. CYP1A1 expression of vascular endothelial cells in the deep blubber of both CHS and IRL dolphins was negatively related to adipocyte size. Reproduction affected CYP1A1 expression of vascular endothelial cells in CHS females. CYP1A1 expression of the deep layer was highest in simultaneously pregnant-lactating dolphins. These dolphins contained the smallest adipocytes in the deep blubber, suggesting intense lipid mobilization in these animals. The concurrent mobilization of AHR agonists may be responsible for the high levels of CYP1A1 expression in the deep blubber layer of the simultaneously pregnant-lactating dolphins. In all dolphins, CYP1A1 expression in the deep blubber layer was significantly related to plasma OH-

PCB concentrations. In this study, we speculate that CYP1A1 in endothelial cells of the blubber and CYP1A1 in the liver could be responsible for a large percentage of identified OH-PCB congeners in CHS dolphins. Mobilization of AHR agonists from the blubber may enhance PCB metabolism and the production of OH-PCBs by induction of CYP1A1 in endothelial cells of the deep blubber and induction of CYP1A1 in hepatocytes. The OH-PCBs may then interfere with thyroid hormone homeostasis.

**KEYWORDS:** CYP1A1, PCBs, OH-PCBs, blubber, adipocyte, bottlenose dolphin

## INTRODUCTION

Marine mammals bioaccumulate persistent organic pollutants (POPs) such as organochlorine pesticides like dichlorodiphenylethanes (i.e. DDTs), dieldrin, chlordanes, and hexachlorocyclohexanes (HCHs), as well as industrial solvents and their byproducts such as chlorinated dibenzo-*p*-dioxins, dibenzofurans, and polychlorinated biphenyls (PCBs) (Blomkvist et al., 1992; DeLong et al., 1973; Kannan et al., 1993; Muir et al., 1996; Ross et al., 2000). In some populations, the levels of POPs in blubber are extremely high, as observed in beluga whales (*Delphinapterus leucas*) from the St. Lawrence Estuary, striped dolphins (*Stenella coeruleoalba*) from the Western Mediterranean, killer whales (*Orcinus orca*) from British Columbia, and bottlenose dolphins (*Tursiops truncatus*) from the Southeast United States (Hansen et al., 2004; Kannan et al., 1993; Muir et al., 1996; Ross et al., 2000). Exposure of marine mammals to these compounds has been associated with mass mortalities and health effects, including reproductive abnormalities and immune dysfunction (DeLong et al., 1973; Kannan et al., 1993; Ross et al., 2000).

Understanding the impacts of environmental chemicals on the health of marine mammals is a daunting task because of ethical, logistical, and legal concerns. Researchers have focused primarily on epidemiological studies of captive animals, remote-biopsy to acquire skin-blubber biopsies, and examination of specimens from strandings or subsistence hunts. Health assessments involving the capture and release of

marine mammal species are favored because of the wealth of life history and veterinary diagnostic data, as well as the numerous biological samples (i.e. blood, full-depth blubber biopsies, urine, and feces) that can be collected for pollutant and biomarker measurements. Integration of these data can provide a method to estimate associated health risks of chemical pollutants. For bottlenose dolphins (*Tursiops truncatus*), a series of health assessment programs have been established along the Eastern United States (Bossart, 2005; Hansen et al., 2004; Wells et al., 2005). One of the goals of these programs is to understand the effect persistent environmental chemicals have on the health of bottlenose dolphins, including how anthropogenic chemicals that bioaccumulate in the blubber may affect biomarkers of exposure and effect such as cytochrome P4501A1 (CYP1A1).

CYP1A1 is induced by ligands that activate the aryl hydrocarbon receptor (AHR). These ligands include planar halogenated aromatic hydrocarbons (PHAHs) (i.e. non-ortho and some mono-ortho substituted PCBs and 2,3,7,8-tetrachlorodibenzo-p-dioxin) and polycyclic aromatic hydrocarbons (PAHs). In rat liver, CYP1A1 is important in phase I oxidative metabolism of PCB congeners with chlorine substituents at one or both *para* positions, and with adjacent non-halogenated *ortho* and *meta* carbons on at least one ring (Kaminsky et al., 1981; Mills et al., 1985). CYP1A1 metabolism of these parent PCB congeners generates hydroxylated metabolites (OH-PCBs) (Kaminsky et al., 1981; Mills et al., 1985; Yoshimura et al., 1987). *In vitro* biotransformation studies using beluga whale liver microsomes have demonstrated the production of OH-PCBs in cetaceans by CYP1A1 (White et al., 2000). OH-PCBs have emerged as important classes of environmental contaminants in marine mammals (Houde et al., 2006; McKinney et al., 2006; Sandala et al., 2004; Sandau, 2000). These compounds interact with the thyroid hormone system and have been recognized as a group of contaminants that may pose a threat to human and marine mammal health (Brouwer et al., 1998; Brouwer et al., 1989; Zoeller, 2002).

CYP1A1 induction is a valuable biomarker of exposure and effect to PHAHs in cetaceans (White et al., 1994; Wilson, 2003; Wilson et al., 2005). Its advantages include

the relatively robust methods that exist for its detection (formalin preservation followed by immunohistochemistry) and the fact that it can be measured in skin-blubber biopsy samples (Angell et al., 2004). In vitro assays have demonstrated CYP1A1 induction in sperm whale (*Physeter macrocephalus*) skin biopsy slices exposed to β-napthoflavone (BNF), a prototypical CYP1A1 inducer, (Godard et al., 2004) and in bottlenose dolphin skin-blubber biopsies exposed to 3,3',4,4'-tetrachlorobiphenyl (PCB126) (E. Montie, unpublished data).

In the integument, CYP1A1 expression is strongest and most frequent in vascular endothelial cells of the arterial system and capillaries within the blubber of cetaceans (Angell et al., 2004). This is consistent with earlier observations that CYP1A is highly inducible in vertebrate endothelial cells (Stegeman et al., 1989). It has been suggested that the movement of AHR agonists from the blubber across the endothelial cells and into the bloodstream (i.e. as occurs during blubber lipid mobilization) could induce CYP1A1 in vascular endothelial cells (Angell et al., 2004). In other vertebrate species, PCBs and DDTs have been shown to move out of adipose tissue during lipid mobilization (Dale et al., 1962; Findlay and De Freitas, 1971; Sodergren and Ulfstrand, 1972). Hence, understanding blubber morphology and lipid dynamics may be important factors in understanding CYP1A1 expression in the blubber biopsy, its relationship to AHR agonists (e.g. non-ortho and mono-ortho PCBs), and its involvement in the production of OH-PCBs.

Previously, we investigated the blubber morphology of wild bottlenose dolphins captured and released in Charleston, South Carolina (CHS) and Indian River Lagoon, Florida (IRL), as part of the Bottlenose Dolphin Health and Risk Assessment (HERA) Project (Chapter 2). In all dolphins examined, histological analysis revealed stratification of the blubber into superficial, middle, and deep layers. Our goal in this study was to integrate the histological analysis of the integument with measures of CYP1A1 expression in vascular endothelial cells of the different blubber layers, and the concentrations of non-ortho and mono-ortho PCB congeners and OH-PCBs. Specifically, the objectives of this study were to: 1) quantitatively test the hypothesis that CYP1A1

expression is stratified in the blubber of these dolphins; 2) compare depth-specific expression between CHS and IRL dolphins; 3) determine if there is a relationship between depth-specific expression and total blubber and plasma 2,3,7,8-TCDD Toxic Equivalents (TEQ); 4) test the hypothesis that blubber dynamics is an important factor in CYP1A1 induction; and 5) investigate the relationship between depth-specific CYP1A1 expression and plasma OH-PCB concentrations. The thorough data collected during the health assessment allowed us to factor these variables into our analysis and determine their influence on CYP1A1 expression in the skin-blubber biopsy.

## METHODS

### *Specimens*

Previously, the blubber morphology of these wild bottlenose dolphins was investigated as part of The Bottlenose Dolphin Health and Risk Assessment (HERA) Project (Chapter 2). Briefly, the HERA project is a collaboration between the National Ocean Service Center for Coastal Environmental Health & Biomolecular Research and Harbor Branch Oceanographic Institution. HERA was initiated in 2003, as a comprehensive, integrated, multi-disciplinary research project designed to assess the health of Atlantic bottlenose dolphins in two southeast coastal regions, Charleston, SC and the Indian River Lagoon, FL. As part of this project, blubber samples were collected from seventy-four bottlenose dolphins that were captured and released in estuarine waters from these two geographic locations: (i) Charleston (CHS), SC in August 2003 (n = 38); and (ii) Indian River Lagoon (IRL), FL in July 2003 (n = 36) (Figure 1). Capture, sampling, and release followed methods previously described (Montie et al., 2006; Scott et al., 1990)(see Chapter 2). Pregnancy status, blubber depth, testes length, and an internal organ exam were determined and evaluated by ultrasound (SonoSite 180plus, Bothell, WA). Age was determined by examination of the post-natal dentine layers from an extracted tooth (Hohn et al., 1989). Males less than 10 years old were classified as reproductively immature sub-adults, while older males (greater than 10 years) were

classified as adults. Female dolphins were divided into five life history categories (reproductively immature sub-adult; adult; pregnant; lactating; and simultaneously pregnant and lactating). For the females with calves, the calf length was recorded and used as an approximation for lactation day.

***Plasma and Blubber Biopsy Collection***

*Plasma*. Blood samples were drawn from the periarterial venous rete in the flukes immediately after the dolphin was restrained. The fluke site was prepared aseptically with a surgical scrub (2% chlorhexidine gluconate) and an alcohol soaked gauze pad. The blood sample was obtained with a 19 gauge needle and a 1.9 cm butterfly catheter with a vacutainer attachment (Becton, Dickinson, and Co., Franklin Lakes, NJ). Samples for chemical analysis were collected in four vacutainer tubes with heparin (Becton, Dickinson, and Co., Franklin Lakes, NJ). The tubes were inverted 8-10 times to mix the blood and heparin to avoid clotting, placed at 40$^{o}$F for 20–40 min, and centrifuged for 15 min at 1200 rpms. The plasma was collected in a Teflon container using hexane rinsed glass Pasteur pipets.

*Blubber*. Chapter 2 describes the methods for blubber biopsy collection in detail. Briefly, biopsies measuring approximately 3 x 5 centimeters (cm) were surgically removed from the left side at a site 5-10 cm caudal to the dorsal fin and 10 cm ventral to the dorsal ridge, which is the standard surgical site for bottlenose dolphin health assessments (Figure 2A) (Hansen et al., 2004; Wells et al., 2005). Immediately after collection, a 0.5 x 1.5 cm x full-depth skin-blubber slice was fixed in 10% neutral buffered formalin (NBF) for histological analysis and CYP1A1 immunohistochemistry (IHC) (Figure 2B). A 1.5 x 3.0 cm x full-depth blubber sub-sample was also stored in a pre-cleaned Teflon container and frozen at -80$^{o}$C until environmental contaminants and lipid content could be measured.

***Immunohistochemistry***

Chapter 2 describes the procedure for slide preparation for hematoxylin- and eosin (H&E) staining and CYP1A1 IHC. Briefly, samples were removed from the 10% NBF solution and routinely processed through an ascending series of alcohol dips (70%, 80%, 95%, and 100%), cleared with xylene, and then infiltrated with 100% paraffin. The samples were embedded in paraffin and sectioned at 5 um using a rotary microtome (Leitz Model 1512, GMI, Ramsey, MN) and mounted on either glass microscope slides (for H&E) or colorfrost plus slides (for CYP1A IHC).

Slides were immunostained with either anti-CYP1A monoclonal antibody (MAb) 1-12-3 (0.3 μg/ml) or a non-specific antibody (MOPC31 against purified mouse myeloma protein, 0.3 μg/mL, Sigma, St. Louis, MO), as previously described (Smolowitz et al., 1991). MAb 1-12-3 was originally raised against CYP1A from the marine fish scup (*Stenotomus chrysops*) (Park et al., 1986). This antibody is specific for mammalian CYP1A1, with poor cross-reactivity towards CYP1A2 (Drahushuk et al., 1998); the epitope recognized is a CYP1A1-specific epitope (J. Stegeman, unpublished data). The slides were developed using a peroxidase anti-peroxidase detection system (Signet Laboratories, Deham, MA) with amino-9-ethylcarbazole as a chromogen substrate (AEC, Signet Laboratories), and counterstained with Mayer's hematoxylin (Sigma). For each IHC run, liver sections from benzo[*a*]pyrene treated scup were used as positive controls for staining intensity.

Chapter 2 describes in detail how the visual representation of the blubber on the H&E slide was divided into the superficial, middle, and deep blubber layers (Figure 2C). Briefly, the superficial blubber layer extended from the ventral borders of the dermal papillae to the boundary where the eosin stain decreased in red intensity (due to an increase in size and number of adipocytes). The middle blubber layer extended from the ventral border of the superficial blubber layer to the boundary where the eosin stain increased in red intensity (due to a decrease in adipocyte size and an increased density of structural fibers). The deep layer extended from the ventral border of the middle blubber

layer to the subdermal sheath that separates the blubber from the underlying muscle. In most cases, the ventral boundary of the deep blubber layer could not be determined.

Each blubber layer was scored separately. Because the H&E and IHC slides were derived from contiguous sections, the marks separating the superficial, middle, and deep blubber layers on the H&E slide were transferred to the IHC slide by overlaying the IHC slide on top of the H&E slide (Figure 2D). To score each layer separately, small pieces of paper were placed over the layers not being scored to avoid scoring overlapping layers. Scoring of the superficial blubber layer included the finger-like connective tissue protrusions called dermal papillae. Each dolphin was scored blindly without knowing its geographic location, sex, age class, and reproductive condition. If a dolphin biopsy sample did not contain a representation of the deep blubber layer, that individual was not included in the data or statistical analyses.

CYP1A1 staining scores were determined using two methods, the "original" method (Angell et al., 2004; Smolowitz et al., 1991) and a "modified" method. For each layer, CYP1A1 staining scores were determined separately for each cell type of the epidermis and blubber using both methods. These cell types included basale, spinosum, corneum, and melanocytes of the epidermis; fibroblasts, adipocytes, arterial smooth muscle cells, arterial endothelial cells, venule endothelial cells, and microcirculation (arterioles and capillaries) endothelial cells of the superficial, middle, and deep blubber layers. For the original method, the CYP1A1 staining score was calculated as the product of the staining intensity (scale of 0-5) and the staining occurrence (scale of 0-3). A staining occurrence of 0 corresponds to no staining, while a staining occurrence of 3 reflects staining in all cells. The staining intensity represents the average intensity for each cell type in that blubber layer that showed staining. A staining intensity score of 0 represents no cell staining or staining equivalent to MOPC31 control antibody. A staining intensity score of 5 corresponds to the intensive staining observed in liver sections of scup treated with benzo[*a*]pyrene, a prototypical CYP1A1 inducer, stained at the same time as sample slides. The maximum possible score using the original method is 15 (5x3). The original staining score method has been shown to reflect accurately the

amount of CYP1A1 protein measured by Western blotting (Woodin et al., 1997). For the "modified" method, the CYP1A1 staining score for each layer was calculated as the product of the stain intensity (scale of 0-5) and the "modified" occurrence score (the number of cells stained divided by the area scored). The area of each layer (superficial, middle, and deep) was determined by manually tracing the blubber layer boundaries and calculating the area using Scion Image software (National Institutes of Health, USA). For both methods, an average CYP1A1 expression score for the total or overall blubber was calculated using the following equation:

$$Y = (A_s/A_t)(X_s) + (A_m/A_t)(X_m) + (A_d/A_t)(X_d)$$

Where Y = average CYP1A1 expression score for the total blubber; $A_s$ = area of superficial blubber layer scored in $mm^2$; $A_m$ = area of middle blubber layer scored in $mm^2$; $A_d$ = area of deep blubber layer scored in $mm^2$; $A_t$ = area of superficial, middle, and deep layers scored in $mm^2$; $X_s$ = CYP1A1 staining score for the superficial blubber layer; $X_m$ = CYP1A1 staining score for the middle blubber layer; $X_d$ = CYP1A1 staining score for the deep blubber layer.

***Chemical Analysis of Blubber and Plasma Samples***

*Blubber*. Blubber PCB data were provided by Greg Mitchum (NOAA). Hansen et al. (2004) describe the methods for blubber PCB analysis in detail. Briefly, blubber samples were macerated in sodium sulfate and extracted in a 33 mL Dionex accelerated solvent extraction (ASE) cell (Dionex, Salt Lake City, UT) with methylene chloride. Internal standards were added to the ASE cell. After extraction, percent lipids were determined gravimetrically. Lipids were removed from the extract by gel permeation chromatography. Interfering polar compounds were then removed by Florisil chromatography and eluted with 20% ethyl ether / 80% petroleum ether. The sample was reduced to approximately 100 uL and transported to a GC vial for analysis. Gas chromatograph / mass spectrometry (GC/MS) analysis was operated in the selected ion

monitoring mode and the chemical products were identified by retention time, target ion, and conformation ion ratios, as compared to know standards.

For the blubber samples analyzed, 87 PCB congeners were determined. These included the following International Union for Pure and Applied Chemistry (IUPAC) #s: 1, 2, 3, 5/8, 9, 12, 15, 18, 20, 26, 28/31, 29, 37, 44, 45, 48, 49, 50, 52, 56/60, 61/74, 63, 66, 69, 70/76, 77, 82, 84, 87/115, 88/95, 89, 92, 99, 101/90, 105, 106/118/123, 107/108, 110, 114, 119, 123, 126, 128/167, 130, 132/153/168, 141, 146, 149, 151, 154, 156, 157, 159, 169, 170/190, 172, 174, 177, 180, 183, 187, 188, 189, 193, 194, 195, 200, 201, 202, 206, 207, and 209. Total blubber PCBs were calculated as the sum of these congeners both as wet and lipid weight concentrations. Total Toxic Equivalents ($TEQ_{98}$) relative to 2,3,7,8-tetrachlorodibenzo-*p*-dioxin (TCDD) were calculated for relevant dioxin-like PCBs (non-ortho PCBs 77, 126, and 169; mono-ortho PCBs 105, 114, 156, 157, and 189) as wet and lipid weight concentrations. The most recent international mammalian Toxic Equivalency Factors ($TEF_{98}$) were used (van den Berg et al., 1998).

*Plasma*. Plasma PCB and OH-PCB data were provided by Magali Houde. The OH-PCB extraction method was developed based on a previous published technique (Sandau, 2000). Houde et al. (2006) describe the methods of plasma PCB and OH-PCB analysis of these dolphins in detail. Briefly, plasma samples (~2g) were spiked with two surrogate recovery standards for PCBs: CB-30 (2,4,6-trichlorophenyl) and CB-204 (2,2',3,4,4',5,6,6'-octachlorophenyl) [National Laboratory of Environmental Testing (NLET), Burlington, Canada], and five $^{13}C$-labeled OH-PCBs (4-HO-CB12, 4-HO-CB29, 4-HO-CB61, 4-HO-CB120, and 4-HO-CB187; 50 ng/ml) (Wellington Laboratories Inc., Guelph, ON, Canada). Plasma was acidified with HCl (6M, 1 ml) and denaturated using iso-propanol (3 ml). The denaturated plasma was extracted three times with methyl-*tert*-butyl ether (MTBE)/hexane (1:1 by volume) and the extracts were combined. Volume was reduced and potassium hydroxide (1M in 1:1 ethanol:water) was used to partition the contaminants into two fractions: neutral (PCB) and phenolic (OH-PCB).

The neutral fraction was cleaned on an acidified silica gel column (22% $H_2SO_4$, 3g). Extracts were reduced in volume and a performance standard (CB 166; 30 ng/ml) was added for mass spectral analysis. Extracts were analyzed by gas chromatography (GC) (Hewlett-Packard 5890, Series II, Wilmington, DE) with a $^{63}$Ni-electron capture detector (ECD). The chromatography was performed on a DB-5 column (60m x 0.25mm, 0.25µm internal film thickness) with $H_2$ as the carrier gas. Quantification was performed using a series of external standards (NLET). Mean recoveries (± standard deviation) of CB-30 and CB-204 were 80 ± 7% and 83 ± 10%, respectively. PCB concentrations were not adjusted for recoveries. The method detection limit (MDL) for PCBs was around 0.1 ng/g wet weight (w.w.) based on signal to noise ratio of 10. A total of 121 PCB congeners (including co-elutions; NLET, Burlington, ON, Canada) were assessed and included IUPAC #s: 4/10, 6, 7/9, 8/5, 12/13, 15/17, 16, 18, 19, 22, 24/27, 25, 26, 31/28, 32, 33/20/53, 40, 41/71, 42, 43, 44, 45, 46, 47/48, 51, 52/49, 54/29, 55, 56/60, 59, 63, 64, 70, 74, 76/98, 82/151, 83, 87, 91, 92/84, 95/66, 97, 99, 100, 101, 105, 107/147, 110, 114, 118, 128, 129/178, 131, 132, 134, 135, 136, 137, 138/158, 141/179, 144, 146, 149/133, 153, 156, 158, 167, 170/190, 171, 172, 174, 175, 176/130, 176/203, 177, 180/193, 182, 183, 185, 187, 189, 191, 194, 195, 197, 198, 199, 201, 202/173, 205, 206, 207, 208, and 209. Total plasma PCBs were calculated as the sum of these congeners as wet weight concentrations. Plasma $TEQ_{98}$ wet weight concentrations were calculated for relevant dioxin-like PCBs (mono-ortho PCBs 105, 114, 118, 156, 167, and 189).

The OH-PCB fraction was acidified with sulfuric acid, re-extracted with MTBE/hexane, dried over sodium sulfate and derivatized with diazomethane. Extracts were then cleaned on an acidified (22%) silica gel column (3g), eluted with 15:85 methylene chloride (DCM):hexane and reduced in volume to 100µl under a gentle stream of nitrogen. The resulting extracts were analyzed by high-resolution gas chromatography mass spectrometry (HRGC/HRMS) on a Micromass Ultima mass spectrometer coupled to an Agilent 6890 GC equipped with a CTC A200s autosampler. The GC injection port was configured for split/splitless injection at a temperature of 280°C. Gas

chromatographic separation prior to MS was achieved using a 60 m X 0.25 mm X 0.25 mm DB5 MS column. The GC column was maintained at 80°C for 1 minute, then ramped at 20°C/min to 170°C, held for 12 min and then ramped at 2°C/min to 285°C and held for an additional 24 min. Helium was used as the carrier gas in constant pressure mode. Sample ionization was performed by electron impact (EI) at an electron voltage ranging from 30 to 40eV depending on the optimization parameters of the instrument. Source temperature was 270°C and the resolving power of the analyzer was 10,000. The mass spectrometer was operated in SIM mode using a total of 8 function groups to analyze the suite of methylated OH-PCB congeners. A total of 47 identified OH-PCB (AccuStandard, Inc., New Haven, CT, USA) congeners were assessed in plasma. Utilizing the nomenclature of Maervoet et al. (2004), these congeners included: 4-HO-CB1, 2-HO-CB2, 4-HO-CB2, 2'-HO-CB5, 2'-HO-CB9, 3-HO-CB9, 4-HO-CB9, 2-HO-CB12, 3'-HO-CB14, 4-HO-CB18, 2'-HO-CB26, 4-HO-CB26, 2'-HO-CB30, 3-HO-CB30, 4'-HO-CB30, 4'-HO-CB50, 4-HO-CB57, 2'-HO-CB61, 3'-HO-CB61, 4'-HO-CB61, 3'-HO-CB65, 4-HO-CB65, 2'-HO-CB66, 2'-HO-CB69, 4'-HO-CB69, 4'-HO-CB86/113, 4'-HO-CB88, 2'-HO-CB106, 4'-HO-CB106, 4-HO-CB107, 2'-HO-CB112, 3-HO-CB118, 4'-HO-CB121, 4'-HO-CB130, 3'-HO-CB138, 4-HO-CB146, 4'-HO-CB159, 4-HO-CB165, 4'-HO-CB172, 3'-HO-CB180, 4-HO-CB187, 4-HO-CB193, 4'-HO-CB199, 4-HO-CB202, 4,4'-diOH-CB202, and 4'-HO-CB208 (Maervoet et al., 2004). The quantification of these congeners used external calibration curves. HRGC/HRMS permitted the identification of numerous unknown peaks as OH-PCBs. Total known plasma OH-PCBs were calculated as the sum of the congeners for which standards were available, while total plasma OH-PCBs were calculated as the sum of the identified and unidentified congeners. All OH-PCBs were reported as wet weight concentrations.

***Adipocyte Area Measurements***

Chapter 2 describes the procedure for adipocyte area measurements of the superficial, middle, and deep blubber layers of these bottlenose dolphins in detail. Briefly, H&E slides were viewed with a Zeiss AxioVert S100 microscope, and color

images were acquired with a Hamamatsu C4742-95 digital camera (Hamamatsu Corporation, Hamamatsu City, Japan). Contiguous images were captured along the entire blubber depth (from the epidermis to the deep blubber layer). Images were consistently acquired every 2.35 mm and were analyzed using Scion Image Beta 4.02 software (2000 Scion Corporation, National Institutes of Health, USA). Within each image or blubber depth interval, a 1 mm x 1mm box was positioned approximately in the center. Adipocyte cell cross-sectional areas were calculated using an area tool in Scion Image and estimated for that specific blubber depth interval by averaging areas of the cells that intersected the upper left diagonal. Adipocyte areas for each blubber depth interval were combined based on the categorization of each interval as superficial, middle, or deep layer (as previously discussed) and averaged for a layer specific measurement. The blubber depth interval was not included in the analysis if it overlapped two layers. All measurements were performed blindly without knowing the animal's identification.

***Statistical Analyses***

Table 1 reviews the objectives and corresponding statistical tests used to determine the interrelationships among CYP1A1 expression, PCBs and OH-PCBs, and blubber dynamics in these bottlenose dolphins. "Original" and "modified" CYP1A1 staining scores were $\log_{10}$ transformed to meet normality assumptions. Correlation analysis was completed to relate "original" and "modified" average staining scores. Separate three-factor general linear models (GLM) were used to investigate the effects of geographic location (CHS vs. IRL), age class (subadult vs. adult), and sex (male vs. female) on average CYP1A1 "modified" staining scores, blubber $TEQ_{98}$, blubber total PCB, plasma $TEQ_{98}$, plasma total PCB, and plasma OH-PCB concentrations. A four-factor GLM with layer as a repeated measure was used to investigate the effects of geographic location, age class, sex, and blubber layer (superficial vs. middle vs. deep) on depth-specific CYP1A1 staining intensity, "modified" occurrence, and "modified" staining scores. Statistical tests were completed on two data sets. One data set included

males and non-pregnant, non-lactating females (N = 61), while the second data set included males and all females (N = 71).

Linear regression analysis was used to determine the relationship between the average "modified" CYP1A1 staining scores of the entire blubber versus blubber $TEQ_{98}$, blubber total PCB, plasma $TEQ_{98}$, and plasma total PCB concentrations. Linear regression analysis was also used to examine the relationship between depth-specific CYP1A1 expression versus plasma $TEQ_{98}$ and plasma total PCB concentrations. The data set combined males and non-pregnant, non-lactating females from both geographic locations (N = 48). Similar linear regression analysis was completed for CHS (N = 19) and IRL (N = 21) males but this analysis also included layer specific adipocyte areas and age as additional independent variables to test in linear regression models. The relationships between CYP1A1 depth-specific expression and blubber chemical concentrations were not performed because blubber chemical analysis was completed on the entire blubber and not the layers.

Linear regression analysis was also used to determine the relationship between blubber $TEQ_{98}$, blubber total PCB, plasma $TEQ_{98}$, plasma total PCB, and plasma total OH-PCB concentrations versus age in CHS (N = 19) and IRL (N = 21) males. Non-linear regression analysis was used to examine the relationship between blubber $TEQ_{98}$, blubber total PCB, plasma $TEQ_{98}$, plasma total PCB, and plasma OH-PCB concentrations versus age in CHS (N = 12) and IRL (N = 6) females.

Separate one-way ANOVAs were used to compare average CYP1A1 "modified" staining scores, total blubber PCB, and blubber $TEQ_{98}$ levels among CHS females of varying reproductive states (subadults, adults with calves, pregnant, lactating, and simultaneously pregnant, lactating). A two-factor GLM with blubber layer as a repeated measure was used to investigate the effects of reproductive status on depth-specific CYP1A1 expression in CHS females. Linear regression analysis was used to determine the relationship between the average "modified" CYP1A1 staining scores of the entire blubber versus blubber $TEQ_{98}$, blubber total PCB, plasma $TEQ_{98}$, plasma total PCB concentrations, and average adipocyte area in CHS (N = 12) and IRL (N = 7) females.

Linear regression analysis was also used to examine the relationship between depth-specific CYP1A1 expression versus plasma $TEQ_{98}$ levels, plasma total PCB concentrations, and layer specific adipocyte area in CHS and IRL females. Backward stepwise multiple regression was used to investigate both blubber $TEQ_{98}$ levels and adipocyte areas as factors in depth-specific CYP1A1 expression in CHS females. The effect of lactation day on depth-specific CYP1A1 expression was determined by performing linear regression analysis on CHS females captured with calves, where calf length was the independent variable and CYP1A1 expression of the superficial, middle, and deep blubber served as the dependent variables.

Concentrations of all OH-PCB congeners were $\log_{10}$ transformed to meet normality assumptions. Linear regression analysis was used to determine the relationship between depth-specific CYP1A1 expression versus total identified plasma OH-PCBs and total identified/unidentified plasma OH-PCBs. Linear regression analysis was then used to determine the relationship between CYP1A1 expression in the deep blubber layer and individual OH-PCB congeners. The data set combined males and females (including pregnant and lactating dolphins) from both geographic locations (N = 59).

In all statistical tests, a pre-determined alpha of 0.05 was used. Tests for normality were completed using the Shapiro Wilk test. The equality of variances was examined using the F-test in the case of two variances and the Levene's test in the case of several variances. In cases where ANOVA assumptions were violated, data transformations were performed. Models were run without the highest order interaction term if the term was not significant. Effects were statistically evaluated using the correct mean-square error. If a significant effect was discovered, pair-wise comparisons were conducted using the Tukey post hoc comparison test with a pre-determined alpha of 0.05. Statistical analyses of the data used SYSTAT Version No. 11.00.01 (Systat Software Inc., Richmond, CA).

## RESULTS

### *CYP1A1 Expression in Skin-Blubber Biopsies*

CYP1A1 expression in skin-blubber biopsies was limited to cells in the blubber. Basale, spinosum, corneum, and melanocyte cells of the epidermis did not express CYP1A1. In the blubber, CYP1A1 expression was strongest and most frequently observed in vascular endothelial cells (Figure 3). CYP1A1 staining was occasionally detected in fibroblasts and arteriole smooth muscle cells but never in adipocytes, elastin, or collagen fibers in the blubber. Therefore, in this study, CYP1A1 scores were reported only for vascular endothelial cells of arterioles and capillaries.

CYP1A1 staining scores were determined using two approaches, the "original" and a "modified" method. An exponential correlation existed between the average original CYP1A1 and the average modified CYP1A1 staining scores of vascular endothelial cells (Figure 4A). A significant linear correlation existed between log average original CYP1A1 and log average modified CYP1A1 staining scores of vascular endothelial cells (Figure 4B; $N = 72$; $R = 0.94$; $P < 0.000001$). The modified technique of scoring was more quantitative and less subjective because cells that expressed CYP1A1 were counted rather than given an arbitrary occurrence score from 0 to 3. For this reason, it was decided to perform statistics and display figures using the CYP1A1 modified staining scores. To compare staining scores to previously published studies, staining scores utilizing the "original" method were also reported (see Table 2).

### *Blubber and CYP1A1 Stratification*

Histological analysis revealed that blubber was morphologically stratified into three layers, as reported previously for these live-captured bottlenose dolphins (Figure 3A) (Chapter 2). These layers are referred to as the "superficial", "middle", and "deep" blubber layers, following the terminology published by previous investigators (Montie et al., 2006; Struntz et al., 2004). Chapter 2 describes the blubber cellular characteristics of these bottlenose dolphins in more detail. Briefly, structural fiber areas were consistently

higher in the superficial blubber layer as compared to the middle layer; the fibers increased in the deep layer near the border of the sub-dermal connective tissue sheath and muscle layer. Adipocyte numbers varied significantly across the blubber depth, with more adipocytes in the middle layer. Adipocyte cross-sectional areas were largest in the middle region, and smallest in the superficial and deep blubber layers. The smaller adipocytes in the deep blubber layer, along with other findings discussed in Chapter 2, provided evidence that this layer is more dynamic with regard to blubber lipids.

We hypothesized that CYP1A1 expression in the blubber would be stratified. When we tested this hypothesis, CYP1A1 expression in vascular endothelial cells was significantly different between the superficial, middle, and deep blubber layers of male and female (non-pregnant and non-lactating) CHS and IRL bottlenose dolphins. Vascular endothelial cells in the middle and deep blubber layers expressed higher levels (i.e. the intensity score) of CYP1A1 than endothelial cells in the superficial blubber layer (Figure 5A; N = 61; P = 0.0000105 for both comparisons). The deep blubber layer contained significantly more vascular endothelial cells expressing CYP1A1 (i.e. the "modified" occurrence score) than both the superficial and middle blubber layers (Figure 5B; N = 61; P = 0.001 and P = 0.038, respectively). The CYP1A1 "modified" staining score, the product of the intensity and "modified" occurrence score, was significantly different between the blubber layers (Figure 5C; N = 61; P = 0.0000001). The deep blubber layer contained the highest CYP1A1 staining score, followed by the middle, and then the superficial layer.

***Effect of Geographic Location, Age Class, and Sex on CYP1A1 Expression***

Enlightened by the findings that CYP1A1 expression differed between the blubber layers, and that the highest expression occurred in the deep blubber, we felt it was important to consider both overall scores of the total blubber and depth-specific staining scores when comparing CYP1A1 expression between geographic locations, age classes, and sexes. Evaluating CYP1A1 expression for the entire blubber sample may obscure effects that would otherwise be significant if a more detailed, layer-specific

examination was undertaken. With this in mind, a four-way general linear model (GLM), with the blubber layer as a repeated measure, was used to examine depth-specific CYP1A1 expression differences between geographic location, age class, gender, and all relevant interactions for males and non-lactating, non-pregnant females.

The overall CYP1A1 staining score of vascular endothelial cells in the total blubber was not significantly different between CHS and IRL dolphins (Table 3; males and non-lactating, non-pregnant females; N = 61; P = 0.06). However, CHS and IRL dolphins differed in depth-specific CYP1A1 expression (Table 3; Figure 6A; N = 61; P = 0.0033). CHS dolphins had significantly higher CYP1A1 staining scores in the deep blubber compared to IRL dolphins (P = 0.0000043) but there were no differences between locations in CYP1A1 staining in the superficial or middle layers (P = 0.148 and P = 0.057, respectively). Furthermore, CHS and IRL dolphins exhibited different depth-specific CYP1A1 expression patterns (Table 3; Figure 6A). In CHS dolphins, CYP1A1 expression levels in the deep blubber layer was significantly higher than that in the superficial and middle blubber (P = 0.00063 and P = 0.0000055, respectively). In IRL dolphins, CYP1A1 was less stratified and no significant differences existed between the layers (Table 3). The difference in CYP1A1 expression and depth-specific patterns between geographic locations was observed in both sexes and both age classes (Figure 6D).

The overall CYP1A1 staining score of vascular endothelial cells in the blubber was not significantly different between reproductively immature subadult dolphins and adult dolphins (males and non-lactating, non-pregnant females; Table 3; N = 61; P = 0.65). However, subadult dolphins had significantly higher CYP1A1 expression than adults in the superficial blubber layer (P = 0.00019) but no differences were found in the middle or deep layers (P = 0.237 and P = 0.809). In adult dolphins, CYP1A1 expression was stratified across the blubber layers, with the highest staining scores occurring in the deep blubber layer, followed by the middle, and then the superficial blubber layer (Table 3). Reproductively immature subadult dolphins did not display this pattern; CYP1A1 was uniformly expressed across the layers. The difference in CYP1A1 expression and

depth-specific patterns between age classes was observed in dolphins from both locations and both sexes (Figure 6D).

Males and non-lactating, non-pregnant females did not differ in overall or depth-specific CYP1A1 expression in vascular endothelial cells ($N = 61$; $P < 0.05$; data not shown). Because female bottlenose dolphins have been shown to transfer a majority of their PCB burden to their calf during reproduction (Wells et al., 2005), we also performed similar three-way ANOVAs including males and all females (including pregnant and lactating individuals) to determine any sex differences. However, overall and depth-specific CYP1A1 expression in vascular endothelial cells did not differ between males and females ($N = 71$; $P < 0.05$; data not shown).

***Relationship between PCB Concentrations and CYP1A1 Expression***

Non-ortho and mono-ortho PCB congeners are important contributors to CYP1A1 induction in wildlife. Hence, it was important to determine if CYP1A1 expression in vascular endothelial cells was related to the concentration of these contaminants. Total Toxic Equivalents ($TEQ_{98}$) relative to TCDD were calculated for relevant non-ortho and mono-ortho PCBs using mammalian Toxic Equivalency Factors ($TEF_{98}$) (van den Berg *et al*. 1998). As previously stated, CHS dolphins had significantly higher CYP1A1 expression in the deep blubber layer compared to IRL dolphins (Figure 6A). Similarly, the blubber $TEQ_{98}$ concentrations (ng/g wet wt) were significantly higher in CHS compared to IRL dolphins (males and non-pregnant, non-lactating females; $N = 56$; Figure 6B; Table 3; $P = 0.0019$).

We examined the relationship between CYP1A1 expression of vascular endothelial cells and blubber and plasma $TEQ_{98}$ concentrations for male and non-lactating, non-pregnant female dolphins combined from both CHS and IRL locations. The log overall CYP1A1 staining score through the whole blubber section showed an increasing trend with blubber $TEQ_{98}$ concentrations (ng/g wet wt), although this was not significant (Figure 7A; Table 4). The log overall CYP1A1 staining score through the whole blubber section showed a significant linear increase with plasma $TEQ_{98}$

concentrations (ng/g wet wt) (Figure 7B; Table 4). With regard to depth-specific expression, the log CYP1A1 staining score of the deep blubber layer displayed a significant positive linear relationship with plasma $TEQ_{98}$ concentrations (ng/g wet wt) (Figures 7C; Table 4). However, no significant relationships existed for the superficial or middle blubber layers.

For CHS and IRL males separately, we investigated the relationship between plasma and blubber $TEQ_{98}$ concentrations and CYP1A1 expression of vascular endothelial cells (Tables 4). Different patterns were observed for CHS and IRL male dolphins. IRL males showed a significant negative relationship between log overall CYP1A1 staining scores through the whole blubber and blubber $TEQ_{98}$ concentrations (ng/g wet wt), while CHS males did not exhibit this pattern (Figures 8A and 8B; Table 4). However, IRL males did not display this pattern when TEQs were normalized for lipid weight. Furthermore, IRL males exhibited a significant positive relationship between log CYP1A1 staining scores of the superficial, middle, and deep blubber layers versus plasma $TEQ_{98}$ concentrations (ng/g wet wt.), while CHS males did not follow this relationship (Figure 8C and 8D; Table 4).

CYP1A1 expression in vascular endothelial cells in the blubber could be dependent on movement of AHR agonists from adipocytes across endothelial cells into the circulatory system (i.e which could occur during lipid mobilization events), as hypothesized by Angell et al. (2004). During lipid mobilization events, adipocyte cross sectional areas, particularly in the deep blubber layer, have been shown to decrease in size in cetaceans, as observed in starved harbor porpoises (Koopman et al., 2002), emaciated bottlenose dolphins (Struntz et al., 2004), and lactating bottlenose dolphins (Chapter 2). Hence, we tested the hypothesis that CYP1A1 expression in vascular endothelial cells would be highest in bottlenose dolphins with the lowest adipocyte cross-sectional areas. The results indicated that both CHS and IRL male dolphins exhibited a significant negative linear relationship between log CYP1A1 staining scores and adipocyte areas in the deep blubber layer but not the superficial or middle layers (Figure 8E and 8F; Table 4).

***Relationship between Reproduction and CYP1A1 Expression***

Males and females often show different patterns of blubber PCB accumulation with age because female cetaceans transfer PCBs to their offspring. In this study, total blubber PCB concentrations (ug/g wet wt) of males increased throughout their lifetime, while levels in females decreased dramatically after reproductive maturity (Figures 9A and 9B; Tables 5 and 6). The total blubber $TEQ_{98}$ levels (ng/g wet wt) did not follow this pattern (Figures 9C and 9D; Tables 5 and 6). Males did not display a significant increase in $TEQ_{98}$ concentrations with age. However, $TEQ_{98}$ levels in CHS females decreased at the time of reproductive maturity, in a non-linear pattern similar to that of total blubber PCBs.

Considering the dramatic decrease in total blubber $TEQ_{98}$ concentrations starting at the time of reproductive maturity, it was important to investigate average and depth-specific CYP1A1 expression in CHS females of various reproductive categories. The females captured included reproductively immature subadults (N = 3), adults captured with calves (N =2), pregnant (N = 2), lactating (N = 3), and simultaneously pregnant and lactating (N = 2) dolphins. We hypothesized that in lactating dolphins, the mobilization of lipids and AHR agonists would induce CYP1A1 of vascular endothelial cells, specifically in the more dynamic, deep blubber layer. The results showed that the overall CYP1A1 staining score of the entire blubber did not differ among the female life history categories (N =12; P = 0.65; data not shown). However, depth-specific differences in CYP1A1 expression were observed (Figure 10A; P = 0.0006). Most interestingly, in the deep blubber layer, simultaneously pregnant-lactating females had the highest CYP1A1 staining scores of all females, and those scores were significantly larger than those of subadults (P = 0.022).

Females of various reproductive states exhibited different depth-specific CYP1A1 expression patterns (Figure 10A; N = 12; P = 0.0006). In subadults and pregnant females, CYP1A1 levels were not significantly different among the superficial, middle, and deep blubber layers (Figure 10A; P > 0.05 for all comparisons). However, adult

CHS females contained higher CYP1A1 staining scores in the deep blubber compared to the superficial and middle layers (P = 0.004 and P = 0.038, respectively). Lactating dolphins followed a similar pattern (P = 0.0002 and P = 0.00034). Simultaneously pregnant and lactating females contained higher CYP1A1 expression in the deep blubber compared to the superficial layer (P = 0.0003) but not the middle.

We investigated whether PCB concentrations in CHS females could explain the differences in CYP1A1 staining scores and depth-specific patterns between females of different reproductive states. Subadults had significantly higher blubber $TEQ_{98}$ concentrations (ng/g wet wt) than lactating and pregnant-lactating females (Figure 10C and 11A; P = 0.008 and P = 0.036, respectively). This was consistent with the high CYP1A1 expression in the superficial blubber observed in subadults (Figure 10A). When we explored the relationship between CYP1A1 expression and $TEQ_{98}$ concentrations, CHS females did show a significant relationship between log overall CYP1A1 staining score of the entire blubber and blubber $TEQ_{98}$ concentrations normalized for lipid weight (Table 7).

To investigate blubber $TEQ_{98}$ levels and adipocyte areas as factors in depth-specific CYP1A1 expression, we used backward stepwise multiple regression to determine the significance of these factors, focusing on CHS females because of the diversity in reproductive states (N = 12). Blubber $TEQ_{98}$ concentration was the only significant predictor for CYP1A1 staining scores of the superficial blubber layer (Figure 11B, 11C; $\beta_1 = 15.94$; $R^2 = 0.37$; P = 0.04). For the middle and deep blubber, $TEQ_{98}$ levels and adipocyte areas were not significant factors involved in CYP1A1 expression (Figure 11B, 11D, and 11E). We also tested similar multiple regression models but excluded the two pregnant females (N =10). In the superficial blubber layer, CYP1A1 was significantly related to blubber $TEQ_{98}$ concentrations but not adipocyte areas, similar to the previous data set ($\beta_1 = 17.55$; $R^2 = 0.55$; P = 0.01). No factors were significant in predicting CYP1A1 in the middle blubber layer. For the deep blubber layer, CYP1A1 was dependent on both the blubber $TEQ_{98}$ levels and the adipocyte area (Figure 11F; $R^2 = 0.83$; $\beta_1 = 13.75$ and $\beta_2 = -0.00097$, respectively; $P_1 = 0.01$ and $P_2 = 0.0006$, respectively).

To further explore the effect of lactation on CYP1A1 expression, we investigated CYP1A1 staining scores in CHS mothers captured with calves. The calf length was used as a surrogate measure for the number of days the respective mother had been lactating. We hypothesized that the increased energetic demands to sustain a larger calf would increase the lipid and contaminant flux across the mother's endothelial cells, specifically in the more dynamic deep layer. Therefore, we expected CYP1A1 expression of the deep blubber to be the highest in mothers with the largest calves. Previous results in Chapter 2 showed that the mother's adipocyte areas significantly decreased with calf length in the deep blubber but not the superficial or middle layers. When depth-specific CYP1A1 staining scores of mothers captured with calves was related to calf length, a significant positive relationship existed for the deep blubber but not the superficial or middle layers (Figure 12A; $\beta_1 = 0.015$; $R^2 = 0.72$; $P = 0.015$ for the deep blubber layer). Blubber $TEQ_{98}$ concentrations (ng/g wet wt) and calf length did not show a significant relationship (Figure 12B).

***Relationship between CYP1A1 Expression and OH-PCBs***

CYP1A, CYP2B, and possibly other CYPs are responsible for the metabolism of PCB parent congeners, resulting in the production of OH-PCB metabolites. The concentrations of identified and unidentified OH-PCB congeners in the plasma of these dolphins have been reported (Houde et al., 2006). In the data set examined in our study, the total concentrations of identified OH-PCBs in plasma were nineteen times higher in CHS dolphins compared to IRL animals (Table 2). In addition, the amount of lower chlorinated OH-PCB congeners as a percentage of the total OH-PCB mix was significantly higher in the CHS animals, while the higher chlorinated congeners were more prevalent in the IRL dolphins (Table 8).

To determine if OH-PCB concentrations in the plasma were positively related to CYP1A1 expression in the blubber, we performed linear regression analysis in which CYP1A1 expression was the independent variable and OH-PCB concentration served as the dependent variable. Combining males and females (including pregnant and lactating

females; N=59) from both CHS and IRL, total identified OH-PCBs and total unidentified OH-PCBs were both positively related to CYP1A1 expression in the deep blubber layer but not the superficial or middle layers ($\beta_1 = 0.33$, $R^2 = 0.08$, $P = 0.02$; $\beta_1 = 0.39$, $R^2 = 0.14$, $P = 0.003$). In light of these findings, individual OH-PCB congeners were tested to determine if their concentrations were correlated with deep blubber CYP1A1 expression (Table 8). The concentrations of 4-HO-CB18, 2'-HO-CB26, 4-HO-CB26, 2'-HO-CB69, 3-HO-CB118, 3'-HO-CB138, 4'-HO-CB159, and 3'-HO-CB180 were positively correlated with deep blubber CYP1A1 levels.

## DISCUSSION

### *CYP1A1 Expression in Skin-Blubber Biopsies*

CYP1A1 expression was strongest and most frequently observed in vascular endothelial cells of arterioles and capillaries, similar to other cetacean studies on CYP1A1 expression in the integument (Angell et al., 2004). CYP1A1 was occasionally detected in fibroblasts and smooth muscle cells, but no staining was observed in cells of the epidermis, adipocytes, or elastin and collagen fibers, also consistent with previous research (Angell et al., 2004). Therefore, the focus of this paper was on CYP1A1 staining in vascular endothelial cells.

From fish to mammals, the endothelium is a major site of extra-hepatic CYP1A1 induction by PHAHs or PAHs (Guiney et al., 1997; Stegeman et al., 1989). Skin-blubber slices from sperm whales exposed to BNF showed a dose-dependent increase in endothelial cell staining scores (Godard et al., 2004). Endothelial cell lines derived from kidney and lung of the bottlenose dolphin exposed to TCDD and BNF displayed a dose-dependent increase in CYP1A1 activity (Garrick et al., 2006). CYP1A1 was highly expressed in endothelium of various organs from Arctic and St. Lawrence beluga whales (Wilson et al., 2005).

CYP1A1 staining scores were determined using two approaches, the "original" and a "modified" method. The data analysis was completed using the modified staining

scores. However, the overall CYP1A1 staining scores of the entire blubber and depth-specific original CYP1A1 staining scores are reported for comparison to other CYP1A1 cetacean integument studies (Table 2). The overall "original" score for CHS male adults (N = 24) was 3.7, and the range was 0.7 to 11.7; the mean "original" score for the deep layer was 5.8. The IRL male adults (N = 19) had a lower score of 2.4, with a range of 0.0 to 9.9; the mean score for the deep layer was 2.9. Previous studies of CYP1A1 in the integument of bottlenose dolphins reported similar staining scores. Biopsy samples from Western Atlantic bottlenose dolphins (N = 141) obtained in 1998 showed staining scores of 3.6 ± 2.6, similar to the scores reported in CHS male adults (Angell et al., 2004). Stranded bottlenose dolphins from the Gulf of Mexico sampled in 1994 (N = 6) displayed mean staining scores of 4.7 ± 2.7 (Angell et al., 2004). Live-captured and released bottlenose dolphins from Sarasota, FL sampled in the summer of 1999, 2000, and 2001 displayed mean staining scores of 3.5 for the "upper" dermis and 5.0 for the "lower" dermis (Wilson, 2003). CHS and Sarasota dolphins show similar CYP1A1 staining scores in the deep blubber layer (i.e. the "lower" dermis).

***Blubber and CYP1A1 Stratification***

Histological analysis revealed that the blubber was morphologically stratified into three layers, as described in Chapter 2 (Figure 3). These layers are referred to as the superficial, middle, and deep blubber layers, following the terminology of Struntz et al. (2004). In bottlenose dolphins in our study and Struntz et al. (2004), the superficial blubber layer was characterized by low adipocyte cell counts and small adipocyte cross-sectional areas; the middle blubber layer contained more and larger adipocytes; and the deep blubber layer had more but smaller adipocytes. These patterns in morphology support the "blubber layer" hypothesis, originally proposed by Aguilar and Borrell (1990), which since then has gained more support (Aguilar and Borrell, 1990; Koopman et al., 1996; Koopman et al., 2002). This hypothesis states that for the thorax site in odontocetes, the "outer" blubber layer is metabolically "inert" and more important in anchoring the epidermis, while the "inner" blubber is "dynamic" with regard to lipid

mobilization and deposition. However, in bottlenose dolphins, the histological findings support a three-layered model (Struntz et al., 2004)(also see Chapter 2). The numerous structural fibers in the superficial blubber layer support the epidermis, while adipocytes in the middle blubber store lipid, which provides insulation. The smaller adipocytes in the deep blubber layer may contain lipids that are used to meet energetic demands, as inferred from the reduction of this "inner" blubber layer in starved harbor porpoises (Koopman et al., 2002).

CYP1A1 expression in vascular endothelial cells was significantly different among the superficial, middle, and deep blubber layers in the bottlenose dolphins in this study (Figure 5). These findings confirm previous CYP1A1 research in bottlenose dolphins live-captured in Sarasota, FL, which showed significantly higher CYP1A1 staining scores in the "lower" dermis compared to the "upper" dermis (Wilson et al., 2003). Our study extends the research of Wilson et al. (2003) by revealing a three-layered model for bottlenose dolphin blubber, in which each of these three layers was given a CYP1A1 intensity score, a less subjective occurrence score, and an overall "modified" occurrence score. Furthermore, detailed histological analysis provided mean adipocyte cross-sectional areas for each blubber layer that was used to determine the influence of blubber dynamics and transport of AHR agonists on CYP1A1 expression in the integument.

The transport of AHR agonists across the endothelial cell from the adipocyte to the capillary or vice versa may be an important factor in CYP1A1 induction in cetacean integument, as suggested by Angell et al. (2004). Hence, it is not surprising that the amount of CYP1A1 protein (the intensity score) was highest in endothelial cells of the deep blubber (Figure 5A). The smaller adipocytes in this layer, as described in Chapter 2, suggest that the lipid here is preferentially mobilized, and perhaps lipophilic contaminants follow this movement, inducing CYP1A1 to a greater degree in deep layer endothelial cells. This is supported by higher total PCB concentrations in the "outer" versus "inner" blubber of ringed seals (*Phoca hispida*), fin whales (*Balaenoptera physalus*), and in male sei whales (*B. borealis*) (Aguilar and Borrel, 1991; Severinsen et

al., 1999). Furthermore, the mobilization of lipids from the "inner" layer may be facilitated by the temperature gradient that exists from the epidermis to the subdermal sheath (Castellini, 2002; Koopman et al., 2002). The inner layer is warmer and experiences higher blood perfusion, while the "outer" layer is colder because of reduced blood flow to conserve heat (Pabst et al., 1999b; Pond and Mattacks, 1985), which could physically impede lipid mobilization (Koopman et al., 2002). The reduction in blood flow to the superficial blubber would decrease the exposure of cells in this layer to circulating AHR agonists, which could partly explain the lower intensity scores observed in this layer (Figure 5A).

The total number of vascular endothelial cells per $mm^2$ expressing CYP1A1 was significantly higher in the deep blubber compared to the superficial and middle layers (Figure 5B). This result could be explained by preferential mobilization of AHR agonists in the deep layer. However, the deep blubber is more vascularized than the superficial and middle layers and hence contains more endothelial cells. Yet, the amount of CYP1A1 protein (i.e. the intensity score) was significantly higher in the middle and deep layers compared to the superficial blubber. This favors the hypothesis that AHR agonists in the deeper blubber are preferentially mobilized, inducing CYP1A1 to a greater degree in deep layer endothelial cells. Future research should combine studies comparing the degree of vascularization, the number of endothelial cells, the contaminant concentrations, and CYP1A1 staining scores between the blubber layers.

### *Effect of Geographic Location on Depth-specific CYP1A1 Expression*

The importance of measuring depth-specific CYP1A1 expression became apparent when comparing CYP1A1 levels between geographic locations. The overall CYP1A1 staining score of the entire blubber was not significantly different between CHS and IRL dolphins; however, CHS animals had significantly higher CYP1A1 levels in the deep blubber (Table 3; Figure 6A). Examining CYP1A1 expression by layer revealed differences not observed with overall values of the total blubber. These findings reinforce the necessity of carefully interpreting the results of cetacean biomarker studies

in which skin-blubber biopsies do not contain full-depth samples or at least a portion of the deep layer. Projectile biopsy techniques often do not acquire a representative sample of the deep blubber, particularly for cetaceans with thick blubber (i.e. killer whales, sperm whales, and mysticete species). Biomarker results using this sampling technique should be viewed with caution.

### *PCB Concentrations and CYP1A1 Induction*

Why did CHS dolphins display higher CYP1A1 levels in the deep blubber compared to IRL dolphins? Were these observations related to differences in the concentrations of AHR agonists? Our results support this hypothesis. CHS dolphins contained higher blubber $TEQ_{98}$ concentrations (ng/g wet wt) than IRL dolphins (Figure 6; Table 3). For all male and non-pregnant, non-lactating females, overall CYP1A1 levels of the total blubber linearly increased with blubber (ng/g lipid wt) and plasma (ng/g wet wt) $TEQ_{98}$ levels, while CYP1A1 staining scores in the deep blubber linearly increased with plasma $TEQ_{98}$ concentrations (Figure 7; Table 4).

Previous marine mammal studies have shown that CYP1A1 expression in endothelial cells is directly related to the concentration of AHR agonists. First, when endothelial cell lines derived from bottlenose dolphin kidney and lung were exposed to TCDD and BNF, they displayed a dose-dependent increase in CYP1A1 activity (Garrick et al., 2006). Second, skin-blubber slices obtained from sperm whales and then exposed to BNF *in vitro* showed a dose-dependent increase in CYP1A1 staining scores of vascular endothelial cells (Godard et al., 2004). Third, captive river otters fed crude oil exhibited a significant relationship between the concentrations of hydrocarbons in the diet and CYP1A1 staining scores in the vascular endothelial cells of skin biopsies (Ben-David et al., 2001).

### *CYP1A1 Expression and Blubber Lipid Mobilization*

*CHS versus IRL*. There was evidence that blubber lipid mobilization was an important factor in CYP1A1 expression in CHS and IRL dolphins. As previously

discussed, mobilization events preferentially use blubber lipids in the deep blubber, causing adipocytes to shrink (Koopman et al., 2002; Struntz et al., 2004)(also see Chapter 2). During these events, it is likely that AHR agonists stored in adipocytes are transported across endothelial cells into the circulatory system, inducing CYP1A1. In this study, we found supporting evidence for this hypothesis. CYP1A1 expression of vascular endothelial cells in the deep blubber of both CHS and IRL dolphins was greater in animals with smaller adipocytes (Table 4; Figure 8E and 8F). Furthermore, CYP1A1 levels of CHS and IRL males and non-pregnant, non-lactating dolphins exhibited a significant positive relationship with plasma $TEQ_{98}$ concentrations for the deep blubber layer only (Table 4; Figure 7C).

Bottlenose dolphins in Sarasota, Florida drastically thin their blubber during summer months, when estuarine water temperatures can reach 32$^{o}$C (~90$^{o}$F) (R. Wells, unpublished data). In these dolphins, total circulating PCB levels were much higher in summer than in winter (R. Wells, unpublished data). Blubber thinning may have mobilized lipids and PCBs from the blubber into the circulatory system. Is it possible that CHS and IRL dolphins were in a state of blubber lipid mobilization? IRL and CHS animals were captured during the summer months of July and August 2003, respectively, when blubber thinning would be expected. The transport of blubber lipids and AHR agonists from the adipocyte across the endothelial cell into the circulatory system may have enhanced CYP1A1 induction in the deeper layers.

Seasonal differences in water temperatures between CHS and IRL locations may explain the findings that CHS and IRL dolphins exhibited differences in depth-specific CYP1A1 expression patterns and in the relationship of CYP1A1 staining scores to blubber and plasma $TEQ_{98}$ levels (Figure 6A; Figure 8A-8D). In chapter 2, we hypothesized that CHS dolphins exhibited higher total blubber lipid content, larger adipocytes, and a higher degree of blubber stratification than IRL dolphins because the water temperature was colder in CHS. CHS dolphins exhibited CYP1A1 blubber stratification, while IRL dolphins did not display any significant differences between the blubber layers (Table 3; Figure 6A). One possible explanation could be extensive

shrinkage of adipocytes in the middle blubber in IRL dolphins, concomitant mobilization of lipids and AHR agonists, and CYP1A1 induction of vascular endothelial cells in the middle layer. Hence, CYP1A1 expression would be less stratified in the blubber. However, for CHS dolphins adapting to colder water temperatures, the middle blubber adipocytes remained larger with little mobilization and induction, leading to blubber stratification with regards to adipocyte size and CYP1A1 expression. Furthermore, it is possible that IRL dolphins removed lipid from the adipocytes of all layers (and hence AHR agonists followed), which decreased the blubber $TEQ_{98}$ levels (ng/g wet wt) but increased the plasma concentrations. This could explain why CYP1A1 expression of the superficial, middle, and deep layers was positively related to increasing plasma $TEQ_{98}$ levels in IRL dolphins but not CHS animals (Figures 8A-8D). A more rigorous test of this hypothesis would involve a longitudinal study and collection of blubber biopsies from the same body site during the summer and winter at a geographic location that experiences drastic differences in water temperature.

Other reasons may exist for the different CYP1A1 expression patterns of CHS and IRL dolphins. These differences could be due to the presence of other CYP1A1 inducers such as PAHs, which were not measured in this study. An oil spill in Charleston Harbor, SC during October 2002 may have contributed to the induction of CYP1A1 in Charleston dolphins. This would cloud any relationships between CYP1A1 and $TEQ_{98}$ levels for CHS dolphins. In addition, $TEQ_{98}$ levels were higher in CHS dolphins, and perhaps in highly contaminated CHS males, CYP1A1 induction was repressed through an AHR repressor mechanism (Figure 8D)(Nishihashi et al., 2006). Alternatively, CYP1A1 expression may have been reduced in these highly contaminated males if CYP1A1 was inactivated or endothelial cells were damaged by excess production of reactive oxygen species (Cantrell et al., 1996; Cantrell et al., 1998; Schlezinger et al., 2006; Schlezinger et al., 1999; Toborek et al., 1995).

*Subadults vs. adults*. Subadults and adults exhibited different depth-specific CYP1A1 expression patterns. Adult dolphins displayed greater CYP1A1 blubber stratification than subadults (Table 3; Figure 6D). We speculate that these differences

may be attributed to biaccumulation and blubber dynamics. In chapter 2, we showed that adult dolphins displayed significantly lower total blubber lipid content than subadults. One possible explanation is that as the dolphin's surface-area-to-volume ratio decreases with growth, there is less demand for insulation but greater demand for energy to support growth (Dunkin et al., 2005; McLellan et al., 2002; Struntz et al., 2004). Furthermore, both male and female adults expend energy for reproduction, and this may decrease the lipid content of blubber and mobilize AHR agonists, inducing CYP1A1. The lipids and AHR agonists are preferentially mobilized from the deeper blubber, which may cause the intense stratification of CYP1A1 observed in adults but not in subadults.

*Reproduction.* Male and female cetaceans display different patterns of PCB accumulation (Addison and Brodie, 1987; Borrell et al., 1995; Ross et al., 2000). Generally, cetacean females transfer a large percentage of their contaminant load from blubber to their offspring during lactation (Borrell et al., 1995; Wells et al., 2005). For example, in bottlenose dolphins from Sarasota, Florida, first-born calves have higher PCB concentrations than subsequent calves of similar age (Wells et al., 2005). In the current study, total blubber PCB concentrations increased with age in males, while levels in females decreased dramatically after reproductive maturity (Table 5 and 6; Figure 9A and 9B). Blubber $TEQ_{98}$ levels in CHS females also decreased at the time of reproductive maturity, in a non-linear pattern similar to that of total blubber PCBs. This indicated either maternal transfer of dioxin-like PCBs, biotransformation, or a combination of both elimination pathways.

Lactation represents the largest energetic cost of reproduction in all female mammals (Iversen, 2002). In bottlenose dolphins, the lipid content of milk is approximately 15%, as compared to 3.8% in humans and 3.7% in cows (Costa, 2002). We hypothesized that the mobilization of lipids (and AHR agonists) from adipocytes across endothelial cells, in response to the high energetic costs of reproduction (including milk production), would induce CYP1A1 of vascular endothelial cells. The induction of CYP1A1 in the deep blubber layer would be higher than the superficial or middle layers

because the lipids in adipocytes of the deep blubber layer are the most dynamic. Three aspects of our data support this hypothesis.

The first line of evidence is focused on the differences of depth-specific CYP1A1 expression and blubber $TEQ_{98}$ levels among the CHS female reproductive categories. Subadults and pregnant females had higher CYP1A1 expression in vascular endothelial cells in the superficial blubber layer compared to adults (captured with weaned calves), lactating females, and simultaneously pregnant-lactating dolphins (Figure 10A). The blubber $TEQ_{98}$ concentrations were significantly higher in subadults compared to lactating and pregnant-lactating females, providing an explanation for the higher CYP1A1 in the superficial layer (Figure 10C). However, a different pattern in the deep blubber layer was observed; CYP1A1 expression was highest in simultaneously pregnant-lactating dolphins (Figure 10A), and blubber $TEQ_{98}$ concentrations of the total blubber were significantly lower than subadults (Figure 10C). Furthermore, CYP1A1 was not stratified among the blubber layers in subadults and pregnant females but was stratified in all dolphins captured with calves (adults, lactating, and simultaneously pregnant-lactating dolphins), with the most intense stratification in simultaneously pregnant-lactating dolphins (Figure 10A). Deep blubber adipocytes were the smallest in pregnant-lactating dolphins (as discussed in Chapter 2), suggesting that the combination of pregnancy and lactation increased the energetic demands, and deep blubber lipids were mobilized and used as energy currency. Concurrent mobilization of AHR agonists from the deep blubber adipocytes across endothelial cells could therefore explain the high CYP1A1 levels of vascular endothelial cells in the deep blubber layer and the intense stratification in simultaneously pregnant-lactating dolphins (Figure 10A).

The second line of evidence that supports our hypothesis included the results of the multiple regression analysis that investigated the importance of blubber $TEQ_{98}$ levels and adipocyte area in predicting depth specific CYP1A1 expression. When excluding pregnant females, the total blubber $TEQ_{98}$ levels (positive relationship) and the adipocyte area (negative relationship) were significant predictors of CYP1A1 expression in the deep blubber (Figure 11F), while only the $TEQ_{98}$ factor (positive relationship) was

significant for the superficial layer (Figure 11B). Pregnant females were excluded because these dolphins seem to follow a different pattern. The adipocytes in the deep blubber of pregnant females were the largest of all females – most likely indicating that these adipocytes were in a depositional state (Figure 11E). In this case, we hypothesize that the net flux of lipophilic contaminants would be moving from the diet, into the circulatory system, across endothelial cells, and into the blubber adipocyte.

The third line of evidence is that deep CYP1A1 expression of mothers captured with calves displayed a significant positive relationship with calf length (Figure 12A). It is possible that the increased energetic demands to sustain a larger calf increased the flux of lipid and AHR agonist from blubber adipocytes, across endothelial cells, and into the circulatory system. Previous results provided evidence that mother's adipocyte cross-sectional areas decreased with calf length, specifically in the deep blubber but not the superficial or middle layers (Chapter 2).

*Other Research Studies Involving CYP1A1 Expression and Fat Dynamics.* Many vertebrates, including some cetacean and pinniped species, exhibit marked seasonal cycles of fattening followed by fasting. For example, Arctic Charr (*Salvelinus alpinus*), an anadromous Arctic fish, can double their body weight and increase lipid stores several fold during the summer feeding migration to seawater (Jorgensen et al., 1997a). During the over-wintering period in freshwater, Arctic Charr lipid stores can be totally depleted (Boivin and Power, 1990; Jorgensen et al., 1997a). In a series of laboratory experiments, winter fasting in Arctic Charr resulted in the redistribution of PCBs from lipid stores such as muscle to the liver and brain (Jorgensen et al., 2006). Hepatic CYP1A activities (EROD, pmol/min/mg protein) increased dramatically from the beginning of the over-wintering period (October) to its end (May). These results support our findings that lipid dynamics (and AHR agonist mobilization) is an important factor in CYP1A1 expression.

A limitation in relating lipid dynamics to CYP1A1 induction is the inability to determine whether or not the adipocyte is in a state of deposition or mobilization. Unfortunately, the molecular signaling pathways involved in lipid dynamics of the blubber of marine mammals are presently unknown. It is important to identify cetacean

homologous receptors (e.g. thyroid hormone and adrenergic receptors) (Liu et al., 2003), proteins (e.g. perilipin) (Moore et al., 2005), and enzymes (e.g. hormone-sensitive lipase, adipose triglyceride lipase, and type 2 deiodinase)(Watanabe et al., 2006; Zimmermann et al., 2004) that have been discovered to be important in lipid storage and utilization in humans and rats. A variety of molecular approaches could be used to identify these candidate genes and proteins. This would not only add to a better interpretation of CYP1A1 expression and the mobilization of environmental chemicals in marine mammals but would also provide valuable information on the molecular control of blubber dynamics.

***Relationship between CYP1A1 Expression and OH-PCBs***

In this study, CYP1A1 expression in the deep blubber was significantly higher in CHS dolphins compared to IRL animals (Figure 6A). In addition, the total identified plasma OH-PCB concentrations and the total OH-PCB/PCB ratios were nineteen times and seven times higher, respectively, in CHS dolphins (Table 3). Furthermore, the total blubber $TEQ_{98}$ levels were significantly higher in CHS dolphins compared to IRL animals, which indicates that the exposure to some PCB congeners was higher in CHS dolphins (Table 3). These findings suggest that the CHS dolphin population may have a higher biotransformation rate than the IRL population, metabolizing parent PCBs to OH-PCB metabolites.

No other enzymes besides the cytochrome P450s are known to hydroxylate PCBs. In humans, there are 59 cytochrome P450 enzymes that have been identified and approximately half of these enzymes belong to CYP subfamilies that are known to include enzymes that can metabolize persistent organic pollutants. CYP1A1, CYP2A, CYP2B, and/or CYP3A are involved in PCB metabolism (Letcher et al., 2000; Yoshimura et al., 1987). The PCB residue patterns in cetaceans, including the dolphins in this study, suggest that CYP2B-like enzyme activity is low (Duinker et al., 1989; Norstrom et al., 1992; Tanabe et al., 1988; Weisbrod, 2000). The low rates of metabolism of 2,2',5,5' in pilot and beluga whale and the low rates of other CYP2B

activities including PROD activity in beluga also support this hypothesis (White et al., 1994; White et al., 2000). Therefore, CYP1A1, CYP2A, and CYP3A are more likely involved in PCB metabolism and OH-PCB production in cetaceans.

*In vitro* biotransformation studies with beluga and pilot whale liver microsomes have shown that some OH-PCB congeners are products of CYP1A1 metabolism (White et al., 2000). Lower chlorinated PCB congeners with chlorine substituents at one or both *para* positions, and with vicinal hydrogens at the *ortho-meta* positions are oxidized by CYP1A1 (Ishida et al., 1991; Kaminsky et al., 1981; Mills et al., 1985; Shimada and Sawabe, 1983). Therefore, the lower chlorinated OH-PCB congeners that were significantly higher in CHS dolphins (i.e. OH-PCB18, 4-OH-CB26, 4'-OH-CB69) may be products of CYP1A1 metabolism from parent PCB congeners that fit these chlorine substitution patterns. In addition, the concentration of specific OH-PCB congeners in plasma was significantly related to the expression of CYP1A1 in the deep blubber layer (Table 8). In this study, it is possible that the majority of the lower chlorinated OH-PCB congeners were products of CYP1A1 metabolism. For example, CYP1A1 could theoretically metabolize 2,3',4-trichlorobiphenyl (PCB25) to form the 4-5 epoxide intermediate. This intermediate could then be opened by epoxide hydrolase and the *meta*-hydrogen and *para*-chlorine could undergo a 1,2-shift to form 4-HO-2,3',5-trichlorobiphenyl (4-HO-CB26), a metabolite comprising 31% of the total identified OH-PCBs (Table 8). These findings suggest that biotransformation by CYP1A1 may be important in shaping the pattern of plasma OH-PCB congeners in bottlenose dolphins from the two different geographic locations.

The concentration of total OH-PCBs in the plasma correlated with the expression of CYP1A1 in vascular endothelial cells of the deep blubber but not the superficial or middle layers. It is possible that as AHR agonists moved from the adipocyte and across the endothelial cell in the more dynamic deep layer, CYP1A1 was induced and metabolized select parent PCB congeners to OH-PCB products. Additionally and/or alternatively, PCBs that are hydroxylated by CYP1A1 (e.g. PCB77) may have been transported to the liver where the predominant phase I metabolism occurred, since

cetacean CYP1A1 activity in liver microsomes has been shown to be higher than that in endothelial cells (Garrick et al., 2006; White et al., 2000). If the cellular environment permits the oxidation of PCBs by endothelia CYP1A1 of the deep blubber, the vasculature in the deep blubber could play a role in metabolism of PCBs and the production of OH-PCBs. For example, it is proposed that endothelia CYP1A of the rete mirabile swimbladder capillary network of the eel (*Anguilla rostrata*) may influence the toxicokinetics of AHR agonists (Schlezinger and Stegeman, 2000).

OH-PCBs are similar in structure to the major circulating thyroid hormone 3,3',5,5'-tetraiodo-L-thyroxine (thyroxine or T4) and have been shown to bind the thyroid hormone transport protein, transythyretin (TTR), in humans (Cheek et al., 1999). This may explain the retention of these metabolites in plasma, as described by Houde et al. (2006). Efforts to demonstrate TTR in cetaceans (beluga whales and bottlenose dolphins) have proved unsuccessful using methodologies established for other mammals (St. Aubin, 2001). However, recently, TTR has been identified in the liver of the Atlantic white-sided dolphin (Appendix 5). In these bottlenose dolphins, the degree of retention of these OH-PCB congeners in plasma might then be a function of their binding to TTR, as well as rates of phase II metabolism (e.g. glucuronidation and sulfation) and subsequent elimination.

Certain OH-PCB metabolites such as 4-HO-CB107 have been shown to interfere with the thyroid hormone system in rodent models (Meerts et al., 2004). Therefore, it is important to determine which OH-PCB metabolites are products of CYP1A1 metabolism. White et al. (2000) used a specific inhibitor of CYP2B to illustrate that CYP1A1 in beluga whale liver microsomes converted 3,3',4,4'-tetrachlorobiphenyl (PCB77) primarily to 4-HO-3,3',4,5'-tetrachlorobiphenyl (4'-HO-CB79 or 4'-HO-3,3',4,5'-tetrachlorobiphenyl) and 5-HO-3,3',4,4'-tetrachlorobiphenyl (4-HO-CB77). Performing similar biotransformation studies with bottlenose dolphin liver microsomes using a more comprehensive list of individual non-ortho, mono-ortho, and di-ortho PCB congeners would help elucidate which CYP enzymes are responsible for the formation of specific environmentally relevant hydroxylated metabolites. Expanding this research to include

biotransformation studies using endothelial cell lines derived from bottlenose dolphins would help determine the importance of extra-hepatic metabolism of non-ortho and mono-ortho PCBs, as well as the importance of extra-hepatic production of OH-PCBs (Garrick et al., 2006).

***Implications for Marine Mammal Toxicology and Health Assessment Studies***

Microscopic inspection of the blubber, prior to analysis of CYP1A1, allowed us to understand the biology and independent roles of the blubber layers and incorporate this knowledge in explaining CYP1A1 integument expression in bottlenose dolphins (see Chapter 2). By analyzing depth-specific CYP1A1 levels, we found differences in CYP1A1 expression between CHS and IRL dolphins; CYP1A1 expression in the deep blubber layer was significantly higher in dolphins from CHS as compared to those from IRL. CYP1A1 levels in the deep blubber increased with total plasma $TEQ_{98}$ concentrations, while no such relationship was found for the superficial or middle layers (except for IRL males). We also discovered that blubber dynamics was an important factor in CYP1A1 induction. CYP1A1 expression of vascular endothelial cells in the deep blubber of both CHS and IRL dolphins was negatively related to adipocyte size. Reproduction affected CYP1A1 expression of vascular endothelial cells in CHS females. CYP1A1 expression of the deep layer was highest in simultaneously pregnant-lactating dolphins, and these dolphins contained the smallest adipocytes in the deep blubber. In all dolphins, CYP1A1 expression in the deep blubber layer was significantly related to plasma OH-PCB concentrations. From these data, we speculate that CYP1A1 could be responsible for a large percentage of the identified OH-PCB congeners in CHS dolphins. All these observations would otherwise have been overlooked if the blubber had been examined as one unit, rather than three independent, biologically relevant layers. The depth specific CYP1A1 differences illustrate the necessity to inspect the morphology of blubber and interpret its biology in cetacean health assessment studies, where the skin-blubber biopsy is providing valuable information on changes in gene expression as a response to environmental chemicals.

Understanding the implications of PCBs on marine mammal health requires knowledge of mobilization of these chemicals from the blubber into the circulatory system. In marine mammals, blubber is the primary storage site for persistent organic pollutants, such as PCBs. During periods of lipid mobilization (as occurs during fasting, starvation, adaptation to warmer water temperatures, lactation, or any combination of these factors), stored blubber lipids and AHR agonists maybe mobilized into the circulatory system, reaching target sites and undergoing bioactivation. Mobilization of AHR agonists from the blubber may enhance PCB metabolism and the production of OH-PCBs by induction of CYP1A1 in endothelial cells of the deep blubber and induction of CYP1A1 in hepatocytes. The OH-PCBs may then interfere with thyroid hormone homeostasis.

**REFERENCES**


Addison RF, Brodie PF. 1987. Organochlorine residues in maternal blubber, milk, and pup blubber from grey seals (*Halichoerus grypus*) from Sable Island, Nova Scotia. Canadian Journal of Fisheries and Aquatic Sciences 44:782-786.

Aguilar A, Borrel A. 1991. Heterogeneous distribution of organochlorine contaminants in the blubber of baleen whales: implications for sampling procedures. Marine Environmental Research 31:275-286.

Aguilar A, Borrell A. 1990. Patterns of lipid content and stratification in the blubber of fin whales (*Balaenoptera physalus*). Journal of Mammalogy 71:544-554.

Angell C, Wilson J, Moore M, Stegeman J. 2004. Cytochrome P4501A1 expression in cetacean integument: implications for detecting contaminant exposure and effects. Marine Mammal Science 20:554-566.

Ben-David M, Kondratyuk T, Woodin B, Snyder P, Stegeman J. 2001. Induction of cytochrome P450 1A expression in captive river otters fed Prudhoe Bay crude oil: evaluation by immunohistochemistry and quantitative RT-PCR. Biomarkers 8:218-235.

Blomkvist G, Roos A, Jensen S, Bignert A, Olsson M. 1992. Concentrations of DDTs and PCBs in seals from Swedish and Scottish waters. Ambio 21(8):539-545.

Boivin TG, Power G. 1990. Winter condition and proximate composition of anadromous Arctic charr (*Salvelinus alpinus*) in eastern Ungava Bay, Quebec. Canadian Journal of Zoology 68:2284-2289.

Borrell A, Bloch D, Desportes G. 1995. Age trends and reproductive transfer of organochlorine compounds in long-finned pilot whales from the Faroe Islands. Environmental Pollution 88:283-292.

Bossart GD. 2005. The Indian River Lagoon Health Assessment Project: a sentinel for emerging marine mammal disease and ecosystem health. In: AZA, editor; 2005; Cocoa Beach, Florida.

Brouwer A, Morse DC, Lans MC, Schuur AG, Murk AJ, Klasson-Wehler E, Bergman A, Visser TJ. 1998. Interactions of persistent environmental organohalogens with the thyroid hormone system: mechanisms and possible consequences for animal and human health. Toxicology and Industrial Health 14(1-2):59-84.

Brouwer A, Reijnders PJH, Koeman JH. 1989. Polychlorinated biphenyl (PCB)-contaminated fish induces vitamin A and thyroid hormone deficiency in the common seal (*Phoca vitulina*). Aquatic Toxicology 15(1):99-106.

Cantrell SM, Lutz LH, Tillitt DE, Hannink M. 1996. Embryotoxicity of 2,3,7,8-tetrachlorodibenzo-p-dioxin (TCDD): the embryonic vasculature is a phsyiological target for TCDD-induced DNA damage and apoptotic cell death in medaka (*Oryzias latipes*). Toxicology and Applied Pharmacology 141:23-34.

Cantrell SM, Schlezinger JJ, Stegeman JJ, Tillitt DE, Hannink M. 1998. Correlation of 2,3,7,8-tetrachlorodibenzo-p-dioxin induced apoptotic cell death in the vasculature with embyrotoxicity. Toxicology and Applied Pharmacology 148:24-34.

Castellini M. 2002. Thermoregulation. In: Perrin WF, Wursig B, Thewissen JGM, editors. Encylopedia of Marine Mammals. San Diego, CA: Academic Press.

Cheek AO, Kow K, Chen J, McLachlan JA. 1999. Potential mechanisms of thyroid disruption in humans: interaction of organochlorine compounds with thyroid receptor, transthyretin, and thyroid-binding globulin. Environmental Health Perspectives 107(4):273-278.

Costa DP. 2002. Energetics. In: Perrin WF, Wursig B, Thewissen JGM, editors. Encylopedia of Marine Mammals. San Diego, CA: Academic Press. p 387-394.

Dale EW, Gaines TB, Hayes WJ. 1962. Storage and excretion of DDT in starved rats. Toxicology and Applied Pharmacology. 4:89-106.

DeLong RL, Gilmartin WG, Simpson JG. 1973. Premature births in California sea lions: association with high organochlorine pollutant residue levels. Science 181(4105):1168-1170.

Duinker JC, Hillebrand MTJ, Zeinstra T, Boon JP. 1989. Individual chlorinated biphenyls and pesticides in tissues of some cetacean species from the North Sea and the Atlantic Ocean; tissue distribution and biotransformation. Aquatic Mammals 15(3):95-124.

Dunkin RC, McLellan WA, Blum JE, Pabst D. 2005. The ontogenetic changes in the thermal properties of blubber from Atlantic bottlenose dolphin *Tursiops truncatus*. The Journal of Experimental Biology 208:1469-1480.

Findlay GM, De Freitas ASW. 1971. DDT movement from adipocyte to muscle cell during lipid utilization. Nature 229(63-65):63-65.

Garrick RA, Woodin BR, Wilson JY, Middlebrooks BL, Stegeman JJ. 2006. Cytochrome P4501A is induced in endothelial cell lines from the kidney and lung of the bottlenose dolphin, *Tursiops truncatus*. Aquatic Toxicology 76(3-4):295-305.

Godard CAJ, Smolowitz RM, Wilson JY, Payne RS, Stegeman JJ. 2004. Induction of cetacean cytochrome P4501A1 by B-napthoflavone exposure of skin biopsy slices. Toxicological Sciences 80:268-275.

Guiney PD, Smolowitz RM, Peterson RE, Stegeman JJ. 1997. Correlation of 2,3,7,8-tetrachlorodibenzo-p-dioxin induction of cytochrome P4501A in vascular endothelium with toxicity in early stages of lake trout. Toxicology and Applied Pharmacology 143:256-273.

Hansen LJ, Schwacke LH, Mitchum GB, Hohn AA, Wells RS, Zolman ES, Fair PA. 2004. Geographic variation in polychorinated biphenyl and organochlorine pesticide concentrations in the blubber of bottlenose dolphins from the US Atlantic coast. The Science of the Total Environment 319:147-172.

Hohn AA, Scott MD, Wells RS, Sweeney JC, Irvine AB. 1989. Growth layers in teeth from known-age, free-ranging bottlenose dolphins. Marine Mammal Science 5(4):315-342.

Houde M, Pacepavicius G, Wells RS, Fair PA, Letcher RJ, Alaee M, Bossart GD, Hohn AA, Sweeney J, Solomon KR, Muir DCG. 2006. Polychlorinated biphenyls (PCBs) and hydroxylated polychlorinated biphenyls (OH-PCBs) in plasma of botlenose dolphins (*Tursiops truncatus*) from the Western Atlantic and the Gulf of Mexico.

Ishida C, Koga N, Hanioka N, Saeki HK, Yoshimura H. 1991. Metabolism in vitro of 3,4,3',4'- and 2,5,2',5'-tetrachlorobiphenyl by rat liver microsomes and highly purified cytochrome P-450. Journal of Pharmacobio-Dynamics 14:276-284.

Iversen SJ. 2002. Blubber. In: Perrin WF, Wursig B, Thewissen JGM, editors. Encylopedia of Marine Mammals. San Diego, CA: Academic Press. p 107-111.

Jorgensen EH, Johansen SJS, Jobling M. 1997a. Seasonal pattern of growth, lipid deposition, and lipid depletion in anadromous Arctic charr. Journal of Fish Biology 51(312-326).

Jorgensen EH, Vijayan MM, Killie JA, Aluru N, Aas-Hansen O, Maule A. 2006. Toxicokinetics and effects of PCBs in Arctic fish: a review of studies on Arctic charr. Journal of Toxicology and Environmental Health, Part A 69:37-52.

Kaminsky LS, Kennedy MW, Adams SM, Guengerich FP. 1981. Metabolism of dichlorobiphenyls by highly purified isozymes of rat liver cytochrome P-450. Biochemistry 20:7379-7384.

Kannan K, Tanabe S, Borrell A, Aguilar A, Focardi S, Tatsukawa R. 1993. Isomer-specific analysis and toxic evaluation of polychlorinated biphenyls in striped dolphins affected by an epizootic in the western Mediterranean Sea. Archives of Environmental Contamination and Toxicology 25(2):227-233.

Koopman HN, Iverson S, Gaskin D. 1996. Stratification and age-related differences in blubber fatty acids of the male harbour porpoise (*Phocoena phocoena*). Journal of Comparative Physiology, B 135:628-639.

Koopman HN, Pabst DA, McLellan WA, Dillaman RM, Read AJ. 2002. Changes in blubber Distribution and morphology associated with starvation in the harbour porpoise (*Phocoena phocoena*): evidence for regional differences in blubber structure and function. Physiological and Biological Zoology 75(5):498-512.

Letcher RJ, Klasson Wehler E, Bergman A. 2000. Methyl sulfone and hydroxylated metabolites of polychlorinated biphenyls. In: Paasivinta J, editor. The Handbook of Environmental Chemistry: New types of Persistent Halogenated Compounds. Heidelberg: Springer-Verlaq. p 314-359.

Liu Y, Schultz JJ, Brent GA. 2003. A thyroid hormone receptor alpha gene mutation (P398H) is associated with visceral adiposity and impaired catecholamine-stimulated lipolysis in mice. The Journal of Biological Chemistry 278(40):38913-38920.

Maervoet J, Covaci A, Schepens P, Sandau CD, Letcher RJ. 2004. A reassessment of the nomenclature of polychlorinated biphenyl (PCB) metabolites. Environmental Health Perspectives 112(3):291-294.

McKinney MA, De Guise S, Martineau D, Beland P, Lebeuf M, Letcher RJ. 2006. Organohalogen contaminants and metabolites in beluga whale (*Delphinapterus leucas*) liver from two Canadian populations. Environmental Toxicology and Chemistry 25(5):30-41.

McLellan WA, Koopman HN, Rommel SA, Read AJ, Potter CW, Nicolas JR, Westgate AJ, Pabst DA. 2002. Ontogenetic allometry and body composition of harbour porpoises (*Phocoena phocoena, L.*) from the western North Atlantic. Journal of Zoology 257:457-471.

Meerts IA, Lilienthal H, Hoving S, van den Berg JHJ, Weijers BM, Bergman A, Koeman JH, Brouwer A. 2004. Developmental exposure to 4-hydroxy-2,3,3',4',5-pentachlorobiphenyl (4-OH-CB107): long-term effects on brain development, behavior, and brain stem auditory evoked potentials in rats. Toxicological Sciences 82(1):207-218.

Mills RA, Millis CD, Dannan GA, Guengerich FP, Aust SD. 1985. Studies on the structure-activity relationships for the metabolism of polybrominated biphenyls by rat liver microsomes. Toxicology and Applied Pharmacology 78:96-104.

Moore HH, Silver RB, Mottillo EP, Bernlohr DA, Granneman JG. 2005. Perilipin targets a novel pool of lipid droplets for lipolytic attack by hormone-sensitive lipase. The Journal of Biological Chemistry 280(52):43109-43120.

Muir DCG, Koczanski K, Rosenberg B, Beland P. 1996. Persistent organochlorines in beluga whales (*Delphinapterus leucas*) from the St. Lawrence River Estuary. 2. Temporal trends, 1982-1994. Environmental Pollution 93(2):235-245.

Nishihashi H, Kanno Y, Tomuro K, Nakahama T, Inouye Y. 2006. Primary structure and organ-specific expression of the rat aryl hydrocarbon receptor repressor gene. Biological and Pharmaceutical Bulletin 29(4):640-647.

Norstrom RJ, Muir DCG, Ford CA, Simon M, Macdonald CR, Beland P. 1992. Indications of P450 monooxygenase activities in beluga (*Delphinapterus leucas*) and narwhal (*Monodon monoceros*) from patterns of PCB, PCDD and PCDF accumulation. Marine Environmental Research 34:267-272.

Pabst DA, Rommel SA, McLellan WA. 1999b. The functional morphology of marine mammals. In: III JER, Rommel SA, editors. Biology of Marine Mammals. Washington, D.C.: Smithsonian Institution.

Park SS, Miller H, Klotz AV, Kloepper-Sams PJ, Stegeman JJ, Gelboin HV. 1986. Monoclonal antibodies to liver microsomal cytochrome P-450E of the marine fish *Stenotamus chrysops* (scup): cross-reactivity with 3-methylcholanthrene induced rat cytochrome P-450. Archives of Biochemistry and Biophysics 249:339-350.

Pond CM, Mattacks CA. 1985. Body mass and natural diet as determinants of the number and volume of adipocytes in eutherian mammals. Journal of Morphology 185:183-193.

Ross PS, Ellis GM, Ikonomou MG, Barrett-Lennard LG, Addison RF. 2000. High PCB concentrations in free-ranging Pacific killer whales, *Orcinus orca*: effects of age, sex and dietary preference. Marine Pollution Bulletin 40(6):504-515.

Sandala GM, Sonne-Hansen C, Dietz R, Muir DCG, Valters K, Bennett ER, Born EW, Letcher RJ. 2004. Hydroxylated and methyl suflone PCB metabolites in adipose and whole blood of polar bear (*Ursus maritimus*) from East Greenland. Science of the Total Environment 331:125-141.

Sandau CD. 2000. Analytical chemistry of hydroxylated metabolites of PCBs and other halogenated phenolic compounds in blood and their relationship to thyroid hormone and retinol homeostasis in humans and polar bears. Ottawa, Ontario: Carleton University. 202 p.

Schlezinger JJ, Stegeman JJ. 2000. Dose and inducer-dependent induction of cytochrome P450 1A in endothelia of the eel, including in the swimbladder rete mirabile, a model microvascular structure. Drug Metabolism and Disposition 28(6):701-708.

Schlezinger JJ, Struntz DJ, Goldstone JV, Stegeman JJ. 2006. Uncoupling of cytochrome P4501A and stimulation of reactive oxygen species production by co-planar polychlorinated biphenyl congeners. Aquatic Toxicology 77(4):422-32.

Schlezinger JJ, White RD, Stegeman JJ. 1999. Oxidative inactivation of cytochrome P4501A stimulated by 3,3',4,4'-tetracholorobiphenyl: production of reactive oxygen by vertebrate CYP1As. Molecular Pharmacology 56:588-597.

Scott M, Wells R, Irvine A. 1990. A long-term study of bottlenose dolphins on the west coast of Florida. In: Leatherwood S, Reeves R, editors. The Bottlenose Dolphin. San Diego, CA, USA: Academic Press. p 235-244.

Severinsen T, Skaare JU, Lydersen C. 1999. Spatial distribution of persistent organochlorines in ringed seal (*Phoca hispida*) blubber. Marine Environmental Research 49:291-302.

Shimada T, Sawabe Y. 1983. Activation of 3,4,3',4'-tetrachlorobiphenyl to protein bound metabolites by the rat liver cytochrome P-448-containing monooxygenase system. Toxicology and Applied Pharmacology 70:486-493.

Smolowitz RM, Hahn ME, Stegeman JJ. 1991. Immunohistochemical localization of cytochrome P450IA1 induced by 3,3',4,4'-tetrachlorobiphenyl and by 2,3,7,8-tetrachlorodibenzofuran in liver and extrahepatic tissues of the teleost *Stenotomus chrysops* (scup). Drug Metabolism and Disposition 19:113-123.

Sodergren A, Ulfstrand S. 1972. DDT and PCB relocate when caged robins use fat reserves. Ambio 1:36-40.

St. Aubin DJ. 2001. Endocrinology. In: Dierauf LA, Gulland FMD, editors. CRC Handbook of Marine Mammal Medicine. Boca Raton, FL: CRC Press. p 165-192.

Stegeman JJ, Miller MR, Hinton DE. 1989. Cytochrome P450IA1 induction and localization in endothelium of vertebrate (teleost) heart. Molecular Pharmacology 36:723-729.

Struntz DJ, McLellan WA, Dillaman R, Blum J, Kucklick J, Pabst D. 2004. Blubber development in bottlenose dolphins (*Tursiops truncatus*). Journal of Morphology 259:7-20.

Tanabe S, Watanabe S, Kan H, Tatsukawa R. 1988. Capacity and mode of PCB metabolism in small cetaceans. Marine Mammal Science 4(2):103-124.

Toborek M, Barger SW, Mattson MP, Espandiari P, Robertson LW, Hennig B. 1995. Exposure to polychlorinated biphenyls cause endothelial cell dysfunction. Journal of Biochemical and Molecular Toxicology 10:219-226.

van den Berg M, Birnbaum L, Bosveld ATC, Brunstrom B, Cook P, Feeley M, Giesy JP, Hanberg A, Hasegawa R, Kennedy SW, Kubiak T, Larsen JC, van Leeuwen FX, Liem AK, Nolt C, Peterson RE, Poellinger L, Safe S, Schrenk D, Tillitt D, Tysklind M, Younes M, Waern F, Zacharewski T. 1998. Toxic equivalency factors (TEFs) for PCBs, PCDDs, PCDFs for humans and wildlife. Environmental Health Perspectives 106:775-792.

Watanabe M, Houten SM, Mataki C, Christoffolete MA, Kim BW, Sato H, Messaddeq N, Harney JW, Ezaki O, Tatsuhiko K, Schoonjans K, Bianco AC, Auwerx J. 2006. Bile acids induce energy expenditure by promoting intracellular thyroid hormone activation. Nature 439:484-489.

Weisbrod AS, D; Moore, MJ; Stegeman, JJ. 2000. Bioaccumulation patterns of polychlorinated biphenyls and chlorinated pesticides in northwest Atlantic pilot whales. Environmental Toxicology and Chemistry 3:667-677.

Wells RS, Tornero V, Borrell A, Aguilar A, Rowles TK, Rhinehart HL, Hofmann S, Jarman WM, Hohn AA, Sweeney JC. 2005. Integrating life-history and reproductive success data to examine potential relationships with organochlorine compounds for bottlenose dolphins (*Tursiops truncatus*) in Sarasota Bay, Florida. Science of the Total Environment 349(1-3):106.

White RD, Hahn ME, Lockhart WL, Stegeman JJ. 1994. Catalytic and immunochemical characterization of hepatic microsomal cytochromes P450 in beluga whale (*Delphinapterus leucas*). Toxicology and Applied Pharmacology 126(1):45-57.

White RD, Shea D, Schlezinger JJ, Hahn ME, Stegeman JJ. 2000. In vitro metabolism of polychlorinated biphenyl congeners by beluga whale (*Delphinapterus leucas*) and pilot whale (*Globicephala melas*) and relationship to cytochrome P450 expression. Comparitive Biochemistry and Physiology Part C 126(3):267-284.

Wilson JY. 2003. Cytochrome P4501A1 and aromatase (CYP19) in cetaceans: enzyme expression and relationship to contaminant exposure. Woods Hole, MA: Massachusetts Institute of Technology / Woods Hole Oceanographic Institution. 260 p.

Wilson JY, Cooke SR, Moore MJ, Martineau D, Mikaelian I, Metner DA, Lockhart WL, Stegeman JJ. 2005. Systemic effects of Arctic pollutants in beluga whales indicated by CYP1A1 expression. Environmental Health Perspectives 113:1594-1599.

Wilson JY, Montie EW, Tuerk K, Kucklick JR, Stegeman J. Cytochrome P450 1A expression in white-sided dolphins (*Lagenorhynchus acutus*) stranded on Cape Cod, MA; 2003.

Woodin BR, Smolowitz R, Stegeman J. 1997. Induction of cytochrome P4501A in the intertidal fish *Anoplarchus purpurescens* by Prudhoe Bay crude oil and environmental induction in fish from Prince William Sound. Environmental Science & Technology 31:1198-1205.

Yoshimura H, Yonemoto Y, Yamada H, Koga N, Oguri K, Saeki S. 1987. Metabolism in vivo of 3,4,3',4'-tetrachlorobiphenyl and toxicological assessment of the metabolites in rats. Xenobiotica 17:897-910.

Zimmermann R, Strauss JG, Haemmerle G, Schoiswohl G, Birner-Gruenberger R, Riederer M, Lass A, Neuberger G, Eisenhaber F, Hermetter A, Zechner R. 2004.

Fat mobilization in adipose tissue is promoted by adipose triglyceride lipase. Science 306:1383-1386.

Zoeller TD, AL; Herzig,CT; Iannacone,EA; Gauger,K; Bansal,R. 2002. Thyroid hormone, brain development, and the environment. Environmental Health Perspectives 110(3):355-361.

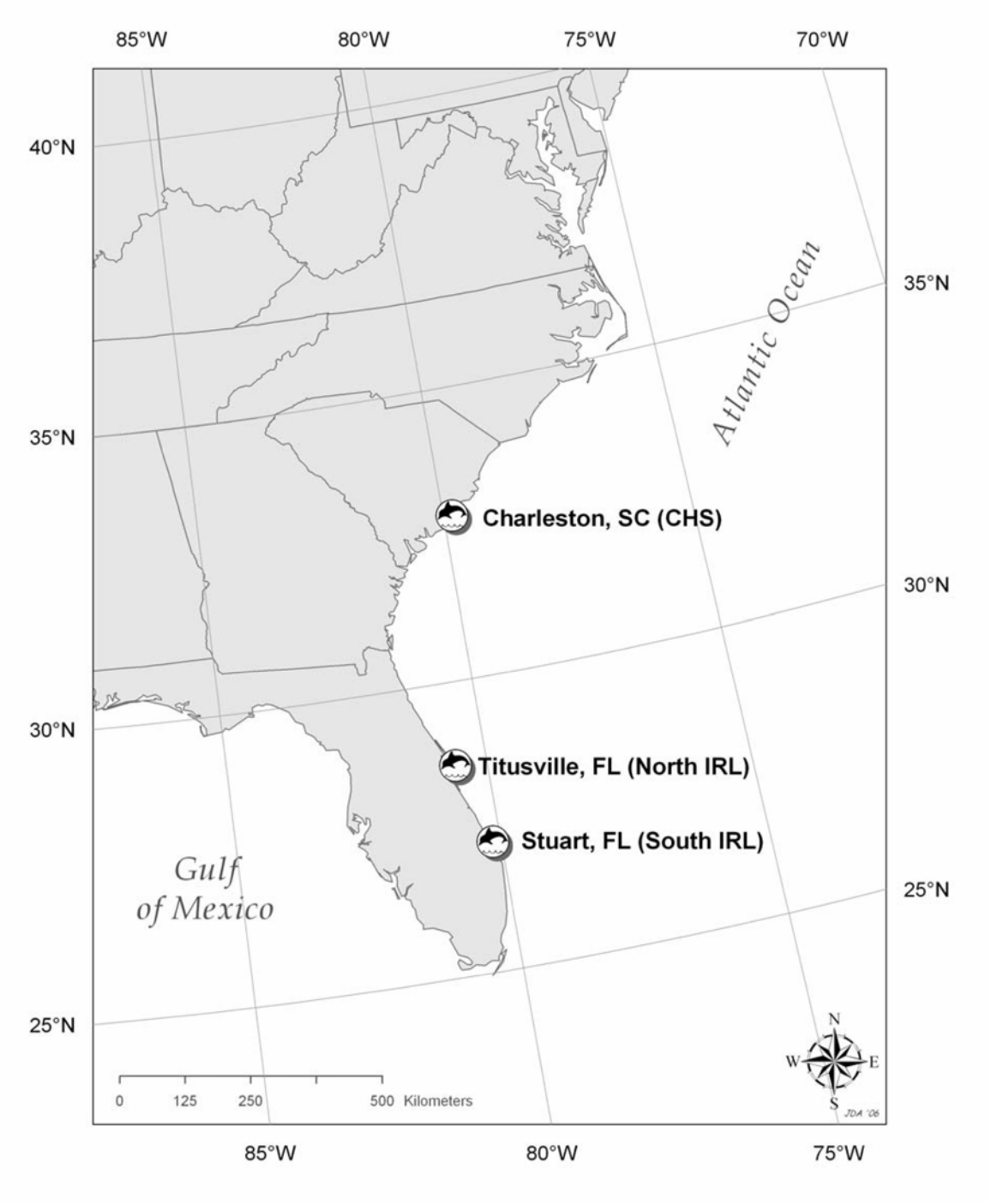


**Figure 1. Map showing the sampling locations of bottlenose dolphins along the Southeast United States Atlantic Coast.**

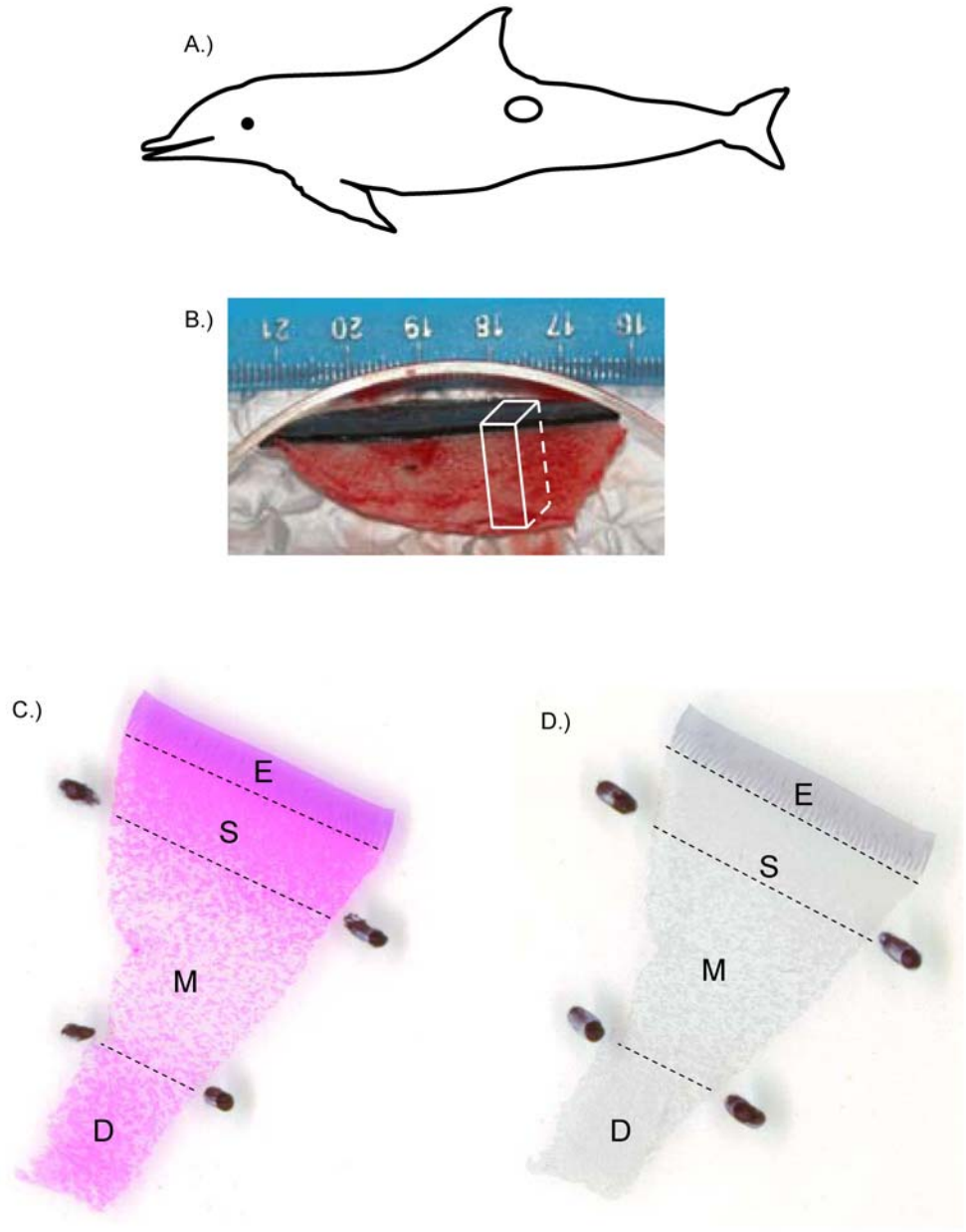


**Figure 2. Skin-blubber biopsy sampling site and subsampling for histology and immunohistochemical (IHC) analysis of cytochrome P4501A1 (CYP1A1) in bottlenose dolphins.** A.) Sampling site on body. B.) Representative photo of skin-blubber biopsy. The white rectangle represents the subsampling site used for IHC. C.) Representative image of a hematoxylin and eosin (H&E) slide. D.) Representative image of the corresponding IHC slide. Dotted lines across the slides represent boundaries of the epidermis (E), superficial (S), middle (M), and deep (D) blubber layers.

**Figure 3. Light micrograph images of the blubber and CYP1A1 staining in the superficial, middle, and deep layers.** A.) Contiguous H&E images from the epidermis to the deep blubber of an adult male captured and released in Charleston, SC illustrating the stratification of the blubber. E = epidermis; S = superficial blubber layer; M = middle blubber layer; D = deep blubber layer. B.) IHC image of the superficial, C.) middle, and D.) deep blubber layers. CYP1A1 staining is in red and demarcated by black arrows. There is no staining in the representative superficial IHC slide. In all images, the left side is closest to the epidermis surface. Dp = dermal papillaie; Ca = capillary; Art = arteriole; Ad = adipocyte; Str = structural fibers.

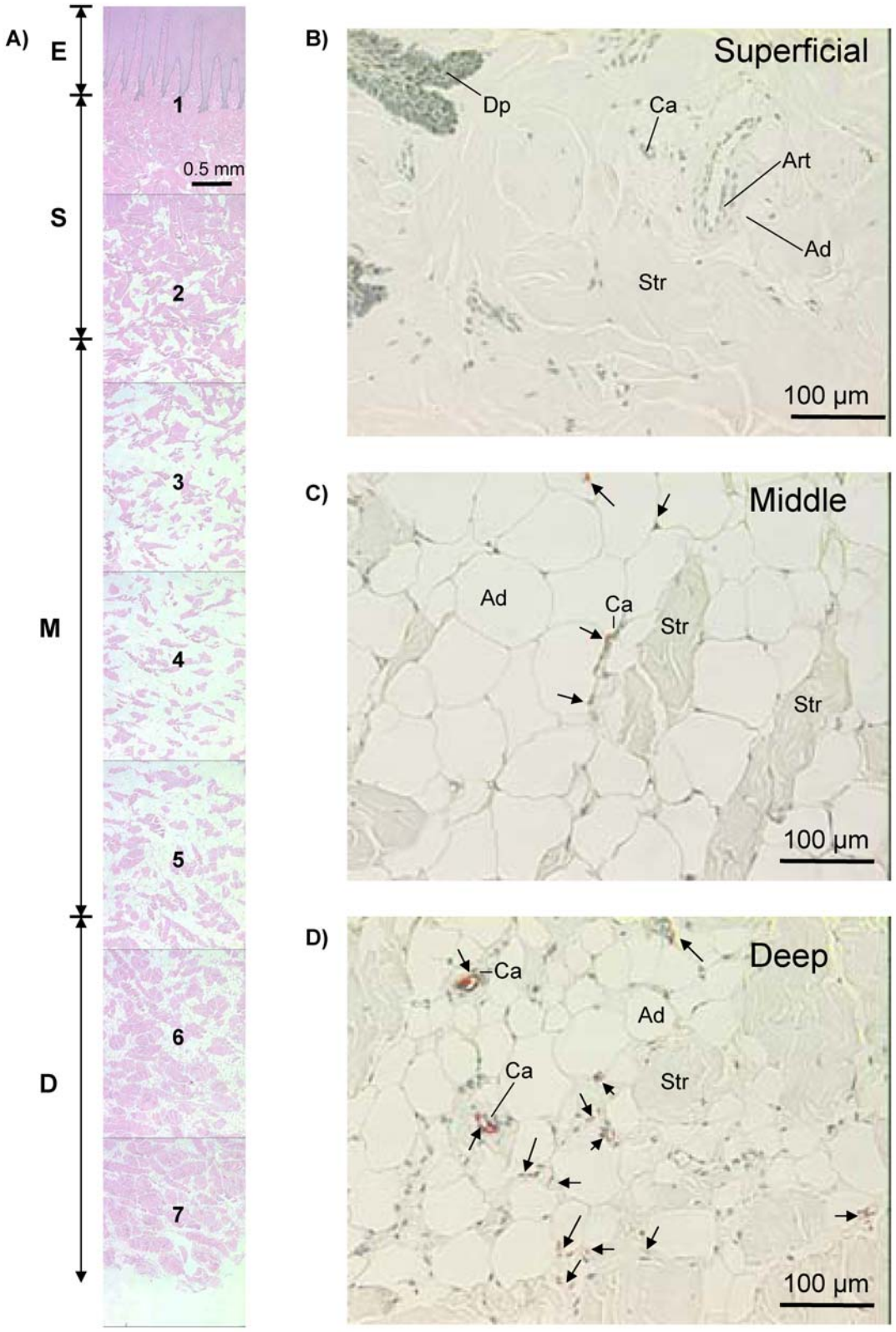
A)
E
S
M
D
1
2
3
4
5
6
7
0.5 mm
B)
Superficial
Dp
Ca
Art
Ad
Str
100 μm
C)
Middle
Ad
Ca
Str
Str
100 μm
D)
Deep
Ca
Ad
Ca
Str
100 μm

**Figure 4. Correlation between "original" and "modified" CYP1A1 staining scores in vascular endothelial cells averaged over blubber layers.** Two dolphins were not included in the statistical analysis because a representation of the deep blubber was not present; N = 72. A.) Raw data. B.) Log transformed.

A.)

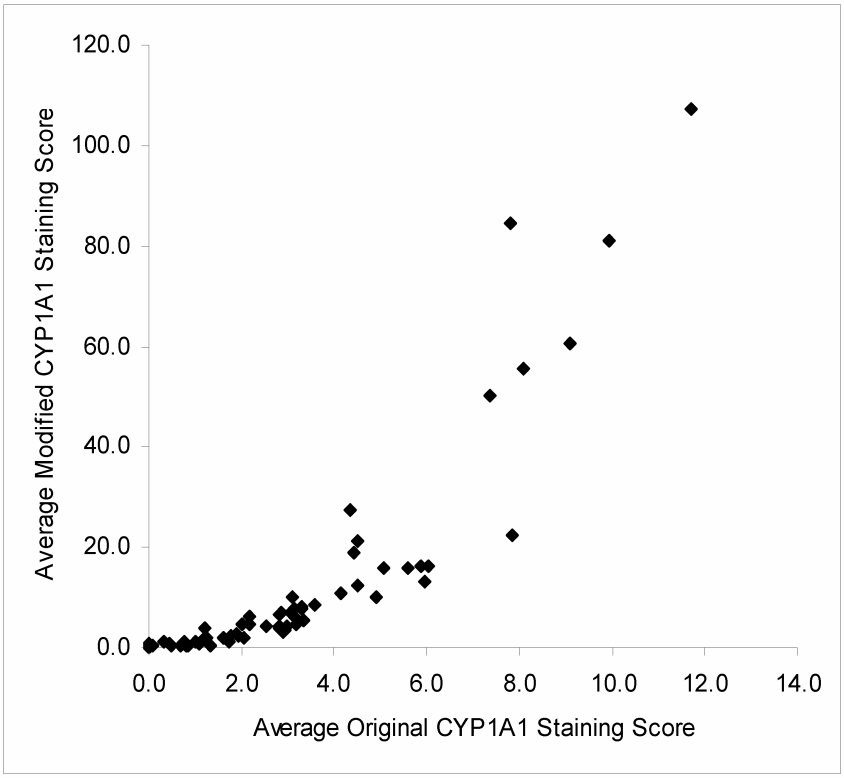
120.0
100.0
80.0
60.0
40.0
20.0
0.0
Average Modified CYP1A1 Staining Score
0.0
2.0
4.0
6.0
8.0
10.0
12.0
14.0
Average Original CYP1A1 Staining Score

B.)

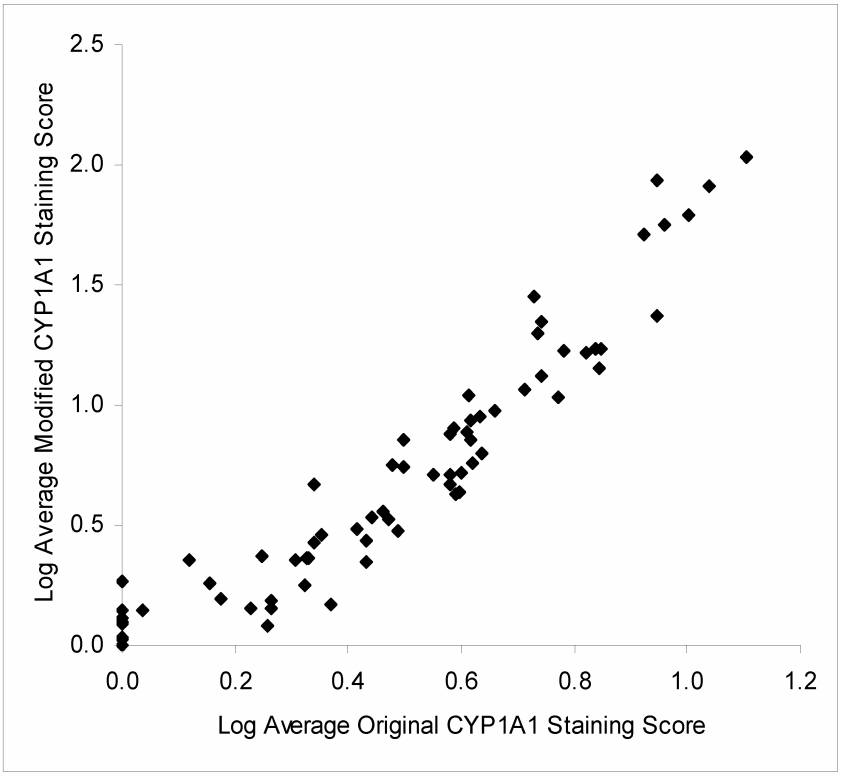
2.5
2.0
1.5
1.0
0.5
0.0
Log Average Modified CYP1A1 Staining Score
0.0
0.2
0.4
0.6
0.8
1.0
1.2
Log Average Original CYP1A1 Staining Score

**Figure 5. Depth specific CYP1A1 expression in vascular endothelial cells in the skin-blubber biopsy of male and female bottlenose dolphins captured and released at Charleston, SC (CHS) and Indian River Lagoon, FL (IRL).** Lactating, pregnant, and females of unknown reproductive state were not included in the analysis (N = 61). Layers that share a similar letter are not significantly different from each other ($P > 0.05$). A.) CYP1A1 intensity score in vascular endothelial cells of the superficial, middle, and deep blubber layers. B.) CYP1A1 "modified" occurrence score (cells/$mm^2$) of vascular endothelial cells in the superficial, middle, and deep blubber layers. C.) CYP1A1 "modified" staining score of vascular endothelial cells in the superficial, middle, and deep blubber layers.

A.)

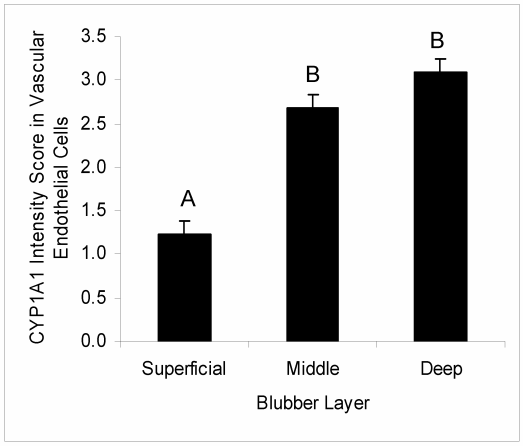
CYP1A1 Intensity Score in Vascular Endothelial Cells
3.5
3.0
2.5
2.0
1.5
1.0
0.5
0.0
A
B
B
Superficial
Middle
Deep
Blubber Layer

B.)

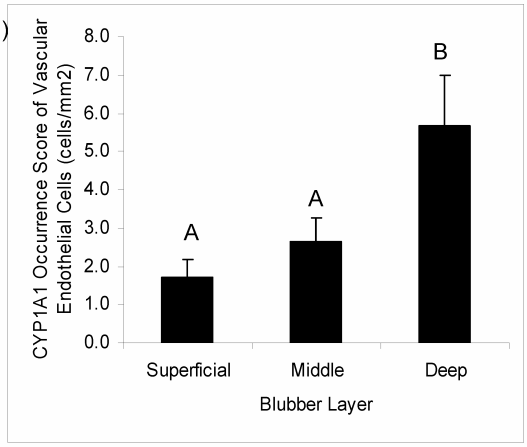
CYP1A1 Occurrence Score of Vascular Endothelial Cells (cells/mm2)
8.0
7.0
6.0
5.0
4.0
3.0
2.0
1.0
0.0
A
A
B
Superficial
Middle
Deep
Blubber Layer

C.)

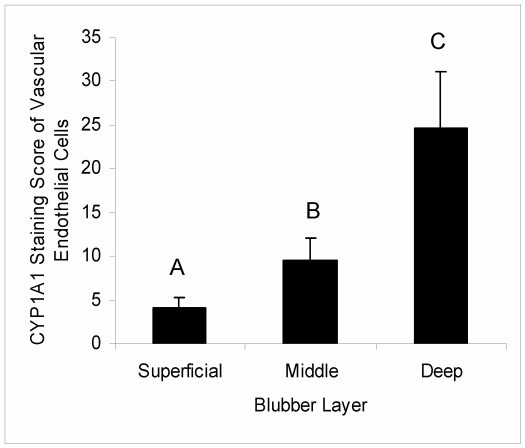
CYP1A1 Staining Score of Vascular Endothelial Cells
35
30
25
20
15
10
5
0
A
B
C
Superficial
Middle
Deep
Blubber Layer

**Figure 6. CYP1A1 expression and Total Toxic Equivalents ($TEQ_{98}$ ng/g wet wt) in male and female bottlenose dolphins captured and released in CHS and IRL locations.** Lactating, pregnant, and females of unknown reproductive state were not included in the analysis. Between categories, blubber layers that share a similar capital letter are not significantly different from each other ($P > 0.05$). Within categories, blubber layers that share a similar lowercase letter are not significantly different from each other ($P>0.05$). A.) CYP1A1 "modified" staining score of vascular endothelial cells of the superficial, middle, and deep blubber layers in CHS (N = 31) and IRL (N = 30) dolphins. B.) Blubber $TEQ_{98}$ concentrations (ng/g wet wt) in CHS (N = 30) and IRL (N = 26) dolphins. C.) Sum plasma $TEQ_{98}$ (ng/g wet wt) in CHS (N = 22) and IRL (N = 26) dolphins. D.) CYP1A1 "modified" staining scores of vascular endothelial cells of the superficial, middle, and deep blubber layers for CHS subadult males (N = 2), CHS adult males (N = 24), CHS subadult females (N =3), CHS non-pregnant and non-lactating adult females (N = 2), IRL subadult males (N = 5), IRL adult males (N = 19), IRL subadult females (N = 3), and IRL non-pregnant and non-lactating adult females (N = 3). Blubber PCB data were provided by Greg Mitchum. Plasma PCB data were provided by Magali Houde.

A.)

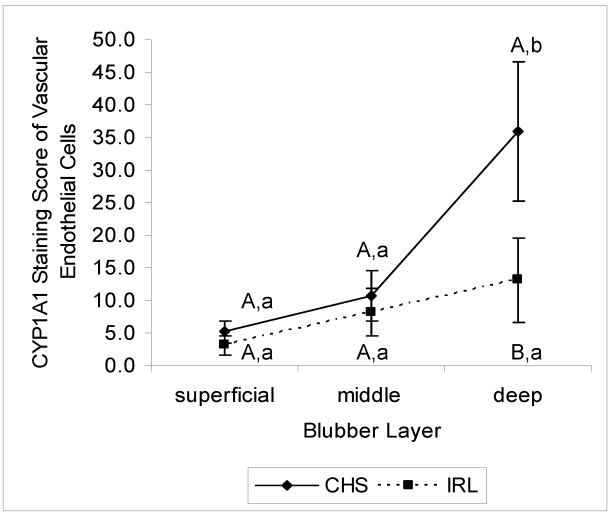
CYP1A1 Staining Score of Vascular Endothelial Cells
50.0
45.0
40.0
35.0
30.0
25.0
20.0
15.0
10.0
5.0
0.0
A,b
A,a
A,a
A,a
B,a
superficial
middle
deep
Blubber Layer
CHS
IRL

B.)

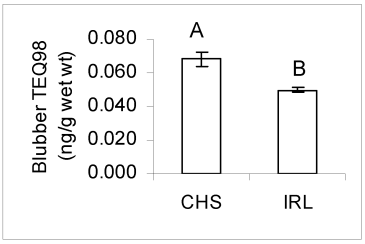
Blubber TEQ98 (ng/g wet wt)
0.080
0.060
0.040
0.020
0.000
A
B
CHS
IRL

C.)

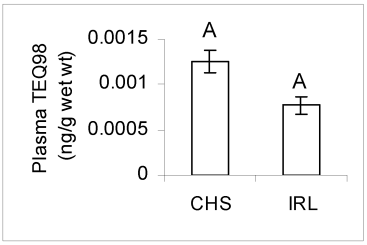
Plasma TEQ98 (ng/g wet wt)
0.0015
0.001
0.0005
0
A
A
CHS
IRL

D.)

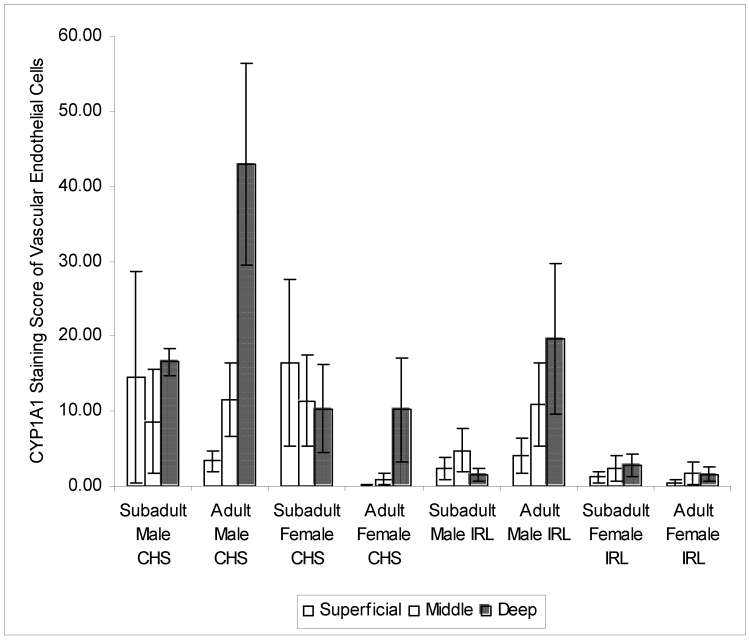
CYP1A1 Staining Score of Vascular Endothelial Cells
60.00
50.00
40.00
30.00
20.00
10.00
0.00
Subadult Male CHS
Adult Male CHS
Subadult Female CHS
Adult Female CHS
Subadult Male IRL
Adult Male IRL
Subadult Female IRL
Adult Female IRL
Superficial
Middle
Deep

**Figure 7. Relationships between CYP1A1 expression of vascular endothelial cells and $TEQ_{98}$ levels in male and female bottlenose dolphins captured and released at CHS and IRL locations.** Lactating, pregnant, and females of unknown reproductive state were not included in the analysis; N = 48. Solid lines indicate a significant relationship ($P < 0.05$). A.) Log average CYP1A1 staining score versus total blubber $TEQ_{98}$ concentrations (ng/g wet wt). B.) Log average CYP1A1 staining score versus plasma $TEQ_{98}$ concentrations (ng/g wet wt). C.) Depth-specific log CYP1A1 staining scores versus plasma $TEQ_{98}$ concentrations (ng/g wet wt). Blubber PCB data were provided by Greg Mitchum. Plasma PCB data were provided by Magali Houde.

A.)

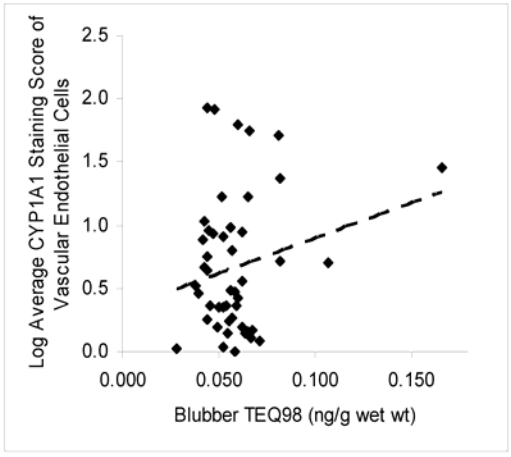
Log Average CYP1A1 Staining Score of Vascular Endothelial Cells
2.5
2.0
1.5
1.0
0.5
0.0
0.000
0.050
0.100
0.150
Blubber TEQ98 (ng/g wet wt)

B.)

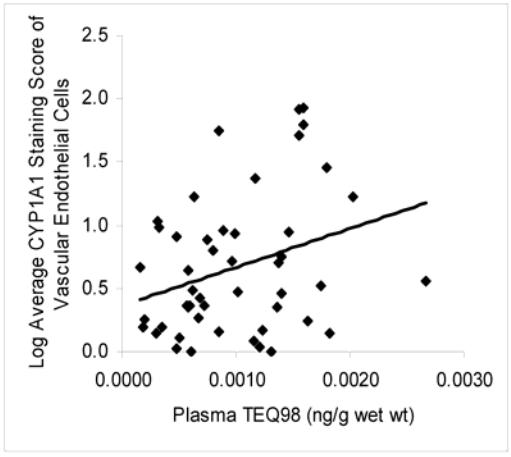
Log Average CYP1A1 Staining Score of Vascular Endothelial Cells
2.5
2.0
1.5
1.0
0.5
0.0
0.0000
0.0010
0.0020
0.0030
Plasma TEQ98 (ng/g wet wt)

C.)

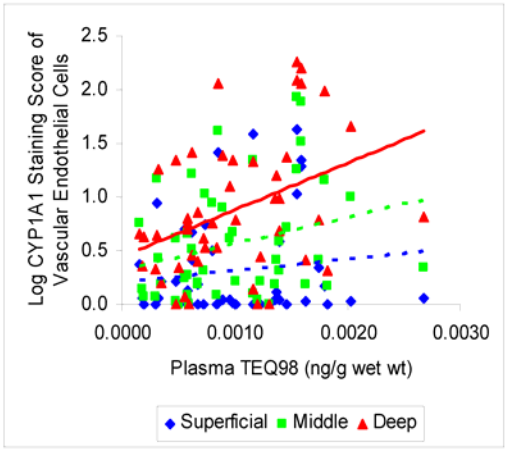
Log CYP1A1 Staining Score of Vascular Endothelial Cells
2.5
2.0
1.5
1.0
0.5
0.0
0.0000
0.0010
0.0020
0.0030
Plasma TEQ98 (ng/g wet wt)
Superficial
Middle
Deep

**Figure 8. Relationships among CYP1A1 expression of vascular endothelial cells, $TEQ_{98}$ concentrations, and adipocyte areas in male bottlenose dolphins captured and released at CHS (N = 19) and IRL (N = 21) locations.** Solid lines indicate a significant relationship ($P < 0.05$). A-B.) Log average CYP1A1 staining score versus blubber $TEQ_{98}$ concentrations (ng/g wet wt). C-D.) Depth specific log CYP1A1 staining score versus plasma $TEQ_{98}$ levels (ng/g wet wt). E-F.) Depth specific log CYP1A1 staining score versus depth-specific adipocyte areas. Blubber PCB data were provided by Greg Mitchum. Plasma PCB data were provided by Magali Houde.

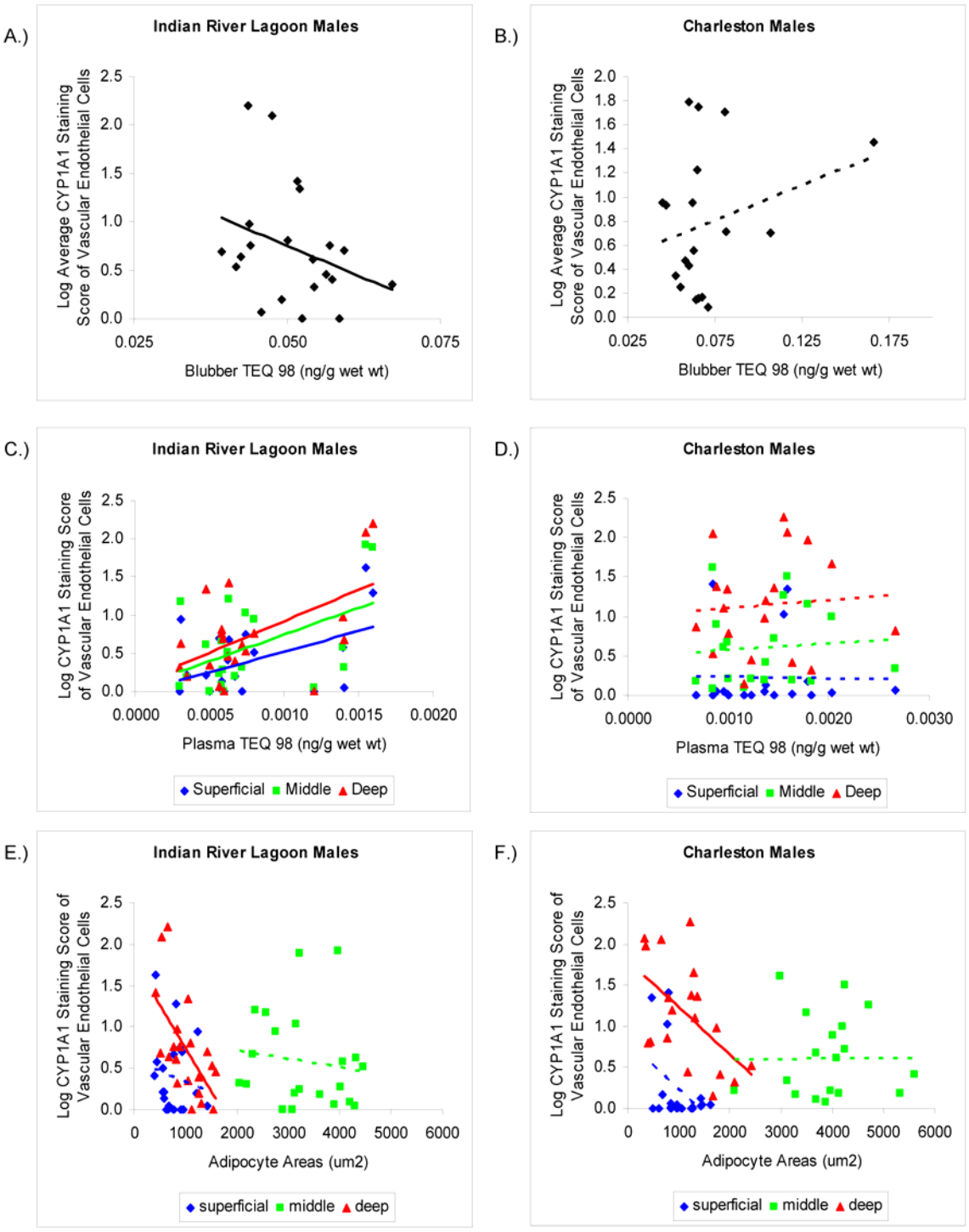
A.)
Indian River Lagoon Males
Log Average CYP1A1 Staining Score of Vascular Endothelial Cells
Blubber TEQ 98 (ng/g wet wt)
B.)
Charleston Males
Log Average CYP1A1 Staining Score of Vascular Endothelial Cells
Blubber TEQ 98 (ng/g wet wt)
C.)
Indian River Lagoon Males
Log CYP1A1 Staining Score of Vascular Endothelial Cells
Plasma TEQ 98 (ng/g wet wt)
Superficial Middle Deep
D.)
Charleston Males
Log CYP1A1 Staining Score of Vascular Endothelial Cells
Plasma TEQ 98 (ng/g wet wt)
Superficial Middle Deep
E.)
Indian River Lagoon Males
Log CYP1A1 Staining Score of Vascular Endothelial Cells
Adipocyte Areas (um2)
superficial middle deep
F.)
Charleston Males
Log CYP1A1 Staining Score of Vascular Endothelial Cells
Adipocyte Areas (um2)
superficial middle deep

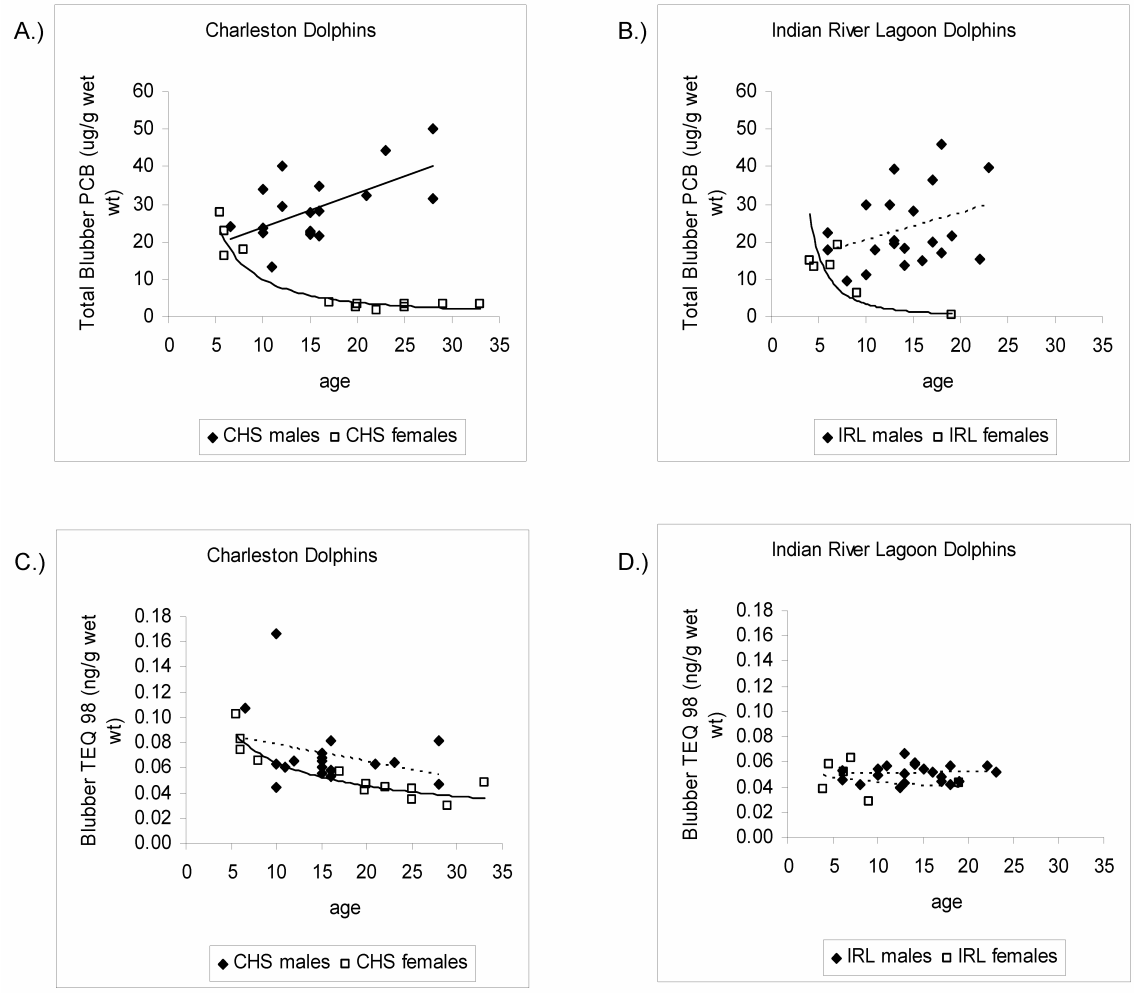


**Figure 9. Relationships of total blubber PCB concentrations and $TEQ_{98}$ levels with age in male and female dolphins from CHS and IRL locations (CHS males N = 19, females N = 12; IRL males N = 21, females N = 6).** Solid lines indicate a significant relationship ($P < 0.05$ or $R^2 > 0.5$). A-B.) Total blubber PCB concentrations (ug/g wet wt) versus age for CHS and IRL males and females. C-D.) Blubber $TEQ_{98}$ concentrations (ng/g wet wt) versus age for CHS and IRL males and females. Blubber PCB data were provided by Greg Mitchum.

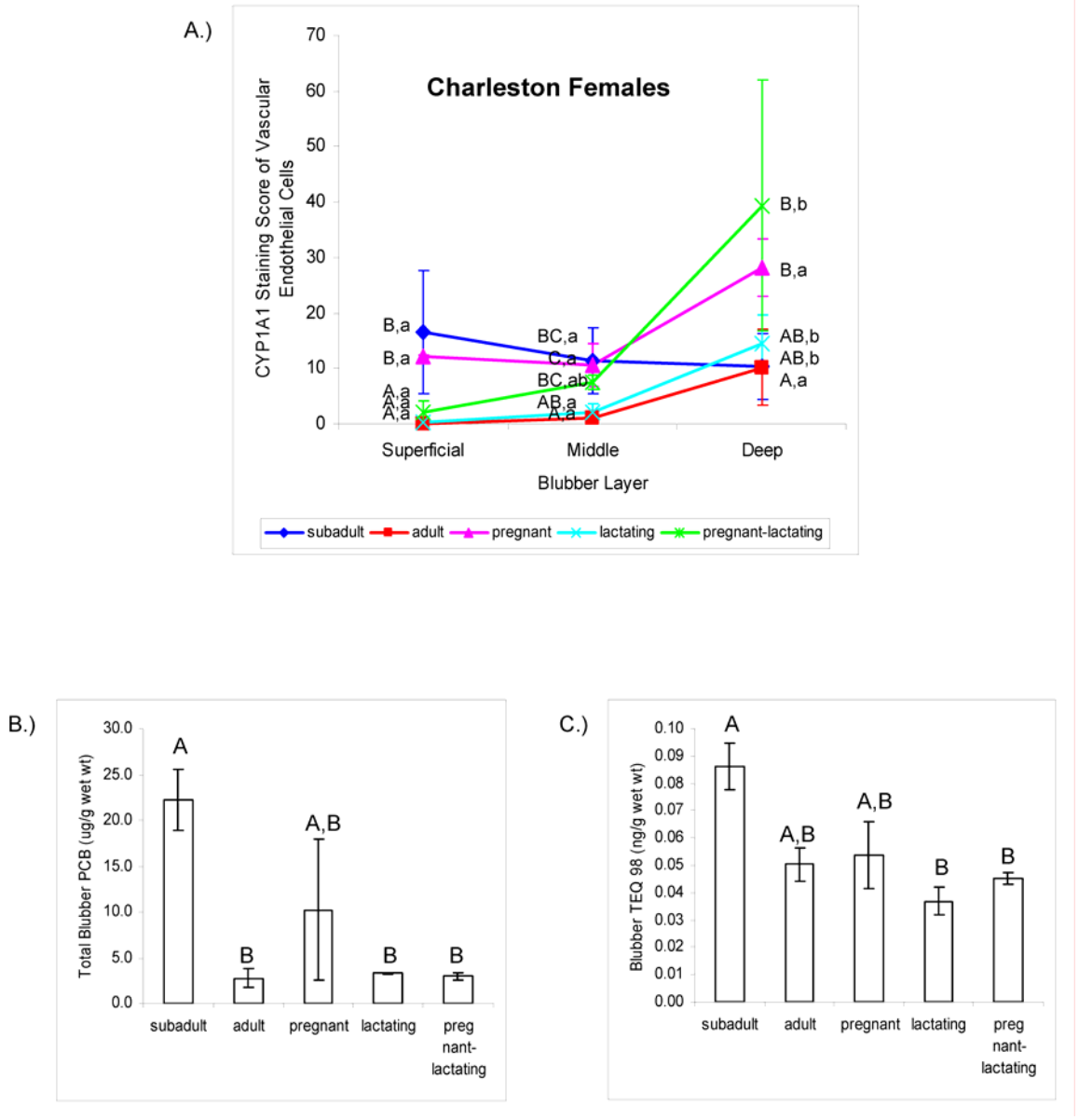


**Figure 10. A.) Depth specific CYP1A1 expression in vascular endothelial cells in the skin-blubber biopsy of subadult (N = 3), adults captured with calves (N = 2), pregnant (N = 2), lactating (N = 3), and simultaneously pregnant and lactating (N = 2) female dolphins captured and released at CHS location.** Between reproductive categories, layers that share a similar capital letter are not significantly different from each other ($P > 0.05$). Within each reproductive category, layers that share a similar lowercase letter are not significantly different from each other ($P > 0.05$). B-C.) Total blubber PCB (ug/g wet wt) and blubber $TEQ_{98}$ (ng/g wet wt) concentrations in CHS female dolphins. Blubber PCB data were provided by Greg Mitchum.

**Figure 11. Relationships among CYP1A1 expression of vascular endothelial cells, $TEQ_{98}$ concentrations, and adipocyte cross-sectional areas in subadult (N = 3), adult (N = 2), pregnant (N = 2), lactating (N = 3), and simultaneously pregnant and lactating (N = 2) CHS female dolphins. Solid lines indicate a significant relationship ($P < 0.05$).** A.) Blubber $TEQ_{98}$ levels versus age. B.) Depth-specific log CYP1A1 staining scores of the superficial, middle, and deep blubber layers versus blubber $TEQ_{98}$ concentrations (ng/g wet wt). C-E.) Depth-specific log CYP1A1 staining scores of the superficial, middle, and deep blubber layers versus depth-specific adipocyte cross-sectional areas. F.) Log CYP1A1 divided by blubber $TEQ_{98}$ concentrations (ng/g wet wt) versus adipocyte areas for the deep blubber layer. Blubber PCB data were provided by Greg Mitchum.

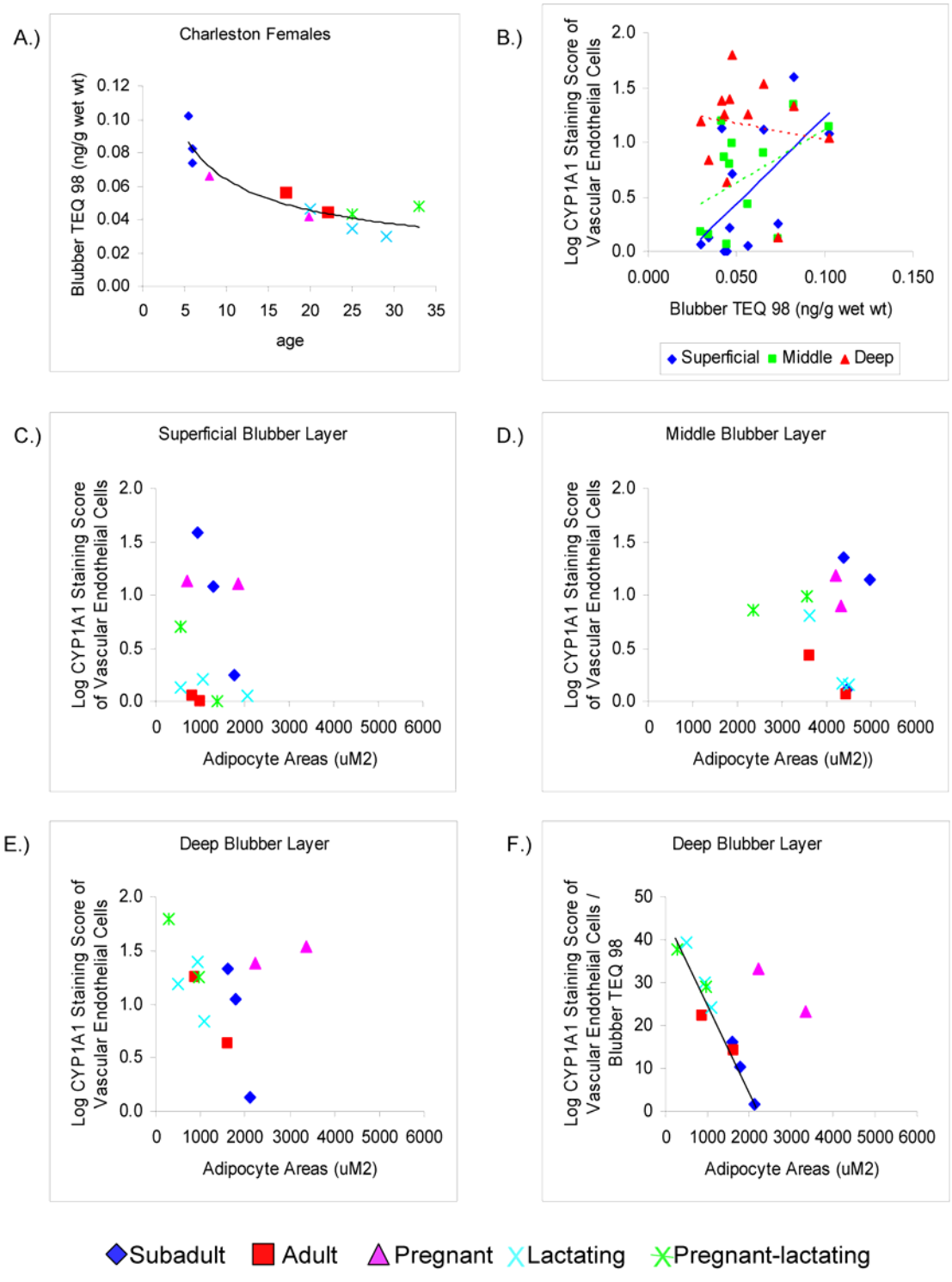
A.)
Charleston Females
Blubber TEQ 98 (ng/g wet wt)
0.12
0.10
0.08
0.06
0.04
0.02
0.00
0 5 10 15 20 25 30 35
age
B.)
Log CYP1A1 Staining Score of Vascular Endothelial Cells
2.0
1.5
1.0
0.5
0.0
0.000 0.050 0.100 0.150
Blubber TEQ 98 (ng/g wet wt)
Superficial Middle Deep
C.)
Superficial Blubber Layer
Log CYP1A1 Staining Score of Vascular Endothelial Cells
2.0
1.5
1.0
0.5
0.0
0 1000 2000 3000 4000 5000 6000
Adipocyte Areas (uM2)
D.)
Middle Blubber Layer
Log CYP1A1 Staining Score of Vascular Endothelial Cells
2.0
1.5
1.0
0.5
0.0
0 1000 2000 3000 4000 5000 6000
Adipocyte Areas (uM2))
E.)
Deep Blubber Layer
Log CYP1A1 Staining Score of Vascular Endothelial Cells
2.0
1.5
1.0
0.5
0.0
0 1000 2000 3000 4000 5000 6000
Adipocyte Areas (uM2)
F.)
Deep Blubber Layer
Log CYP1A1 Staining Score of Vascular Endothelial Cells / Blubber TEQ 98
50
40
30
20
10
0
0 1000 2000 3000 4000 5000 6000
Adipocyte Areas (uM2)
Subadult Adult Pregnant Lactating Pregnant-lactating

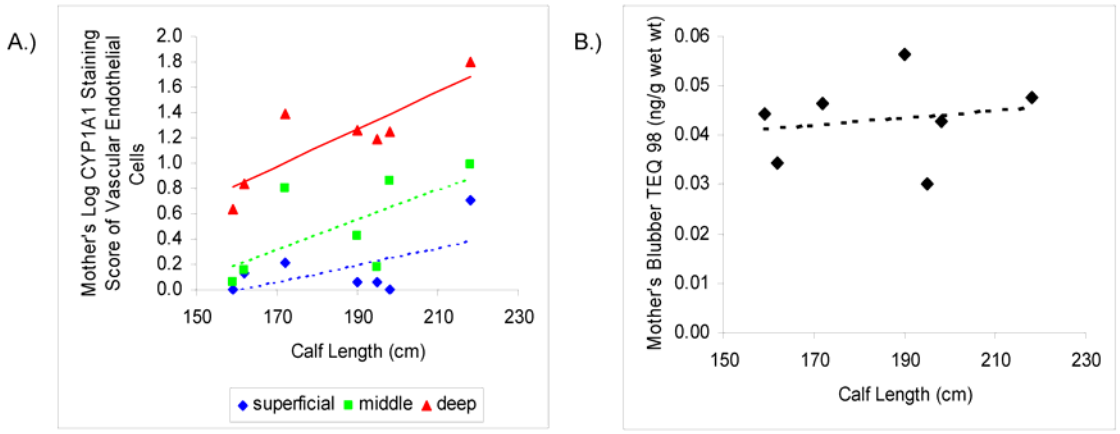


**Figure 12. $TEQ_{98}$ levels and CYP1A1 expression of vascular endothelial cells in CHS female dolphins captured with calves (N = 7).** Solid lines indicate a significant relationship ($P < 0.05$). A.) Calf length versus mother's depth-specific log CYP1A1 staining score. B.) Calf length versus mother's blubber $TEQ_{98}$ concentrations (ng/g wet wt.). Blubber PCB data were provided by Greg Mitchum.

Table 1. Objectives and Statistical Tests to Determine the Interrelationships among CYP1A1 Expression, PCBs and OH-PCBs, and Blubber Dynamics of Bottlenose Dolphins Live-captured and Released in Charelston, SC and Indian River Lagoon, FL during July and August 2003.

| Objective | Animal Group(s) | Independent Variable(s) | Dependent Variable(s) | Statistical Test |
|---|---|---|---|---|
| **METHODOLOGY** | | | | |
| 1. Relationship between "original" and "modified" CYP1A1 staining scores | N = 72 (all dolphins) | NA | NA | Correlation |
| | | | | |
| **EFFECT OF LAYER, GEOGRAPHIC LOCATION, AGE CLASS,AND SEX ON CYP1A1** | | | | |
| 1. Test the hypothesis that CYP1A1 expression is stratified.<br>2. Determine the effects of geographic location, age class, and sex on average and depth-specific CYP1A1. | N = 61 (no lactating or pregnant) or N = 71 (all animals) | Geographic location, age class, sex, and blubber layer | Depth-specific CYP1A1 intensity, occurrence, or staining score | Four-factor GLM with layer as a repeated measure |
| | N = 61 (no lactating or pregnant) or N = 71 (all animals) | Geographic location, age class, and sex | Average CYP1A1 | Three-factor GLM |
| | | | | |
| **RELATIONSHIP BETWEEN PCBS AND CYP1A1** | | | | |
| 1. Determine the effects of geographic location, age class, and sex on blubber and plasma PCB levels. | N = 56 for blubber PCB & TEQs<br>N = 48 for plasma PCB & TEQs<br>(no lactating or pregnant) | Geographic location, age class, and sex | Blubber TEQ, blubber total PCB, plasma TEQ, or plasma total PCB | Three-factor GLM |
| | | | | |
| 2. Determine the relationship between PCBs and average or depth-specific CYP1A1 expression<br>3. Determine the relationship between age and average or depth-specific CYP1A1 expression<br>4. Determine the relationship between layer specific adipocyte area and average or depth-specific CYP1A1 expression. | N = 48 (CHS and IRL combined) (no lactating or pregnant) | Blubber TEQ, blubber total PCB, plasma TEQ, or plasma total PCB | Average CYP1A1 | Linear Regression |
| | | | | |
| | N = 48 (CHS and IRL combined) (no lactating or pregnant) | Plasma TEQ or plasma total PCB | Depth-specific CYP1A1 | Linear Regression |
| | | | | |
| | N = 19 (CHS males) or N = 12 (CHS all females) | Blubber TEQ, blubber total PCB, plasma TEQ, plasma total PCB, layer specific adipocyte area, or age | Average CYP1A1 | Linear Regression |
| | | | | |
| | N = 19 (CHS males) or N = 12 (CHS all females) | Plasma TEQ, plasma total PCB, layer specific adipocyte area, or age | Depth-specific CYP1A1 | Linear Regression |
| | | | | |
| | N = 21 (IRL males) or N = 7 (IRL all females) | Blubber TEQ, blubber total PCB, plasma TEQ, plasma total PCB, layer specific adipocyte area, or age | Average CYP1A1 | Linear Regression |
| | | | | |
| | N = 21 (IRL males) or N = 7 (IRL all females) | Plasma TEQ, plasma total PCB, layer specific adipocyte area, or age | Depth-specific CYP1A1 | Linear Regression |
| | | | | |

Table 1. (*Continued*)

| | | | | |
|---|---|---|---|---|
| **RELATIONSHIP BETWEEN REPRODUCTION AND CYP1A1** | | | | |
| 1. Determine the relationship of age and PCB levels . | N = 19 (CHS males) or N = 21 (IRL males) | Age | Blubber TEQ, blubber total PCB, plasma TEQ, plasma total PCB, or plasma OH-PCB | Linear Regression |
| | N = 12 (CHS all females) or N = 6 (IRL all females) | Age | Blubber TEQ, blubber total PCB, plasma TEQ, plasma total PCB, or plasma OH-PCB | Non- linear Regression |
| 2. Determine the effects of reproductive state on average and depth-specific CYP1A1 expression. | N = 12 (CHS all females) | Reproductive state | Average CYP1A1 | One way ANOVA |
| | N = 12 (CHS all females) | Reproductive state | Depth-specific CYP1A1 | Two-factor GLM with layer as a repeated measure |
| 3. Investigate blubber TEQ levels and adipocyte areas as factors in depth-specific CYP1A1 expression. | N = 12 (CHS all females) or N = 10 (CHS; no pregnant) | Blubber TEQ and layer-specific adipocyte area | Depth-specific CYP1A1 | Backward stepwise multiple regression |
| 4. Determine the relationship of lactation day and depth-specific CYP1A1 expression | N = 7 (CHS females captured w/ calves) | Calf length | Depth-specific CYP1A1 | Linear regression |
| **RELATIONSHIP BETWEEN CYP1A1 AND OH-PCBs** | | | | |
| 1. Determine the effects of geographic location, age class, and sex on plasma OH-PCBs. | N = 45 (no lactating or pregnant) | Geographic location, age class, and sex | Total plasma OH-PCB or OH-PCB / PCB ratio | Three-factor GLM |
| 2. Determine if the percentage of individual OH-PCB congeners of the total OH-PCB mix was different between CHS dolphins and IRL dolphins. | N = 59 (CHS & IRL) | Geographic location | OH-PCB congener percent | T-test |
| 3. Determine the relationship of CYP1A1 expression and plasma OH-PCB levels. | N = 59 (CHS & IRL) | Depth-specific CYP1A1 | Total identified OH-PCB or all OH-PCB | Linear regression |
| 4. Determine the relationship of CYP1A1 expression in the deep blubber and individual OH-PCB congeners. | N = 59 (CHS & IRL) | Deep CYP1A1 | Individual OH-PCB congeners | Linear regression |

NA = not applicable.
TEQ = $TEQ_{98}$
CYP1A1 = measured endpoint is the "modified" staining score unless otherwise noted.

Table 2. Cytochrome P450 1A1 Expression of Vascular Endothelial Cells in the Blubber of Bottlenose Dolphins Live-captured and Released in Charleston, SC and Indian River Lagoon, FL during July and August 2003.

| | | | | Original CYP1A1 Staining Score | | | | Modified CYP1A1 Staining Score | | | |
|---|---|---|---|---|---|---|---|---|---|---|---|
| Location | Sex | Age Class | | Superficial | Middle | Deep | Average | Superficial | Middle | Deep | Average |
| Charleston, SC | male | subadult | N of cases | 2 | 2 | 2 | 2 | 2 | 2 | 2 | 2 |
| | | | Minimum | 0.5 | 2.5 | 3.0 | 2.6 | 0.3 | 1.6 | 14.8 | 4.1 |
| | | | Maximum | 6.0 | 4.0 | 5.0 | 4.4 | 28.5 | 15.7 | 18.3 | 18.9 |
| | | | **Mean** | **3.3** | **3.3** | **4.0** | **3.5** | **14.4** | **8.6** | **16.6** | **11.5** |
| | | | **Std. Error** | **2.8** | **0.7** | **1.0** | **0.9** | **14.1** | **7.0** | **1.7** | **7.4** |
| Charleston, SC | male | adult | N of cases | 24 | 24 | 24 | 24 | 24 | 24 | 24 | 24 |
| | | | Minimum | 0.0 | 1.0 | 1.0 | 0.7 | 0.0 | 0.2 | 0.4 | 0.2 |
| | | | Maximum | 10.0 | 12.5 | 12.5 | 11.7 | 25.1 | 114.0 | 262.5 | 107.3 |
| | | | **Mean** | **1.4** | **3.6** | **5.8** | **3.7** | **3.3** | **11.6** | **42.9** | **16.5** |
| | | | **Std. Error** | **0.6** | **0.6** | **0.7** | **0.6** | **1.4** | **4.9** | **13.4** | **5.4** |
| Charleston, SC | female | subadult | N of cases | 3 | 3 | 3 | 3 | 3 | 3 | 3 | 3 |
| | | | Minimum | 0.5 | 0.0 | 0.0 | 0.1 | 0.8 | 0.3 | 0.4 | 0.4 |
| | | | Maximum | 5.0 | 6.0 | 10.0 | 7.9 | 37.8 | 21.1 | 20.6 | 22.4 |
| | | | **Mean** | **3.3** | **3.5** | **4.8** | **4.1** | **16.5** | **11.4** | **10.3** | **11.6** |
| | | | **Std. Error** | **1.4** | **1.8** | **2.9** | **2.3** | **11.0** | **6.0** | **5.8** | **6.4** |
| Charleston, SC | female | adult | N of cases | 2 | 2 | 2 | 2 | 2 | 2 | 2 | 2 |
| | | | Minimum | 0.0 | 0.0 | 2.0 | 0.4 | 0.0 | 0.2 | 3.3 | 0.8 |
| | | | Maximum | 0.0 | 2.0 | 6.0 | 3.6 | 0.1 | 1.7 | 17.0 | 8.5 |
| | | | **Mean** | **0.0** | **1.0** | **4.0** | **2.0** | **0.1** | **0.9** | **10.1** | **4.7** |
| | | | **Std. Error** | **0.0** | **1.0** | **2.0** | **1.6** | **0.1** | **0.8** | **6.9** | **3.9** |

Table 2. (*Continued*)

| | | | | | | | | | | | | |
|---|---|---|---|---|---|---|---|---|---|---|---|---|
| Indian River Lagoon, FL | male | subadult | N of cases | 5 | 5 | 5 | 5 | 5 | 5 | 5 | 5 |
| | | | Minimum | 0.0 | 0.0 | 0.0 | 0.0 | 0.0 | 0.1 | 0.0 | 0.1 |
| | | | Maximum | 6.0 | 6.0 | 2.0 | 4.9 | 7.7 | 14.0 | 3.8 | 9.9 |
| | | | **Mean** | **1.6** | **2.3** | **0.8** | **1.8** | **2.4** | **4.8** | **1.5** | **3.5** |
| | | | **Std. Error** | **1.2** | **1.2** | **0.5** | **1.0** | **1.6** | **2.8** | **0.8** | **1.9** |
| Indian River Lagoon, FL | male | adult | N of cases | 19 | 19 | 19 | 19 | 19 | 19 | 19 | 19 |
| | | | Minimum | 0.0 | 0.0 | 0.0 | 0.0 | 0.0 | 0.0 | 0.0 | 0.0 |
| | | | Maximum | 7.5 | 10.0 | 12.5 | 9.9 | 41.2 | 82.8 | 159.3 | 84.4 |
| | | | **Mean** | **1.3** | **2.6** | **2.9** | **2.4** | **4.0** | **10.9** | **19.5** | **11.5** |
| | | | **Std. Error** | **0.5** | **0.7** | **0.8** | **0.6** | **2.3** | **5.6** | **10.0** | **5.8** |
| Indian River Lagoon, FL | female | subadult | N of cases | 3 | 3 | 3 | 3 | 3 | 3 | 3 | 3 |
| | | | Minimum | 0.0 | 0.0 | 0.0 | 0.0 | 0.0 | 0.0 | 0.0 | 0.0 |
| | | | Maximum | 2.0 | 2.0 | 3.0 | 2.0 | 2.3 | 5.5 | 5.0 | 4.6 |
| | | | **Mean** | **1.0** | **1.3** | **1.7** | **1.3** | **1.2** | **2.4** | **2.8** | **2.3** |
| | | | **Std. Error** | **0.6** | **0.7** | **0.9** | **0.7** | **0.7** | **1.6** | **1.5** | **1.3** |
| Indian River Lagoon, FL | female | adult | N of cases | 3 | 3 | 3 | 3 | 3 | 3 | 3 | 3 |
| | | | Minimum | 0.0 | 0.0 | 0.0 | 0.0 | 0.0 | 0.1 | 0.0 | 0.1 |
| | | | Maximum | 2.0 | 3.0 | 3.0 | 2.8 | 1.3 | 4.7 | 3.5 | 3.7 |
| | | | **Mean** | **0.7** | **1.3** | **1.3** | **1.2** | **0.5** | **1.7** | **1.6** | **1.4** |
| | | | **Std. Error** | **0.7** | **0.9** | **0.9** | **0.8** | **0.4** | **1.5** | **1.0** | **1.1** |

Pregnant and lactating females are not included.

Table 3. Cytochrome P450 1A1 Expression of Vascular Endothelial Cells in the Blubber and PCB Concentrations of Bottlenose Dolphins Live-captured and Released in Charleston, SC and Indian River Lagoon, FL during July and August 2003.[1]

| | | Modified CYP1A1 Staining Score | | | | Blubber PCB concentrations (ng/g) | | | | Plasma PCB concentrations (ng/g) | | | |
|---|---|---|---|---|---|---|---|---|---|---|---|---|---|
| Category | | Superficial | Middle | Deep | Average | TEQ98 (wet wt.) | TEQ98 (lipid wt.) | Total PCB (wet wt.) | Total PCB (lipid wt.) | TEQ98 (wet wt.) | Total PCB[4] (wet wt.) | Total OH-PCB[4] (wet wt.) | Total OH-PCB / PCB[4] ratio |
| CHS dolphins | N of cases | 31 | 31 | 31 | 31 | 30 | 30 | 30 | 30 | 22 | 22 | 19 | 19 |
| | Minimum | 0.0 | 0.2 | 0.4 | 0.2 | 0.042 | 0.104 | 1691 | 4539 | 0.00019 | 33.5 | 2.7 | 0.02 |
| | Maximum | 37.8 | 114.0 | 262.5 | 107.3 | 0.167 | 0.458 | 64518 | 255010 | 0.00267 | 1066.7 | 192.0 | 0.45 |
| | | A[2],a | A,a | A,b | A | A | A | A | A | A | A | A | A |
| | **Mean** | **5.1** | **10.7** | **35.9** | **15.0** | **0.068** | **0.194** | **28037** | **84833** | **0.00125** | **371.2** | **57.4** | **0.15** |
| | **Std. Error** | **1.8** | **3.9** | **10.6** | **4.2** | **0.004** | **0.014** | **2482** | **10820** | **0.00012** | **44.8** | **12.3** | **0.03** |
| IRL dolphins | N of cases | 30 | 30 | 30 | 30 | 26 | 26 | 26 | 26 | 26 | 26 | 26 | 26 |
| | Minimum | 0.0 | 0.0 | 0.0 | 0.0 | 0.028 | 0.091 | 429 | 1520 | 0.00015 | 53.2 | 0.1 | 0.00 |
| | Maximum | 41.2 | 82.8 | 159.3 | 84.4 | 0.067 | 0.295 | 45986 | 227291 | 0.00174 | 715.6 | 13.3 | 0.06 |
| | | A,a[3] | A,a | B,a | A | B | A | A | A | A | A | B | B |
| | **Mean** | **3.1** | **8.1** | **13.1** | **8.3** | **0.050** | **0.169** | **20892** | **74254** | **0.00077** | **245.2** | **3.2** | **0.02** |
| | **Std. Error** | **1.5** | **3.6** | **6.5** | **3.8** | **0.002** | **0.011** | **2110** | **10430** | **0.00009** | **35.6** | **0.6** | **0.00** |
| Subadult dolphins | N of cases | 13 | 13 | 13 | 13 | 10 | 10 | 10 | 10 | 7 | 7 | 6 | 6 |
| | Minimum | 0.0 | 0.0 | 0.0 | 0.0 | 0.038 | 0.097 | 9528 | 25306 | 0.00031 | 69.6 | 1.1 | 0.00 |
| | Maximum | 37.8 | 21.1 | 20.6 | 22.4 | 0.107 | 0.252 | 29219 | 70074 | 0.00174 | 674.5 | 76.6 | 0.23 |
| | | A,a | A,a | A,a | A | A | A | A | A | A | A | A | A |
| | **Mean** | **7.2** | **6.3** | **6.2** | **6.4** | **0.067** | **0.159** | **19808** | **47798** | **0.00109** | **304.3** | **14.6** | **0.05** |
| | **Std. Error** | **3.4** | **2.0** | **2.0** | **2.1** | **0.008** | **0.015** | **2025** | **4277** | **0.00019** | **74.4** | **12.4** | **0.04** |
| Adult dolphins | N of cases | 48 | 48 | 48 | 48 | 46 | 46 | 46 | 46 | 41 | 41 | 39 | 39 |
| | Minimum | 0.0 | 0.0 | 0.0 | 0.0 | 0.028 | 0.091 | 429 | 1520 | 0.00015 | 33.5 | 0.1 | 0.00 |
| | Maximum | 41.2 | 114.0 | 262.5 | 107.3 | 0.167 | 0.458 | 64518 | 255010 | 0.00267 | 1066.7 | 192.0 | 0.45 |
| | | B,a | A,b | A.c | A | A | A | A | A | B | A | A | A |
| | **Mean** | **3.3** | **10.3** | **29.7** | **13.1** | **0.058** | **0.188** | **25787** | **86904** | **0.00097** | **302.7** | **27.9** | **0.08** |
| | **Std. Error** | **1.1** | **3.3** | **8.0** | **3.6** | **0.003** | **0.010** | **2003** | **8789** | **0.00009** | **32.3** | **7.3** | **0.02** |

[1] The data includes males and non-pregnant, non-lactating females.

[2] Between categories, blubber layers that share a similar capital letter are not significantly different from each other ($P > 0.05$).

[3] Within categories, blubber layers that share a similar lowercase letter are not significantly different from each other ($P > 0.05$).

[4] Houde et al. (2006) report plasma PCB and OH-PCB concentrations in these dolphins. The mean values reported here represent a different combination of individuals than reported in Houde et al. (2006 OH-PCB levels and ratios in this table represent the sum of all identified congeners.

Table 4. Slope $\beta_1$, $R^2$, and P-values of the Simple Linear Regression Equations for Cytochrome P450 1A1 Expression of Vascular Endothelial Cells in Bottlenose Dolphins Live-captured and Released in Charleston, SC and Indian River Lagoon, FL during July and August 2003.

| Independent Variables | Dependent Variables: Log CYP1A1 Staining Score of Vascular Endothelial Cells | | | | | | | | | | | |
|---|---|---|---|---|---|---|---|---|---|---|---|---|
| | Average | | | Superficial[1] | | | Middle[1] | | | Deep[1] | | |
| | $\beta_1$ | $R^2$ | P | $\beta_1$ | $R^2$ | P | $\beta_1$ | $R^2$ | P | $\beta_1$ | $R^2$ | P |
| **CHS and IRL (N = 48)[2]** | | | | | | | | | | | | |
| Blubber $TEQ_{98}$ (ng/g wet wt) | 5.57 | 0.04 | 0.15 | | | | | | | | | |
| Blubber $TEQ_{98}$ (ng/g lipid wt) | **2.44** | **0.10** | **0.03** | | | | | | | | | |
| Blubber Total PCBs (ng/g wet wt) | <0.01 | 0.03 | 0.24 | | | | | | | | | |
| Blubber Total PCBs (ng/g lipid wt) | <0.01 | 0.04 | 0.15 | | | | | | | | | |
| Plasma $TEQ_{98}$ (ng/g wet wt) | **303.51** | **0.10** | **0.03** | 107.93 | 0.02 | 0.39 | 245.99 | 0.07 | 0.07 | **435.58** | **0.15** | **<0.01** |
| Plasma Total PCBs (ng/g wet wt) | <0.01 | <0.01 | 0.65 | <-0.01 | <0.01 | 0.52 | <0.01 | <0.01 | 0.86 | <0.01 | 0.02 | 0.38 |
| **CHS males (N = 19)** | | | | | | | | | | | | |
| Blubber $TEQ_{98}$ (ng/g wet wt) | 5.83 | 0.07 | 0.26 | | | | | | | | | |
| Blubber $TEQ_{98}$ (ng/g lipid wt) | 2.11 | 0.09 | 0.21 | | | | | | | | | |
| Blubber Total PCBs (ng/g wet wt) | <-0.01 | 0.01 | 0.68 | | | | | | | | | |
| Blubber Total PCBs (ng/g lipid wt) | <0.01 | <0.01 | 0.99 | | | | | | | | | |
| Plasma $TEQ_{98}$ (ng/g wet wt) | 127.19 | 0.01 | 0.65 | -20.31 | <0.01 | 0.93 | 79.52 | <0.01 | 0.75 | 99.27 | <0.01 | 0.75 |
| Plasma Total PCBs (ng/g wet wt) | <-0.01 | <0.01 | 0.77 | <-0.01 | 0.03 | 0.51 | <-0.01 | 0.01 | 0.65 | <-0.01 | 0.01 | 0.65 |
| Layer Specific Adipocyte Area ($uM^2$) | <-0.01 | 0.09 | 0.22 | <-0.01 | 0.18 | 0.07 | <0.01 | <0.01 | 0.99 | **<-0.01** | **0.29** | **0.02** |
| age | -0.01 | 0.01 | 0.61 | <-0.01 | <0.01 | 0.86 | <-0.01 | <0.01 | 0.68 | -0.02 | 0.03 | 0.49 |
| **IRL males (N = 21)** | | | | | | | | | | | | |
| Blubber $TEQ_{98}$ (ng/g wet wt) | **-36.07** | **0.22** | **0.03** | | | | | | | | | |
| Blubber $TEQ_{98}$ (ng/g lipid wt) | 1.84 | 0.04 | 0.40 | | | | | | | | | |
| Blubber Total PCBs (ng/g wet wt) | <0.01 | 0.05 | 0.34 | | | | | | | | | |
| Blubber Total PCBs (ng/g lipid wt) | <0.01 | 0.10 | 0.15 | | | | | | | | | |
| Plasma $TEQ_{98}$ (ng/g wet wt) | **709.83** | **0.27** | **0.01** | **542.61** | **0.22** | **0.03** | **698.81** | **0.24** | **0.03** | **827.42** | **0.31** | **<0.01** |
| Plasma Total PCBs (ng/g wet wt) | <0.01 | 0.02 | 0.58 | <0.01 | <0.01 | 0.80 | <0.01 | 0.01 | 0.62 | <0.01 | 0.03 | 0.49 |
| Layer Specifc Adipocyte Area ($uM^2$) | <-0.01 | 0.11 | 0.14 | <-0.01 | 0.02 | 0.50 | <-0.01 | 0.02 | 0.56 | **<-0.01** | **0.37** | **<0.01** |
| age | 0.05 | 0.17 | 0.06 | 0.02 | 0.04 | 0.38 | 0.05 | 0.18 | 0.06 | **0.06** | **0.22** | **0.03** |

[1] Linear regression equations relating CYP1A1 depth-specific expression and blubber $TEQ_{98}$ were not performed because blubber chemical analysis was completed on the entire blubber and not the layers.

[2] Combines males and non-pregnant, non-lactating females from both CHS and IRL locations.
Significant differences are in bold and underlined.

Table 5. Slope $\beta_1$, $R^2$, and P-values of the Linear Regression Equations for $TEQ_{98}$, Total PCB, and OH-PCB concentrations Versus Age in Male Bottlenose Dolphins Live-captured and Released in Charleston, SC and Indian River Lagoon, FL during July and August 2003.

| Dependent Variables | Independent Variable: Age | | |
|---|---|---|---|
| | $\beta_1$ | $R^2$ | P |
| **CHS males (N = 19)** | | | |
| Blubber $TEQ_{98}$ (ng/g wet wt) | <-0.01 | 0.08 | 0.23 |
| Blubber $TEQ_{98}$ (ng/g lipid wt) | <-0.01 | 0.02 | 0.52 |
| Blubber Total PCBs (ng/g wet wt) | **900.11** | **0.34** | **<0.01** |
| Blubber Total PCBs (ng/g lipid wt) | **3874.09** | **0.21** | **0.05** |
| Plasma $TEQ_{98}$ (ng/g wet wt) | <0.01 | 0.01 | 0.81 |
| Plasma Total PCBs (ng/g wet wt) | **17.02** | **0.25** | **0.03** |
| Plasma OH-PCBs (ng/g wet wt)[1, 2] | 2.39 | 0.07 | 0.32 |
| **IRL males (N = 21)** | | | |
| Blubber $TEQ_{98}$ (ng/g wet wt) | <0.01 | <0.01 | 0.78 |
| Blubber $TEQ_{98}$ (ng/g lipid wt) | **0.01** | **0.34** | **<0.01** |
| Blubber Total PCBs (ng/g wet wt) | 716.64 | 0.11 | 0.14 |
| Blubber Total PCBs (ng/g lipid wt) | **5648.77** | **0.24** | **0.02** |
| Plasma $TEQ_{98}$ (ng/g wet wt) | <0.01 | 0.02 | 0.49 |
| Plasma Total PCBs (ng/g wet wt) | 4.65 | 0.02 | 0.56 |
| Plasma OH-PCBs (ng/g wet wt)[1] | -0.03 | <0.01 | 0.85 |

[1] Linear regression equations were completed on the sum of all identified OH-PCB congeners. The equations reported here were completed on a different combination of individuals than reported in Houde et al. (2006).

[2] N = 17

Significant differences are in bold and underlined.

Table 6. Slope $\beta_1$, $R^2$, and P-values of the Non-linear Regression Equations for TEQ98, Total PCB, and OH-PCB concentrations Versus Age in Female Bottlenose Dolphins Live-captured and Released in Charleston, SC and Indian River Lagoon, FL during July and August 2003.

| Dependent Variables | Independent Variable: Age | |
|---|---|---|
| | $\beta_1$ | $R^2$ |
| **CHS females (N = 12)**[1] | | |
| Blubber $TEQ_{98}$ (ng/g wet wt) | -0.51 | 0.86 |
| Blubber $TEQ_{98}$ (ng/g lipid wt) | -0.17 | 0.22 |
| Blubber Total PCBs (ng/g wet wt) | -1.46 | 0.93 |
| Blubber Total PCBs (ng/g lipid wt) | -1.15 | 0.91 |
| Plasma $TEQ_{98}$ (ng/g wet wt)[2] | NA | NA |
| Plasma Total PCBs (ng/g wet wt)[2] | NA | NA |
| Plasma OH-PCBs (ng/g wet wt)[3, 4] | NA | NA |
| **IRL females (N = 6)**[1] | | |
| Blubber $TEQ_{98}$ (ng/g wet wt) | -0.13 | 0.06 |
| Blubber $TEQ_{98}$ (ng/g lipid wt) | -0.13 | 0.07 |
| Blubber Total PCBs (ng/g wet wt) | -0.78 | 0.55 |
| Blubber Total PCBs (ng/g lipid wt) | -1.14 | 0.91 |
| Plasma $TEQ_{98}$ (ng/g wet wt) | -2.44 | 0.94 |
| Plasma Total PCBs (ng/g wet wt) | -2.21 | 0.62 |
| Plasma OH-PCBs (ng/g wet wt)[3] | -1.13 | 0.53 |

[1] Includes pregnant and lactating females.

[2] N = 8

[3] Non-linear regression equations were completed on the sum of all identified OH-PCB congeners. The equations reported here were completed on a different combination of individuals than reported in Houde et al. (2006).

[4] N = 7

The non-linear equation tested was $y = \beta_0 x^{\beta 1}$.

NA = not applicable because no plasma chemical analysis was available for subadult females.
Significant differences are in bold and underlined.

Table 7. Slope $\beta_1$, $R^2$, and P-values of the Simple Linear Regression Equations for Cytochrome P450 1A1 Expression of Vascular Endothelial Cells in Female Bottlenose Dolphins Live-captured and Released in Charleston, SC and Indian River Lagoon, FL during July and August 2003.

| Independent Variables | Dependent Variables: Log CYP1A1 Staining Score of Vascular Endothelial Cells | | | | | | | | | | | |
|---|---|---|---|---|---|---|---|---|---|---|---|---|
| | Average | | | Superficial[1] | | | Middle[1] | | | Deep[1] | | |
| | $\beta_1$ | $R^2$ | P | $\beta_1$ | $R^2$ | P | $\beta_1$ | $R^2$ | P | $\beta_1$ | $R^2$ | P |
| **CHS females (N = 12)[2]** | | | | | | | | | | | | |
| Blubber $TEQ_{98}$ (ng/g wet wt) | 5.34 | 0.07 | 0.40 | | | | | | | | | |
| Blubber $TEQ_{98}$ (ng/g lipid wt) | **7.02** | **0.35** | **0.04** | | | | | | | | | |
| Blubber Total PCBs (ng/g wet wt) | <0.01 | 0.06 | 0.43 | | | | | | | | | |
| Blubber Total PCBs (ng/g lipid wt) | <0.01 | 0.11 | 0.30 | | | | | | | | | |
| Plasma $TEQ_{98}$ (ng/g wet wt)[3] | -123.36 | 0.02 | 0.71 | 346.13 | 0.10 | 0.45 | 33.10 | <0.01 | 0.93 | -220.18 | 0.10 | 0.45 |
| Plasma Total PCBs (ng/g wet wt)[3] | <-0.01 | 0.07 | 0.53 | <0.01 | <0.01 | 0.95 | <-0.01 | 0.04 | 0.64 | <0.01 | 0.10 | 0.45 |
| Layer Specific Adipocyte Area ($uM^2$) | <0.01 | <0.01 | 0.97 | <-0.01 | 0.01 | 0.73 | <-0.01 | 0.02 | 0.64 | <-0.01 | 0.03 | 0.57 |
| **IRL females (N = 7)[2]** | | | | | | | | | | | | |
| Blubber $TEQ_{98}$ (ng/g wet wt) | -7.11 | 0.12 | 0.44 | | | | | | | | | |
| Blubber $TEQ_{98}$ (ng/g lipid wt) | -1.83 | 0.08 | 0.54 | | | | | | | | | |
| Blubber Total PCBs (ng/g wet wt) | <-0.01 | 0.16 | 0.38 | | | | | | | | | |
| Blubber Total PCBs (ng/g lipid wt) | <-0.01 | 0.14 | 0.40 | | | | | | | | | |
| Plasma $TEQ_{98}$ (ng/g wet wt) | -76.58 | 0.03 | 0.72 | -119.16 | 0.04 | 0.65 | -124.50 | 0.07 | 0.55 | 43.13 | <0.01 | 0.85 |
| Plasma Total PCBs (ng/g wet wt) | <-0.01 | 0.18 | 0.33 | <-0.01 | 0.13 | 0.43 | <-0.01 | 0.20 | 0.31 | <-0.01 | 0.09 | 0.50 |
| Layer Specifc Adipocyte Area ($uM^2$) | <0.01 | 0.14 | 0.41 | <-0.01 | 0.39 | 0.14 | <0.01 | 0.26 | 0.24 | <0.01 | 0.07 | 0.58 |

[1] Linear regression equations relating CYP1A1 depth-specific expression and blubber $TEQ_{98}$ were not performed because blubber chemical analysis was completed on the entire blubber and not the layers.

[2] Includes pregnant and lactating females.

[3] N = 8

Significant differences are in bold and underlined.

Table 8. Relationship between OH-PCB Concentrations and Cytochrome P450 1A1 Expression of Vascular Endothelial Cells of the Deep Blubber Layer in Bottlenose Dolphins Live-captured and Released in Charleston, SC and Indian River Lagoon, FL during July and August 2003.[1, 2]

| Abbreviation | Full Chemical Name | CHS % of OH-PCBs[3] | IRL % of OH-PCBs[3] | Avg % of OH-PCBs | Observed Relationship[4, 5] | | |
|---|---|---|---|---|---|---|---|
| | | | | | $\beta_1$ | $R^2$ | P |
| Trichlorobiphenyls | | | | | | | |
| 4-OH-CB18 | 4-OH-2,2',5-trichlorobiphenyl | **11.29 ± 4.60** | 1.83 ± 0.47 | 5.84 ± 2.04 | **0.4957** | **0.0682** | **0.0457** |
| 2'-OH-CB26 | 2'-OH-2,3',5-trichlorobiphenyl | **9.45 ± 3.42** | 0.03 ± 0.00 | 4.02 ± 1.56 | **0.7062** | **0.1390** | **0.0036** |
| 4-OH-CB26 | 4-OH-2,3',5-trichlorobiphenyl | **55.89 ± 5.46** | 12.74 ± 3.71 | 31.02 ± 4.19 | **1.1801** | **0.1893** | **0.0006** |
| Tetrachlorobiphenyls | | | | | | | |
| 4-OH-CB57 | 4-OH-2,3,3',5-tetrachlorobiphenyl | 0.01 ± 0.00 | **4.34 ± 1.00** | 2.51 ± 0.64 | -0.4925 | 0.1105 | 0.0101 |
| 2'-OH-CB69 | 2'-OH-2,3',4,6-tetrachlorobiphenyl | **2.56 ± 0.79** | 0.03 ± 0.01 | 1.10 ± 0.37 | **0.8269** | **0.2120** | **0.0002** |
| 4'-OH-CB69 | 4'-OH-2,3',4,6-tetrachlorbiphenyl | **7.06 ± 2.31** | 2.17 ± 0.48 | 4.25 ± 1.05 | 0.1205 | 0.0028 | 0.6910 |
| Pentachlorobiphenyls | | | | | | | |
| 4'-OH-CB88 | 4'-OH-2,2',3,4,6-pentachlorobiphenyl | 0.71 ± 0.36 | 2.85 ± 1.04 | 1.94 ± 0.63 | 0.1068 | 0.0063 | 0.5502 |
| 2'-OH-CB106 | 2'-OH-2,3,3',4,5-pentachlorobiphenyl | 0.05 ± 0.04 | **0.95 ± 0.32** | 0.56 ± 0.19 | -0.0735 | 0.0069 | 0.5319 |
| 4-OH-CB107 | 4-OH-2,3,3',4',5-pentachlorobiphenyl | 6.50 ± 0.86 | **24.29 ± 5.75** | 16.75 ± 3.51 | 0.3708 | 0.0462 | 0.1019 |
| 3-OH-CB118 | 3-OH-2,3',4,4',5-pentachlorobiphenyl | 0.09 ± 0.04 | 0.02 ± 0.00 | 0.05 ± 0.02 | **0.2123** | **0.1011** | **0.0141** |
| Hexachlorobiphenyls | | | | | | | |
| 4'-OH-CB130 | 4'-OH-2,2',3,3',4,5'-hexachlorobiphenyl | 0.05 ± 0.01 | **0.36 ± 0.14** | 0.23 ± 0.08 | 0.2849 | 0.0619 | 0.0575 |
| 3'-OH-CB138 | 3'-OH-2,2',3,4,4',5'-hexachlorobiphenyl | 0.08 ± 0.03 | 0.16 ± 0.09 | 0.12 ± 0.05 | **0.5369** | **0.239** | **0.0001** |
| 4-OH-CB146 | 4-OH-2,2',3,4',5,5'-hexachlorobiphenyl | 0.03 ± 0.01 | 1.45 ± 0.81 | 0.85 ± 0.48 | 0.1811 | 0.029 | 0.197 |
| 4'-OH-CB159 | 4'-OH-2,3,3',4,5,5'-hexachlorobiphenyl | 0.49 ± 0.24 | 0.06 ± 0.02 | 0.24 ± 0.10 | **0.2813** | **0.0889** | **0.0218** |
| Heptachlorobiphenyls | | | | | | | |
| 3'-OH-CB180 | 3'-OH-2,2',3,4,4',5,5'-heptachlorobiphenyl | 0.03 ± 0.01 | 0.06 ± 0.05 | 0.05 ± 0.03 | **0.352** | **0.151** | **0.0023** |
| 4-OH-CB187 | 4-OH-2,2',3,4',5,5',6-heptachlorobiphenyl | 0.07 ± 0.02 | **1.52 ± 0.25** | 0.91 ± 0.17 | -0.1151 | 0.0209 | 0.2740 |
| 4-OH-CB193 | 4-OH-2,3,3',4',5,5',6-heptachlorobiphenyl | 0.03 ± 0.01 | 1.09 ± 0.66 | 0.64 ± 0.39 | 0.1677 | 0.0262 | 0.2204 |
| Octachlorobiphenyls | | | | | | | |
| 4'-OH-CB199 | 4'-OH-2,2',3,3',4,5,5',6'-octachlorobiphenyl | 0.17 ± 0.07 | **28.70 ± 5.25** | 16.61 ± 3.53 | -0.1222 | 0.0044 | 0.6148 |
| 4-OH-CB202 | 4'-OH-2,2',3,3',5,5',6,6'-octachlorobiphenyl | 0.22 ± 0.07 | **14.91 ± 4.82** | 8.68 ± 2.92 | -0.1196 | 0.0051 | 0.5912 |
| Nonachlorobiphenyls | | | | | | | |
| 4'-OH-CB208 | 4'-OH-2,2',3,3',4,5,5',6,6'-nonachlorobiphenyl | 0.35 ± 0.12 | **1.38 ± 0.30** | 0.95 ± 0.19 | 0.0323 | 0.0010 | 0.8118 |

[1] Houde et al. (2006) report plasma OH-PCB concentrations in these dolphins in greater detail.

[2] Combines males and all females (including pregnant and lactating dolphins) from both CHS and IRL locations; N = 59.

[3] Significant differences between CHS and IRL are indicated in bold and underlined.

[4] Combines both CHS and IRL locations; N = 59.

[5] Significant positive relationships between CYP1A1 expression and OH-PCB concentrations are in bold and underlined.

# CHAPTER IV:
# NEUROANATOMY AND BRAIN VOLUMES OF THE ATLANTIC WHITE-SIDED DOLPHIN (*LAGENORHYNCHUS ACUTUS*) FROM MAGNETIC RESONANCE IMAGES

**ABSTRACT**

In this study, I devised a novel, quantitative approach to assess neurodevelopment in the Atlantic white-sided dolphin (*Lagenorhynchus acutus*) by determining the volumes of brain structures from magnetic resonance (MR) images of fresh, post-mortem brains *in situ* (i.e. the brain intact within the skull with the head still attached to the body). It is important to develop these approaches because emerging chemicals (PBDEs and OH-PCBs) and legacy chemicals (PCBs) that bioaccumulate in odontocetes may affect neurodevelopment of the cerebellum, corpus callosum, hippocampus, and cochlea. We provide, for the first time, an anatomically labeled MRI-based atlas of the fetal and subadult Atlantic white-sided dolphin brain. These dolphin brains displayed the classic hallmarks of odontocete brains – foreshortened orbital lobes and pronounced bitemporal width. Olfactory structures were absent, while auditory system structures were enlarged (e.g. relatively large inferior colliculi). In all post-mortem MRI scans of Atlantic white-sided dolphins, the hippocampus was identifiable, in contrast to prior MRI studies on formalin-fixed odontocete brains. Myelination patterns during ontogenesis were also examined. White matter (WM): grey matter (GM) volume ratios of the entire brain increased from the fetus to adult. Specifically, the white matter tracts of the fetal hindbrain and cerebellum were pronounced, but in the telencephalon, the white matter tracts were much less distinct. In addition, the white matter tracts of the auditory pathways in the fetal brains were myelinated, indicated by the T2 hypo-intensity signal for the inferior colliculus, the cochlear nuclei, and trapezoid body. This provides an indication that hearing and auditory processing regions mature early during ontogeny (prenatally). Quantitative measurements from MR images were obtained for the cerebellum (WM and GM volumes), corpus callosum (mid-sagittal area), and hippocampus (left and right hippocampal formations and surrounding fluid structure volumes) of Atlantic white-sided dolphins. In this study, the cerebellum (WM and GM volumes combined) of subadult and adult specimens ranged between 13.8 to 15.0% of the total brain size. These findings were within the range of measurements found in bottlenose dolphins and common dolphins. The corpus callosum area to brain mass ratios

(CCA/BM) ranged between 0.088 and 0.137. These measurements were within the range of CCA/BM ratios observed in other odontocete studies. The small hippocampi of the Atlantic white-sided dolphin compared to carnivores and ungulates were consistent with previous qualitative findings on the hippocampus in the bottlenose dolphin. In this study, we establish an approach for accurately determining the size of brain structures from MR images of brains *in situ* of stranded, dead dolphins. Therefore, we can use this approach to quantify the potential impacts of natural toxins (such as domoic acid) and anthropogenic chemicals (such as PCBs, PBDEs, and their hydroxylated metabolites) on the size of brain regions in marine mammal species. These studies are underway.

**KEYWORDS:** MRI; odontocete; Atlantic white-sided dolphin; brain; cerebellum; corpus callosum; hippocampus; ontogeny

## INTRODUCTION

Odontocetes (toothed whales, dolphins, and porpoises) have undergone unique anatomical adaptations to an aquatic environment. One of the most prominent modifications has been in brain size. In fact, several odontocete species have encephalization quotients (a measure of relative brain size) that are second only to modern humans (Marino, 1998; Ridgway and Brownson, 1984). Several studies have been completed on odontocete neuroanatomy, as reviewed in Morgane et al. (1986) and Ridgway (1990). However, few studies have focused on quantitative measurements of odontocete brain structures (Marino et al., 2000; Tarpley and Ridgway, 1994). Fewer studies have focused on odontocete prenatal neuroanatomy or on quantitative data on prenatal brain structures (Marino et al., 2001b).

For odontocetes, there is a paucity of data on the size of individual brain structures through an ontogenetic series from fetus to adult. This is important information not only for comparative evolutionary studies but also for marine mammal health concerns. Emerging threats to marine mammal health include anthropogenic chemicals such as hydroxylated polychlorinated biphenyls (OH-PCBs) (McKinney et al.,

2006; Sandala et al., 2004) and polybrominated diphenyl ethers (PBDEs)(de Boer et al., 1998); land-based pathogen pollution (Conrad et al., 2005); and biotoxins from harmful algal blooms (HABs)(Scholin et al., 2000). These chemical and biological agents can target the brain. For example, domoic acid (a type of biotoxin produced by some diatom *Pseudo-nitzschia* species and associated with HABs) is neurotoxic and has been shown to cause bilateral hippocampal atrophy in California sea lions (Silvagni et al., 2005).

Of particular concern in odontocetes is the bioaccumulation of PCBs, PBDEs, and their hydroxylated metabolites (i.e OH-PCBs and HO-PBDEs). In some populations, the levels of persistent organic pollutants in blubber are extremely high, as observed in beluga whales (*Delphinapterus leucas)* from the St. Lawrence Estuary (Muir et al., 1996), striped dolphins (*Stenella coeruleoalba*) from the Western Mediterranean (Kannan et al., 1993), killer whales (*Orcinus orca*) from British Columbia (Ross et al., 2000), bottlenose dolphins (*Tursiops truncatus*) from the Southeast United States (Hansen et al., 2004; Wells et al., 2005), and Atlantic white-sided dolphins (*Lagenorhynchus acutus*) from the Northeast United States (Tuerk et al., 2005). Generally, odontocete females transfer a large percentage of their contaminant load from blubber to their offspring during lactation (Borrell et al., 1995; Wells et al., 2005). For example, in bottlenose dolphins from Sarasota, Florida, first-born calves have higher PCB concentrations than subsequent calves of similar age (Wells et al., 2005).

In laboratory animals and wildlife, PCBs, PBDEs, and their hydroxylated metabolites can interfere with the thyroid hormone system (as reviewed by Birnbaum and Staskal, 2004; Brouwer et al., 1998; Zoeller, 2002). Thyroid hormones play an integral role in neuro-development, particularly in Purkinje cell dendritic arborization in the cerebellum (Kimura-Kuroda et al., 2002), axonal myelination of the corpus callosum (Schoonover et al., 2004), proliferation of dentate gyrus granule cells in the hippocampus (Rami et al., 1986), and cochlear development (Knipper et al., 2000). In mouse cerebellar culture assays, OH-PCBs inhibit thyroid-hormone-dependent arborization of cerebellar Purkinje cell dendrites (Kimura-Kuroda et al., 2005). In fetal rats, Aroclor 1254 (a PCB mixture) decreases the cell density of the corpus callosum (Sharlin et al.,

2006). Hence, there is concern that PCBs, PBDEs, and their metabolites may affect neuro-development in odontocetes.

It is important to develop methods to assess the effects of environmental chemicals on neurodevelopment in odontocetes. Magnetic resonance imaging (MRI), a common diagnostic tool in human medicine, has recently been used to study the comparative neuroanatomy of the beluga whale (Marino et al., 2001a), the fetal common dolphin (*Delphinus delphis*)(Marino et al., 2001b), the bottlenose dolphin (Marino et al., 2001c), the harbor porpoise (*Phocoena phocoena*) (Marino et al., 2003b), the dwarf sperm whale (*Kogia simus*) (Marino et al., 2003a), the spinner dolphin (*Stenella longirostris orientalis*) (Marino et al., 2004b), and the killer whale (Marino et al., 2004a). These studies were completed on formalin fixed brains rather than fresh tissue. MR imaging offers a non-invasive and non-destructive method of acquiring a permanent archive of external and internal brain structure data. In addition, MR imaging, coupled with advanced software image analysis, can accurately determine regional brain volumes, while traditional dissection and photography introduce greater possibility of error in performing quantitative measurements.

Our goal in this study was to devise a novel, quantitative approach to assess neurodevelopment in the Atlantic white-sided dolphin by determining the volumes of brain structures from MR images of the post-mortem brain intact within the skull with the head still attached to the body (i.e. *in situ*). Specifically, the objectives of this study were to: a) validate our techniques by determining if MR imaging coupled with advanced software image processing and segmentation could accurately determine volumes; b) provide an anatomically labeled MRI-based atlas of the fetal and subadult Atlantic white-sided dolphin brain; c) determine the white matter and grey matter volumes of the total brain and cerebellum along an ontogenetic series using MR images; d) from MR images, determine the mid-sagittal area of the corpus callosum and the volumes of the left and right hippocampal formation.

## METHODS

### *Specimens*

The Atlantic white-sided dolphin specimens used in this study had been stranded live on the beaches of Cape Cod, Massachusetts between 2002 and 2005. Stranded animals were usually first reported by the public and then responded to by the Cape Cod Stranding Network (CCSN) in Buzzards Bay, MA. The specimens were either found freshly dead or euthanized by stranding response personnel or by local veterinarians because of poor health. Less than 24 hours had passed since the time of death in all cases. The specimens were then immediately transported to the Woods Hole Oceanographic Institution (WHOI) necropsy facility where total body weights and morphometric measurements were recorded. Some specimens were then prepared for magnetic resonance (MR) imaging (Table 1). The headcoil of the MRI scanners had a circumference of 80 cm. Therefore, the blubber, nuchal fat, and semispinalis muscle of specimens that had an axillary girth greater than 80cm were removed from the head region. The pectoral and dorsal fins were removed in all carcasses. The specimens were then washed, dried, and placed in transport bags with ice surrounding the head. The specimens were then immediately transported to the MRI facility or temporarily stored at 40$^{o}$F until imaging could be completed. The time of the MRI was recorded. After imaging, the specimen was transported back to WHOI and stored at 40$^{o}$F overnight. A complete necropsy was performed the next day. Cerebrospinal fluid (CSF) was collected. The brain was removed, weighed, and archived in 10% neutral buffered formalin for histological analysis or at –80$^{o}$C for contaminant analysis (see Appendix 7).

The specimens were classified as fetuses, neonates (126 cm to 140 cm), subadults (defined as reproductively immature, i.e. females of body length from 141 to 201 cm, and males of body length from 141 to 210 cm), or adults. Total length measurements were used in this classification, consistent with those previously determined by Sergeant et al. (1980). In addition, reproductive state (lactation and pregnancy indicated sexual maturity for females) and measurement of gonads (weight and macroscopic examination) also

helped in classification of the specimens into the appropriate age class. Teeth were archived for future aging of dolphins.

***Magnetic Resonance Data Acquisition***

Magnetic resonance imaging of the entire brain was completed with the brain intact with the skull and the head attached to the body. MR images were acquired in the coronal and sagittal planes with either a 1.5-T Siemens Vision scanner (Siemens, Munich, Germany) at the Massachusetts Eye and Ear Infirmary (MEEI), Massachusetts General Hospital, Boston, MA or a 1.5-T Siemens Symphony scanner (Siemens, Munich, Germany) at Shields MRI and CT of Cape Cod, Hyannis, MA (Table 4). Two-dimensional proton density (PD) and T2-weighted images were acquired using a fast spin-echo sequence with the following parameters: TE = 15/106 ms for PD and T2 respectively; TR = 9000 ms; slice thickness = 2mm; Flip angle = $180^{o}$; FOV = 240 x 240mm; matrix = 256 x 256; voxel size = 0.9 x 0.9 x 2.0 mm. For fetal brains, the parameters were altered because of the small size of the brain: TE = 15/106 ms for PD and T2 respectively; TR = 8000 ms; slice thickness = 2mm; Flip angle = $180^{o}$; FOV = 200 x 200mm; matrix = 256 x 256; voxel size = 0.8 x 0.8 x 2.0 mm.

***Image Processing***

The visualization, processing, segmentation (i.e. assigning pixels to a particular structure such as white matter or hippocampus), three-dimensional reconstructions, and volume analysis of MRI data was performed using the software program AMIRA 3.1.1 (Mercury Computer Systems, San Diego, CA). Native (i.e no processing of MRI data) T2 and PD-weighted images from each specimen were loaded into AMIRA, and the quality of images was evaluated. The data were then processed to ensure adequate threshold segmentation of the brain and cerebellum into white matter (WM), grey matter (GM), and cerebrospinal fluid (CSF) using methods similar to those described by Evans et al. (2006). Threshold segmentation is an automated technique that allows the software user to select pixels with signal intensity values of a defined range.

The image processing consisted of the following steps. First, the T2 and PD-weighted images were corrected for image intensity non-uniformity by applying a Gaussian filter to the originally acquired images (i.e. native). The processed results (i.e. intensity values) were then subtracted from the original images to generate a "filtered" data set. Second, the new data set was rotated and realigned around the y-axis to correct for head tilt and/or differences in head position. From this "filtered and realigned" data set, a brain surface mask was produced to remove head blubber, muscle, skull, and any other remaining head anatomy. The mask was constructed by manually tracing the surface of the brain and selecting all pixels within this trace for each MR image. These resulting data are referred to as the "processed" PD and T2 images (as compared to the originally acquired "native" PD and T2 images).

Rilling and Insel (1999) describe the theory of why image processing is necessary for accurate threshold segmentation (Rilling and Insel, 1999). An MR image is a map of pixels that are described by different signal intensities. In PD- and T2-weighted images, pixel signal intensity values are lowest for WM, higher for GM, and highest for CSF. AMIRA software can be instructed to select pixels with signal intensity values of a defined range. Thus, in principle, it should be easy to separate WM, GM, and CSF of native PD and T2-weighted images using computerized thresholding. However, most MRI scans contain gradients of signal intensity values, which cause WM, GM, and CSF in one part of the image to have different signal intensities than those in another region. Hence, a single threshold range cannot capture the WM, GM, or CSF for an entire slice. This problem is remedied by the application of a Gaussian filter to the native images (i.e. where each pixel is defined by a signal intensity value) to generate filtered results (i.e. a new set of signal intensity values) followed by subtraction of these filtered results from the native images to produce the "processed" images (i.e. where each pixel of the image set is now defined by a new signal intensity value). This processing corrects for the uneven illumination of the scene that is inherent in MR images.

However, a drawback of image processing is a loss of resolution, as observed by Evans (2006). Because of this, we chose to manually segment structures such as the

corpus callosum and hippocampus from native images (see Method section, Segmentation Analysis). In addition, it was not necessary to correct for signal intensity non-uniformity because manual tracing of structures does not depend on threshold segmentation.

***Volume Validation Experiments***

*Comparisons of Expected and Segmented Volumes of Water*. Processing of MR images was required for threshold segmentation of brains into WM, GM, and CSF, as described previously. Therefore, it was important to determine if our segmentation technique from processed images was accurate. In this experiment, MR imaging was completed on three separate vials containing a weighed amount of water (~20 mL or the expected volume). Water was used because of the high signal intensity observed in PD- and T2-weighted images. Two-dimensional PD- and T2-weighted images were acquired using a fast spin-echo sequence with parameters similar to those used for specimen scanning: TE = 15/106 ms for PD and T2 respectively; TR = 2500 ms; slice thickness = 2mm; Flip angle = $180^{o}$; FOV = 240 x 240 mm; matrix = 256 x 256; voxel size = 0.9 x 0.9 x 2.0 mm. Native T2 and PD-weighted images from each vial were loaded into AMIRA, and the quality of images was evaluated. The image processing of the T2 and PD native images of the vials followed steps similar to those taken in processing the images of the specimen brains, including the correction for image intensity non-uniformity and realignment. Three different processing conditions were applied to native PD and T2 images and these included: 1) application of a Gauss filter three successive times with sigma = 10 and kernel = 21 followed by subtraction of these results; 2) application of a Gauss filter sixteen successive times with sigma = 10 and kernel = 21 followed by subtraction of these results; 3) application of a Gauss filter three successive times with sigma = 10 and kernel = 21 followed by subtraction of these results and then realignment, which consisted of rotating the images $3^{o}$ around the y-axis. These sigma and kernel values were chosen because these values were used in the processing of native PD and T2 specimen images. Rotation of $3^{o}$ around the global y-axis was evaluated as

the realignment parameter because this rotation was often applied to specimen images to remove head tilt. The volumes of water for these different image-processing conditions were then determined using techniques identical to those used in specimen segmentation (i.e. specifying a defined range of signal intensities for water followed by manual editing). Three measurement replicates were completed. The segmented volumes were compared to the expected volumes and root mean squared errors (RMSE) and percent errors (% error) were calculated for each condition.

*Comparisons of Expected and Segmented Volumes of Brain Tissue.* We also performed an experiment with actual brain tissue to determine if the image processing and segmentation procedure in this study was accurate. In this experiment, MR imaging was completed on two dissected regions of the cerebellum from a formalin-fixed brain (CCSN05-038-La). These regions were comprised of WM and GM. Two-dimensional PD- and T2-weighted images were acquired using a fast spin-echo sequence with parameters similar to those used for specimen scanning: TE = 15/106 ms for PD and T2 respectively; TR = 4060 ms; slice thickness = 2mm; Flip angle = $180^{o}$; FOV = 240 x 240 mm; matrix = 256 x 256; voxel size = 0.9 x 0.9 x 2.0 mm. After MRI, the total volumes displaced by the cerebellum samples (i.e. expected total slice volume) were measured separately. The WM and GM were then dissected and separated, and the volumes displaced by each tissue type (i.e. expected WM and GM volumes) were also measured. Native PD and T2-weighted images from each cerebellum sample were loaded into AMIRA, and the quality of images was evaluated. The image processing of the PD and T2 native images of the vials followed steps similar to those taken in processing the images of the specimen brains, including the correction for image intensity non-uniformity and realignment. A Gauss filter (sigma = 10; kernel = 21) was applied to the PD native images ten successive times. The filter results were then subtracted from the native PD images to acquire a new image set. These images were then rotated $2^{o}$ around the y-axis. The volumes of WM and GM of the native and processed PD image set were then determined using techniques identical to those used in specimen segmentation.

Three measurement replicates were completed. The segmented volumes were compared to the expected volumes and RMSEs and % errors were calculated for each condition.

*Comparisons of Manual and Threshold Segmentation Volumes.* Rilling and Insel (1999) describe the theory of why image processing is necessary for threshold segmentation of the brain into WM, GM, and CSF, as previously discussed. We performed an experiment that compared threshold segmentation derived volumes (of WM, GM, and CSF) of both native and processed PD images (with the application and subtraction of a Gauss filter but not realignment) to manual segmentation volumes (of WM, GM, and CSF) derived from manually tracing the boundaries of WM, GM, and CSF. This experiment was completed on three coronal PD-weighted brain sections from separate specimens (CCSN05-040-La, CCSN05-037-La, and CCSN05-231-La) at the level of the inferior and superior colliculi. The Gauss filter processing of the PD images in this experiment followed the same steps as those taken in the processing of the specimen brains. The volumes of WM, GM, and CSF of the native and processed PD images were then determined using techniques identical to those used in specimen threshold segmentation. Three measurement replicates were completed. The threshold volumes were compared to the manual volumes and RMSEs and % errors were calculated for each condition.

### *Anatomic Labeling and Nomenclature*

Anatomical structures were identified and labeled in coronal and sagittal MR images of the subadult (CCSN05-084-La) and fetus (CCSN05-040-Fetus-La) brains. In the subadult, native PD-weighted images were used in the labeled schematics. For the fetal-labeled illustrations, native T2-weighted images were used because these images were higher resolution than PD-weighted images, which was most likely a function of the higher levels of water in fetal brains (Almajeed et al., 2004). The anatomical nomenclature was adopted from Morgane et al. (1980). MR images of the subadult and fetal brains in this study were also compared to previous findings of the bottlenose dolphin and of the fetal common dolphin (Marino et al., 2001c; Marino et al., 2001b).

***Segmentation Analysis***

For specimens in which the MRIs were of high quality, image segmentation produced the following measures:

- Total brain volume from "processed" PD weighted images;
- Total brain tissue (GM, WM, and CSF) volumes from "processed" T2-weighted images (for fetus segmenation) or "processed" PD-weighted images (for subadult and adult segmentation);
- Histogram of signal intensity values for the entire brain;
- Cerebellum tissue (GM and WM) volumes by manual segmentation of the previously generated total brain tissue label map (using a visual representation of the segmentation);
- Corpus callosum mid-sagittal area from native and processed PD-weighted sagittal images;
- Hippocampus and surrounding fluid structure volumes from native T2-weighted images.

These measurements are described below.

*Total Brain*. The brain surface mask was produced to remove head blubber, muscle, skull, and any other remaining head anatomy. This segmentation was constructed through a combination of computerized thresholding based on signal intensities that defined the brain surface and manual editing. Total brain segmented volumes were calculated by integrating the area of the selected tissue for each slice. Virtual brain weight was calculated by multiplying the total brain segmented volume by the specific gravity of brain tissue, 1.036 g/cm$^3$ (Stephan et al., 1981).

Total brain WM, GM, and CSF volumes were determined by threshold segmentation of the brain surface mask followed by manual editing of each slice. Specifically, this procedure involved thresholding for signal intensity ranges that captured the boundaries of WM, GM, and CSF followed by visual inspection and manual editing to ensure that the WM, GM, and CSF were properly defined. WM, GM, and CSF

volumes were determined three times for each specimen. WM:GM volume ratios of the total brain were also calculated three times .

*Cerebellum.* WM and GM volumes of the cerebellum were determined by manually editing the label map of the whole brain, which had been generated previously. The WM and GM volumes of the cerebellum included the vermis and the cerebellar hemispheres but did not include the white or grey matter of the pons, the auditory nerve, the cochlear nucleus, trapezoid body, the lateral lemniscus white matter tracts, inferior olive, or spinal cord. WM and GM volumes were determined three times for each specimen. WM:GM volume ratios of the cerebellum were also calculated. For each specimen, the percentage of the brain occupied by the cerebellum was calculated by dividing the sum of the cerebellar WM and GM volumes by the sum of the total brain WM and GM volumes multiplied by 100. For the neonate, subadults, and adults, volumes from processed PD-weighted images were used. For fetuses, volumes from processed T2-weighted images were used.

*Corpus Callosum*. The mid-sagittal area of the corpus callosum was determined by manually tracing the callosal perimeter of the midline sagittal section of both the "native" and "processed" sagittal PD images. The area was calculated using AMIRA software. During MR acquisition in the sagittal plane for each specimen, special care was taken to obtain MR images that would give an accurate longitudinal midline section. Therefore, during processing of the sagittal images, it was not necessary to perform any realignment. The mid-sagittal areas were determined three times from both the "native" and "processed" PD images. The areas obtained from the "native" PD images were favored because image processing decreased the resolution of images, as described previously. Mid-sagittal corpus callosum areas relative to the total brain weight (CCA/BW) were also calculated by dividing the area (from native PD-weighted images) by the total brain weight.

*Hippocampus.* Left and right hippocampi and surrounding fluid structure volumes were determined by manual segmentation of native, coronal T2-weighted images with the contrast reversed. The native images were used because of the higher

resolution compared to the processed images (i.e. filtered and realigned). The T2-weighted images were used because they were better at highlighting fluid structures surrounding the hippocampus as compared to the PD images. These fluid structures served as boundaries of the hippocampus and were defined by higher signal intensities. Reversing the contrast of the T2-weighted images (i.e. CSF now appears black rather than white) aided the manual segmentation of the hippocampus because it sharpened the boundaries between the hippocampus and these fluid structures.

The anatomical landmarks and boundaries of the hippocampus used for the segmentation in this study were based on the extensive description of the bottlenose dolphin hippocampus by Jacobs et al. (1979). An additional anatomical consultation was provided by a neuroanatomical expert (Prof. G. Schneider, Dept. of Brain and Cognitive Sciences, MIT, Cambridge, MA). Pantel et al. (2000) also served as a guide for segmenting the hippocampus. In most specimens, the hippocampal formation could be distinguished from other structures of the medial temporal lobe with sufficient accuracy to perform manual segmentation. The hippocampal formation refers to the assemblage of anatomical structures, that include the subiculum, Ammon's horn (hippocampus proper), and the dentate gyrus. In these MR images, the various structures of the hippocampal formation could not be adequately distinguished and were collectively grouped and referred to as the hippocampus.

Segmented volumes for the left and right hippocampal formations (i.e. hippocampus) and surrounding fluid spaces (i.e CSF of the inferior horn of the lateral ventricle, CSF of the hippocampal sulcus, CSF of the parahippocampal sulcus, and CSF of the subarachnoid space including the transverse fissure of Bichat) were determined. The tracing of the hippocampal head started with the slice that first exhibited a distinct fluid spot (black in T2 with contrast reversed), which demarcated the dorsal boundary of the amygdala (the posterior portion of the amygdala lies just above the hippocampus). The medial boundary was the tentorium cerebelli and CSF of the subarachnoid space. The ventral and lateral boundaries were CSF of the parahippocampal sulcus. In the body of the hippocampus, CSF of the inferior horn of the lateral ventricle served as the lateral

boundary, while the tentorium cerebelli and CSF of the subarachnoid space served as the medial boundary. The CSF of the parahippocampal sulcus served as the ventral boundary, while the CSF of the transverse fissure of Bichat and the fimbria (which was excluded) served as the dorsal boundary. In the tail of the hippocampus, the ascending crus of the fornix, the fimbria, and CSF of the inferior horn of the lateral ventricles served as the lateral boundary, while the tentorium cerebelli and CSF of the subarachnoid space served as the medial boundary. The CSF of the parahippocampal sulcus served as the ventral boundary, while the CSF of the transverse fissure of Bichat and the pulvinar of the thalamus served as the dorsal boundary.

Left and right hippocampus volumes were determined three times, separately. For each specimen, the percentage of brain occupied by the left or right hippocampus was calculated by dividing the hippocampus volume (from the native T2-weighted images) by the sum of the WM and GM volumes of the whole brain (i.e. from the processed PD-weighted images) multiplied by 100.

## RESULTS

### *Volume Analysis Validation*

*Comparisons of Expected and Segmented Volumes of Water*. Processing of MR images was required for threshold segmentation of brains into WM, GM, and CSF, as described in the methods section. Therefore, it was important to validate our segmentation technique from processed images. In this experiment, MR imaging was completed on known amounts of water using acquisition protocols similar to those of specimen scanning. The segmentation analysis of water used techniques identical to those used in specimen segmentation. The segmented volumes of water calculated from the native PD and T2 weighted images closely approximated the expected volume (Table 2). The percent errors were less than 4%. The segmented volumes from processed PD and T2 weighted images (with Gaussian filter application and subtraction) were more accurate than the segmented volumes from native images (Table 2). Furthermore, realignment of both the PD and T2 weighted images around the global y-axis (a

technique used in threshold segmentation of specimens for symmetry of the left and right hemispheres) did not introduce any errors into the volume analysis.

Fetal brains were segmented into WM, GM, and CSF from processed T2-weighted images; while subadult and adult brains were segmented from processed PD-weighted images (see Methods for explanation). Therefore, it was necessary to determine if segmented volumes from processed PD images differed from segmented volumes from processed T2-weighted images. The results of this experiment revealed that the segmented volumes of water derived from PD- and T2-weighted images did not differ (Table 2).

*Comparisons of Expected and Segmented Volumes of Brain Tissue.* We performed an experiment that allowed us to determine the accuracy of the image processing and segmentation procedure with actual brain tissue. MR imaging was completed on formalin fixed cerebellar sections using acquisition protocols similar to those of specimen scanning. After MRI, the total volume displaced by the cerebellum sample was measured. The WM and GM were then dissected and separated, and the volume displaced by each tissue type was also measured (Table 3). Segmented volume measurements by computerized thresholding followed by manual editing were completed for the total cerebellum sample, the WM, and GM from both native and processed PD-weighted images (Table 3). In most cases, the segmented volumes from processed PD images were more accurate than the segmented volumes from native PD images (Table 3). For example, the segmented volumes of the cerebellum slice 1 indicated that the segmentation of the processed images contained smaller errors than the segmentation of the PD native images (total slice, 3.3% vs. 10.3%; WM, 5.5% vs. 8.3%; GM, 5.2% vs. 15.3%). However, a larger percent error was observed in larger segmented volumes. For example and generally, the pattern of errors for the segmented volumes of processed brain tissue was that the total slice error was the lowest followed by WM and GM errors. These errors were larger than the errors in the water experiment. Possible reasons for the increased errors in the brain tissue experiments compared to the water experiments are the smaller volumes of brain tissue segmented compared to the larger volumes of water

segmented. In addition, the error associated with the dissection of WM and GM may have caused the expected volume of WM and GM to be inaccurate. Additionally or alternatively, the larger errors of the segmented brain tissue may be associated with the errors associated with measuring the water displaced by the tissue.

*Comparisons of Manual and Threshold Segmentation Volumes.* The processing of images (i.e. Gaussian filter application and subtraction) allowed a single threshold range to define the WM, GM, or CSF for an entire slice. We performed experiments that validated this approach by performing computerized threshold segmentation into WM, GM, and CSF materials from a native and processed PD image (Figure 1; Table 4). These segmented volumes were compared to volumes in which the WM, GM, and CSF was manually outlined from the same native PD image. In all replicates, the manually segmented volumes from the native PD images were more similar to the threshold volumes (for WM and GM) derived from processed PD images than the threshold volumes derived from the native PD images (Table 4). In summary, the processing of native PD images improved the accuracy of computerized threshold segmentation in determining the volumes of WM and GM.

### *Brain Weight and Length Relationships*

Brain weight in males and females increased with body length (Figure 2A) and body weight (Figure 2B).

### *Three-dimensional Reconstructions and Neuroanatomy of the Subadult Brain*

*Three-Dimensional Reconstruction*. Three-dimensional reconstructions of the brain from magnetic resonance images of the subadult (CCSN05-084-La) revealed distinguishing characteristics of odontocete brains, as previously observed in other MRI studies of formalin-fixed toothed whale brains (Marino et al., 2001a; Marino et al., 2004a; Marino et al., 2004b; Marino et al., 2003a; Marino et al., 2003b; Marino et al., 2001c) (Figure 3). The most striking feature was the foreshortened frontal lobes and the pronounced bitemporal width. This gave the brain "a boxing glove" appearance typical

of odontocetes and first noted by Morgane et al. (1980). No olfactory structures were observed in the frontal lobe region. The mesencephalic and pontine flexures that resemble brainstem flexure patterns in the embryonic stage of terrestrial mammals were observed, as in other MRI studies. These flexure patterns were also seen in adult specimens.

*Anatomically Labeled Two-Dimensional MR Images.* Two-dimensional magnetic resonance images of the subadult (CCSN05-084-La) also revealed distinguishing features of odontocete brains, as previously observed in other MRI studies of formalin-fixed toothed whale brains (Marino et al., 2001a; Marino et al., 2004a; Marino et al., 2004b; Marino et al., 2003a; Marino et al., 2003b; Marino et al., 2001c) (Figures 4-19). Figures 4-11 display an anterior-to-posterior sequence of PD native, 2.0 mm-thick coronal MR brain sections at 10 mm intervals. Panels A illustrate the position of the brain in the coronal plane relative to surrounding head structures of the native PD image; panels B show labeled schematics of each brain section removed from the head structure with the contrast reversed so white matter appears white and CSF appears black; panels C display the orientation and level at which the native PD section was taken in the sagittal plane.

Figures 12-19 display a midline-to-lateral sequence of native PD, 2.0 mm-thick sagittal MR brain sections at 10 mm intervals through the left hemisphere. Panels A illustrate the position of the brain in the sagittal plane relative to surrounding head structures of the native PD image; panels B show labeled images of each brain section cut away from the head structure with the contrast reversed; panels C display the orientation and level at which the native PD section was taken in the coronal plane. These figures illustrate the preservation of spatial relationships among brain structures and surrounding head anatomy that is gained from MR imaging of fresh post-mortem brains intact within the skull with the head still attached to the body (*in situ* imaging).

*Telencephalon.* The MR images showed distinguishing features of the odontocete telencephalon. The neocortex is highly convoluted (Figures 4B-19B). The limbic and paralimbic clefts, which divide the limbic, paralimbic, and supralimbic lobes were seen (Figures 4B-8B). Structures of the basal ganglia (such as the caudate nucleus and the

putamen) were recognized (Figures 5B, 6B, 12B, and 13B). Unlike previous reports of odontocete MRI studies of formalin-fixed brains (Marino et al., 2001a; Marino et al., 2001c; Marino et al., 2004a; Marino et al., 2004b; Marino et al., 2003a; Marino et al., 2003b; Marino et al., 2001c), the hippocampus was located and was found to be quite small relative to the overall size of the brain (Figures 7B, 8B, and 15B). This observation was similar to the findings on the bottlenose dolphin hippocampus observed by Jacobs et al. (1979). Despite the large hemispheres, the corpus callosum is relatively small (Figures 5B-8B; 12B-14B).

*Diencephalon*. The MR images revealed a large diencephalon in the Atlantic white-sided dolphin. The thalamus was easily recognized in the MR images and is massive (Figures 6B-8B; 12B-15B), as expected from the size of the hemispheres.

*Mesencephalon*. The MR images of the subadult Atlantic white-sided dolphin brain illustrate the enlargement of auditory processing regions that occurred during odontocete brain evolution. For example, the inferior colliculus was much larger than the superior colliculus (Figure 8B; 13B).

*Metencephalon and myelencephalon*. The MR images showed typical characteristics of the odontocete metencephalon and myelencephalon. Auditory pathways were easily observed, including the large auditory nerve (Figure 6B) and the cochlear nuclei (Figure 7B). The cerebellum is large and the WM and GM are easily distinguishable (Figures 6B-11B; 12B-16B). Hindbrain structures including the pons and inferior olive, as well as the spinal cord (including the dorsal and ventral horns) could be identified (Figures 6B-11B; 12B, 13B).

***Neuroanatomy and Three-dimensional Reconstructions of the Fetus Brain***

*Three-Dimensional Reconstruction*. Three-dimensional reconstructions of the fetal brain (CCSN05-040-Fetus-La) from magnetic resonance images also revealed distinguishing characteristics of odontocete brains (Figure 20) (Marino et al., 2001). This brain (from a 54cm fetus; approximately 7 months old) had already taken its adult shape (i.e. foreshortened frontal lobes and the pronounced bitemporal width) and that “boxing

glove" appearance, previously described by Morgane et al. (1980). No olfactory structures were observed in the frontal lobe of this embryo, in contrast to previous MR findings of a common dolphin (*Delphinus delphis*) fetal brain (Marino et al., 2001b). The mesencephalic and pontine flexures could be identified.

*Anatomically Labeled Two-Dimensional MR Images.* Magnetic resonance images of the fetus (CCSN05-040-La) revealed interesting features of neurodevelopment in odontocete brains (Figures 21-33), as previously described by Marino et al. (2001b). Figures 21-27 display an anterior-to-posterior sequence of T2 native, 2.0 mm-thick coronal MR brain sections at 6 mm intervals. Figures 28-33 display a midline-to-lateral sequence of native T2, 2.0 mm-thick sagittal MR brain sections at 6 mm intervals through the left hemisphere. The figures (panels A, B, and C) were organized similarly to the MR images of the subadult. These figures also illustrate the preservation of spatial relationships among brain structures and surrounding head anatomy that is gained from *in situ* MR imaging of fresh post-mortem fetal brains.

*Telencephalon.* The MR images of the telencephalon showed hallmark features of fetal brains in general and of odontocetes in particular. The native T2 images illustrate the lack of myelination (see white matter tracts; dark in native T2 images; white in contrast reversed images) in the telencephalon this early in development (Figures 21B-27B; 30B-32B) compared to the subadult brain (Figures 4B-11B; Figures 14B-17B). Structures of the basal ganglia (such as the caudate nucleus and the putamen) could be recognized in this fetus (Figures 21B-23B). In addition, the hippocampus could be identified, contrary to a previous *in situ* MR imaging study of a fetal common dolphin preserved in formalin (Marino et al., 2001b). In this study, the hippocampal formation had already taken its characteristic tear-dropped shape but was quite small relative to the overall size of the brain (Figure 24B), similar to the subadult (Figures 7B, 8B and 15B). The corpus callosum was small, similar to subadults (Figures 22B-24B; 28B-30B). However, it appears already to be myelinated at this stage of development.

*Diencephalon.* The large thalamus was easily recognized in the fetal MR images (Figures 23B, 24B, and 28B).

*Mesencephalon*. The inferior colliculus was well developed and already myelinated (Figures 25B, 28B, and 29B). It had reached its adult proportion and far exceeded the size of the superior colliculus.

*Metencephalon and myelencephalon*. Auditory pathways were easily observed at this fetal stage, including the cochlear nuclei (Figure 25B), the trapezoid body (Figures 28B, 29B), and the lateral lemniscus (Figure 29B). These structures exhibited myelination (i.e. appeared white in native T2 images with the contrast reversed). The cerebellum was large and well developed (Figures 24B-27B; 28B-31B). It was already heavily myelinated. Hindbrain structures including the pons and inferior olive could be identified as could the spinal cord (Figures 23B, 24B, and 28B) and were also already heavily myelinated.

**Brain Volumes**

WM, GM, and CSF segmented volumes of the total brain and cerebellum were determined for all dolphins except animals exhibiting gross brain pathologies and dolphins in which MRIs were of poor quality for computerized thresholding (i.e. poor quality because of signal intensity loss of occipital lobes and cerebellum) (Table 5). In the fetuses, the mid-sagittal area of the corpus callosum and hippocampus volumes were not determined because the boundaries were difficult to ascertain (due to poorer resolution of the fetal MRIs) (Table 6). The mid-sagittal area of the corpus callosum for CCSN05-037-La was not determined because the sagittal MRI did not provide an accurate midline section.

*Total Brain.* Threshold segmentation of processed PD-weighted images was used to select for the brain surface (Figure 34A). These segmentations were then used to calculate the total brain volume (Table 5). As expected, segmented volumes of the brain were strongly and significantly related to the total brain weight (Figure 34B; $R^2$ = 0.9996).

A visual comparison of the degreee of myelination of major white matter tracts among the MR images of a fetus, neonate, and adult brain at the level of the inferior and

superior colliculi revealed an increase with development (Figures 35). Because the virtual images of the brain were removed from the head, a histogram of signal intensity values for the brain (with no head structure) could be compared among the dolphins of different life history stages (fetus, neonate, and adult) (Figure 36A). The visual comparison of the degree of myelination among the dolphins of different age class categories was substantiated by the observed increase in WM:GM volume ratios (obtained from our segmentation) with increasing body length (Figure 36B).

*Cerebellum.* A visual comparison of the degreee of myelination of major white matter tracts among the MR images of a fetus, neonate, and adult cerebellum at the level of the inferior and superior colliculi also revealed an increase in white matter tracts with development (Figures 35). These observed findings were substantiated by the increase in WM:GM volume ratios (obtained from our segmentation) of the cerebellum with increasing body length (Figure 36C). However, the larger fetus (CCSN05-040-Fetus-La) had a WM:GM volume ratio approximately equivalent to that of the subadults and adults. In addition, the GM segmented volumes of the cerebellum increased with length for both males and females (Figure 37).

*Corpus Callosum.* The mid-sagittal area of the corpus callosum in adult females was larger than that of the neonate dolphin (Figure 38). It will require a larger number of adult cases to substantiate the larger callosal area of females compared to males.

*Hippocampus.* In all post-mortem MRI scans of Atlantic white-sided dolphins in this study, the hippocampus was identified. The hippocampus was buried deep in the medial wall of the very large temporal lobes (Figure 39-40). The boundaries of the hippocampus were best observed in native T2-weighted images, rather than the PD-weighted images (Figure 39). This can be best explained by the CSF surrounding this structure, as observed by the hyperintensity of the inferior horn of the lateral ventricle (lateral border), the hyperintensity of the parahippocampal sulcus (ventral border), and the hyperintensity of the subarachnoid space (the medial and dorsal borders).

The hippocampi of adult females were larger than that of the neonate female (Figure 39). Furthermore, the neonate hippocampus contained more CSF in the inferior

horn of the lateral ventricle, the transverse fissure of Bichat, and within the hippocampus itself (Figures 39A-F).

## DISCUSSION

This study presents a novel, quantitative approach to assess neurodevelopment in the Atlantic white-sided dolphin by determining the volumes of brain structures from *in situ* brain MR images obtained from freshly dead specimens. In addition, this study provides the first anatomically labeled MRI-based atlas of the fetal and subadult Atlantic white-sided dolphin brain. It is different from previous MRI-based atlases completed on cetaceans in that it has been created from images of the brain *in situ* as compared to brains that were removed and formalin fixed. We also present WM:GM volume ratios of the total brain and cerebellum along an ontogenetic series from fetus to adult using MR images. In addition, hippocampus volumes were determined; these have not been reported previously for a cetacean species.

### *Atlantic White-sided Dolphin Neuroanatomy - Comparisons to Other Cetacean Brain MRI Studies*

The brain of the Atlantic white-sided dolphin, as revealed in the MR images collected during this study, displayed the classic hallmarks of odontocete brains, as described in previous studies (Marino et al., 2001a; Marino et al., 2001b; Marino et al., 2004a; Marino et al., 2004b; Marino et al., 2003a; Marino et al., 2003b; Marino et al., 2001c; Morgane et al., 1980). The most prominent characteristic was the general shape of the brain – its "foreshortened orbital lobes" and "pronounced bitemporal width", as Marino et al. (2001a) observed in other odontocete brains. This brain shape is different from that of other mammals and may be a result of evolutionary changes that occurred during migration of the blowhole and telescoping of the skull (Marino et al., 2001a; Morgane et al., 1980). On the other hand, there is adequate evidence that the brain changed shape because olfactory structures were lost (as observed in the Alantic white-sided dolphin specimens in this study) and acoustic structures were enlarged (e.g. the

large inferior colliculi observed in the specimens of this study) (Marino et al., 2001a; Morgane et al., 1980).

To date, MRI studies of odontocete brains have been unable to identify the hippocampus (Marino et al., 2001a; Marino et al., 2001b; Marino et al., 2004a; Marino et al., 2004b; Marino et al., 2003a; Marino et al., 2003b; Marino et al., 2001c). Those studies were performed on brains that were removed and fixed in formalin, except for the common dolphin fetal specimen which was pressure perfused with formalin and placed in alcohol with brain intact (Marino et al., 2001b). In all post-mortem MRI scans of Atlantic white-sided dolphins in the current study, the hippocampus was identified. The hippocampus was buried deep in the medial wall of the very large temporal lobes, similar to what has been observed in bottlenose dolphins (Jacobs et al., 1979).

It is possible that the key factor in finding the hippocampus in odontocete MR images is performing the imaging of the brain *in situ*, as completed in this study. A key to finding the hippocampus was to recognize its boundaries, in particular the surrounding fluid structures. These boundaries were the CSF of the inferior horn of the lateral ventricle, the parahippocampal sulcus, and the transverse fissure of Bichat. These structures were best observed in native T2-weighted images rather than PD-weighted images because of the hyperintensity of fluid. It is possible that severing the head and removing the brain, as completed in previous odontocete MRI studies, leads to the leakage of CSF and therefore reduces the ability to perceive the hippocampus boundaries. This possibility, in conjunction with the weight of the brain on the hippocampus and its potential thinning in the dorsal-ventral direction, may impede the visual perception of the hippocampal formation from MR images of formalin fixed brains. Additionally or alternatively, it is also possible that the medial temporal lobes are damaged by the tentorium during brain removal or the effects of formalin blur the delineation of the hippocampus.

### *Myelination Patterns during Ontogenesis*

The myelination of axons is a critical phase during fetal brain development, since myelin is critical for normal axon function. In humans, it begins in the third trimester and continues well after birth (Hayman et al., 1992). Myelin contains more lipids than proteins (70:30) (as cited by Almajeed et al., 2004), which leads to a T2 hypo-intensity signal. Thus, T2-weighted images can be used to study myelination changes during ontogeny by threshold segmentation and volume analysis of WM and GM. In this study, we used WM:GM volume ratios of the entire brain to show how the degree of myelination increases from the fetus to adult in the Atlantic white-sided dolphin brain (Figure 35E). WM:GM volume ratios during ontogeny have not been reported previously in any cetacean species.

A universal principle in brain development is that structures that develop first in the brain become myelinated first. In this study, the white matter tracts of the fetal hindbrain and cerebellum were prominent (Figure 35A). However, in the telencephalon, the white matter tracts were far less developed. Evolutionarily, the hindbrain and cerebellum are the more primitive brain stuctures and develop first during ontogenesis (Allman, 1999). In addition, the white matter tracts of the auditory pathways in the fetal brains were myelinated, indicated by the T2 hypointensity signal of the inferior colliculus, the cochlear nuclei, and trapezoid body. This provides evidence that hearing and auditory processing regions develop early during ontogeny, as described in previous odontocete studies (Solntseva, 1999). Further studies are warranted.

### *Measurements of Brain Structures*

*Cerebellum.* The large cerebellum in Atlantic white-sided dolphins, noted in this study, was consistent with previous findings of the cerebellum in other delphinid species (Marino et al., 2000; Ridgway, 1990). In our study, the cerebellum (WM and GM volumes combined) of subadult and adult specimens ranged between 13.8 to 15.0% of the total brain size. These findings were within the range of measurements found in bottlenose dolphins and common dolphins (Marino et al., 2000). For Atlantic white-

sided, bottlenose, and common dolphins, the cerebellum, which average about 15% of the total brain size, are relatively much larger than those of the human (10.3 %) and some nonhuman primates (9.2% for Cercopithecidae, i.e. baboons, rhesus monkeys, and mangabeys,; and 9.3% for Cebidae, i.e. cebus and squirrel monkeys) (Marino et al, 2000).

Why do dolphins have such a large cerebellum? In reviewing the evidence, Marino et al. (2000) and Ridgway et al. (2000) suggest that the cerebellum may play an important role in acoustic processing, in addition to its function in the control and coordination of movements. This speculation is based on the findings in echolocating bats, as reviewed by Marino et al. (2000). For example, in the big brown bat (*Eptesicus fuscus*), cerebellar neurons function in representation of sound location (Kamada and Jen, 1990). In addition, qualitative observations of the paramedian lobules and paraflocculus of echolocating odontocetes reveal that these regions of the cerebellum are expanded as reviewed by Ridgway (1990). These brain structures are more enlarged in echolocating bats as compared to non-echolocating bats, as reviewed by Marino et al. (2000). In this regard, we note the huge expansion of the cerebellum of Mormyrid electric fishes in which this structure functions in the localization of objects by their distortion of electric fields (Bullock and Heiligenberg, 1986).

*Corpus Callosum*. The small corpus callosum in Atlantic white-sided dolphins, noted in this study, was consistent with previous findings of the corpus callosum in other odontocete species (Tarpley and Ridgway, 1994). In the current study, the corpus callosum area ($mm^2$) to brain mass (g) ratio (CCA/BM) ranged between 0.088 and 0.137. These CCA/BM ratios were within the range of measurements found in other odontocete studies (Tarpley and Ridgway, 1994). For example, the bottlenose dolphin has a CCA/BM ratio range of 0.143 - 0.227 (N = 15), while the Pacific white-sided dolphin has a CCA/BM ratio range of 0.159 - 0.198 (N = 3).

The odontocete CCA/BM ratio is much smaller than in most mammals, including humans (the CCA/BM in humans is approximately 0.9), as reviewed by Tarpley and Ridgway (1994). The corpus callosum plays a key role in transferring information between the two hemispheres. Ridgway (1990) suggested that the smaller corpus

callosum area would result in greater hemispheric independence. In fact, recordings of brain activity of the bottlenose dolphin revealed that the cerebral hemispheres can produce electroencephalograph waveforms indicative of wakefulness in one hemisphere and sleep in the opposite hemisphere (Mukhametov et al., 1977). Ridgway and Tarpley (1994) suggest that hemispheric independence (for whatever reasons) in cetaceans may have been favored during evolution; despite the evolutionary pressure for interhemispheric coordination and asymmetry in movement patterns of the body.

*Hippocampus*. Hippocampal volumes in cetaceans have not been reported previously. However, the small hippocampus in the Atlantic white-sided dolphin specimens, noted in this study, was consistent with previous qualitative findings of the hippocampus in the bottlenose dolphin (Jacobs et al., 1979). Compared to the carnivora and ungulates, the hippocampus is considerably reduced in cetaceans, except for the ventral portion of the temporal lobes. When the hippocampus of a bottlenose dolphin was compared to that in a human brain of the same size and weight, transverse sections at the histological level revealed that the dolphin hippocampus was smaller (Jacobs et al., 1979). In a group of human subjects with a mean age of 20.4 (± 2.2) years, Pantel et al. (2000) found the mean volume of the hippocampal formation to be 1.975 $cm^3$ in the left hemisphere and 1.987 $cm^3$ in the right hemisphere. In our study, the left hippocampus ranged from 0.544 to 1.043 $cm^3$; the right hippocampus ranged from 0.462 to 0.967 $cm^3$.

The mammalian hippocampus is required for some aspects of spatial learning and memory. O'Keefe and Nadel (1978) proposed that hippocampal neurons together form a cognitive map of our surroundings. Recently, the brains of humans with extensive navigation experience (i.e. licensed London taxi drivers) exhibited an enlarged posterior hippocampus compared to control subjects, as observed from structural MR imaging and voxel-based morphometry (i.e. segmentation) (Maguire et al., 2000). In odontocetes, the role of the hippocampus in spatial navigation is not known.

### *Implications for Marine Mammal Health*

Emerging threats to marine mammal health include biotoxins (e.g. domoic acid or DA) and anthropogenic chemicals (e.g. OH-PCBs and PBDEs), in addition to legacy chemicals such as PCBs. These natural toxins and anthropogenic chemicals may affect the size of certain brain structures. For example, DA has been shown to cause hippocampal atrophy in California sea lions (Silvagni et al., 2005). In mouse cerebellar culture assays, OH-PCBs inhibit thyroid-hormone-dependent arborization of cerebellar Purkinje cell dendrites (Kimura-Kuroda et al., 2005). In fetal rats, Aroclor 1254 (a PCB mixture) decreases the cell density of the corpus callosum in a similar but not identical mechanism as hypothyroidism (Sharlin et al., 2006). In the current study, we have established an approach for accurately determining the size of brain structures from *in situ* MR images of stranded, dead dolphins. Therefore, we can use the approach in this study to understand the potential impacts of natural toxins (such as domoic acid) and anthropogenic chemicals (such PCBs, PBDEs, and their hydroxylated metabolites) on the size of brain regions. These studies are underway.

## REFERENCES


Allman JM. 1999. Evolving Brains. New York: Scientific American Library.

Almajeed AA, Adamsbaum C, Langevin F. 2004. Myelin characterization of fetal brain with mono-point estimated T1-maps. Magnetic Resonance Imaging 22:565-572.

Birnbaum LS, Staskal DF. 2004. Brominated Flame Retardents: Cause for Concern? Environmental Health Perspectives 112(1):9-17.

Borrell A, Bloch D, Desportes G. 1995. Age trends and reproductive transfer of organochlorine compounds in long-finned pilot whales from the Faroe Islands. Environmental Pollution 88:283-292.

Brouwer A, Morse DC, Lans MC, Schuur AG, Murk AJ, Klasson-Wehler E, Bergman A, Visser TJ. 1998. Interactions of persistent environmental organohalogens with the thyroid hormone system: mechanisms and possible consequences for animal and human health. Toxicology and Industrial Health 14(1-2):59-84.

Bullock TH, Heiligenberg W., editors. 1986. Electroreception. New York: Wiley.

Conrad PA, Miller MA, Kreuder C, James ER, Mazet J, Dabritz H, Jessup DA, Gulland F, Grigg ME. 2005. Transmission of *Toxoplasma*: clues from the study of sea otters as sentinels of *Toxoplasma gondii* flow into the marine environment. International Journal of Parasitology 35:155-1168.

de Boer J, Wester PG, Klamer HJ, Lewis WE, Boon JP. 1998. Do flame retardants threaten ocean life? Nature 394:28-29.

Evans AC. 2006. The NIH MRI study of normal brain development. NeuroImage 30:184-202.

Hansen LJ, Schwacke LH, Mitchum GB, Hohn AA, Wells RS, Zolman ES, Fair PA. 2004. Geographic variation in polychorinated biphenyl and organochlorine pesticide concentrations in the blubber of bottlenose dolphins from the US Atlantic coast. The Science of the Total Environment 319:147-172.

Hayman LA, McArdle CB, Shah YP. 1992. Neonatal brain. Clinical Brain Imaging 2:45-52.

Jacobs MS, McFarland WL, Morgane PJ. 1979. The anatomy of the brain of the bottlenose dolphin (*Tursiops truncatus*). rhinic lobe (rhinencephalon): the Archicortex. Brain Research Bulletin 4(1):1-108.

Kamada T, Jen PH. 1990. Auditory response properties and direction sensitivity of cerebellar neurons of the echolocationg bat, *Eptesicus fycus*. Brain Research 528:123-129.

Kannan K, Tanabe S, Borrell A, Aguilar A, Focardi S, Tatsukawa R. 1993. Isomer-specific analysis and toxic evaluation of polychlorinated biphenyls in striped dolphins affected by an epizootic in the western Mediterranean Sea. Archives of Environmental Contamination and Toxicology 25(2):227-233.

Kimura-Kuroda J, Nagata I, Kuroda Y. 2005. Hydroxylated metabolites of polychlorinated biphenyls inhibit thyroid-hormone-dependent extension of cerebellar Purkinje cell dendrites. Developmental Brain Research 154:259-263.

Kimura-Kuroda J, Nagata I, Negishi-Kato M, Kuroda Y. 2002. Thyroid hormone-dependent development of mouse cerebellar Purkinje cells in vitro. Developmental Brain Research 137(1):55-65.

Knipper M, Zinn C, Maier H, Praetorius M, Rohbock K, Kopschall I, Zimmermann U. 2000. Thyroid hormone deficiency before the onset of hearing causes irreversible damage to peripheral and central auditory systems. Journal of Neurophysiology 83(5):3101-3112.

Maguire EA, Gadian DG, Johnsrude IS, Good CD, Ashburner J, Frackowiak RSJ, Firth CD. 2000. Navigation-related structural change in the hippocampi of taxi drivers. Proceedings of the National Academy of Sciences 97(8):4398-4403.

Marino L. 1998. A comparison of encephalization between odontocete cetaceans and anthropoid primates. Brain, Behavior, and Evolution 51(4):230-238.

Marino L, Murphy TL, Deweerd AL, Morris JA, Fobbs AJ, Humblot N, Ridgway SH, Johnson JI. 2001a. Anatomy and three-dimensional reconstructions of the brain of the white whale (*Delphinapterus leucas*) from magnetic resonance images. The Anatomical Record 262(4):429-439.

Marino L, Murphy TL, Gozal L, Johnson JI. 2001b. Magnetic resonance imaging and three-dimensional reconstructions of the brain of a fetal common dolphin, *Delphinus delphis*. Anatomy and Embryology 203:393-402.

Marino L, Rilling JK, Lin SK, Ridgway SH. 2000. Relative volume of the cerebellum in dolphins and comparison with anthropoid primates. Brain, Behavior and Evolution 56(4):204-211.

Marino L, Sherwood CC, Delman BN, Tang CY, Naidich TP, Hof PR. 2004a. Neuroanatomy of the killer whale (*Orcinus orca*) from magnetic resonance images. The Anatomical Record A:1-7.

Marino L, Sudheimer K, McLellan WA, Johnson JI. 2004b. Neuroanatomical structures of the spinner dolphin (*Stenella longirostris orientalis*) brain from magnetic resonance images. The Anatomical Record Part A 279A:601-610.

Marino L, Sudheimer K, Pabst DA, McLellan WA, Johnson JI. 2003a. Magnetic resonance images of the brain of a dwarf sperm whale (*Kogia simus*). Journal of Anatomy 203:57-76.

Marino L, Sudheimer K, Sarko D, Sirpenski G, Johnson JI. 2003b. Neuroanatomy of the harbor porpoise (*Phocoena phocoena*) from magnetic resonance images. Journal of Morphology 257:308-347.

Marino L, Sudheimer KD, Murphy TL, Davis KK, Pabst DA, McLellan WA, Rilling JK, Johnson JI. 2001c. Anatomy and three-dimensional reconstructions of the brain of a bottlenose dolphin (*Tursiops truncatus*) from magnetic resonance images. The Anatomical Record 264(4):397-414.

McKinney MA, De Guise S, Martineau D, Beland P, Lebeuf M, Letcher RJ. 2006. Organohalogen contaminants and metabolites in beluga whale (*Delphinapterus leucas*) liver from two Canadian populations. Environmental Toxicology and Chemistry 25(5):30-41.

Morgane PJ, Jacobs MS, Galaburda A. 1986. Evolutionary morphology of the dolphin brain. Dolphin cognition and behavior. 5-29.

Morgane PJ, Jacobs MS, MacFarland WL. 1980. The anatomy of the brain of the bottlenose dolphin (*Tursiops truncatus*). surface configurations of the telencephalon of the bottlenose dolphin with comparative anatomical observations in four other Cetacean species. Brain Research Bulletin 5 (suppl.):1-107.

Muir DCG, Koczanski K, Rosenberg B, Beland P. 1996. Persistent organochlorines in beluga whales (*Delphinapterus leucas*) from the St. Lawrence River Estuary. 2. Temporal trends, 1982-1994. Environmental Pollution 93(2):235-245.

Mukhametov LM, Supin AY, Polyakova IG. 1977. Interhemispheric asymmetry of the electroencephalographic sleep patterns in dolphins. Brain Research 134:581-584.

O'Keefe J, Nadel L. 1978. The hippocampus as a cognitive map: Clarendon Press.

Pantel J, O'Leary DS, Cretsinger K, Bockholt HJ, Keefe H, Magnotta VA, Andreasen NC. 2000. A new method for the in vitro volumetric measurement of the human hippocampus with high neuroanatomical accuracy. Hippocampus 10:752-758.

Rami A, Patel AJ, Rabie A. 1986. Thyroid hormone and development of the rat hippocampus: Morphological alterations in granule and pyramidal cells. Neuroscience 19(4):1217-1226.

Ridgway SH. 1990. The Bottlenose Dolphin. The Central Nervous System of the Bottlenose Dolphin. p 69-97.

Ridgway SH, Brownson RH. 1984. Relative brain sizes and cortical surface areas in odontocetes. Acta Zoologica Fennica 172:149-152.

Rilling JK, Insel TR. 1999. The primate neocortex in comparative perspective using magnetic resonance imaging. Journal of Human Evolution 37:191-223.

Ross PS, Ellis GM, Ikonomou MG, Barrett-Lennard LG, Addison RF. 2000. High PCB concentrations in free-ranging Pacific killer whales, *Orcinus orca*: effects of age, sex and dietary preference. Marine Pollution Bulletin 40(6):504-515.

Sandala GM, Sonne-Hansen C, Dietz R, Muir DCG, Valters K, Bennett ER, Born EW, Letcher RJ. 2004. Hydroxylated and methyl suflone PCB metabolites in adipose and whole blood of polar bear (*Ursus maritimus*) from East Greenland. Science of the Total Environment, 331:125-141.

Scholin CA, Gulland F, Doucette GJ, Benson S, Busman M, Chavez FP, Cordaro J, DeLong R, De Vogelaere A, Harvey J, Haulena M, Lefebvre K, Lipscomb T, Van

Dolah FM, et al. 2000. Mortality of sea lions along the central California coast linked to a toxic diatom bloom. Nature 6765:80-84.

Schoonover CM, Seibel MM, Jolson DM, Stack MJ, Rahman RJ, Jones SA, Mariash CN, Anderson GW. 2004. Thyroid hormone regulates oligodendrocyte accumulation in developing rat brain white matter tracts. Endocrinology 145(11):5013-5020.

Sergeant DE, St. Aubin DJ, Geraci JR. 1980. Life history and Northwest Atlantic status of the Atlantic white-sided dolphin, *Lagenorhynchus acutus*. Cetology 37(5):12.

Sharlin DS, Bansal R, Zoeller RT. 2006. Polychlorinated biphenyls exert selective effects on cellular composition of white matter in a manner inconsistent with thyroid hormone insufficiency. Endocrinology 147(2):846-858.

Silvagni PA, Lowenstine LJ, Spraker T, Lipscomb TP, Gulland FMD. 2005. Pathology of domoic acid toxicity in California sea lions (*Zalophus californianus*). Veterinary Pathology 42:184-191.

Solntseva G. 1999. The comparison of the development of the auditory and vestibular structures in toothed whales -- beluga (Cetacea: Odontoceti - *Delphinapterus leucas*). Dokl Akad Nauk 364(5):714-718.

Stephan H, Frahm H, Baron G. 1981. New and revised data on volumes of brain structures in insectivores and primates. Folia Primatologica 25:1-29.

Tarpley RL, Ridgway SH. 1994. Corpus callosum size in delphinid cetaceans. Brain, Behavior, and Evolution 44:156-165.

Tuerk KJ, Kucklick JR, McFee WE, Pugh RS, Becker PR. 2005. Factors influencing persistent organic pollutant concentrations in the Atlantic white-sided dolphin (*Lagenorhynchus acutus*). Environmental Toxicology and Chemistry 24(5):1079-1087.

Wells RS, Tornero V, Borrell A, Aguilar A, Rowles TK, Rhinehart HL, Hofmann S, Jarman WM, Hohn AA, Sweeney JC. 2005. Integrating life-history and reproductive success data to examine potential relationships with organochlorine compounds for bottlenose dolphins (*Tursiops truncatus*) in Sarasota Bay, Florida. Science of the Total Environment 349(1-3):106.

Zoeller TD, Herzig CT, Iannacone EA, Gauger K, Bansal R. 2002. Thyroid hormone, brain development, and the environment. Environmental Health Perspectives 110(3):355-361.

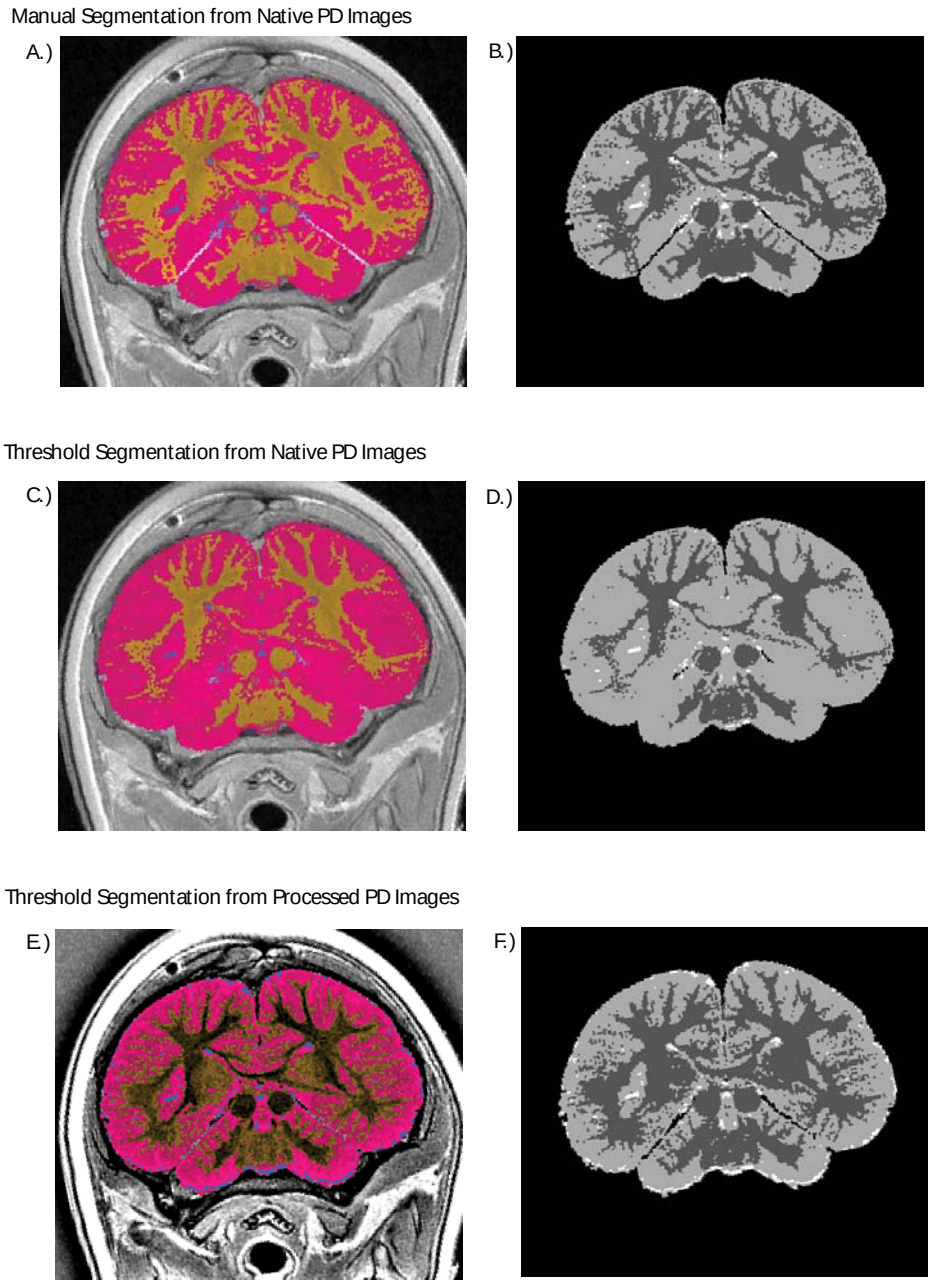


**Figure 1. A comparison between manual and threshold segmentation of native and processed images.** The proton density- (PD) weighted label maps of white matter (WM), grey matter (GM), and cerebrospinal fluid (CSF) are from the same specimen at the level of the inferior and superior colliculus. A - B.) Manual segmentation from native PD images. C – D.) Threshold segmentation from native PD images. E – F.) Threshold segmentation from processed PD images. In panels A, C, and E, WM is yellow, GM is magenta, and CSF is blue. In panels B, D, and F, the label map of the brain has been removed from the head structure. WM is dark grey, GM is light grey, and CSF is white.

**Figure 2. Total brain weights and total brain volumes for Atlantic white-sided dolphins that stranded along the beaches of Cape Cod, MA between 2002 and 2005.** A.) Brain weight (g) versus body length (cm). Encircled points represent individuals in which post-mortem MR imaging was completed of the brain intact within the skull with the head still attached to the body (*in situ* imaging). B.) Brain weight (kg) versus body weight of individuals in which post-mortem magnetic resonance (MR) imaging was completed. Brain volume analysis was not completed on dolphins that exhibited gross brain pathologies, as indicated by MRI and dissection. Encircled points represent these individuals.

A.)

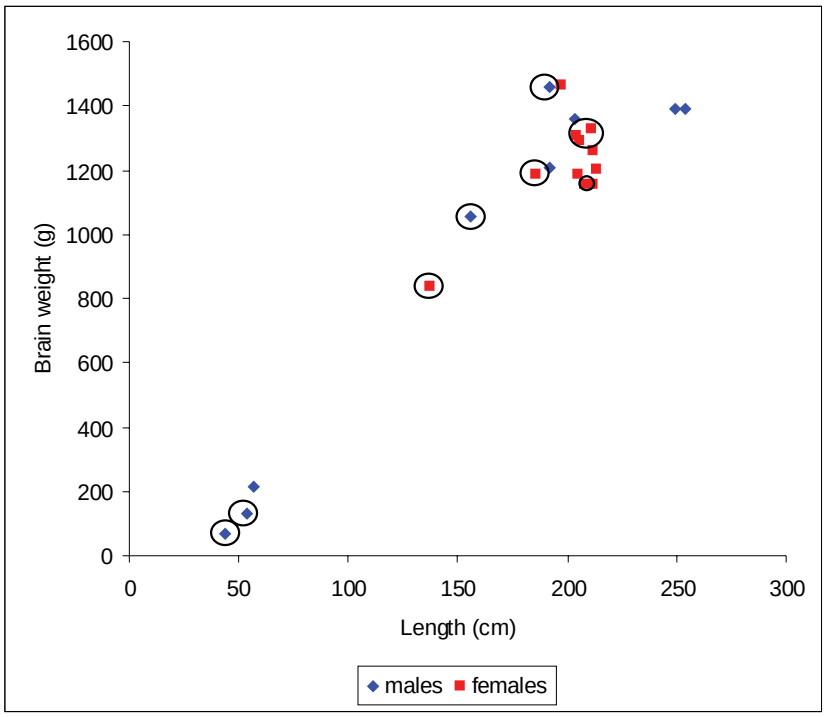
1600
1400
1200
1000
800
600
400
200
0
Brain weight (g)
0
50
100
150
200
250
300
Length (cm)
males
females

B.)

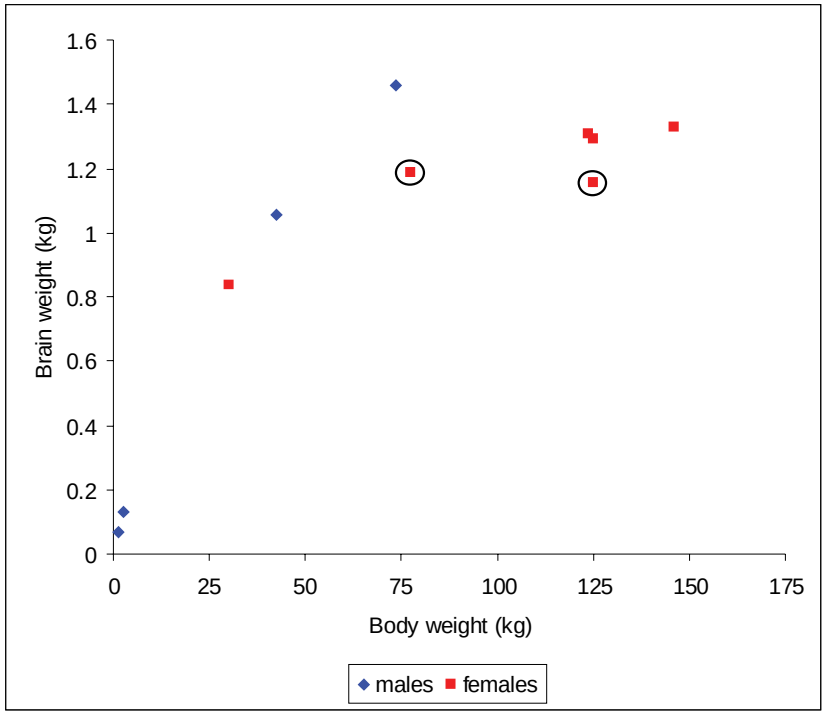
1.6
1.4
1.2
1
0.8
0.6
0.4
0.2
0
Brain weight (kg)
0
25
50
75
100
125
150
175
Body weight (kg)
males
females

**Figure 3. Three-dimensional reconstruction of the brain of specimen CCSN05-084-La from magnetic resonance (MR) images.** A.) Anterior view of brain. B.) Posterior view of brain. C.) Dorsal view of brain. D.) Ventral view of brain. E.) Left view of brain. F.) Right view of brain.

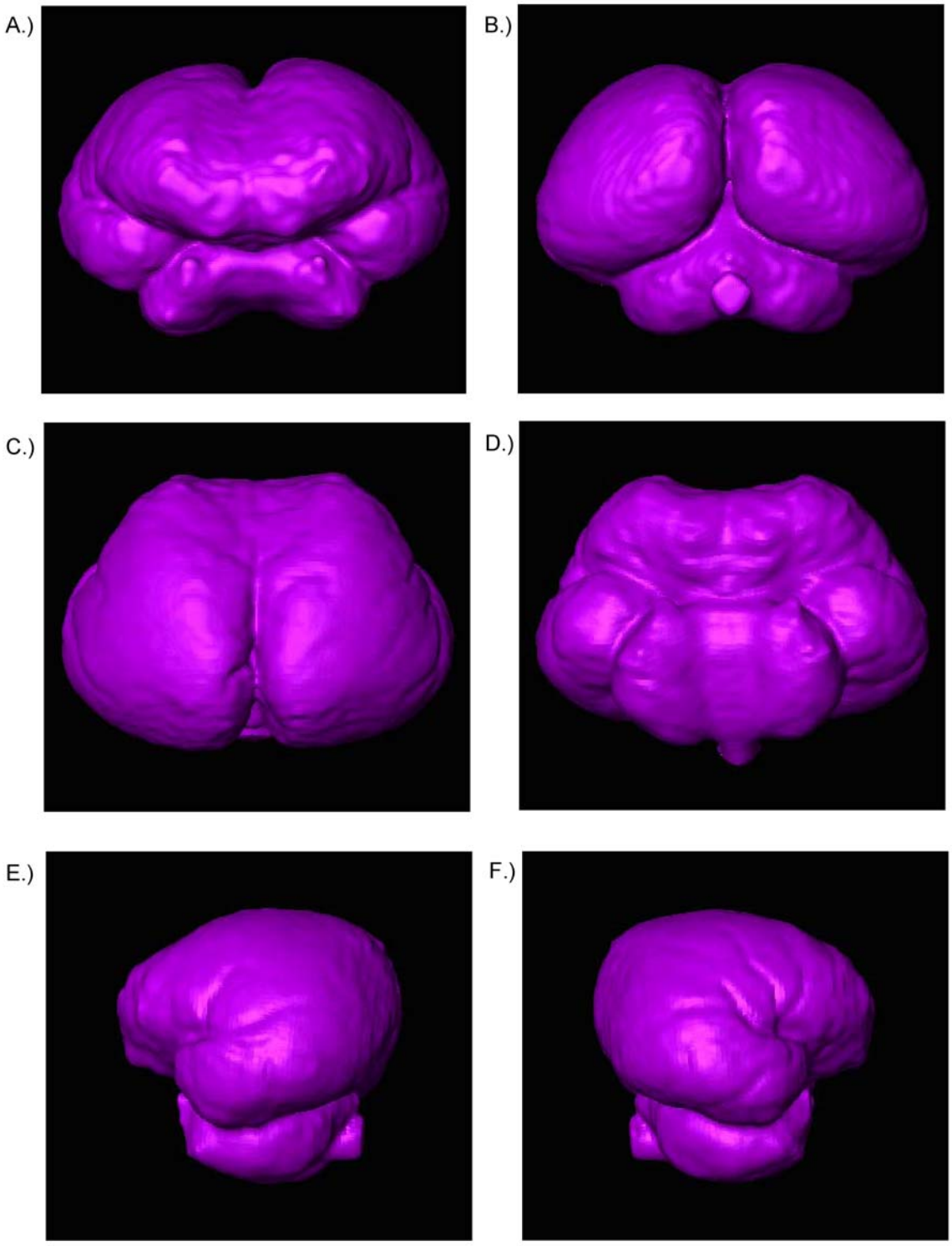
A.)
B.)
C.)
D.)
E.)
F.)

**Figures 4-11. Anterior-to-posterior, post-mortem MRI sequence of a subadult male brain (CCSN05-084-La) intact within the skull.** A.) Native proton density- (PD) weighted 2.0 mm-thick coronal MR brain sections at 10 mm intervals. B.) Labeled brain cutout of each section with contrast reversed. C.) Sagittal MR images of the brain intact within the skull depicting the orientation of the section. Orange lines illustrate the span of the MRI sequence. Blue lines represent the plane of section. D = dorsal; V = ventral; L = left; R = right; A = anterior; and P = posterior.

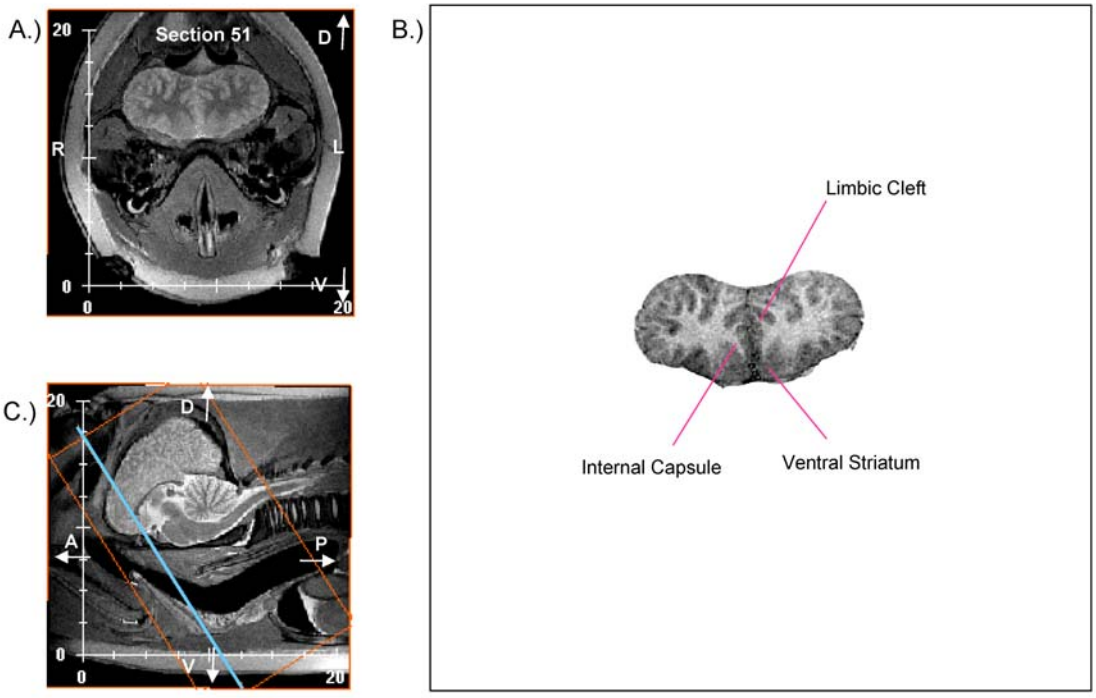


Figure 4.

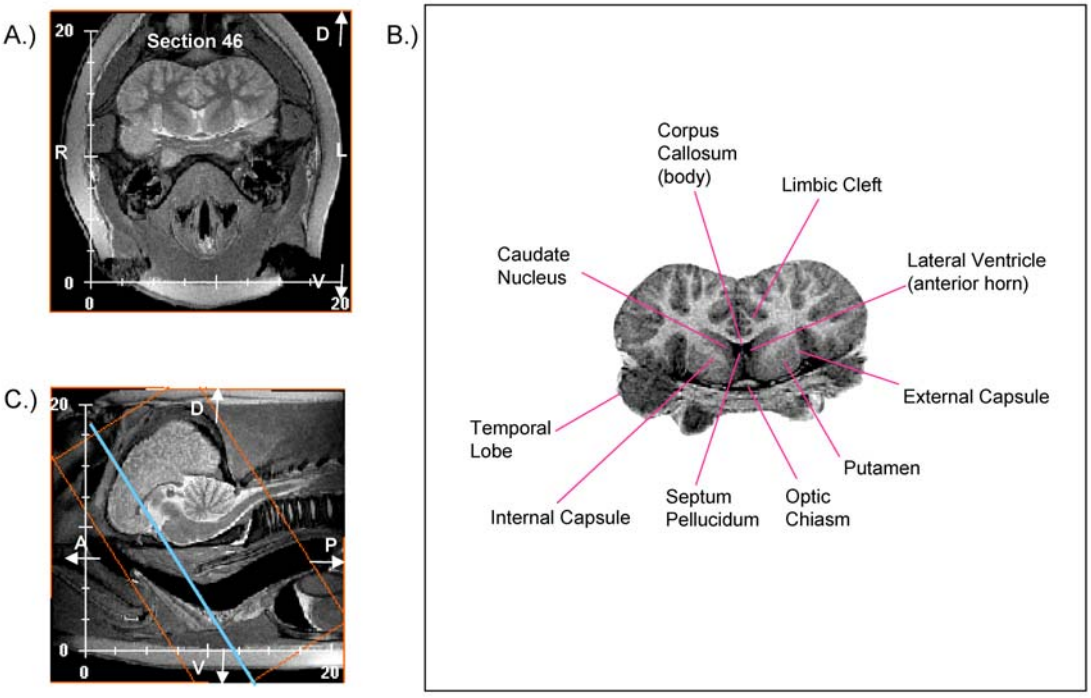


Figure 5.

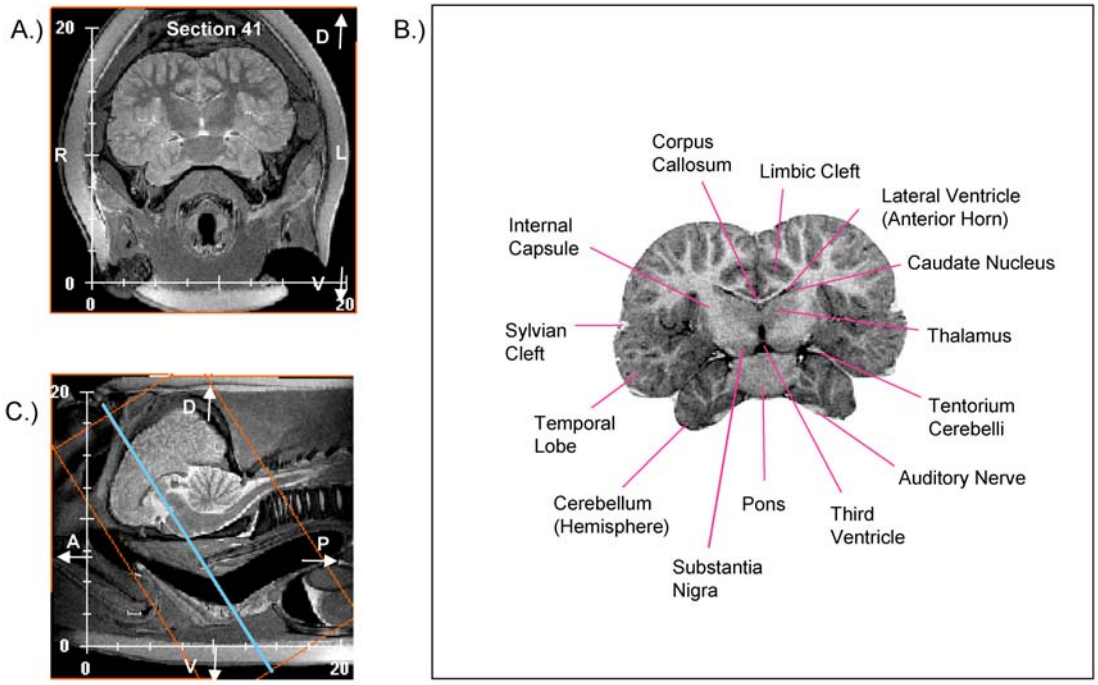


Figure 6.

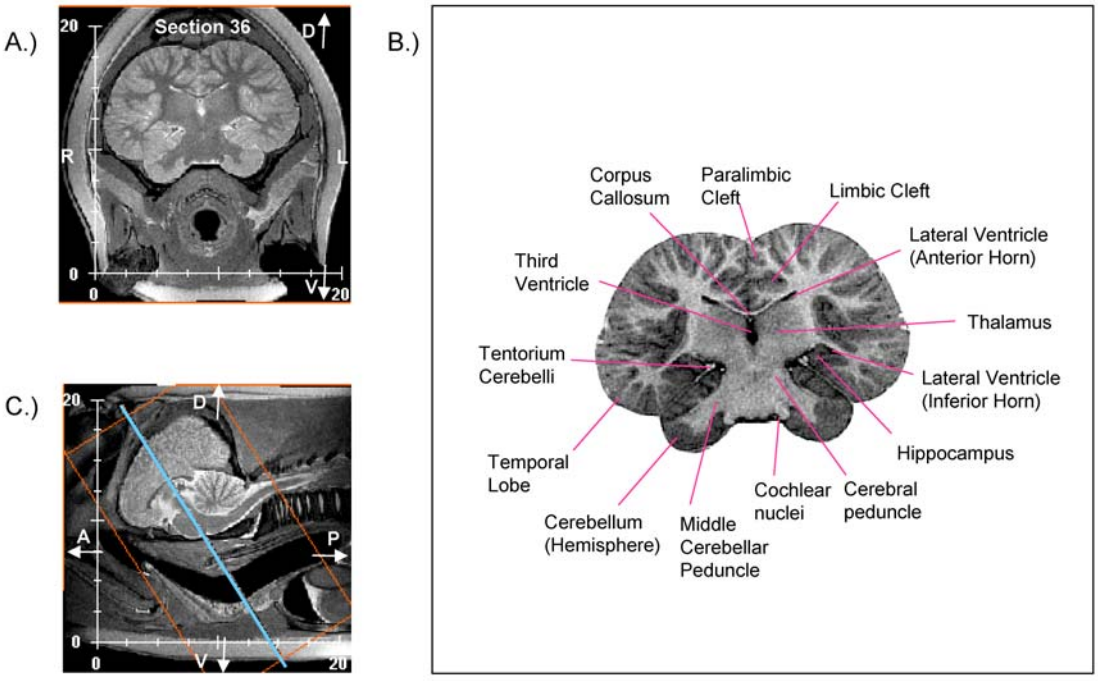


Figure 7.

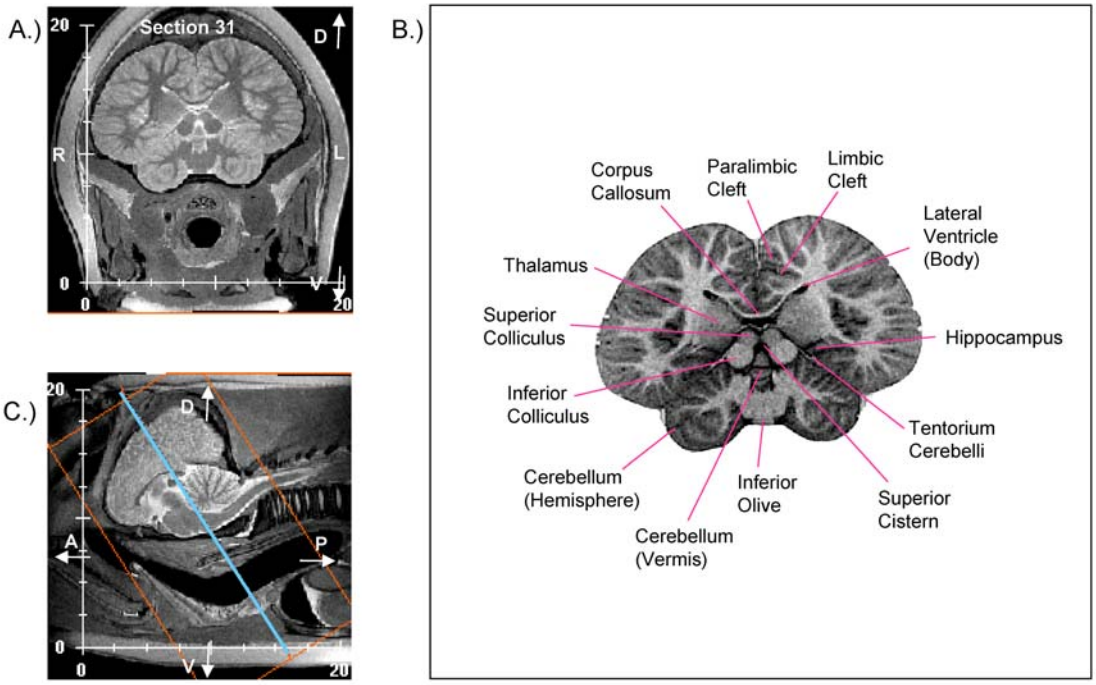


Figure 8.

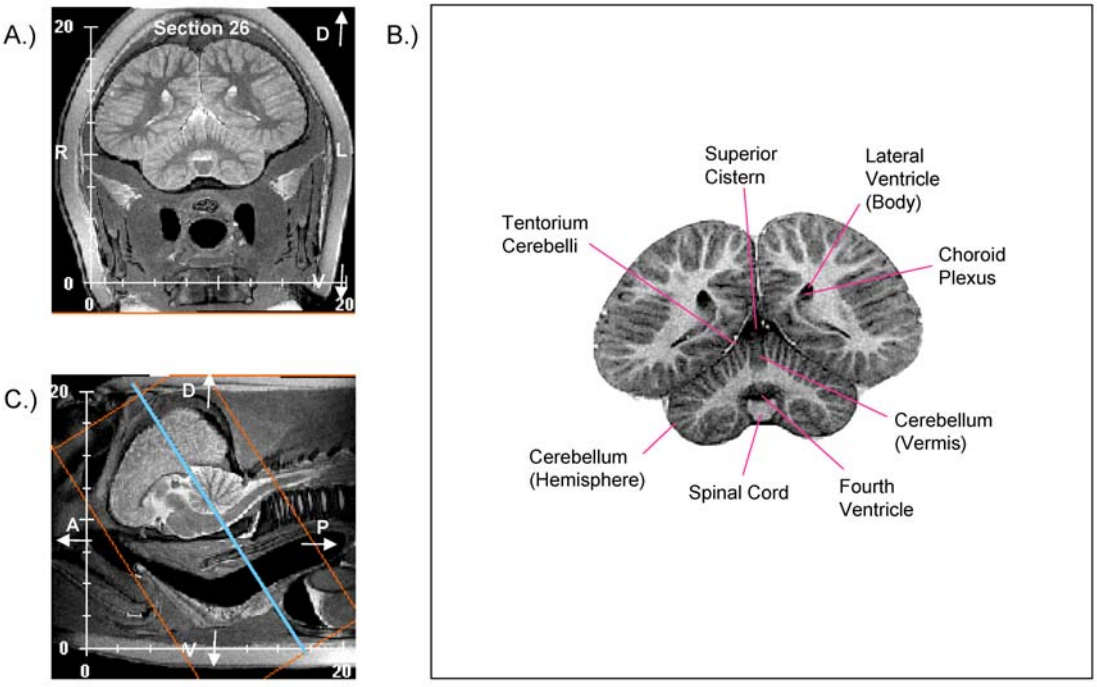


Figure 9.

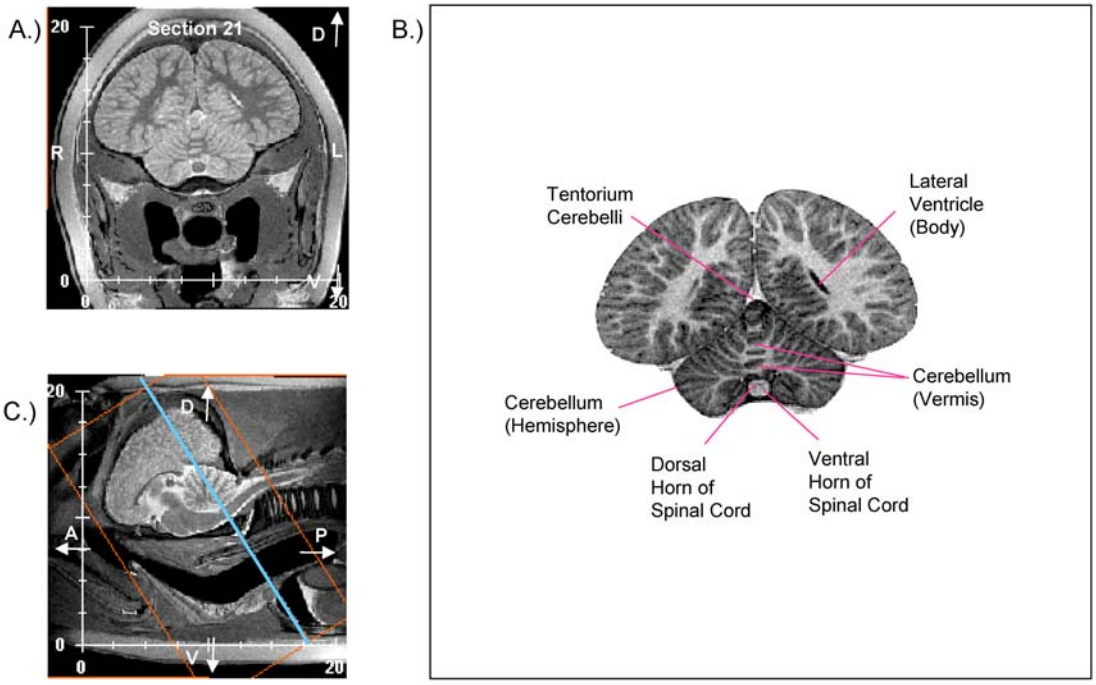


Figure 10.

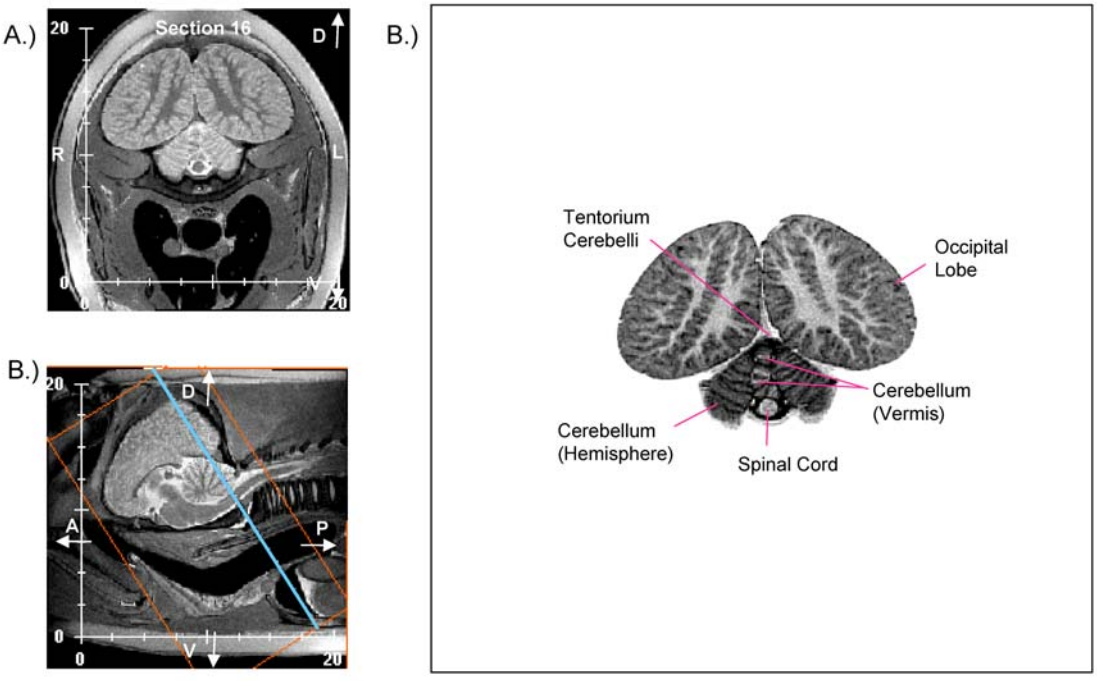


Figure 11.

**Figures 12-19. Midline-to-lateral, post-mortem MRI sequence of a subadult male brain (CCSN05-084-La) intact within the skull.** A.) Native proton-density (PD) weighted 2.0 mm-thick sagittal MR brain sections of the left hemisphere at 10 mm intervals. B.) Labeled brain cutout of each section with contrast reversed. C.) Coronal MR images of the brain intact within the skull depicting the orientation of the section. Orange lines illustrate the span of the MRI sequence. Blue lines represent the plane of section. D = dorsal; V = ventral; L = left; R = right; A = anterior; and P = posterior.

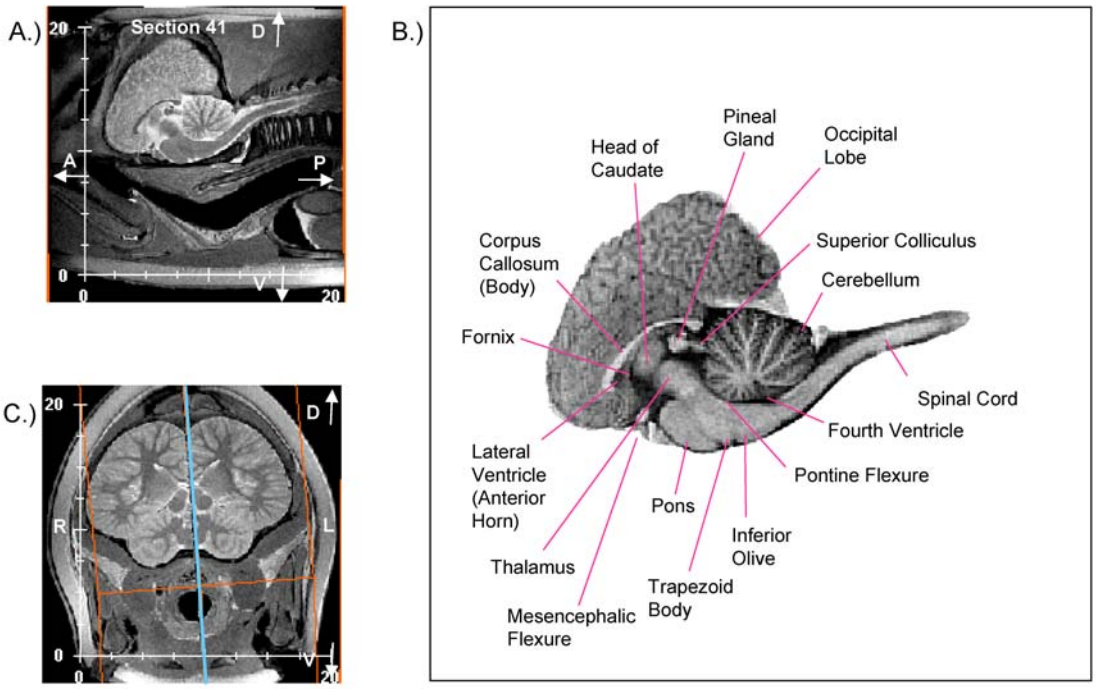


Figure 12.

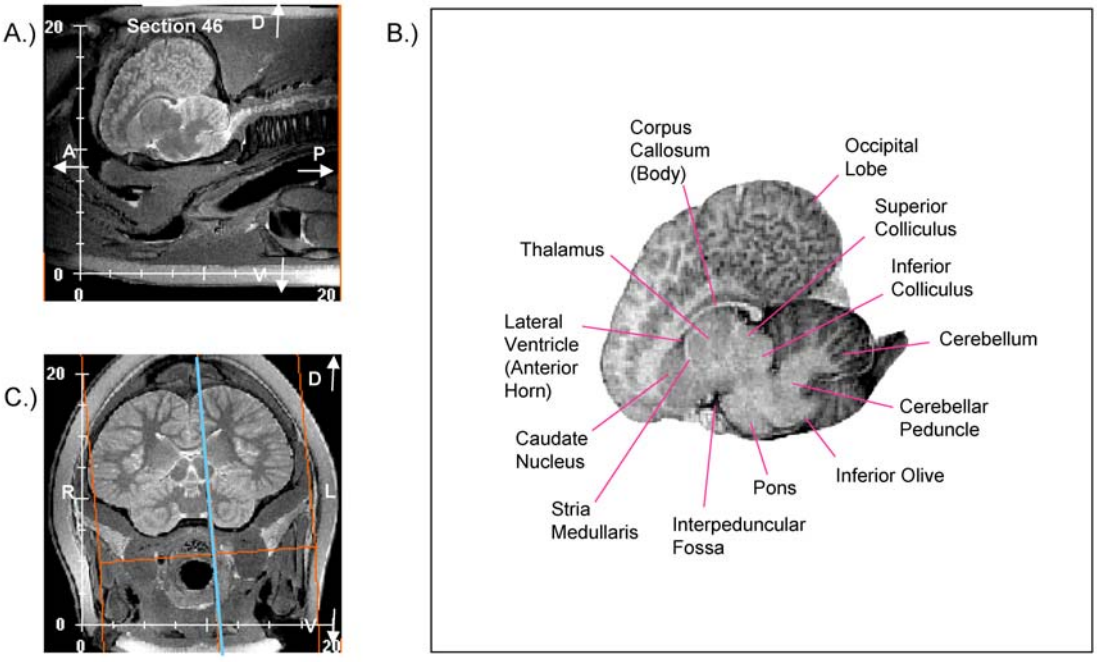


Figure 13.

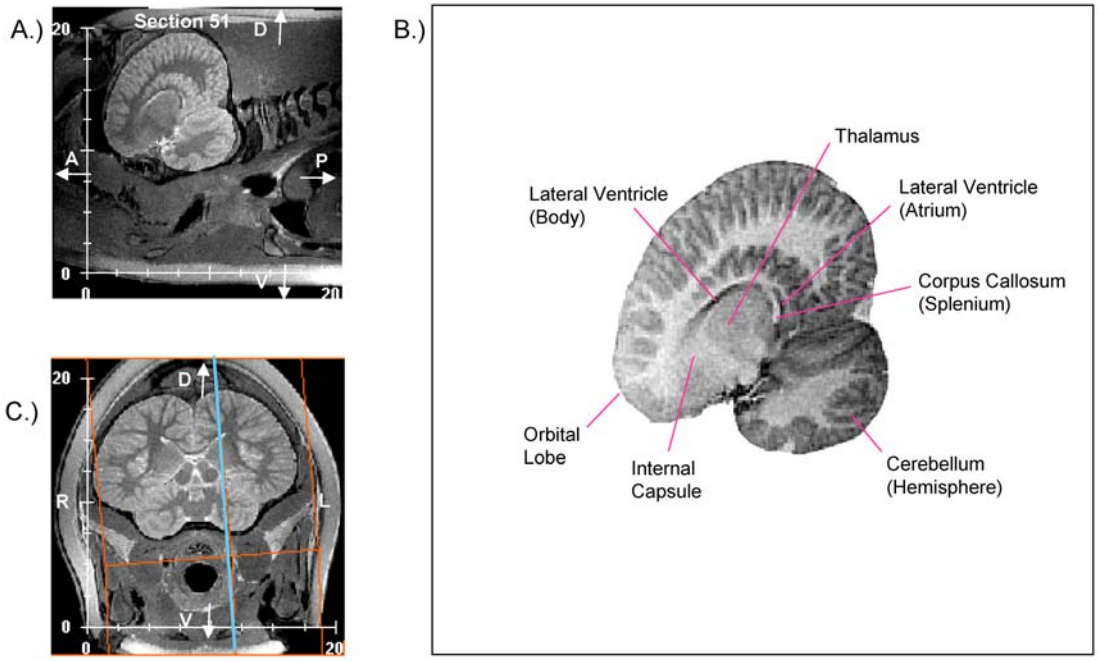


Figure 14.

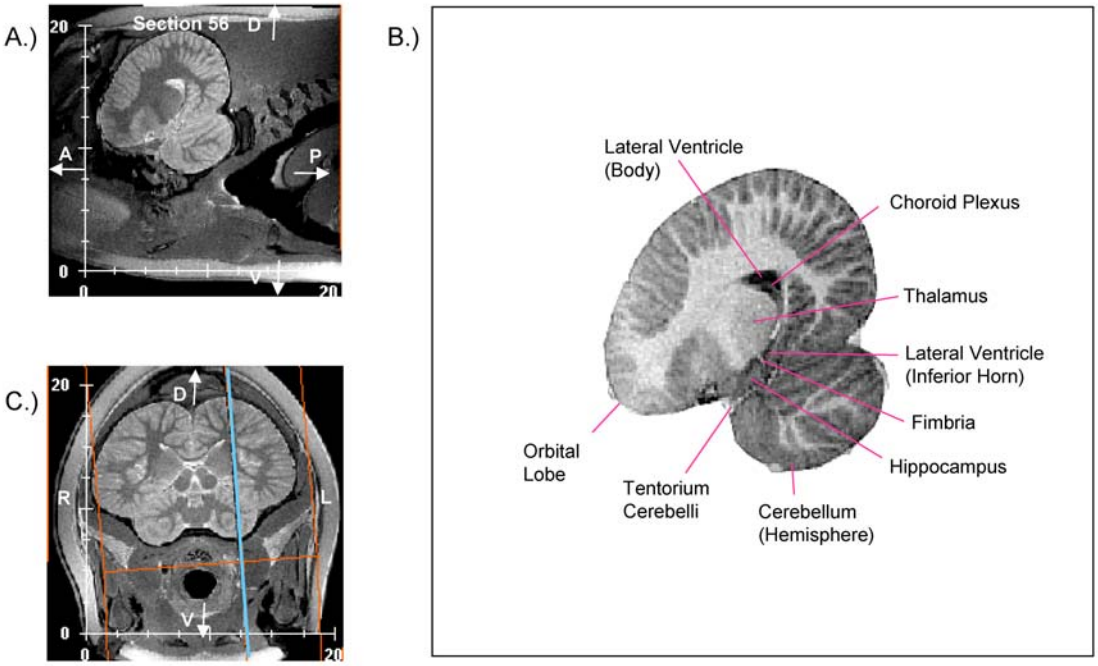


Figure 15.

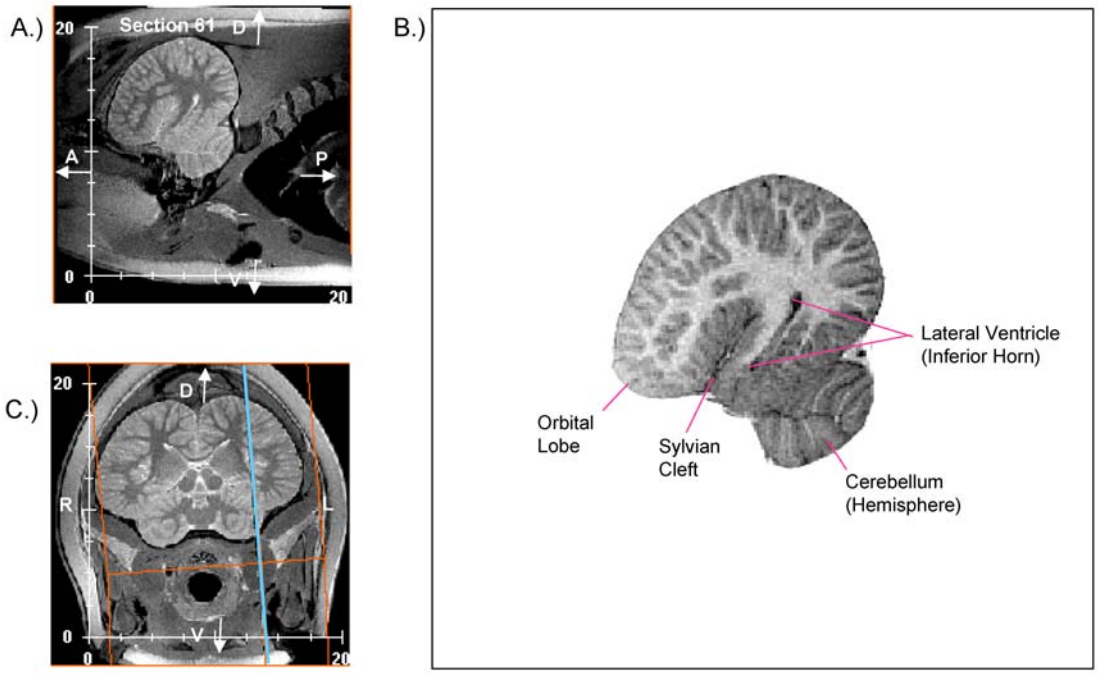


Figure 16.

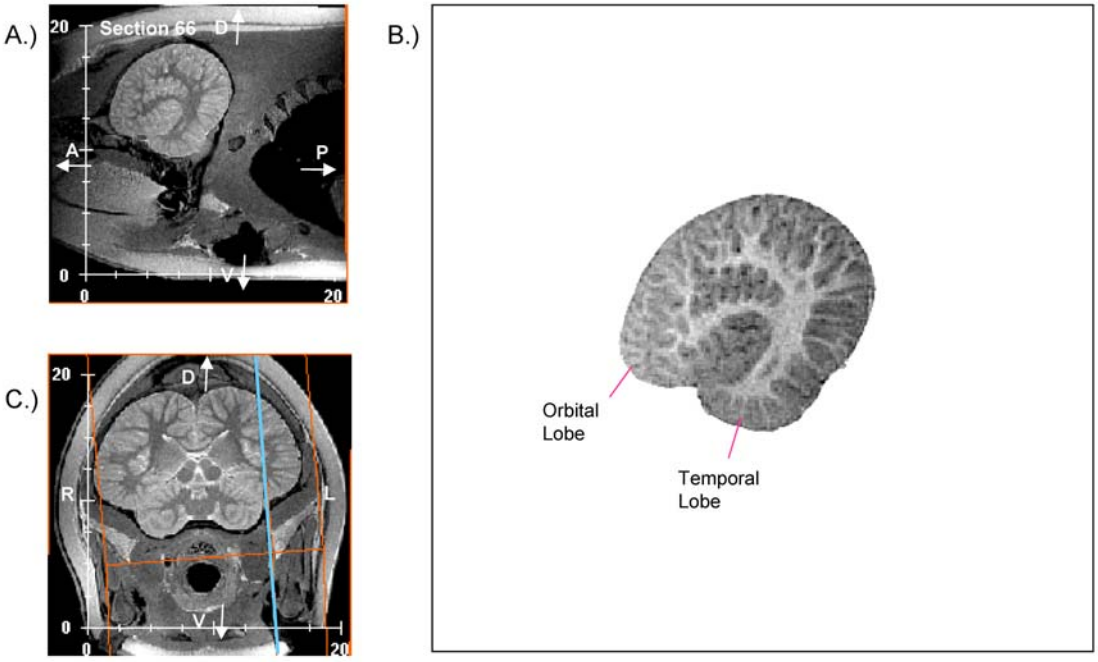


Figure 17.

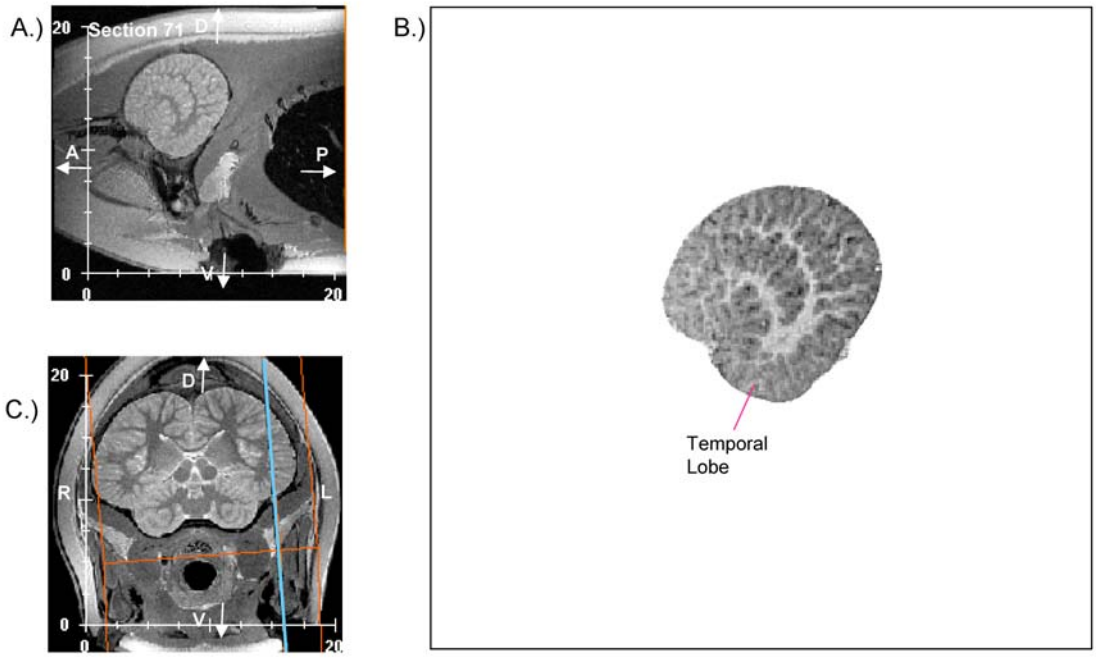


Figure 18.

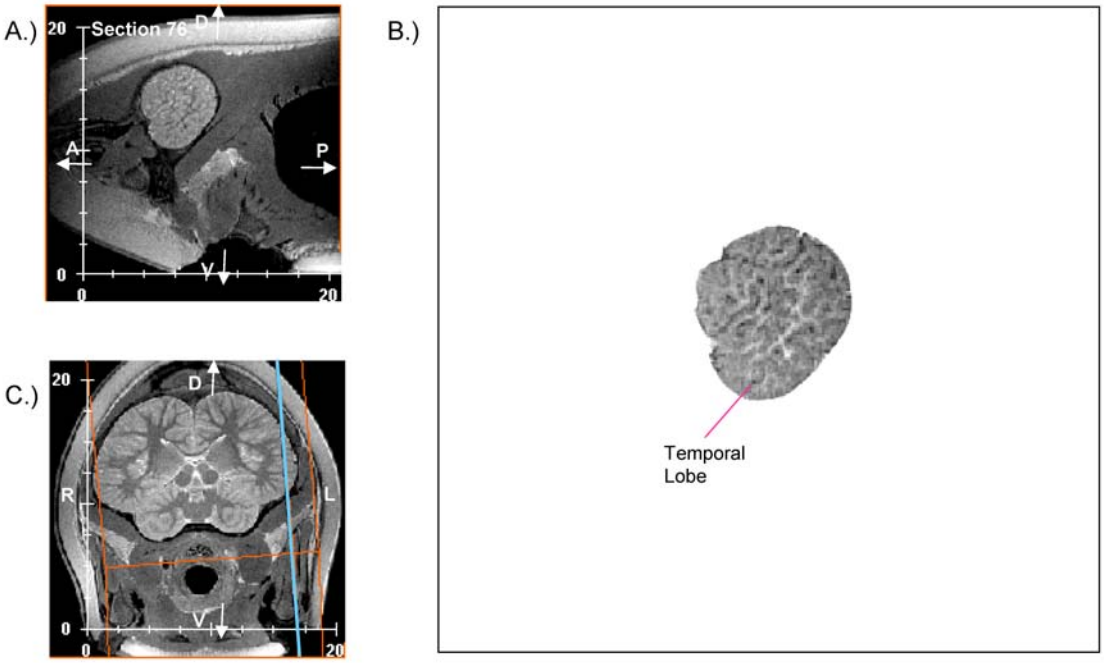


Figure 19.

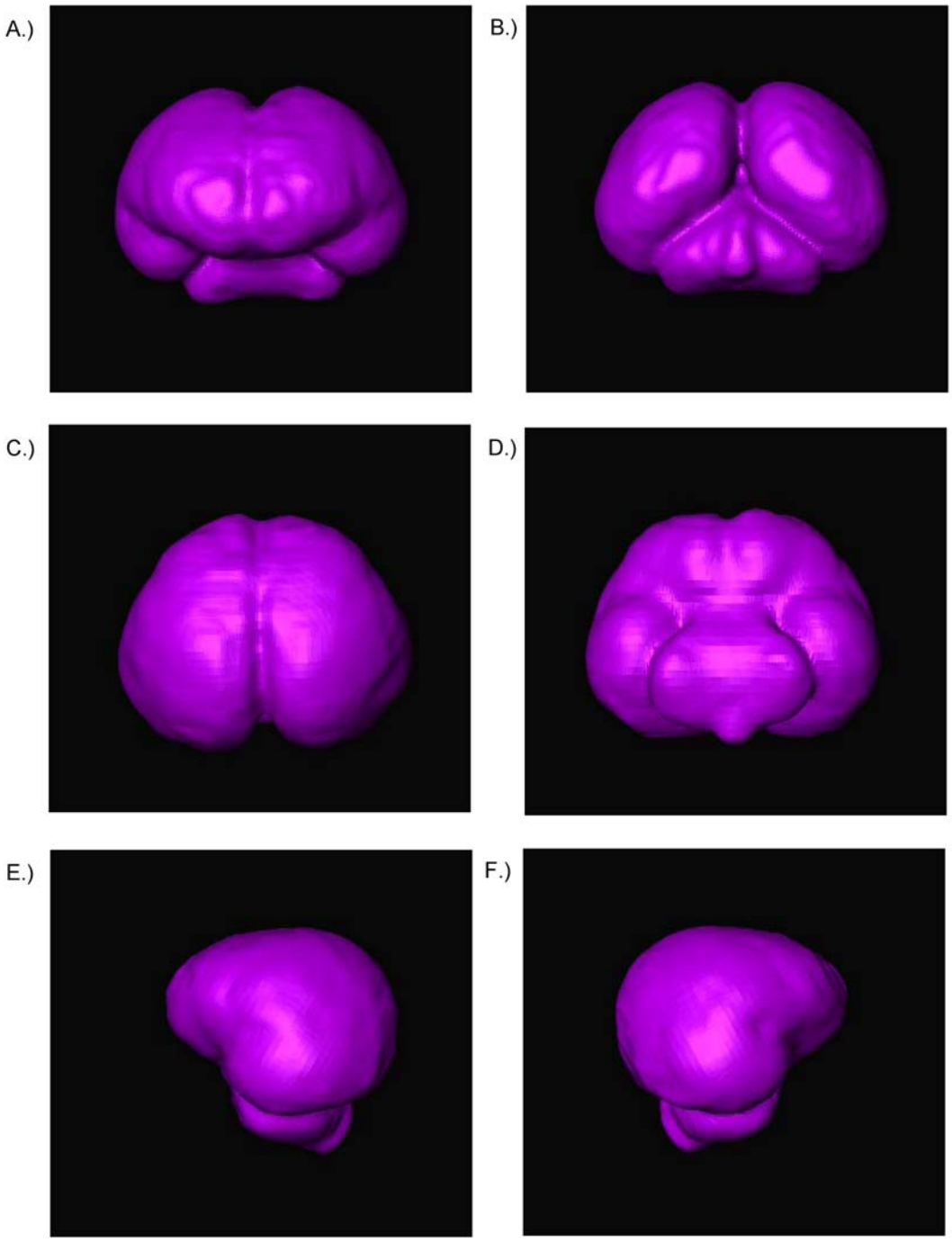


**Figure 20. Three-dimensional reconstruction of the brain of specimen CCSN05-040-Fetus-La from magnetic resonance (MR) images.** A.) Anterior view of brain. B.) Posterior view of brain. C.) Dorsal view of brain. D.) Ventral view of brain. E.) Left view of brain. F.) Right view of brain.

**Figures 21-27. Anterior-to-posterior, post-mortem MRI sequence of a male fetus brain (CCSN05-040-Fetus-La) intact within the skull.** A.) Native T2-weighted 2.0 mm-thick coronal MR brain sections at 6 mm intervals. B.) Labeled brain cutout of each section with contrast reversed. C.) Sagittal MR images of the brain intact within the skull depicting the orientation of the section. Orange lines illustrate the span of the MRI sequence. Blue lines represent the plane of section. D = dorsal; V = ventral; L = left; R = right; A = anterior; and P = posterior.

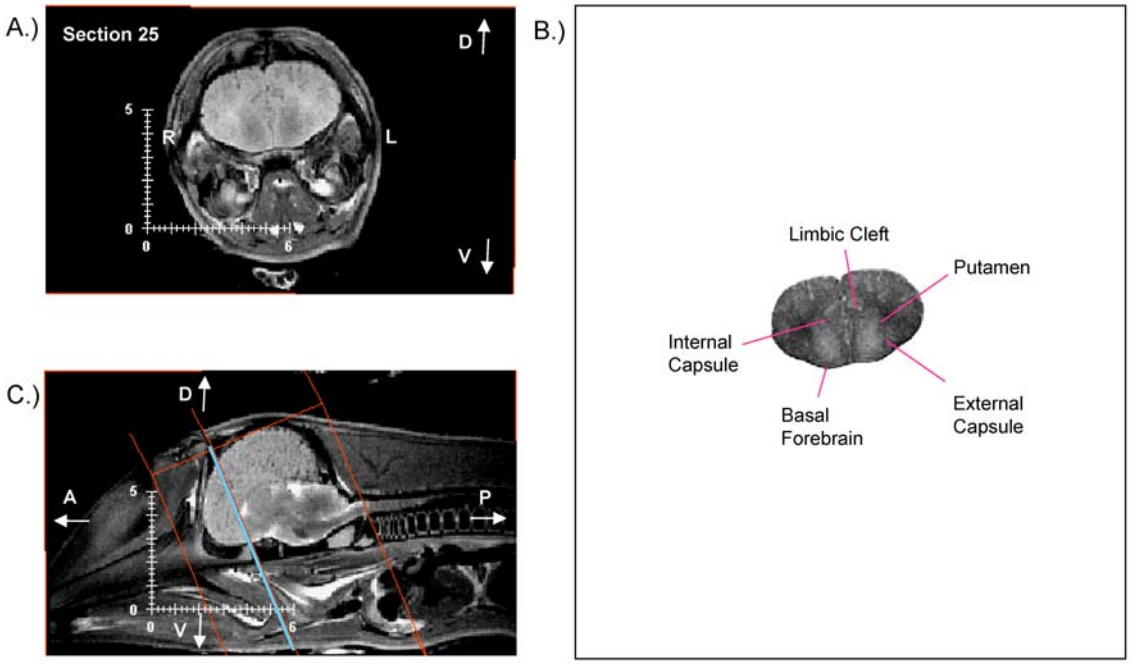


Figure 21.

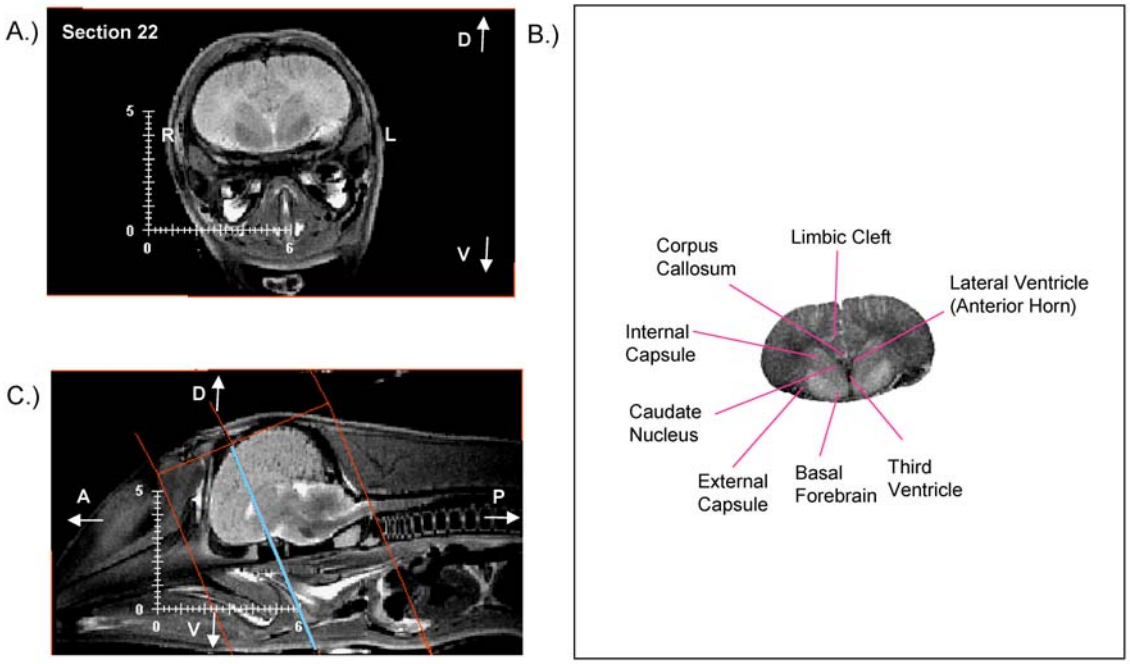


Figure 22.

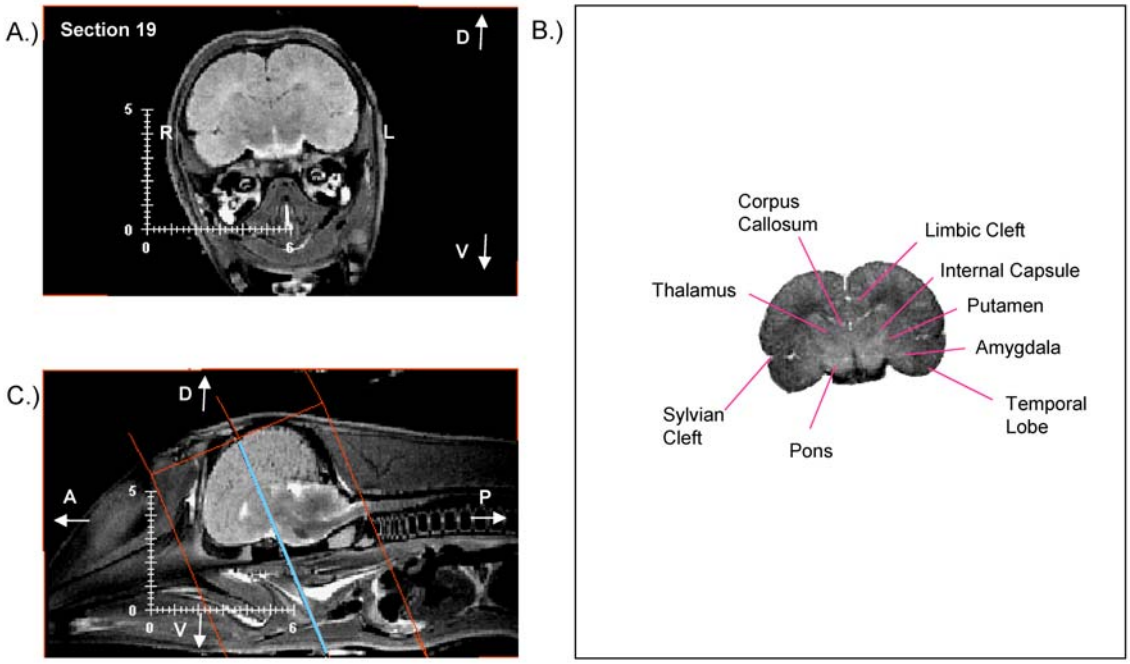


Figure 23.

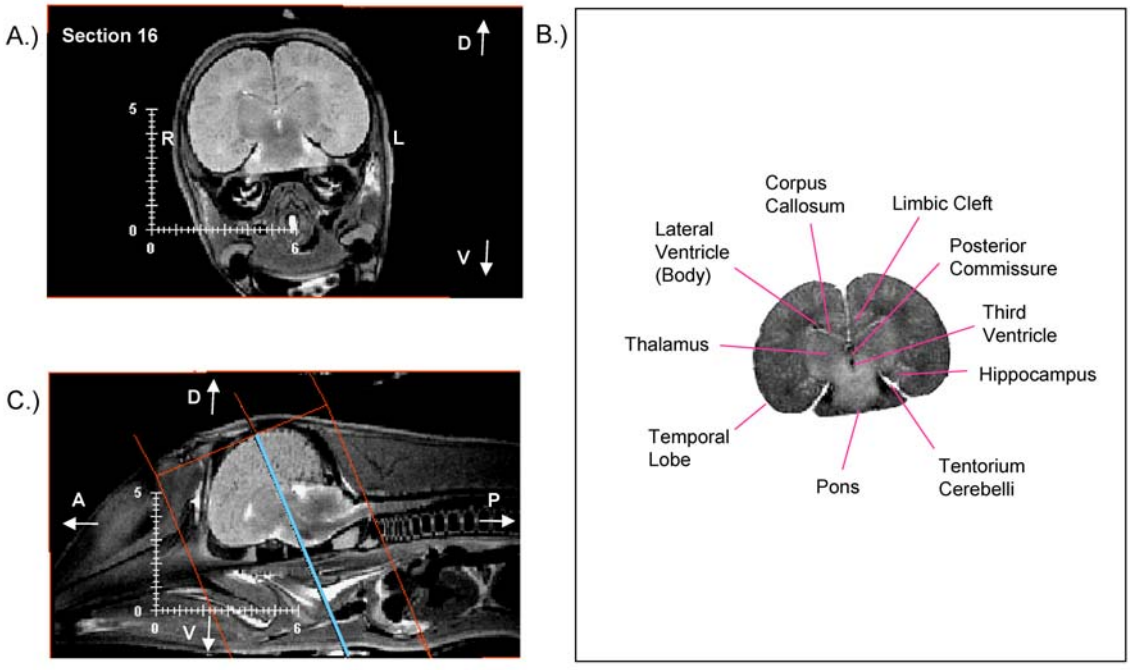


Figure 24.

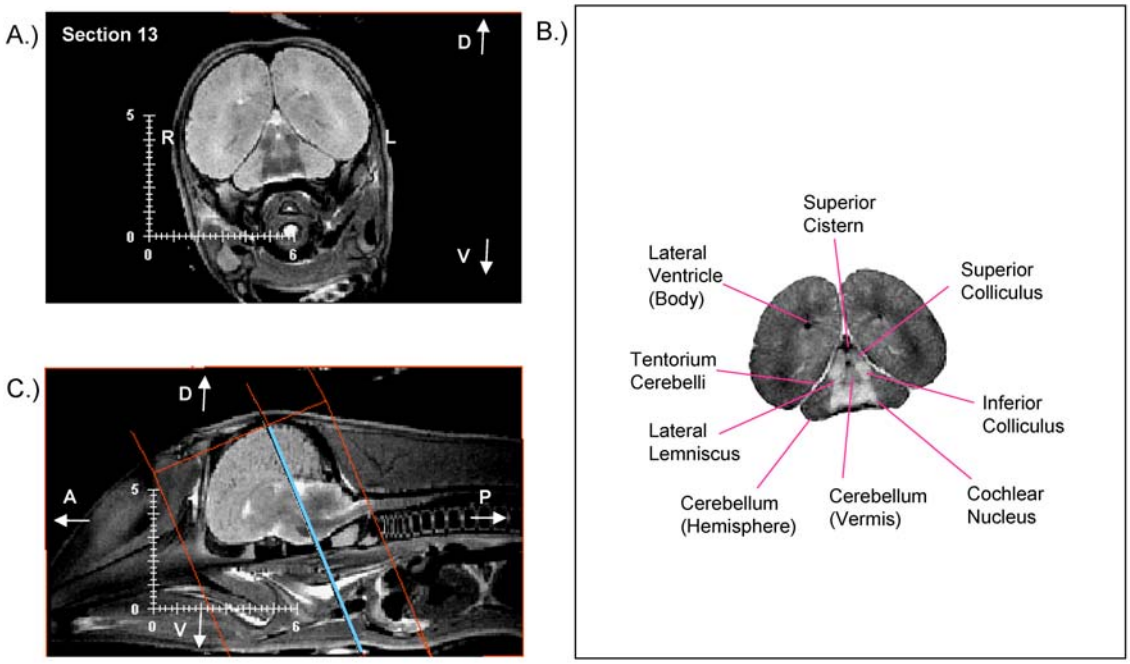


Figure 25.

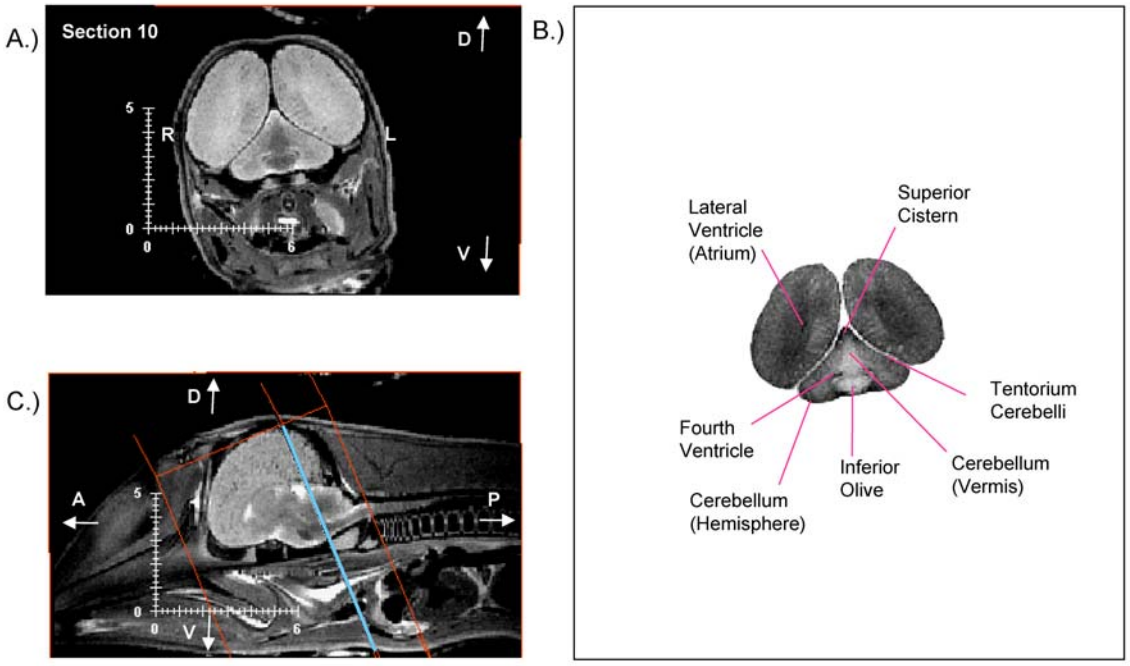


Figure 26.

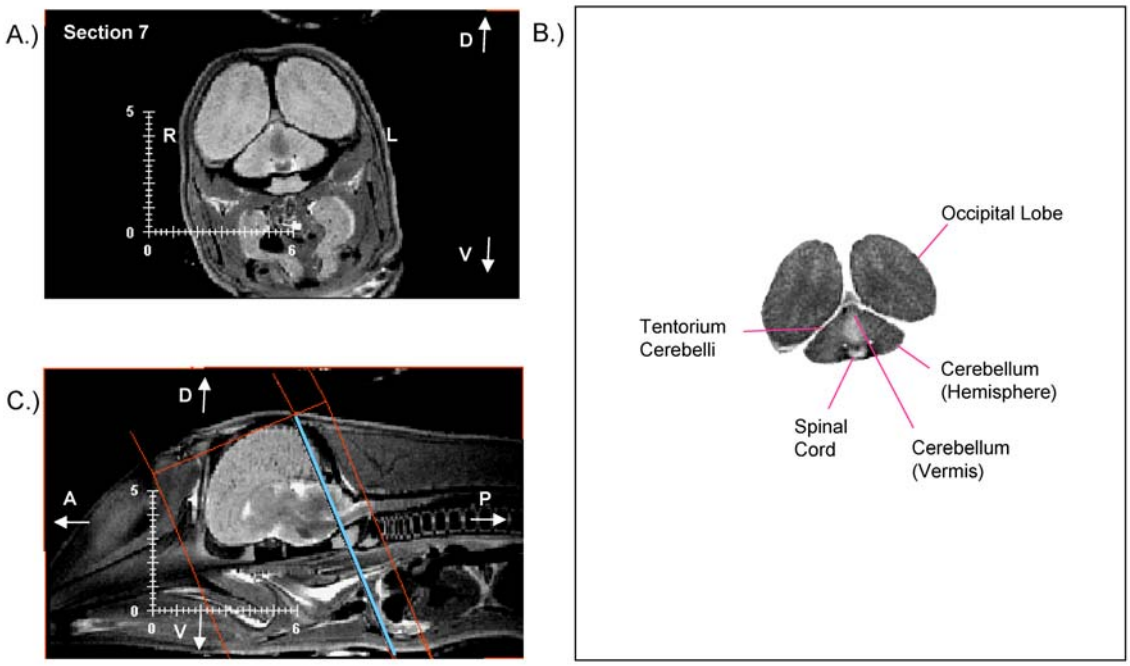


Figure 27.

**Figures 28-33. Midline-to-lateral, post-mortem MRI sequence of a male fetus brain (CCSN05-040-Fetus-La) intact within the skull.** A.) Native T2-weighted 2.0 mm-thick sagittal MR brain sections of the left hemisphere at 6 mm intervals. B.) Labeled brain cutout of each section with contrast reversed. C.) Coronal MR images of the brain intact within the skull depicting the orientation of the section. Orange lines illustrate the span of the MRI sequence. Blue lines represent the plane of section. D = dorsal; V = ventral; L = left; R = right; A = anterior; and P = posterior.

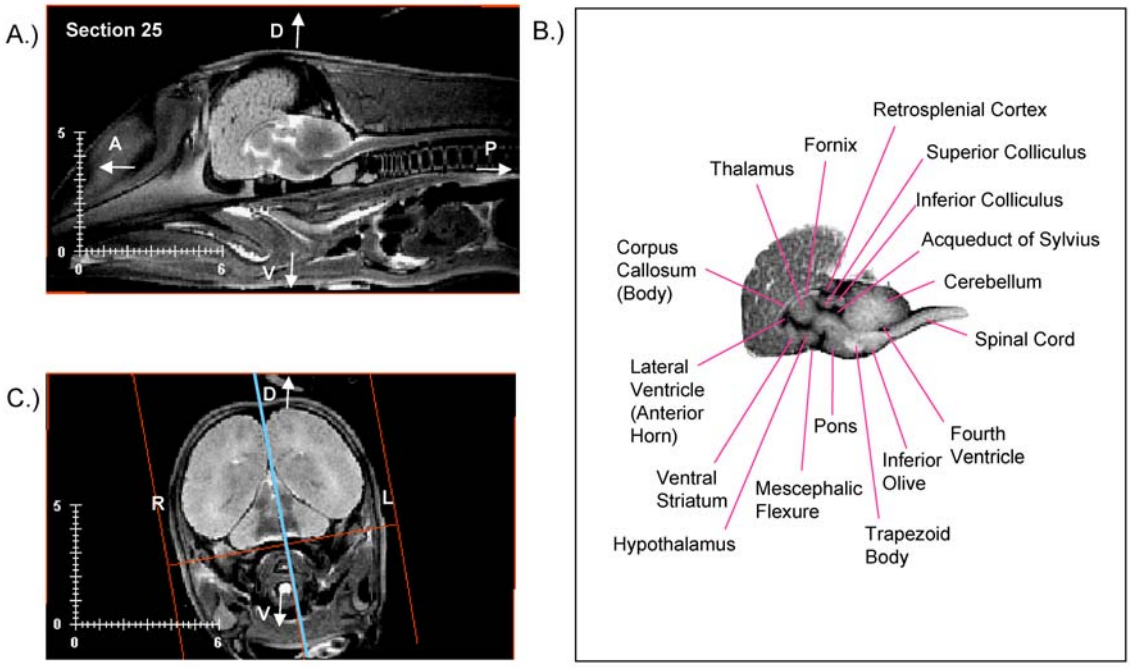


Figure 28.

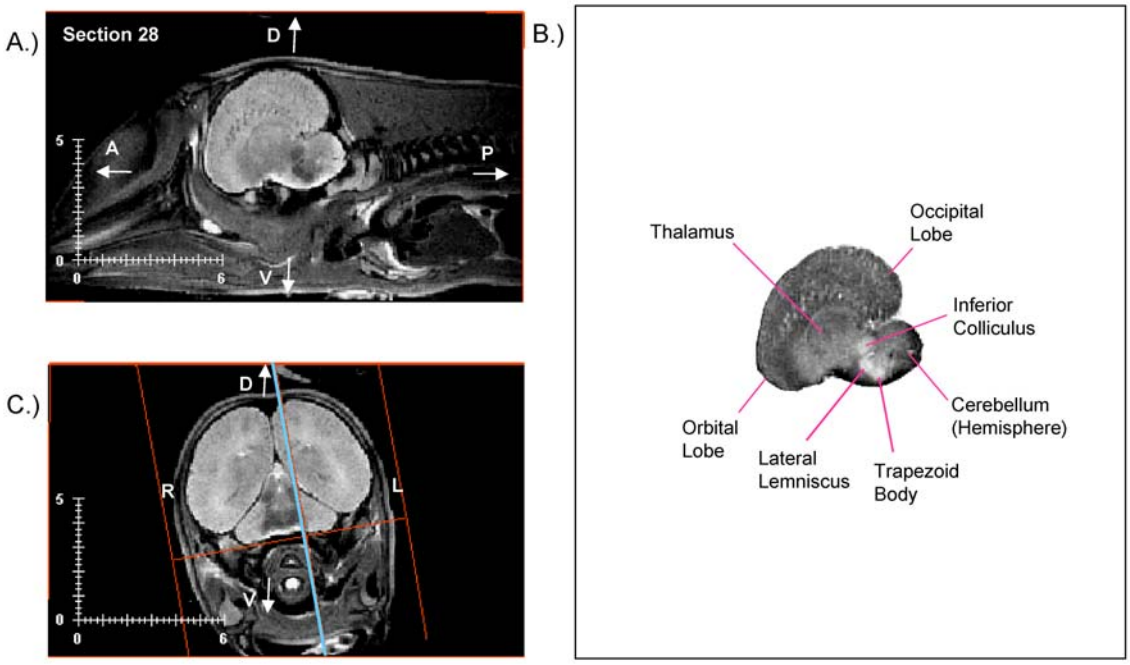


Figure 29.

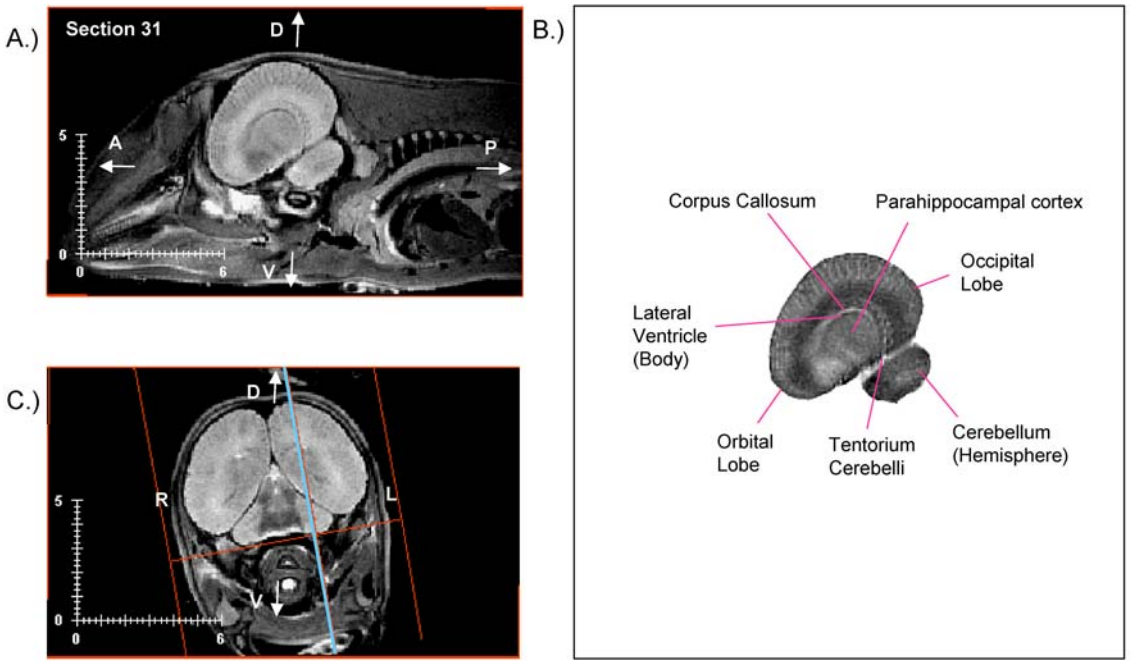


Figure 30.

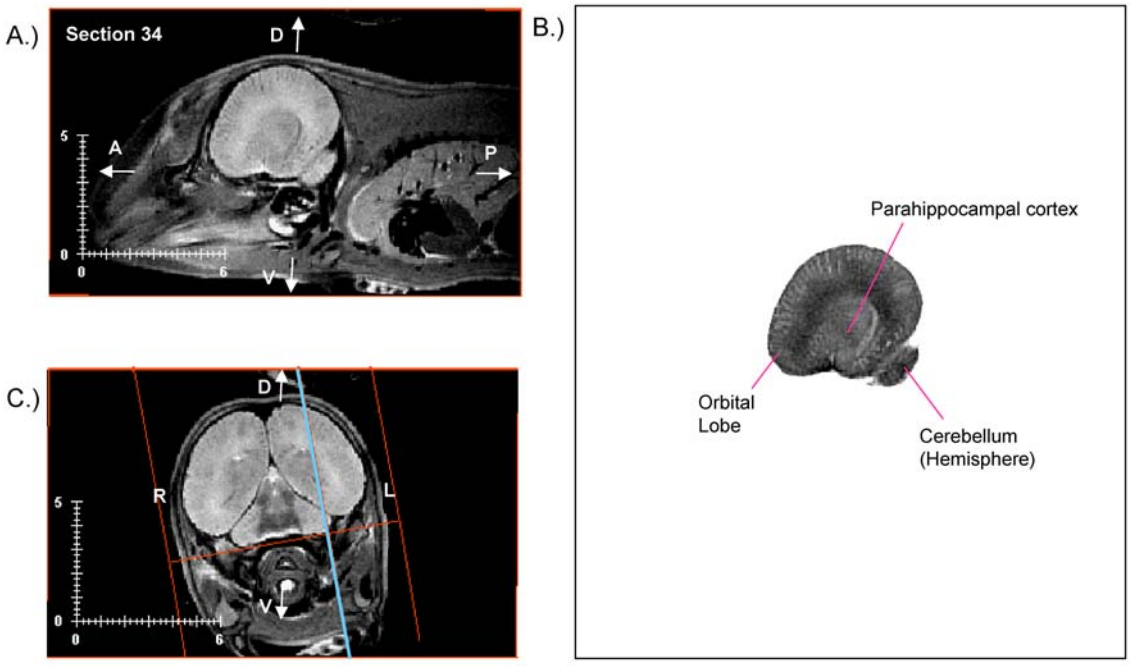


Figure 31.

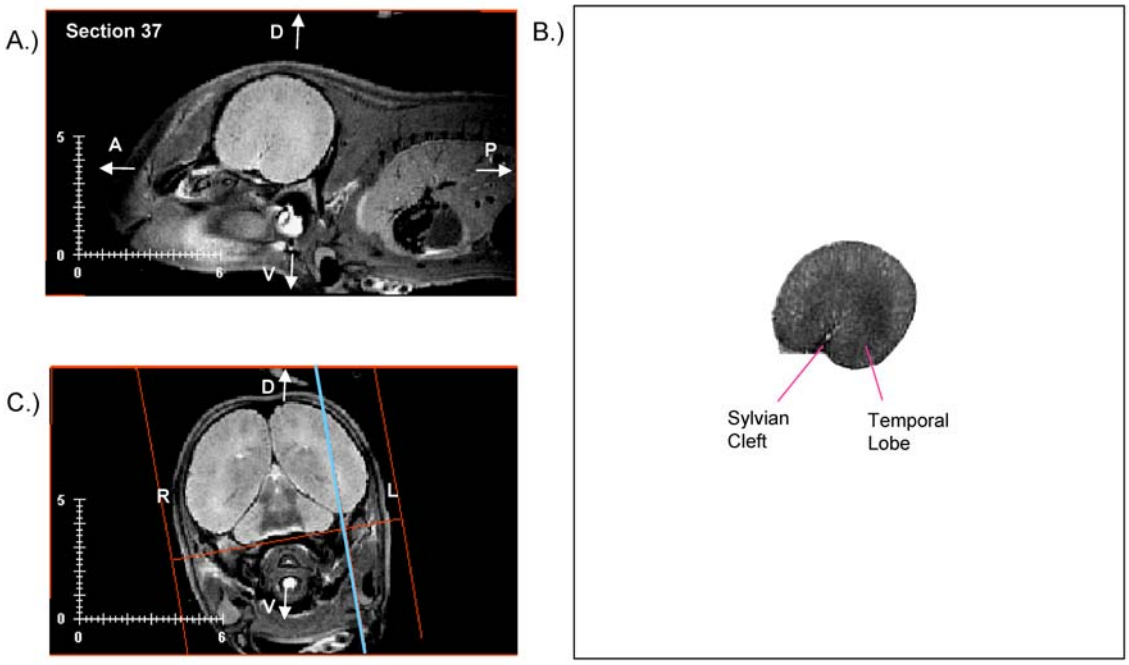


Figure 32.

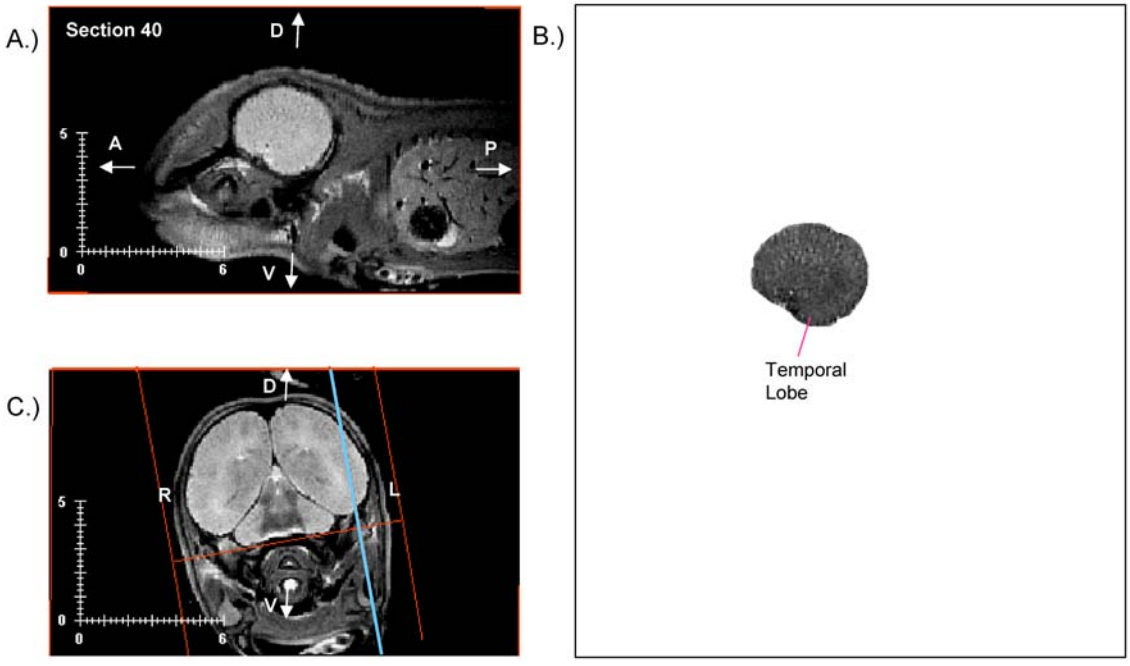


Figure 33.

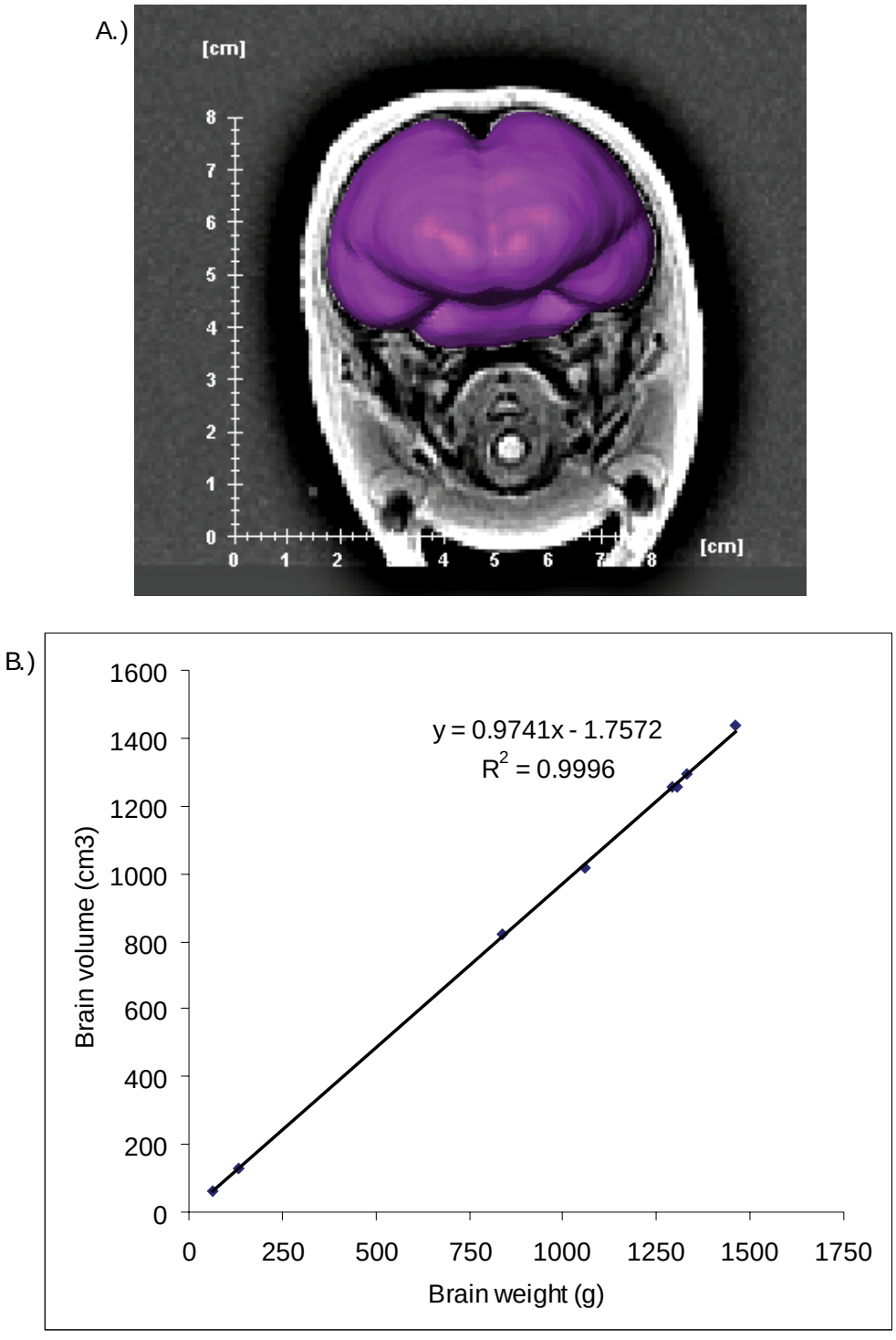


**Figure 34. A.) Three-dimensional reconstruction of fetal brain surface (CCSN05-039-fetus-La). B.) Measured brain volume ($cm^3$) versus actual brain weight (g).**

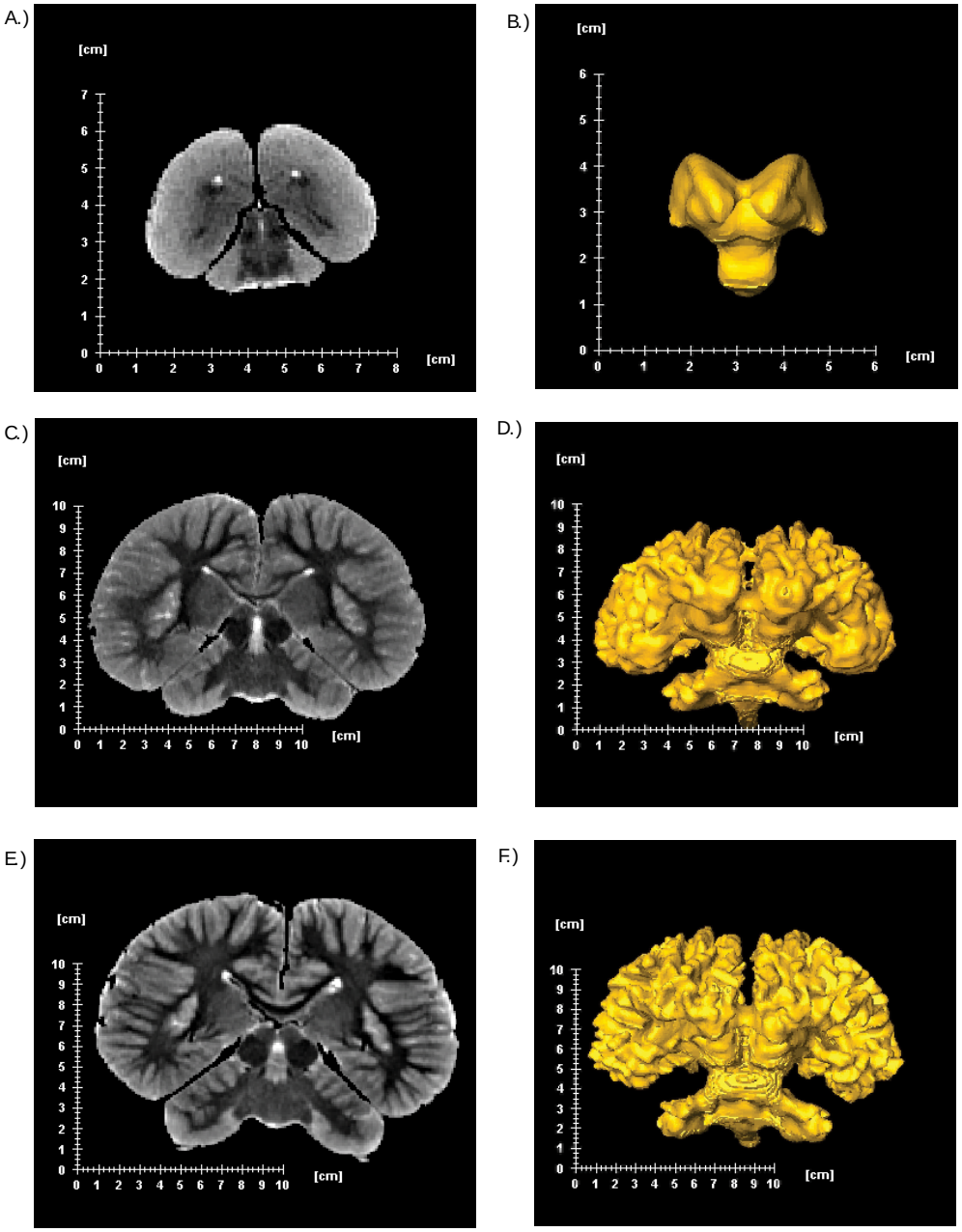


**Figure 35. A visual comparison of the degreee of myelination (i.e white matter tracts) during ontogeny.** A-B.) Fetal specimen CCSN05-039-Fetus-La. C-D.) Neonate specimen CCSN05-231-La. E-F.) Adult specimen CCSN05-040-La. All brain MR sections are at the level of the inferior and superior colliculi. The panels to the right represent three-dimensional reconstructions of the white matter. D.) A histogram of signal intensity values for CCSN05-039-Fetus-La, CCSN05-231-La, and CCSN05-040-La. E.) White matter (WM): grey matter (GM) volume ratios of the total brain versus length. F.) WM:GM volume ratios of the cerebellum versus length.

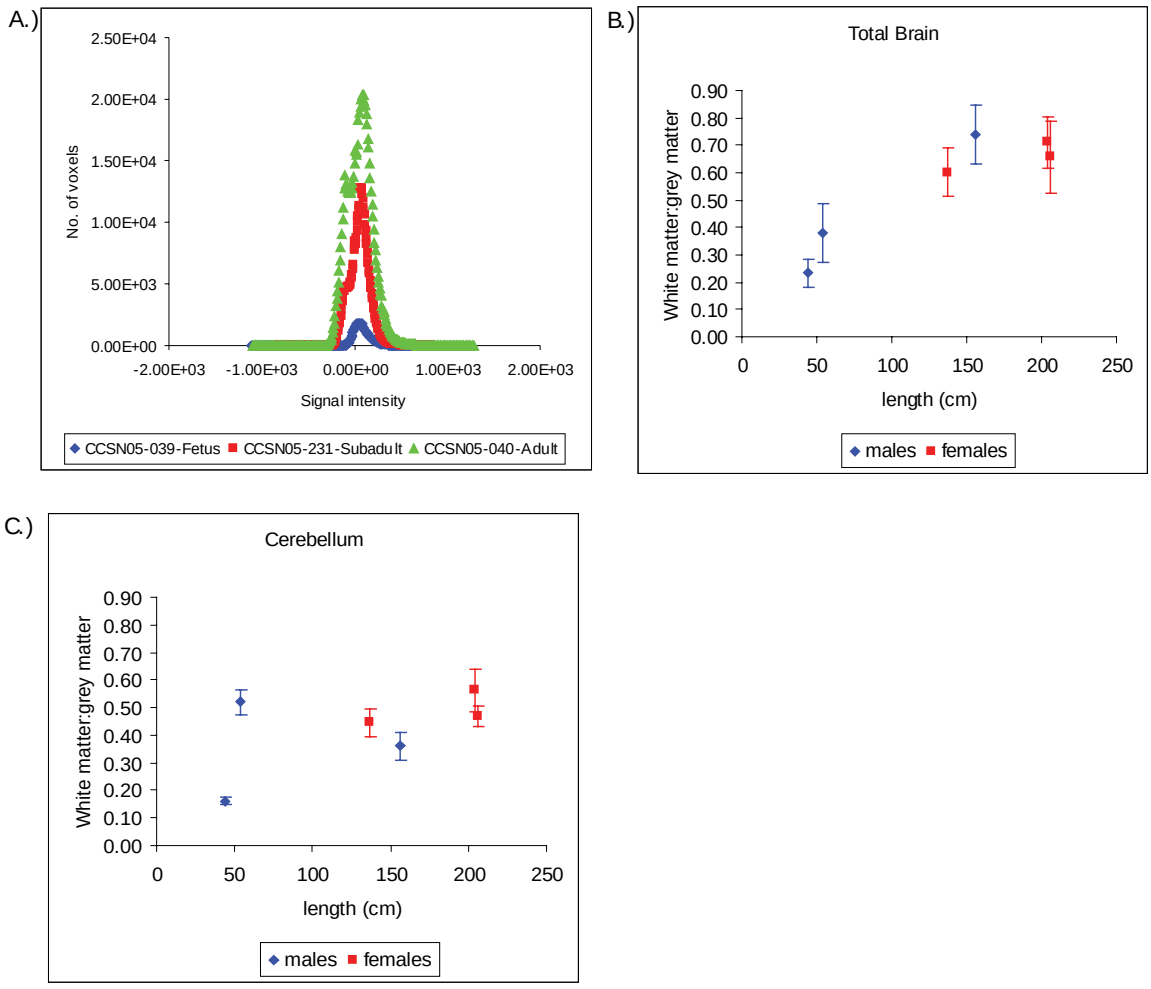


**Figure 36. A quantitative comparison of the degreee of myelination (i.e white matter tracts) during ontogeny.** A.) A histogram of signal intensity values for CCSN05-039-Fetus-La, CCSN05-231-La, and CCSN05-040-La. B.) White matter (WM): grey matter (GM) volume ratios of the total brain versus length. C.) WM:GM volume ratios of the cerebellum versus length.

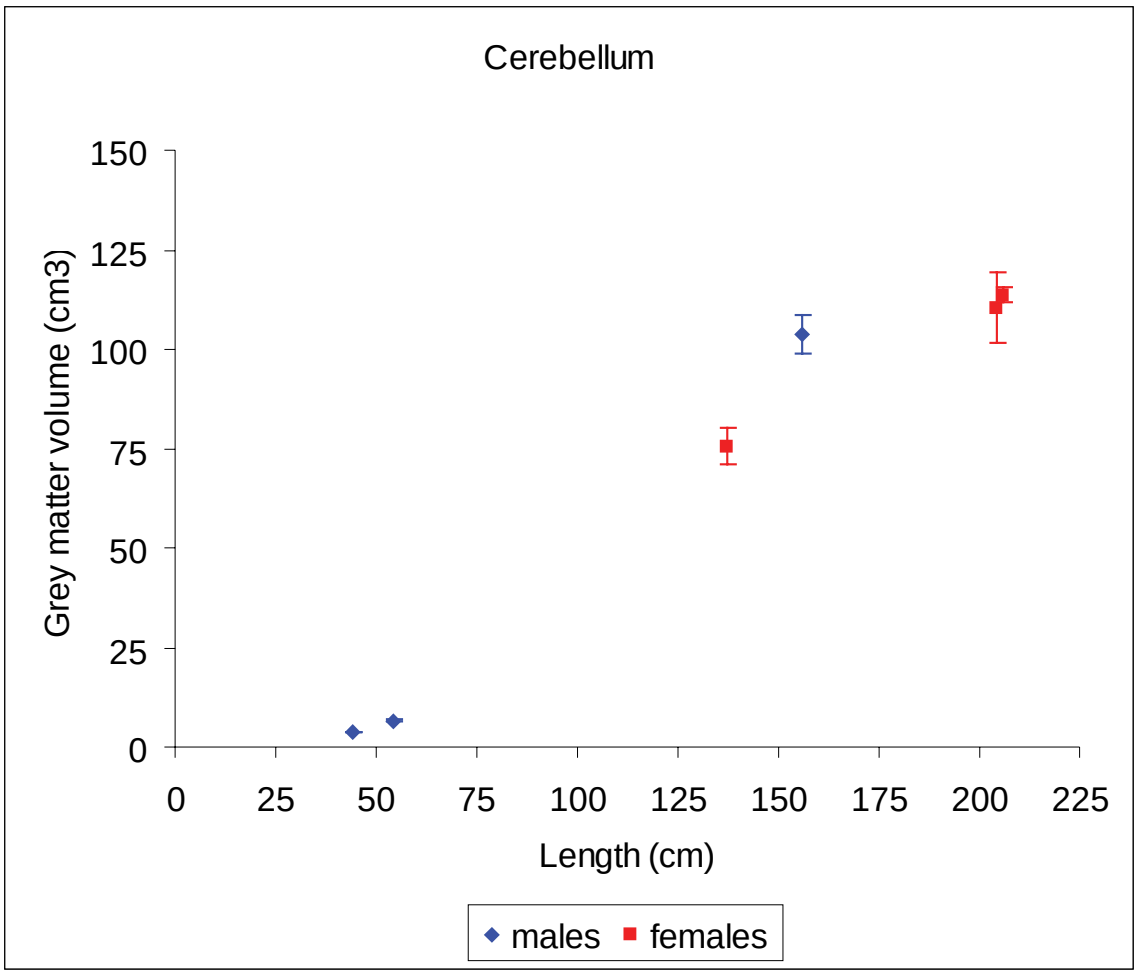


**Figure 37. Volumes ($cm^3$) of the cerebellum grey matter versus length (cm).**

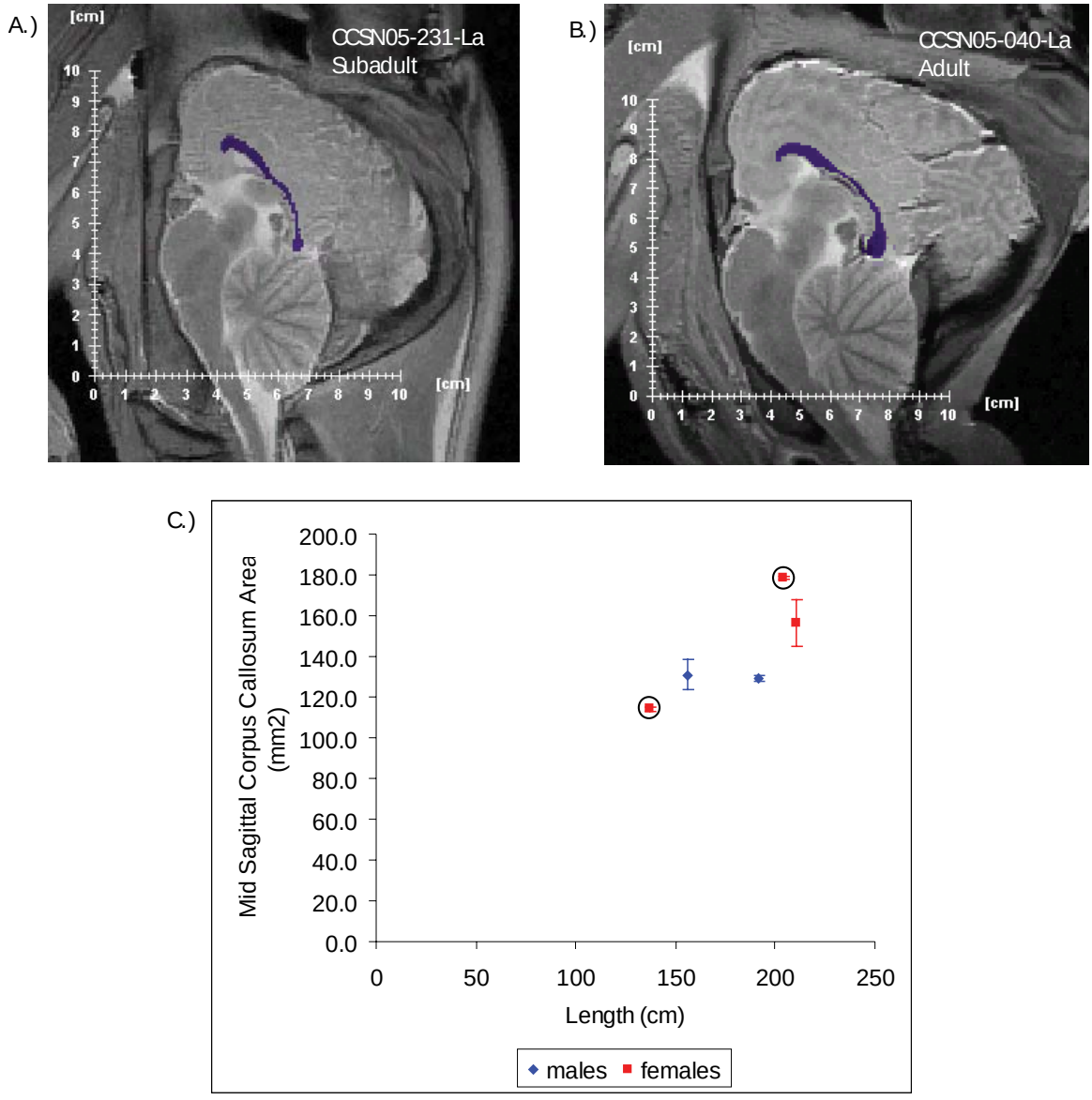


**Figure 38. Segmentation label maps and mid-sagittal areas of the corpus callosum.** A.) Pixels selected to calculate the mid-sagittal area of the corpus callosum for the neonate specimen CCSN05-231-La. B.) Pixels selected to calculate the mid-sagittal area of the corpus callosum for the adult specimen CCSN05-040-La. C.) Mid-sagittal area of the corpus callosum ($mm^2$) versus length (cm). CCSN05-231-La and CCSN05-040-La data points are encircled.

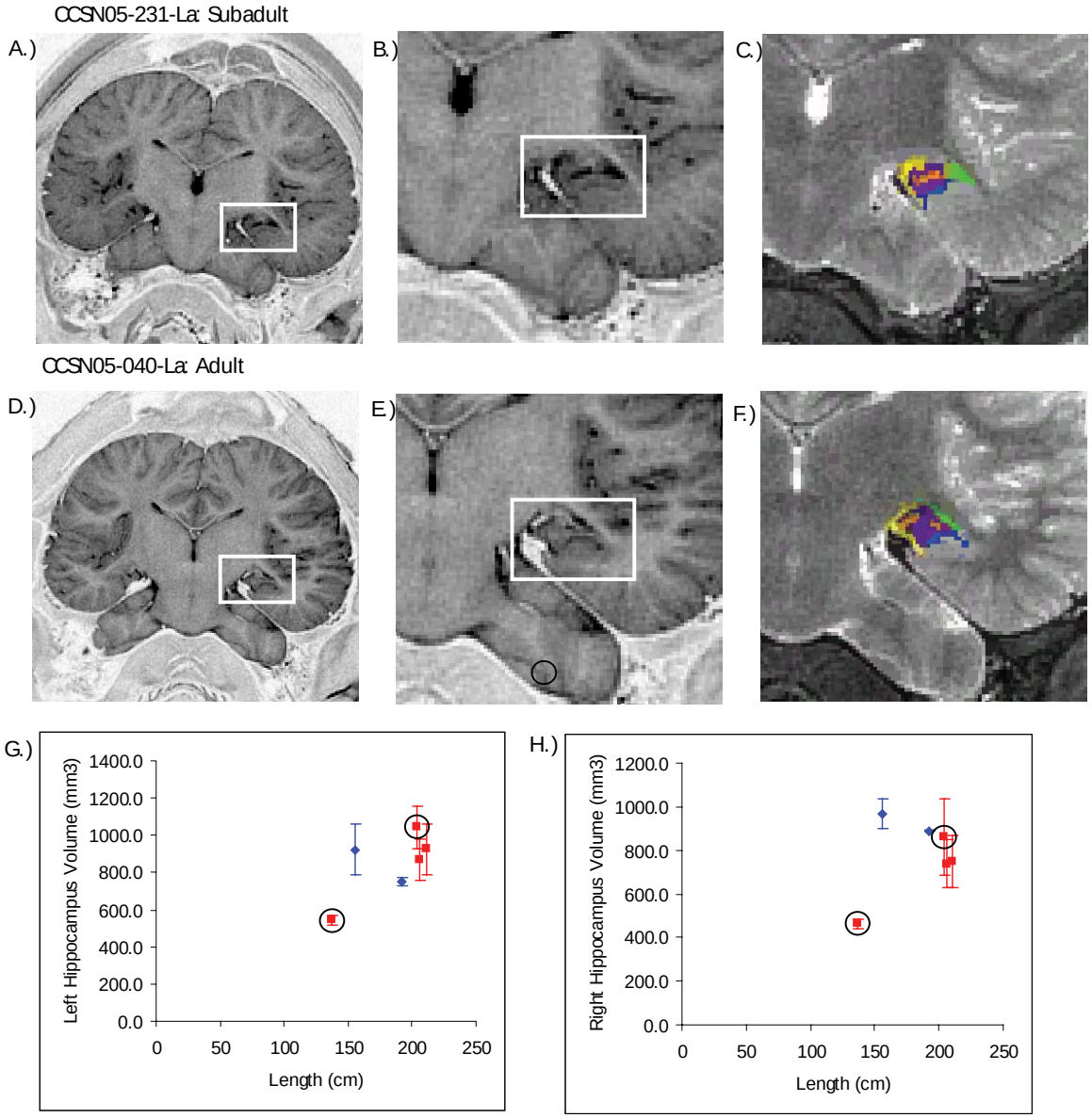


**Figure 39. Segmentation label maps and volumes of the hippocampus.** A – C.) Hippocampus of neonate specimen CCSN05-231-La. D – F.) Hippocampus of adult specimen CCSN05-040-La. Panels A and D demarcate the position of the left hippocampus in the medial wall of the temporal lobe. The hippocampus is highlighted with a white box in the native PD-weighted images (with contrast reversed). Panels B and E are an enlargement of panels A and D, respectively. Panels C and F show the hippocampus label map in native T2-weighted images (normal contrast). Purple = hippocampus; green = CSF of the inferior horn of the lateral ventricle; blue = CSF of the parahippocampal sulcus; yellow = CSF of the subarachnoid space and the transverse fissure of Bichat; orange = hippocampal fluid. G.) Volume of the left hippocampus ($mm^3$) versus length (cm). H.) Volume of the right hippocampus ($mm^3$) versus length (cm).

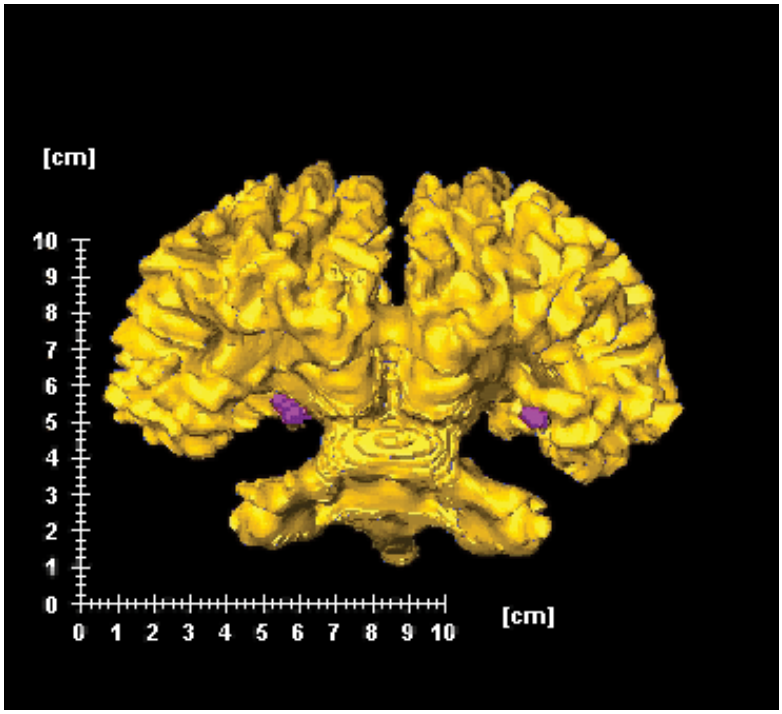


**Figure 40. Three-dimensional reconstruction of the adult specimen brain CCSN05-040-La illustrating the spatial relationship of the hippocampus with the rest of the brain.** White matter = yellow; hippocampus = purple.

Table 1. Stranding and Life History Information of Atlantic White-sided Dolphin Specimens in Which Magnetic Resonance Imaging (MRI) Was Performed.[1]

| FIELD ID: | Date/time of death | Location | Hours to MRI | Condition Code[2] | Stranding type | Sex | Length (cm) | Age Class | Weight (kg) | Brain Lesion[3] |
|---|---|---|---|---|---|---|---|---|---|---|
| CCSN04-195-La | Sept 14, 2004 at 17:36 | Herring River Gut, Wellfleet, MA | 3 | 1 | single | m | 192 | subadult | 73.5 | no |
| CCSN05-037-La | Feb15, 2005 at 14:30 | Chipman's Cove, Wellfleet, MA | 10 | 1 | mass | f | 206 | adult | 125 | no |
| CCSN05-038-La[4] | February 15, 2005 | Chesequesset Neck, Wellfleet, MA | <24 | 2 | mass | f | 208 | lactating adult | 125 | yes |
| CCSN05-039-La | February 15, 2005 | Chesequesset Neck, Wellfleet, MA | <24 | 2 | mass | f | 211 | pregnant adult | 146 | no |
| CCSN05-039-Fetus-La | February 15, 2005 | Chesequesset Neck, Wellfleet, MA | <24 | 2 | mass | m | 44 | fetus | 1.394 | no |
| CCSN05-040-La | February 15, 2005 | Chesequesset Neck, Wellfleet, MA | <24 | 2 | mass | f | 204 | pregnant adult | 123.6 | no |
| CCSN05-040-Fetus-La | February 15, 2005 | Chesequesset Neck, Wellfleet, MA | <24 | 2 | mass | m | 54 | fetus | 2.431 | no |
| CCSN05-084-La | March 19, 2005 at 14:15 | Wellfleet, MA | 5 | 1 | single | m | 156 | subadult | 42.56 | no |
| CCSN05-231-La | Sept 26, 2005 at 13:30 | Sandy Neck, Barnstable, MA | 10 | 1 | single | f | 137 | neonate | 30 | no |
| CCSN05-232-La[4] | Oct 4, 2005 at 12:22 | Nauset Beach, Eastham, MA | 11 | 1 | single | f | 185.5 | subadult | 77.5 | yes |

[1] Only specimens in which MRIs were completed are included.

[2] A condition code of 1 indicates that the dolphin was euthanized, while a condition code of 2 indicates that the dolphin was found dead but the specimen was in fresh condition (i.e. less than 24 hours had passed since the time of death).

[3] Brain pathologies were found using MR images.

[4] Segmentation was not completed on these specimens because of gross brain pathologies. These lesions are described in Appendix 1.

MRIs were completed of the brain intact within the skull and the head attached to the body.

Table 2. Comparisons of Expected and Segmented Volumes of Water.

| | Expected Volume (mL) | Segmented Volume (mL) | RMSE | % error |
|---|---|---|---|---|
| PD native[1] | 19.8 ± 0.2 | 20.5 ± 0.6 | 0.9 ± 0.6 | 3.9 ± 2.4 |
| PD Gauss 3x[2] | 19.8 ± 0.2 | 19.8 ± 0.3 | 0.2 ± 0.1 | 1.0 ± 0.4 |
| PD Gauss 16x[3] | 19.8 ± 0.2 | 20.2 ± 0.2 | 0.4 ± 0.1 | 2.2 ± 0.3 |
| PD Gauss 3x (realigned)[4] | 19.8 ± 0.2 | 19.7 ± 0.2 | 0.2 + 0.1 | 0.9 ± 0.6 |
| T2 native[5] | 19.8 ± 0.2 | 20.0 ± 0.3 | 0.6 ± 0.3 | 2.8 ± 1.3 |
| T2 Gauss 3x[6] | 19.8 ± 0.2 | 19.8 ± 0.2 | 0.1 ± 0.0 | 0.5 ± 0.1 |
| T2 Gauss 16x[7] | 19.8 ± 0.2 | 20.3 ± 0.1 | 0.6 ± 0.1 | 2.7 ± 0.5 |
| T2 Gauss 3x (realigned)[8] | 19.8 ± 0.2 | 19.8 ± 0.2 | 0.1 ± 0.1 | 0.7 ± 0.2 |

N = 3 for each processing condition. Three replicate volume measurements were made.
Volumes are reported as means and standard deviations.

[1] Segmentation was completed using native (no Amira processing) PD-weighted images.

[2] A gauss filter (sigma=10; kernel=21) was applied to the PD native images three successive times. The results of the filter were then subtracted from the native PD images to acquire a new image set.

[3] A gauss filter (sigma=10; kernel=21) was applied to the PD native images sixteen successive times. The results of the filter were then subtracted from the native PD images to acquire a new image set.

[4] A gauss filter (sigma=10; kernel=21) was applied to the PD native images three successive times. The results of the filter were then subtracted from the native PD images to acquire a new image set. These images were then rotated 3° around the global y-axis.

[5] Segmentation was completed using native (no Amira processing) T2-weighted images.

[6] A gauss filter (sigma=10; kernel=21) was applied to the T2 native images three successive times. The results of the filter were then subtracted from the native T2 images to acquire a new image set.

[7] A gauss filter (sigma=10; kernel=21) was applied to the T2 native images sixteen successive times. The results of the filter were then subtracted from the native T2 images to acquire a new image set.

[8] A gauss filter (sigma=10; kernel=21) was applied to the T2 native images three successive times. The filter was then subtracted from the native T2 images to acquire a new image set. These images were then rotated 3° around the global y-axis.

Table 3. Comparisons of Expected and Segmented Volumes of Brain Tissue.

| | Total Slice | | | | White matter | | | | Grey matter | | | |
|---|---|---|---|---|---|---|---|---|---|---|---|---|
| | Expected Volume (mL) | Segmented Volume (mL) | RMSE | % error | Expected Volume (mL) | Segmented Volume (mL) | RMSE | % error | Expected Volume (mL) | Segmented Volume (mL) | RMSE | % error |
| Cerebellum slice 1: | | | | | | | | | | | | |
| PD native [1] | 7.0 | 7.7 ± 0.3 | 0.8 | 10.3 ± 4.3 | 3.0 | 2.9 ± 0.3 | 0.3 | 8.3 ± 4.7 | 4.0 | 4.6 ± 0.5 | 0.7 | 15.3 ± 11.6 |
| PD filtered & realigned [2] | 7.0 | 7.2 ± 0.3 | 0.3 | 3.3 ± 4.6 | 3.0 | 3.0 ± 0.2 | 0.2 | 5.5 ± 2.3 | 4.0 | 4.0 ± 0.3 | 0.2 | 5.2 ± 2.5 |
| Cerebellum slice 2: | | | | | | | | | | | | |
| PD native [1] | 2.5 | 2.5 ± 0.2 | 0.1 | 4.6 ± 3.5 | 1.5 | 1.4 ± 0.1 | 0.1 | 7.7 ± 3.5 | 1.0 | 1.0 ± 0.0 | 0.0 | 2.0 ± 1.6 |
| PD filtered & realigned [2] | 2.5 | 2.6 ± 0.1 | 0.1 | 4.5 ± 3.7 | 1.5 | 1.4 ± 0.0 | 0.1 | 6.8 ± 2.0 | 1.0 | 1.1 ± 0.0 | 0.1 | 8.5 ± 3.0 |

Volumes are reported as means and standard deviations.

[1] Segmentation was completed using native (no Amira processing) PD-weighted images.

[2] A gauss filter (sigma=10; kernel=21) was applied to the PD native images ten successive times. The results of the filter were then subtracted from the native PD images to acquire a new image set. These images were then rotated 2° around the global y-axis.

Table 4. A Comparison of Manual Segmentation Volumes and Threshold Segmentation Volumes of White Matter, Grey Matter, and Cerebrospinal Fluid from Native Proton Density (PD) and Processed PD Images.

| | White Matter | | | | Grey matter | | | | Cerebrospinal fluid | | | |
|---|---|---|---|---|---|---|---|---|---|---|---|---|
| | Manual Volume (mL) | Threshold Volume (mL) | RMSE | % error | Manual Volume (mL) | Threshold Volume (mL) | RMSE | % error | Manual Volume (mL) | Threshold Volume (mL) | RMSE | % error |
| CCSN05-040-La (section 35): | | | | | | | | | | | | |
| PD native [1] | 14.58 + 0.37 | 12.21 + 0.86 | 2.43 | 16.31 + 4.51 | 18.43 + 0.37 | 22.01 + 3.74 | 4.60 | 19.32 + 18.87 | 0.47 + 0.00 | 0.92 + 0.00 | 0.45 | 95.62 + 0.23 |
| PD filtered [2] | 14.58 + 0.37 | 15.84 + 0.97 | 1.67 | 9.83 + 7.54 | 18.43 + 0.37 | 17.12 + 1.01 | 1.72 | 7.85 + 5.99 | 0.47 + 0.00 | 0.60 + 0.00 | 0.14 | 29.16 + 0.28 |
| CCSN05-037-La (section 33): | | | | | | | | | | | | |
| PD native [1] | 12.52 + 0.06 | 11.62 + 2.74 | 2.38 | 16.89 + 10.73 | 19.73 + 0.03 | 20.66 + 2.84 | 2.49 | 11.32 + 7.00 | 0.71 + 0.02 | 0.80 + 0.00 | 0.10 | 13.16 + 4.49 |
| PD filtered [2] | 12.52 + 0.06 | 13.17 + 1.55 | 1.64 | 8.02 + 10.44 | 19.73 + 0.03 | 18.78 + 1.32 | 1.45 | 4.97 + 6.63 | 0.71 + 0.02 | 1.00 + 0.30 | 0.39 | 48.08 + 33.31 |
| CCSN05-231-La (section 30): | | | | | | | | | | | | |
| PD native [1] | 10.45 + 0.03 | 9.34 + 4.47 | 3.81 | 36.27 + 5.46 | 13.39 + 0.03 | 14.54 + 4.59 | 3.92 | 29.00 + 4.61 | 0.27 + 0.00 | 0.17 + 0.00 | 0.10 | 36.34 + 0.37 |
| PD filtered [2] | 10.45 + 0.03 | 10.35 + 0.41 | 0.33 | 2.51 + 2.35 | 13.39 + 0.03 | 13.00 + 0.45 | 0.52 | 3.41 + 2.31 | 0.27 + 0.00 | 0.56 + 0.01 | 0.29 | 107.10 + 2.24 |

Volumes are reported as means and standard deviations.

[1] Segmentation was completed using native (no Amira processing) PD-weighted images.

[2] A gauss filter (sigma=10; kernel=21) was applied to the PD native images three successive times. The results of the filter were then subtracted from the native PD images to acquire a new image set.

Table 5. Brain and Cerebellum Volume Data of Atlantic White-sided Dolphins.

| FIELD ID: | Sex | Length (cm) | Age Class | Brain Weight (g) | Brain Volume ($cm^3$)[1] | Virtual Brain weight (g)[2] | | Brain ($cm^3$)[3] | | | | Cerebellum ($cm^3$)[4] | | | |
|---|---|---|---|---|---|---|---|---|---|---|---|---|---|---|---|
| | | | | | | | | CSF | WM | GM | WM:GM | WM | GM | WM:GM | % of Brain[5] |
| CCSN05-037-La | f | 206 | adult | 1292.2 | 1253.9 | 1299.0 | mean | 67.8 | 467.0 | 718.6 | 0.7 | 53.2 | 113.7 | 0.5 | 14.1 |
| | | | | | | | stdev | 12.9 | 64.1 | 53.2 | 0.1 | 3.4 | 2.0 | 0.0 | 0.0 |
| CCSN05-039-La | f | 211 | pregnant adult | 1329.7 | 1293.6 | 1340.2 | mean | NA | NA | NA | NA | NA | NA | NA | NA |
| | | | | | | | stdev | NA | NA | NA | NA | NA | NA | NA | NA |
| CCSN05-040-La | f | 204 | pregnant adult | 1305.3 | 1255.2 | 1300.3 | mean | 105.0 | 475.8 | 673.3 | 0.7 | 61.7 | 110.4 | 0.6 | 15.0 |
| | | | | | | | stdev | 9.8 | 34.0 | 41.7 | 0.1 | 3.7 | 8.8 | 0.1 | 0.6 |
| CCSN05-231-La | f | 137 | neonate | 839.0 | 821.2 | 850.8 | mean | 29.5 | 296.6 | 494.8 | 0.6 | 33.5 | 75.5 | 0.4 | 13.8 |
| | | | | | | | stdev | 4.6 | 30.4 | 26.2 | 0.1 | 2.0 | 4.7 | 0.1 | 0.4 |
| CCSN04-195-La | m | 192 | subadult | 1460.3 | 1439.9 | 1491.8 | mean | NA | NA | NA | NA | NA | NA | NA | NA |
| | | | | | | | stdev | NA | NA | NA | NA | NA | NA | NA | NA |
| CCSN05-039-Fetus-La | m | 211 | fetus | 65.4 | 63.0 | 65.2 | mean | 3.7 | 11.3 | 48.2 | 0.2 | 0.6 | 3.8 | 0.2 | 7.5 |
| | | | | | | | stdev | 0.5 | 2.1 | 1.6 | 0.1 | 0.1 | 0.0 | 0.0 | 0.0 |
| CCSN05-040-Fetus-La | m | 54 | fetus | 131.9 | 127.9 | 132.5 | mean | 7.7 | 32.4 | 86.0 | 0.4 | 3.4 | 6.6 | 0.5 | 8.4 |
| | | | | | | | stdev | 5.4 | 7.6 | 4.7 | 0.1 | 0.2 | 0.3 | 0.0 | 0.4 |
| CCSN05-084-La | m | 156 | subadult | 1057.8 | 1019.4 | 1056.1 | mean | 44.8 | 413.2 | 561.3 | 0.7 | 37.2 | 103.8 | 0.4 | 14.5 |
| | | | | | | | stdev | 7.8 | 38.5 | 31.8 | 0.1 | 3.6 | 4.6 | 0.0 | 0.2 |

[1] Segmentation was completed from filtered and realigned PD weighted images.

[2] Virtual brain weight was calculated by multiplying the brain volume by the specific gravity of brain tissue or 1.036 $g/cm^3$ (Stephan et al., 1981).

[3] Segmentation of brain into cerebrospinal fluid (CSF), white matter (WM), and grey matter (GM) was completed from filtered and realigned T2 weighted images for fetuses and filtered and realigned PD weighted images for neonates, subadults, and adults.

[4] Segmentation of cerebellum into WM and GM was completed from filtered and realigned T2 weighted images for fetuses and filtered and realigned PD weighted images for neonates, subadults, and adults.

[5] Percentage of total brain occupied by the cerebellum = WM plus GM volumes of cerebellum divided by the WM plus GM volumes of the whole brain multiplied by 100% For neonate, subadults, and adults, volumes from processed PD-weighted images were used. For fetuses, volumes from processed T2-weighted images were used.

NA = data not available

Table 6. Corpus Callosum Area and Hippocampus Volume Measurements of Atlantic White-sided Dolphins.

| FIELD ID: | Sex | Length (cm) | Age Class | | Corpus Callosum Area ($mm^2$) [1] | | | Left Hippocampus ($mm^3$) [2] | | | | | |
|---|---|---|---|---|---|---|---|---|---|---|---|---|---|
| | | | | | Native | Processed | CCA / BW [3] | Hippocampus | % of Brain [4] | Inf. Horn | Hippo. Fluid | Parahippo. sulcus | Subarach. |
| CCSN05-037-La | f | 206 | adult | mean | NA | NA | NA | 868.3 | 0.073 | 133.6 | 197.5 | 345.1 | 695.5 |
| | | | | stdev | NA | NA | NA | 112.5 | 0.010 | 14.1 | 19.6 | 102.3 | 59.1 |
| CCSN05-039-La | f | 211 | pregnant adult | mean | 156.1 | 153.8 | 0.117 | 927.5 | NA | 104.3 | 79.1 | 230.3 | 315.2 |
| | | | | stdev | 11.4 | 7.8 | 0.009 | 135.8 | NA | 2.0 | 0.0 | 19.8 | 43.4 |
| CCSN05-040-La | f | 204 | pregnant adult | mean | 178.4 | 185.7 | 0.137 | 1043.5 | 0.091 | 263.1 | 69.1 | 486.3 | 605.3 |
| | | | | stdev | 0.9 | 9.7 | 0.001 | 112.3 | 0.010 | 28.0 | 16.2 | 10.1 | 11.2 |
| CCSN05-231-La | f | 137 | neonate | mean | 114.0 | 100.5 | 0.136 | 544.3 | 0.069 | 150.6 | 99.6 | 147.7 | 434.2 |
| | | | | stdev | 1.0 | 6.2 | 0.001 | 24.9 | 0.003 | 2.0 | 1.0 | 0.0 | 0.0 |
| CCSN04-195-La | m | 192 | subadult | mean | 129.1 | 130.9 | 0.088 | 752.0 | NA | 310.0 | 88.2 | 157.2 | 789.8 |
| | | | | stdev | 1.4 | 1.6 | 0.001 | 21.9 | NA | 5.1 | 2.6 | 2.6 | 13.5 |
| CCSN05-039-Fetus-La | m | 211 | fetus | mean | NA | NA | NA | NA | NA | NA | NA | NA | NA |
| | | | | stdev | NA | NA | NA | NA | NA | NA | NA | NA | NA |
| CCSN05-040-Fetus-La | m | 54 | fetus | mean | NA | NA | NA | NA | NA | NA | NA | NA | NA |
| | | | | stdev | NA | NA | NA | NA | NA | NA | NA | NA | NA |
| CCSN05-084-La | m | 156 | subadult | mean | 131.0 | 132.1 | 0.124 | 924.0 | 0.095 | 173.4 | 59.2 | 311.1 | 604.1 |
| | | | | stdev | 7.6 | 5.9 | 0.007 | 133.7 | 0.014 | 30.3 | 1.0 | 49.5 | 54.3 |

[1] Manual segmentation of corpus callosum was completed from native PD images and filtered-realigned PD images.

[2] Manual segmentation of hippocampus and surrounding structures was completed on native T2 images.

[3] CCA / BW = midsagittal area of the corpus callosum from native PD-weighted images divided by the brain weight (g).

[4] Percentage of total brain occupied by the left or right hippocampus = left or right hippocampus volume (from native T2 weighted images) divided by the WM plus GM volumes of the whole brain (from processed PD weighted images) multiplied by 100%.

NA = data not available

Inf. Horn = cerebrospinal fluid (CSF) of the inferior horn of the lateral ventricle abutting the hippocampus.

Hippo. Fluid = fluid in the hippocampus.

Parahippo. Sulcus = CSF of the parahippocampal sulcus ventral to the hippocampus.

Subarach. = CSF of the subarachnoid space medial to the hippocampus including the transverse fissure of Bichat.

Table 6. (*Continued*)

| Right Hippocampus ($mm^3$) [2] | | | | | |
|---|---|---|---|---|---|
| Hippocampus | % of Brain[4] | Inf. Horn | Hippo. Fluid | Parahippo. sulcus | Subarach. |
| | | | | | |
| 736.5 | 0.062 | 98.4 | 123.6 | 267.2 | 425.4 |
| 109.0 | 0.010 | 6.3 | 14.3 | 81.5 | 48.7 |
| | | | | | |
| 745.8 | NA | 107.2 | 49.2 | 222.6 | 545.5 |
| 119.6 | NA | 0.0 | 16.8 | 48.5 | 64.6 |
| | | | | | |
| 861.3 | 0.075 | 160.0 | 75.6 | 294.1 | 530.3 |
| 173.6 | 0.015 | 4.7 | 30.4 | 74.1 | 29.4 |
| | | | | | |
| 462.3 | 0.058 | 135.3 | 87.3 | 284.8 | 536.1 |
| 24.4 | 0.003 | 0.0 | 1.0 | 0.0 | 9.1 |
| | | | | | |
| 887.7 | NA | 199.5 | 135.7 | 218.8 | 1114.6 |
| 4.4 | NA | 12.8 | 3.9 | 2.6 | 7.7 |
| | | | | | |
| NA | NA | NA | NA | NA | NA |
| NA | NA | NA | NA | NA | NA |
| | | | | | |
| NA | NA | NA | NA | NA | NA |
| NA | NA | NA | NA | NA | NA |
| | | | | | |
| 967.9 | 0.099 | 193.9 | 64.5 | 427.7 | 719.5 |
| 68.0 | 0.007 | 19.8 | 3.7 | 42.2 | 43.7 |

# CHAPTER V:
# CONCLUSIONS AND FUTURE DIRECTIONS

Cetacean blubber is the primary site for lipid storage and persistent organic pollutants (POPs). During periods of lipid mobilization such as lactation, POPs from the blubber are mobilized into the circulatory system. The maternal transfer of these chemicals and their metabolites may interfere with neurodevelopment of offspring. In the research described in this thesis, I used three approaches to investigate and develop methods to determine how POPs might affect neurodevelopment of cetaceans (Figure 1). In Chapter 2, I identified factors (i.e water temperature, ontogeny, and reproductive state) that influenced the blubber morphology and blubber dynamics in the bottlenose dolphin (Figure 1). These data contributed to the overall objective of the thesis by identifying factors that are involved in lipid mobilization (and hence chemical mobilization) from blubber adipocytes. In Chapter 3, I integrated the blubber morphology data acquired in Chapter 2 to better understand CYP1A1 expression in the blubber biopsy of bottlenose dolphins, its relationship to concentration of AHR agonists in blubber and blood, and its involvement in the production of OH-PCBs (Figure 1). In Chapter 4, I established an approach that accurately obtained the size of brain structures from *in situ* MR imaging of stranded, dead Atlantic white-sided dolphins. This technique, coupled with chemical analysis of brain regions, can be used to determine if thyroid hormone disrupting chemicals (THDCs) are associated with changes in the size of brain structures during ontogeny (Figure 1).

***Blubber Morphology and Chemical Mobilization***

Reproductive state affected the blubber morphology in bottlenose dolphins (Chapter 2). Throughout the blubber, adipocyte area was larger in pregnant females than in simultaneously pregnant & lactating dolphins. The smaller adipocyte size of simultaneously pregnant & lactating dolphins suggests that the combination of pregnancy and lactation increased the energetic demands, and blubber lipids were used as energy currency. Adipocytes in the deep blubber layer were significantly smaller in lactating and simultaneously pregnant & lactating animals compared to pregnant dolphins, further supporting the hypothesis that the deep blubber is more dynamic during periods of

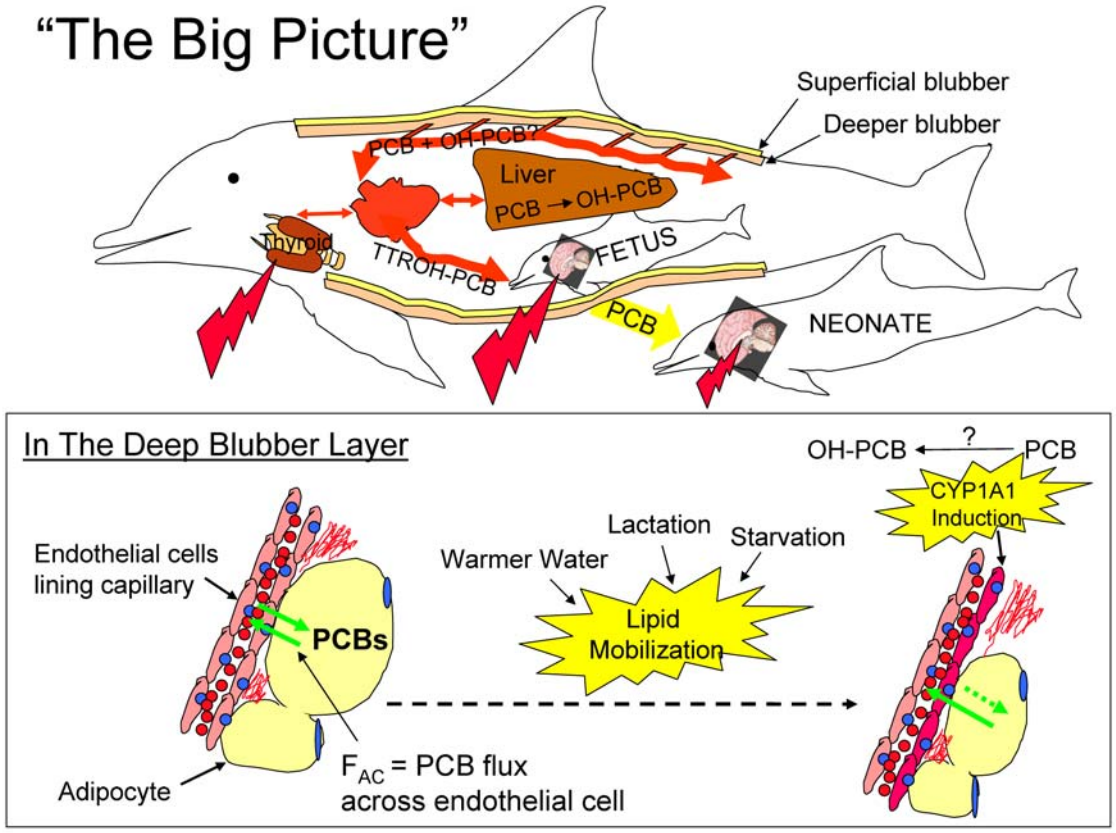


**Figure 1. An integration of major findings of this thesis and working hypotheses.** Warmer water, lactation, and starvation are important factors in lipid mobilization from adipocytes in the deep layer. PCBs, including congeners that are AHR agonists, move out of adipocytes during lipid mobilization events following the lipid gradient. The increased flux of these PCB congeners across the endothelial cells and into the circulatory system induces CYP1A1 in vascular endothelial cells in the deep layer. The induction of CYP1A1 in the blubber and liver may enhance the biotransformation of PCBs to OH-PCBs. Both the parent compounds and biotransformed metabolites may then interfere with neurodevelopment of the fetus in two ways. First, these chemicals may alter the thyroid hormone supply of the mother causing cretinism in the fetus (since in most mammals, the fetal thyroid gland is not fully developed and the fetus depends on the thyroid hormone supply of the mother). Second, the transfer of OH-PCBs from the mother to the fetus by transthyretin may affect the thyroid hormone supply of the fetus also causing cretinism; alternatively or additionally OH-PCBs may directly interfere with fetal neurodevelopment. Additional toxicity can occur later during neonatal development when PCBs are transferred from the mother to the calf through milk.

energetic stress. Total blubber lipid content and adipocyte size in the deep blubber of mothers with calves linearly decreased with calf length, since larger calves are presumed to require more milk than smaller calves. This provided evidence that the energetic

demands of lactation cause mobilization of lipids that affect blubber morphology in bottlenose dolphins similar to the effects of starvation in harbor porpoises (Koopman et al., 2002).

Findings in Chapter 2 reinforce previous findings on the maternal transfer of persistent organic pollutants during gestation and nursing but also offer some new insights. In many marine mammal species, there is a strong correlation between increasing blubber residue levels of persistent organic pollutants (POPs) and age, until animals reach sexual maturity (Borrell et al., 1995; Cockcroft et al., 1989; Ross et al., 2000; Wells et al., 2005). From this time onward, females experience a pronounced decrease in contaminant burdens in the blubber, while males continue to accumulate POPs throughout their lives. This reduction in contaminant burdens in sexually mature females has been best explained by the transfer of these burdens from the maternal blubber to offspring during lactation, with minimal transfer during gestation. The extensive lipid loss and decrease in adipocyte size in the deep blubber of mothers with larger calves, as noted in Chapter 2, explains the extensive transfer of POPs during lactation. Furthermore, pregnant females contained large adipocyte cross-sectional areas in all three blubber layers, which supports minimal transfer of POPs to the fetus. A key finding was the dramatic lipid loss (as indicated by the smaller adipocyte size of the blubber) in simultaneously pregnant & lactating females. It is possible that pregnant females that are lactating may transfer more PCBs to their fetus than pregnant females that are not lactating because more lipids (and hence POPs) are mobilized from the blubber in simultaneously pregnant & lactating females.

Charleston dolphins contained higher total blubber lipids than Indian River Lagoon dolphins, and this difference was reflected in larger adipocytes of the middle blubber layer in CHS animals, possibly reflecting the colder mean yearly water temperatures in South Carolina versus Florida waters. It has been shown that bottlenose dolphins in Sarasota, Florida drastically thin their blubber during summer months, when estuarine water temperatures can reach approximately 90$^{o}$F (R. Wells, unpublished data with permission). In these dolphins, total circulating PCB levels were much higher in summer than in winter (R. Wells, unpublished data with permission). As dolphins adapt to warmer water temperatures, the loss of lipid from the adipocytes in the middle blubber

layer may mobilize POPs from the blubber into the circulatory system. Simultaneously pregnant & lactating females, exposed to warmer water temperatures in the summer months, may experience greater mobilization and transfer of environmental chemicals from their blubber to their fetus and calf.

***Implications of CYP1A1 Induction***

Chapter 3 measured the induction of CYP1A1 in endothelial cells of the blubber layers. AHR agonists can also cause systemic high-level expression of CYP1A1 in hepatocytes, endothelial cells in the lung, and both endothelium and transitional epithelium forming the bladder mucosa, as observed in beluga whales from the Arctic and St. Lawrence estuary (Wilson et al., 2005). In humans, CYP1A has been shown to activate potential bladder carcinogens (Gonzalez and Gelboin, 1994). CYP1A expression in primary transitional cell tumors of the urinary bladder has been correlated with tumor severity (Murray et al., 1995). Furthermore, in mice, the induction of CYP1A1 in endothelial cells can cause vascular endothelial cell dysfunction and an inflammatory response, through an oxidative stress mechanism (Hennig et al., 2002). This disease pathway may lead to the development of artherosclerosis (Hennig et al., 2001) and/or damage to the blood-brain barrier that can allow further secondary damage to the CNS (Filbrandt et al., 2004).

In this thesis, I speculate that CYP1A1 could be responsible for the production of some identified OH-PCB congeners in bottlenose dolphins. OH-PCBs have been shown to bind to transthyretin (TTR) and the thyroid hormone receptor alpha in human *in vitro* assays and have been shown to affect fetal and maternal thyroid hormone homeostasis in the rat (Arulmozhiraja et al., 2005; Cheek et al., 1999; Meerts et al., 2002). In fact, pregnant rats exposed to 4-HO-CB107 have been shown to maternally transfer this metabolite (via TTR) to the fetal cerebellum (Meerts et al., 2002). Moreover, pigeons exposed to Aroclor 1254 and a starvation / re-feeding cycle appeared to accumulate PCB metabolites in the brain, particularly during the re-feeding stage (Barradas et al., 2001). Cetaceans that undergo cycles of lipid mobilization and deposition may be particularly sensitive to the accumulation of PCB metabolites in the brain. Currently, the bioaccumulation of OH-PCBs in brain regions of cetaceans is unknown. (See Appendix 7

for preliminary analysis of cerebellum grey matter samples in Atlantic white-sided dolphins).

Thyroid hormones are essential for skeletal growth, development of the brain and inner ear, immune system function, maintenance of metabolic rate, fat metabolism, and sexual function (Guyton and Hall, 1996; O'Malley et al., 1995; Segal and Ingbar, 1982). OH-PCBs have been shown to negatively impact some of these processes. For example, in mouse cerebellar culture assays, OH-PCBs have been shown to inhibit thyroid-hormone-dependent extension of cerebellar Purkinje cell dendrites (Kimura-Kuroda et al., 2005). In rats, OH-PCBs and parent PCB congeners have been shown to cause both locomotor and auditory deficits through a thyroid hormone dependent mechanism (Goldey and Crofton, 1998; Meerts et al., 2004). Considering the importance of echolocation and the auditory sensory modality to cetaceans, future research should explore the potential impact of CYP1A1 derived OH-PCBs and their parent PCB congeners on hearing in cetaceans.

Bottlenose dolphins from the SE United States could be particularly sensitive to these health effects. Late term pregnancy, parturition, and early nursing often coincide with seasonal warming and blubber thinning (R. Wells, unpublished data). In fact, in the dolphins studied in Chapters 2 and 3, 10 of the 14 adult female dolphins captured and released during the summer months were pregnant and/or lactating. These additive lipid mobilization events may transport a larger burden of AHR agonists from the deep blubber into the circulatory system, inducing endothelial and hepatic CYP1A1. CYP1A1 could then mediate PCB metabolism and OH-PCB production. In addition, PCB congeners that are not metabolized by CYP1A1 could be mobilized and metabolized by other CYPs. These bio-activated products may then interfere with the development of the brain and inner ear of the fetus / calf via a thyroid hormone dependent mechanism. First-born calves may be most sensitive to this toxic mechanism because of the substantial body burden accumulated by nulliparous females (Wells et al., 2005).

### *Developmental Timing of the Brain and Exposure to THDCs*

Based on the dramatic transfer of parent PCB congeners that occurs during nursing as opposed to gestation, brain regions that develop post-natally could be more

sensitive to developmental defects caused by PCBs of their metabolites. In Chapter 4, myelination patterns of the Atlantic white-sided dolphin during ontogeny indicated that white matter tracts were still developing post-natally throughout the brain. White matter tract development of the hindbrain, cerebellum, and auditory pathways were more advanced than the telencephalon early during ontogeny. Considering that the bulk of PCB exposure occurs during nursing, the white matter tracts of the hindbrain, cerebellum, and auditory pathways may be more resistant to myelination defects because of their advanced growth early in development. However, if OH-PCBs are transferred from the mother to the fetus or if the mother experiences severe hypothyroidism, congenital defects of these brain structures could occur. More research is needed on developmental timing of brain regions for delphinid cetaceans.

## FUTURE DIRECTIONS

### *Biomarker Assessment in Skin-blubber Biopsies*

The importance of measuring depth-specific CYP1A1 expression became apparent when comparing CYP1A1 levels between geographic locations. The average CYP1A1 staining score of the total blubber was not significantly different between CHS and IRL dolphins; however, CHS animals had significantly higher CYP1A1 levels in the deep blubber (Chapter 3). Examining CYP1A1 expression by layer revealed differences not observed with average values. These findings reinforce the necessity of carefully interpreting the results of cetacean biomarker studies in which skin-blubber biopsies do not contain full-depth samples or at least a portion of the deep layer. Projectile biopsy techniques often do not acquire a representative sample of the deep blubber, particularly for cetaceans with thick blubber (i.e. killer whales, sperm whales, and mysticetes). Biomarker results using this sampling technique should be viewed with caution. Furthermore, other biomarkers in skin-blubber biopsies (such as Type 2 Iodothyronine Deiodinase or D2; see below) could behave as CYP1A1 and should be analyzed in a similar manner, as presented in Chapter 3 (i.e. depth-specific expression).

A limitation in relating lipid dynamics to CYP1A1 induction is the inability to determine whether the adipocyte is in a state of deposition or mobilization. Unfortunately, the molecular signaling pathways involved in lipid dynamics of the

blubber of marine mammals are presently unknown. It is important to identify cetacean homologs of receptors (e.g. thyroid hormone and adrenergic receptors) (Liu et al., 2003), membrane proteins (e.g. perilipin) (Moore et al., 2005), and enzymes (e.g. hormone-sensitive lipase, adipose triglyceride lipase, and type 2 deiodinase)(Watanabe et al., 2006; Zimmermann et al., 2004) that have been discovered to be important in lipid storage and utilization in humans and rats. A variety of molecular approaches could be used to identify and characterize these candidate genes and proteins. This would not only add to a better interpretation of CYP1A1 expression and the mobilization of environmental chemicals in marine mammals but would also provide valuable information on the molecular control of blubber dynamics.

***The Role of Cytochrome P450 Enzymes in Production of OH-PCBs***

CYP2B and other CYP enzymes were not measured in the dolphins studied in Chapter 3. However, blubber biopsy sections were embedded in paraffin and an adjacent blubber slice was flash frozen for all dolphins studied in Chapters 2 and 3. CYP2B and other CYP enzymes could be measured in these samples at the mRNA, protein, and enzyme activity levels. These measurements are important because CYP enzymes may also contribute to the production of OH-PCBs. The positive relationship between CYP1A1 and some OH-PCB congeners may be a result of CYP1A1 covariance with other CYPs, such as CYP2B, CYP2A, and CYP3A type isoforms.

In delphinid cetaceans, it is also important to determine which OH-PCB metabolites are products of CYP1A1 metabolism. White et al. (2000) used a specific inhibitor of CYP2B to illustrate that CYP1A1 in beluga whale liver microsomes converted 3,3',4,4'-tetrachlorobiphenyl (PCB77) primarily to 4-OH-3,3',4,5'-tetrachlorobiphenyl (4'-OH-CB79 or 4'-OH-3,3',4,5'-tetrachlorobiphenyl) and 5-OH-3,3',4,4'-tetrachlrobiphenyl (5-OH-CB77). Performing similar biotransformation studies with bottlenose dolphin liver microsomes using a more comprehensive list of individual non-ortho, mono-ortho, and di-ortho PCB congeners would help elucidate which CYP enzymes are responsible for the formation of specific OH-PCB congeners that are environmentally relevant. Expanding this research to include biotransformation studies using endothelial cell lines derived from bottlenose dolphin blubber samples would help

determine the importance of extra-hepatic metabolism of non-ortho and mono-ortho PCBs, as well as the importance of extra-hepatic production of OH-PCBs (Garrick et al., 2006).

***Type 2 Iodothyronine Deiodinase (D2): A Biomarker of Effect for THDCs?***

D2 activates the prohormone thyroxine (T4) to form the active hormone T3 (reviewed in (Kohrle, 1999)). D2 is expressed in the brain, inner ear, severely hypothyroid anterior pituitary, placenta, skin, and brown adipose tissue in rodents (Bates et al., 1999; Campos-Barros et al., 2000; Kohrle, 1999; Schroder-van der Elst et al., 1998; Tu et al., 1997). D2 is especially important because of its apparent role in the development of the central nervous system and the cochlea (Bates et al., 1999; Campos-Barros et al., 2000), its essential role for adaptive thermogenesis in brown adipose tissue (de Jesus, 2001), and its reaction to hypothyroidism (Schroder-van der Elst et al., 1998). These observations have led to the theory that D2 produces T3 for local cellular demands independent of circulating T3 (Kohrle, 2000).

Such a role for D2 activity has been further supported in rats made mildly hypothyroidic by an antithyroid chemical PTU or PCBs (Crofton et al., 2000; Goldey and Crofton, 1998; Goldey et al., 1995; Herr et al., 1996). In fact, rats treated with dioxin show a dose-dependent decrease in circulating T4 and an increase in brown adipose tissue D2 activity (Viluksela et al., 2004). These studies provide some evidence that D2 could be used as a biomarker of effect for marine mammals exposed to thyroid hormone disrupting chemicals such as PCBs, PBDEs, and their hydroxylated metabolites. However, the structural and functional characteristics of D2 in marine mammals are currently unknown.

In this thesis, a 750-bp fragment of a D2 cDNA (as assessed by RT-PCR) was identified in a skin-blubber biopsy sample from a bottlenose dolphin live-captured and released during the CHS and IRL health assessments discussed in Chapters 2 and 3 (see Appendix 4). Future studies will obtain the complete D2 bottlenose dolphin sequence and measure the D2 mRNA levels in the skin-blubber biopsies previously analyzed in Chapters 2 and 3. The expression of D2 in individual animals will be compared to levels of relevant contaminants (PCBs, PBDEs, and their hydroxylated metabolites). The

relationship of D2 expression to other variables such as sex, geographic location, and circulating levels of THs will also be determined.

***Transthyretin: A Biomarker of Susceptibility for THDCs***

During vertebrate evolution, the capacity of the plasma to hold onto T4 increased in two ways (reviewed in Schreiber and Richardson, 1997). First, a multi-network system of thyroid hormone transport proteins evolved, which included albumin, TTR, and thyroxine binding globulin (TBG). Second, the affinity of TTR for thyroxine increased (Chang et al., 1999). The increased capacity of the plasma to bind T4 during vertebrate evolution may have been driven by the increase in relative sizes of lipid pools and the massive explosion of brain size (Chang et al., 1999; Schreiber and Richardson, 1997; Schreiber et al., 2001).

Toothed whales add an interesting twist regarding the evolution of thyroid hormone binding proteins. As odontocetes evolved from terrestrial vertebrates and adapted to an aquatic environment, they developed a large lipid pool (blubber) and underwent a dramatic increase in brain size (Marino, 2002). A large lipid pool and brain in odontocetes may have increased the selection pressure for increased capacity of the plasma to bind T4 in order to avoid permeation into blubber since T4 is lipophilic.

A characteristic of human and rat TTR is its ability to bind hydroxylated PCB metabolites and related compounds with higher affinity than the natural ligand, T4 (Brouwer et al., 1986; Cheek et al., 1999; Ghosh et al., 2000). How do marine mammals compare to rats and humans? Do we expect a difference in TTR ligand-binding characteristics? Currently, the structural and functional characteristics of TTR in marine mammals are not known. In fact, efforts to demonstrate TTR in belugas and bottlenose dolphins have proved unsuccessful using methodologies established for other mammals [8]. These unknowns limit our understanding of how POPs and halogenated phenolics interact with the thyroid hormone system.

In this thesis, a 280-bp fragment of a TTR cDNA (as assessed by RT-PCR) was identified in a liver sample from an Atlantic white-sided dolphin (see Appendix 5). Future studies will obtain the complete TTR sequence for the Atlantic white-sided dolphin. The cloned TTR can then be produced *in vitro* to study its ligand-binding

characteristics, including its affinity for T4, T3, selected PCB and PBDE congeners, and their hydroxylated metabolites (OH-PCBs and OH-PBDEs).

***Chemical Analysis of Brain Regions in Adult and Fetal Specimens***

For all specimens in which MRIs were performed, plasma, blubber, liver, and brain regions were collected for the analysis of PCBs, OH-PCBs, $MeSO_2$-PCBs, PBDEs, OH-PBDEs, DDTs and $MeSO_2$–DDEs, cyclodienes including dieldrin and chlordanes, toxaphenes, HCHs, hexachlorobenzene, and pentachlorophenol. These brain regions included cerebrospinal fluid (CSF), frontal cortex, corpus callosum, choroid plexus, hypothalamus, hippocampus, cerebellum grey matter, and cerebellum white matter. Chemical analyses of grey matter of the cerebellum were performed for specimens CCSN05-037-La, CCSN05-039-La, and CCSN05-040-La (see results in Appendix 3).

Chemical analyses of the fetal brains are a priority in the future. No information is known about the maternal transfer of halogenated phenolics in marine mammals during gestation or nursing. TTR is thought to be responsible for maternal to fetal transport of thyroxine (T4) across the placenta (Achen et al., 1992). The high binding affinity of xenobiotics such as OH-PCBs and other halogenated phenolics to TTR is hypothesized to result in facilitated transport of these compounds across the placenta to the fetus (Meerts et al., 2002). By performing chemical analyses of the fetal brains collected in the current study, we will answer important questions regarding the maternal transfer of halogenated phenolics (including OH-PCBs and OH-PBDEs) during gestation in delphinid cetaceans.

The chemical analysis of choroid plexus and CSF samples are also a priority for future studies. Since TTR is synthesized in the choroid plexus and is secreted into the CSF, it is possible that these tissues retain higher levels of OH-PCBs, OH-PBDEs, and other halogenated phenolics, specifically chemicals that have a high affinity for TTR. Recently, Takasuga et al. (2004) observed that the levels of OH-PCBs in human CSF were higher than the levels of PCBs, which was reversed in the serum.

***Relationships between the Size of Brain Structures and Environmental Chemicals***

The ability to determine the volumes of brain structures in delphinid cetaceans (and other marine vertebrates) from *in situ* MR imaging provides a powerful approach

that can be used specifically to study whether environmental chemicals (e.g. PCBs, PBDEs, and/or hydroxylated metabolites) affect the development of brain structures that depend on thyroid hormones for maturation. With a larger sample size, we can begin to test specific hypotheses about THDCs. These hypotheses focus on myelination of the telencephalon and corpus callosum during ontogeny, cerebellar growth, hippocampal development, and maturation of auditory pathways in delphinid cetaceans exposed to THDCs.

*Myelination*. Thyroid hormones (THs) control several aspects of white matter tract development (i.e. myelination), including the proliferation and survival of oligodendrocyte precursor cells (reviewed in Bernal, 2002) and the number of oligodendrocytes (Schoonover et al., 2004). Since PCBs interfere with thyroid function in animals and THs are important in white matter tract development, PCBs and chemicals with similar mechanisms of action may affect myelination. I hypothesize that neonates and subadults that contain high levels of THDCs will have less myelination. This hypothesis can be tested by determining the WM:GM volume ratios of the left and right hemispheres during ontogeny (see Chapter 4; Figure 35) and relating these measurements to the concentrations of THDCs in the brain. A small WM:GM volume ratio would indicate less myelination.

*Corpus Callosum Midsagittal Area.* Recently, Sharlin et al. (2006) observed that in fetal rats, exposure to Aroclor 1254 (a PCB mixture) decreases the cell density of the corpus callosum (a large white matter tract that bridges the two hemispheres) in a similar but not identical manner as hypothyroidism. Hence, I hypothesize that neonate and subadult dolphins that contain high levels of THDCs will have a smaller corpus callosum area than those individuals with lower concentrations of THDCs.

*Cerebellum Grey Matter.* In mouse cerebellar cultures, thyroid hormones are essential for the development of Purkinje cell dendrites (Kimura-Kuroda et al., 2002). Addition of T3 or T4 in culture resulted in dendritic arborization of Purkinje cells that was highly elaborate. The growth of dendrites was dependent on the concentration of T4 and was confirmed with the addition of amiodarone (i.e. an inhibitor of deiodinases *in vitro*), which impeded dendritic branching. Minimal dendritic growth occurred in the control cultures. The addition of OH-PCB congeners ( i.e. either 4-OH-2',3,3',4',5,5'-

hexachlorobiphenyl or 4-OH-2',3,3',4',5'-pentachlorobiphenyl) to cerebellar cultures disturbed the development of Purkinje cell dendrites (Kimura-Kuroda et al., 2005). The dendrites exhibited poor growth and the secondary branches shrunk, which significantly decreased the dendritic area of the Purkinje cells. Because the dendrites of the Purkinje cells comprise the bulk of the cerebellum grey matter and some THDCs impede the arborization of dendrites, I hypothesize that the grey matter volumes of the cerebellum of dolphins exposed to higher levels of THDCs during development would be smaller than those of animals with lower concentrations of THDCs.

*Hippocampus*. THs are also important in the development of the hippocampus (reviewed in Anderson, 2001). In rats, a deficiency of thyroid hormones during late brain development decreases the number of dentate gyrus granule cells in the hippocampal formation. In addition, the volume of the mossy fiber system is reduced in rats that are deprived of THs. Furthermore, hypothyroidism in rats causes stunted growth of the dendrites in CA3 pyramidal cells of the hippocampus and a corresponding decrease in volume of the CA3 layer. Thus, I hypothesize that the hippocampal volumes of dolphins exposed to higher levels of THDCs during development would be smaller than those of animals with lower concentrations of THDCs.

*Auditory Pathways*. Thyroid hormones are important in the development of hearing as indicated by congenital deafness observed in cretinism (i.e. hypothyroidism during fetal development). Hypothyroidism impedes the differentiation of the inner sulcus and the sensory epithelium (i.e hair cell development) and causes malformation of the tectorial membrane (i.e. it is enlarged) (reviewed by Forrest et al. (2002)). Furthermore, exposure of rat offspring to PCBs results in severe hearing loss (Goldey and Crofton, 1998). These deficits are accompanied by a drastic decrease in circulating T4, and the deficits are attenuated by T4 replacement therapy. Cochlear pathologies in these rats reveal outer hair cell losses very similar to pathologies that result from severe hypothyroidism (Crofton et al., 2000; Goldey, 1995a). It is possible that dolphins exposed to high levels of THDCs during ontogeny may experience hearing deficits.

Animal and human studies have shown that congenital deafness causes degenerative changes in the central auditory pathway of the brain (Emmorey et al., 2003; Nishiyama et al., 2000). These degenerative changes include reductions in cochlear

nucleus volume (cited in Nishiyama et al. (2000)) and soma areas of the inferior colliculus (Nishiyama et al., 2000). If PCBs were to cause hearing deficits in delphinid cetaceans, it is possible that auditory deprivation could result in degeneration of auditory pathways in the brain such as the auditory nerve, cochlear nucleus, trapezoid body, lateral lemniscus, and inferior colliculus. In Chapter 4, these structures were identified in the MR images of the Atlantic white-sided dolphin and could be segmented and their volumes determined. I hypothesize that the volumes of auditory structures of dolphins exposed to higher levels of THDCs during development would be smaller than those of animals with lower concentrations of THDCs.

A problem in addressing these hypotheses will be assessing exposure when exposure and effects are separated in time. Brain volume and THDC measurements of subadult or adult dolphins will reflect only recent exposure rather than the more toxicologically relevant exposure that occurred during brain development early in life. Reconstructing exposure during development will be important in addressing this biomedical problem. This may be accomplished by studying dolphin populations such as the one in Sarasota Bay, Florida, where researchers have studied the population for thirty-years.

*MR Imaging Protocols*. Future *in situ* MR imaging of stranded specimens should focus on increasing the resolution of images. Segmentation of brain structures and volume determination in fetal brains was not completed because of poor resolution of these images. Furthermore, the boundaries of the hippocampal formation were difficult but not impossible to ascertain. Increasing the resolution of images would increase the accuracy of segmented volumes of all brains (including the fetal brain structures and the hippocampal formation).

Resolution enhancement could be completed through a variety of approaches. In the current study, imaging was completed using 1.5 Tesla MRI scanners. Using MRI scanners with stronger magnets (i.e 3.0 T or 7.0 T MRI scanners) would greatly enhance resolution of the entire brain for all age class categories. For fetal scans, using imaging parameters discussed by Whitby et al. (2006) may enhance the resolution of MR images of post-mortem fetal specimens acquired using 1.5 T scanners. Increasing the resolution

of hippocampus images may be possible using 1.5 T scanners if the field of view is decreased and focusing the MRI on the hippocampus with thinner sliced sections.

In conclusion, this thesis investigated and developed methods to study how persistent organic pollutants might affect neurodevelopment in delphinid cetaceans. Because delphinid cetaceans live in a niche in the marine environment that is analogous to the human niche in the terrestrial environment, understanding the impacts of POPs on neurodevelopment in cetaceans can help to understand the potential effects of these chemicals on children's health. In addition, the fact that odontocetes bioaccumulate and biomagnify extremely high levels of persistent organic pollutants in their blubber and transfer a majority of this chemical burden to their first-born calf makes odontocetes an important animal model to study this biomedical problem (i.e. the effects of THDCs on neurodevelopment of first-borns). In addition, the dolphin brain is more similar to the human brain in overall and regional structure than the rat brain is to the human. Furthermore, the human and dolphin brain share similar developmental patterns of structures during ontogeny. For example, the early development of auditory pathways during gestation is shared by both dolphins and humans, quite unlike the post-natal development of hearing in rats. The techniques described in this thesis can be used to study the impacts of persistent organic pollutants on neurodevelopment in both humans and marine mammals.

## REFERENCES

Achen MG, Harms PJ, Thomas T, Richardson SJ, Wettenhall REH, Schreiber G. 1992. Protein synthesis at the blood-brain barrier. The major protein secreted by amphibian choroid plexus is a lipocalin. Journal of Biological Chemistry 267(32):23170-23174.

Anderson G. 2001. Thyroid hormones and the brain. Frontiers in Neuroendocrinology 22(1):1-17.

Arulmozhiraja S, Shiraishi F, Okumura T, Iida M, Takigami H, Edmonds JS, Morita M. 2005. Structural requirements for the interaction of 91 hydroxylated polychlorinated biphenyls with estrogen and thyroid hormone receptors. Toxicological Sciences 84:49-62.

Barradas PC, Vieira RS, De Freitas MS. 2001. Selective effect of hypothyroidism on expression of myelin markers during development. Journal of Neuroscience Research 66(2):254-261.

Bates JM, St Germain DL, Galton VA. 1999. Expression profiles of the three iodothyronine deiodinases, D1, D2, and D3, in the developing rat. Endocrinology 140(2):844-851.

Bernal J. 2002. Action of thyroid hormone in brain. Journal of Endocrinological Investigation 25(3):268-288.

Borrell A, Bloch D, Desportes G. 1995. Age trends and reproductive transfer of organochlorine compounds in long-finned pilot whales from the Faroe Islands. Environmental Pollution 88:283-292.

Brouwer A, van den Berg KJ, Blaner WS, Goodman DS. 1986. Transthyretin (prealbumin) binding of PCBs, a model for the mechanism of interference with vitamin A and thyroid hormone metabolism. Chemosphere 15(9-12):1699-1706.

Campos-Barros A, Amma LL, Faris JS, Shailam R, Kelley MW, Forrest D. 2000. Type 2 iodothyronine deiodinase expression in the cochlea before the onset of hearing. Proceedings of the National Academy of Sciences, USA 97(3):1287-1292.

Chang L, Munro SL, Richardson SJ, Schreiber G. 1999. Evolution of thyroid hormone binding by transthyretins in birds and mammals. European Journal of Biochemistry / FEBS 259(1-2):534-542.

Cheek AO, Kow K, Chen J, McLachlan JA. 1999. Potential mechanisms of thyroid disruption in humans: interaction of organochlorine compounds with thyroid receptor, transthyretin, and thyroid-binding globulin. Environmental Health Perspectives 107(4):273-278.

Cockcroft VG, De Kock AC, Lord DA, Ross GJB. 1989. Organochlorines in bottlenose dolphins (*Tursiops truncatus*) from the East coast of South Africa. South African Journal of Marine Science 8:207-217.

Crofton K, Ding D, Padich R, Taylor M, Henderson D. 2000. Hearing loss following exposure during development to polychlorinated biphenyls: a cochlear site of action. Hearing Research 144(1-2):196-204.

de Jesus LC, SD; Ribeiro, MO; Schneider, M; Kim, S-W; Harney, JW; Larsen, PR; Bianco, AC. 2001. The type 2 iodothyronine deiodinase is essential for adaptive thermogenesis in brown adipose tissue. The Journal of Clinical Investigation 108(9):1379-1385.

Emmorey K, Allen JS, Bruss J, Schenker N, Damasio H. 2003. A morphometric analysis of auditory brain regions in congenitally deaf adults. Proceedings of the National Academy of Sciences 100(17):10049-10054.

Filbrandt CR, Wu Z, Zlokovic B, Opanashuk L, Gasiewicz TA. 2004. Presence and functional activity of the aryl hydrocarbon receptor in isolated murine cerebral vascular endothelial cells and astrocytes. Neurotoxicology 25:605-616.

Forrest D, Reh TA, Ruesch A. 2002. Neurodevelopmental control by thyroid hormone receptors. Current Opinion in Neurobiology 12(1):49-56.

Garrick RA, Woodin BR, Wilson JY, Middlebrooks BL, Stegeman JJ. 2006. Cytochrome P4501A is induced in endothelial cell lines from the kidney and lung of the bottlenose dolphin, *Tursiops truncatus*. Aquatic Toxicology 76(3-4):295-305.

Ghosh M, Meerts IA, Cook A, Bergman A, Brouwer A, Johnson LN. 2000. Structure of human transthyretin complexed with bromophenols: a new mode of binding. Acta Crystallographica Section D, Biological Crystallography 56(Pt 9):1085-1095.

Goldey EK, LS; Lau,C; Rehnberg,GL; Crofton,KM. 1995a. Developmental exposure to polychlorinated biphenyls (Aroclor 1254) reduces circulating thyroid hormone concentrations and causes hearing deficits in rats. Toxicology and Applied Pharmacology 135(1):77-88.

Goldey ES, Crofton KM. 1998. Thyroxine replacement attenuates hypothyroxinemia, hearing loss, and motor deficits following developmental exposure to Aroclor 1254 in rats. Toxicological Sciences 45(1):94-105.

Goldey ES, Kehn LS, Rehnberg GL, Crofton KM. 1995. Effects of developmental hypothyroidism on auditory and motor function in the rat. Toxicology and Applied Pharmacology 135(1):67-76.

Gonzalez FJ, Gelboin HV. 1994. Role of human cytochromes P450 in the metabolic activation of chemical carcinogens and toxins. Drug Metabolism Review 26:165-183.

Guyton AC, Hall JE. 1996. The thyroid metabolic hormones. Textbook of Medical Physiology 9th Edition. Philadelphia, PA: W.B. Saunders Company. p 945-956.

Hennig B, Meerarani P, Slim R, Toborek M, Daugherty A, Silverstone AE, Robertson LW. 2002. Proinflammatory properties of coplanar PCBs: in vitro and in vivo evidence. Toxicology and Applied Pharmacology 181(3):174-183.

Hennig B, Slim R, Toborek M, Robertson LW. 2001. PCBs and cardiovascular disease: endothelial cells as a target for PCB toxicity. In: Robertson, Hansen, editors. PCBs: Recent Advances in Environmental Toxicity and Health Effects. Lexington, KY: Univ. Press of Kentucky. p 211-220.

Herr DW, Goldey ES, Crofton KM. 1996. Developmental exposure to Aroclor 1254 produces low-frequency alterations in adult rat brainstem auditory evoked responses. Fundamental and Applied Toxicology 33:129-128.

Kimura-Kuroda J, Nagata I, Kuroda Y. 2005. Hydroxylated metabolites of polychlorinated biphenyls inhibit thyroid-hormone-dependent extension of cerebellar purkinje cell dendrites. Developmental Brain Research 154:259-263.

Kimura-Kuroda J, Nagata I, Negishi-Kato M, Kuroda Y. 2002. Thyroid hormone-dependent development of mouse cerebellar Purkinje cells in vitro. Developmental Brain Research 137(1):55-65.

Kohrle J. 1999. Local activation and inactivation of thyroid hormones: the deiodinase family. Molecular and Cellular Endocrinology 151(1-2):103-119.

Kohrle J. 2000. The deiodinase family: selenoenzymes regulating thyroid hormone availability and action. Cellular and Molecular Life Sciences 57(13-14):1853-1863.

Koopman HN, Pabst DA, McLellan WA, Dillaman RM, Read AJ. 2002. Changes in blubber distribution and morphology associated with starvation in the harbour porpoise (*Phocoena phocoena*): evidence for regional differences in blubber structure and function. Physiological and Biological Zoology 75(5):498-512.

Liu Y, Schultz JJ, Brent GA. 2003. A thyroid hormone receptor alpha gene mutation (P398H) is associated with visceral adiposity and impaired catecholamine-stimulated lipolysis in mice. The Journal of Biological Chemistry 278(40):38913-38920.

Marino L. 2002. Brain Size Evolution. In: Perrin WF, Wursig B, Thewissen JGM, editors. Encyclopedia of Marine Mammals. San Diego, San Francisco, New York, Boston, London, Sydney, Tokyo: Academic Press. p 158-162.

Meerts IA, Assink Y, Cenijn PH, Van Den Berg JH, Weijers BM, Bergman A, Koeman JH, Brouwer A. 2002. Placental transfer of a hydroxylated polychlorinated biphenyl and effects on fetal and maternal thyroid hormone homeostasis in the rat. Toxicological Sciences 68(2):361-371.

Meerts IA, Lilienthal H, Hoving S, van den Berg JHJ, Weijers BM, Bergman A, Koeman JH, Brouwer A. 2004. Developmental exposure to 4-hydroxy-2,3,3',4',5-pentachlorobiphenyl (4-OH-CB107): long-term effects on brain development, behavior, and brain stem auditory evoked potentials in rats. Toxicological Sciences 82(1):207-218.

Moore HH, Silver RB, Mottillo EP, Bernlohr DA, Granneman JG. 2005. Perilipin targets a novel pool of lipid droplets for lipolytic attack by hormone-sensitive lipase. The Journal of Biological Chemistry 280(52):43109-43120.

Murray GI, Taylor VE, McKay JA, Weaver RJ, Ewen SW, Melvin WT, al. e. 1995. Expression of xenobiotic metabolizing enzymes in tumours of the urinary bladder. International Journal of Experimental Pathology 76:271-276.

Nishiyama N, Hardie NA, Shepherd RK. 2000. Neonatal sensorineural hearing loss affects neurone size in cat auditory midbrain. Hearing Research (140):18-22.

O'Malley BW, Jr., Li D, Turner DS. 1995. Hearing loss and cochlear abnormalities in the congenital hypothyroid (hyt/hyt) mouse. Hearing Research 88(95):181-189.

Ross PS, Ellis GM, Ikonomou MG, Barrett-Lennard LG, Addison RF. 2000. High PCB concentrations in free-ranging Pacific killer whales, *Orcinus orca*: effects of age, sex and dietary preference. Marine Pollution Bulletin 40(6):504-515.

Schoonover CM, Seibel MM, Jolson DM, Stack MJ, Rahman RJ, Jones SA, Mariash CN, Anderson GW. 2004. Thyroid hormone regulates oligodendrocyte accumulation in developing rat brain white matter tracts. Endocrinology 145(11):5013-5020.

Schreiber G, Richardson SJ. 1997. The evolution of gene expression, structure, and function of transthyretin. Comparative Biochemistry and Physiology, B 116(2):137-160.

Schreiber G, Richardson SJ, Prapunpoj P. 2001. Structure and expression of the transthyretin gene in the choroid plexus: a model for the study of the mechanism of evolution. Microscopy Research and Technique 52(1):21-30.

Schroder-van der Elst JP, van der Heide D, Morreale de Escobar G, Obregon MJ. 1998. Iodothyronine deiodinase activities in fetal rat tissues at several levels of iodine deficiency: a role for the skin in 3,5,3'-triiodothyronine economy? Endocrinology 139(5):2229-2234.

Segal J, Ingbar SH. 1982. Specific binding sites for triiodothyronine in the plasma membrane of rat thymocytes. Journal of Clinical Investigation 70:919-926.

Sharlin DS, Bansal R, Zoeller RT. 2006. Polychlorinated biphenyls exert selective effects on cellular composition of white matter in a manner inconsistent with thyroid hormone insufficiency. Endocrinology 147(2):846-858.

Takasuga T, Senthilkumar K, Watanabe K, Takemori H, Shoda T, Kuroda Y. 2004. Ultratrace analysis of polychlorinated biphenyls (PCBs) and their hydroxylated metabolites (s) in human serum and cerebrospinal fluid (CSF) samples. Organhalogen Compounds 66:2529-2534.

Tu HM, Kim SW, Salvatore D, Bartha T, Legradi G, Larsen PR, Lechan RM. 1997. Regional distribution of type 2 thyroxine deiodinase messenger ribonucleic acid in rat hypothalamus and pituitary and its regulation by thyroid hormone. Endocrinology 138(8):3359-3368.

Viluksela M, Raasmaja A, Lebofsky M, Stahl BU, Rozman KK. 2004. Tissue-specific effects of 2,3,7,8-tetrachlorodibenzo-p-dioxin (TCDD) on the activity of 5'-deiodinases I and II in rats. Toxicology Letters 147(2):133-142.

Watanabe M, Houten SM, Mataki C, Christoffolete MA, Kim BW, Sato H, Messaddeq N, Harney JW, Ezaki O, Tatsuhiko K, Schoonjans K, Bianco AC, Auwerx J. 2006. Bile acids induce energy expenditure by promoting intracellular thyroid hormone activation. Nature 439:484-489.

Wells RS, Tornero V, Borrell A, Aguilar A, Rowles TK, Rhinehart HL, Hofmann S, Jarman WM, Hohn AA, Sweeney JC. 2005. Integrating life-history and reproductive success data to examine potential relationships with organochlorine compounds for bottlenose dolphins (*Tursiops truncatus*) in Sarasota Bay, Florida. Science of the Total Environment 349(1-3):106.

Whitby EH, Paley MNJ, Cohen M, Griffiths PD. 2006. Post-mortem fetal MRI: what do we learn from it? European Journal of Radiology 57:250-255.

White RD, Shea D, Schlezinger JJ, Hahn ME, Stegeman JJ. 2000. In vitro metabolism of polychlorinated biphenyl congeners by beluga whale (*Delphinapterus leucas*) and pilot whale (*Globicephala melas*) and relationship to cytochrome P450 expression. Comparitive Biochemistry and Physiology Part C 126(3):267-284.

Wilson JY, Cooke SR, Moore MJ, Martineau D, Mikaelian I, Metner DA, Lockhart WL, Stegeman JJ. 2005. Systemic effects of Arctic pollutants in beluga whales indicated by CYP1A1 expression. Environmental Health Perspectives 113:1594-1599.

Zimmermann R, Strauss JG, Haemmerle G, Schoiswohl G, Birner-Gruenberger R, Riederer M, Lass A, Neuberger G, Eisenhaber F, Hermetter A, Zechner R. 2004. Fat mobilization in adipose tissue is promoted by adipose triglyceride lipase. Science 306:1383-1386.

## APPENDIX 1:

## Brain Pathologies in Common Dolphins (*Delphinus delphis*) and Atlantic White-sided Dolphins (*Lagenorhynchus acutus*) from the Northwest Atlantic Discovered by Magnetic Resonance Imaging

Between 2004 and 2005, magnetic resonance imaging was completed on 21 marine mammals. These included one harbor seal (*Phoca Vitulina*), one grey seal (*Halichoerus grypus*), nine common dolphins (Delphinus delphis), and ten Atlantic white-sided dolphins (*Lagenorhynchus acutus*). MR imaging revealed that two common dolphins and two Atlantic white-sided dolphins contained brain lesions (i.e. 4 out of 16 dolphins randomly imaged contained a brain lesion) (Figures 1-4; Table 1). All dolphins that had a lesion contained a heavy infestation of the nematode Stenurus in the cranial and otic sinuses. In at least three cases, histological findings suggest parasite migration as the causative agent. However, no adults of ova were observed in the brain. Future directions will include a more detailed investigation of the causative agent. We will also test the hypothesis that dolphins exhibiting lesions contain high levels of persistent organic pollutants.

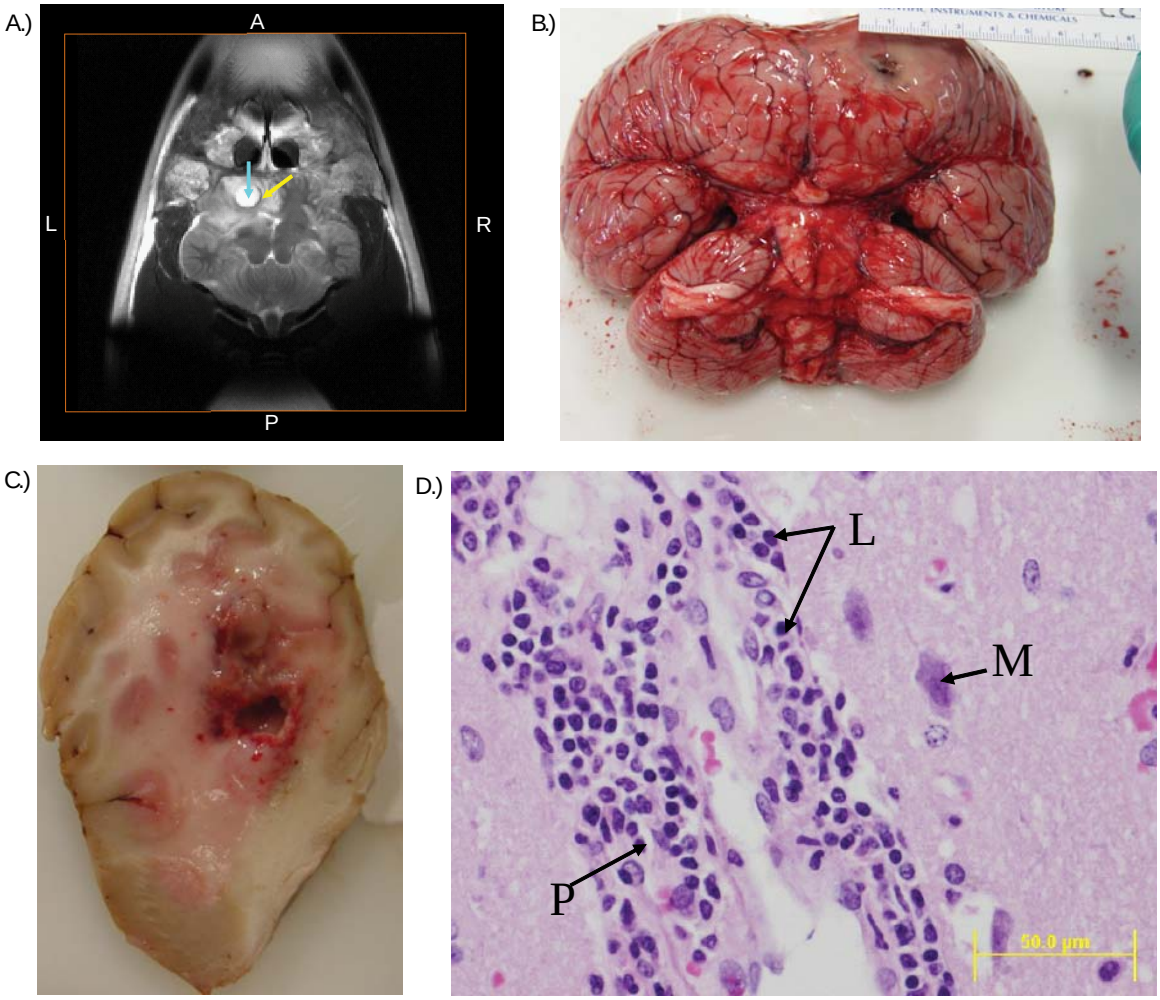


**Figure 1. Brain lesion in CCSN04-177-Dd.** A.) The MR image indicated a 2 cm spherical abscess identified in the left frontal lobe. A halo of damaged tissue is noted by the yellow arrow. A fluid filled necrotic core is indicated by the turquoise arrow. B) Brain removal revealed pus in the left frontal lobe. C.) The lesion was revealed during the dissection. D.) Histological analysis revealed abundant and active lymphocytes (L), microglia (M), and plasma (P) cells. *Dr. David Rotstein (Univ. of Tennessee) performed the histological analysis.*

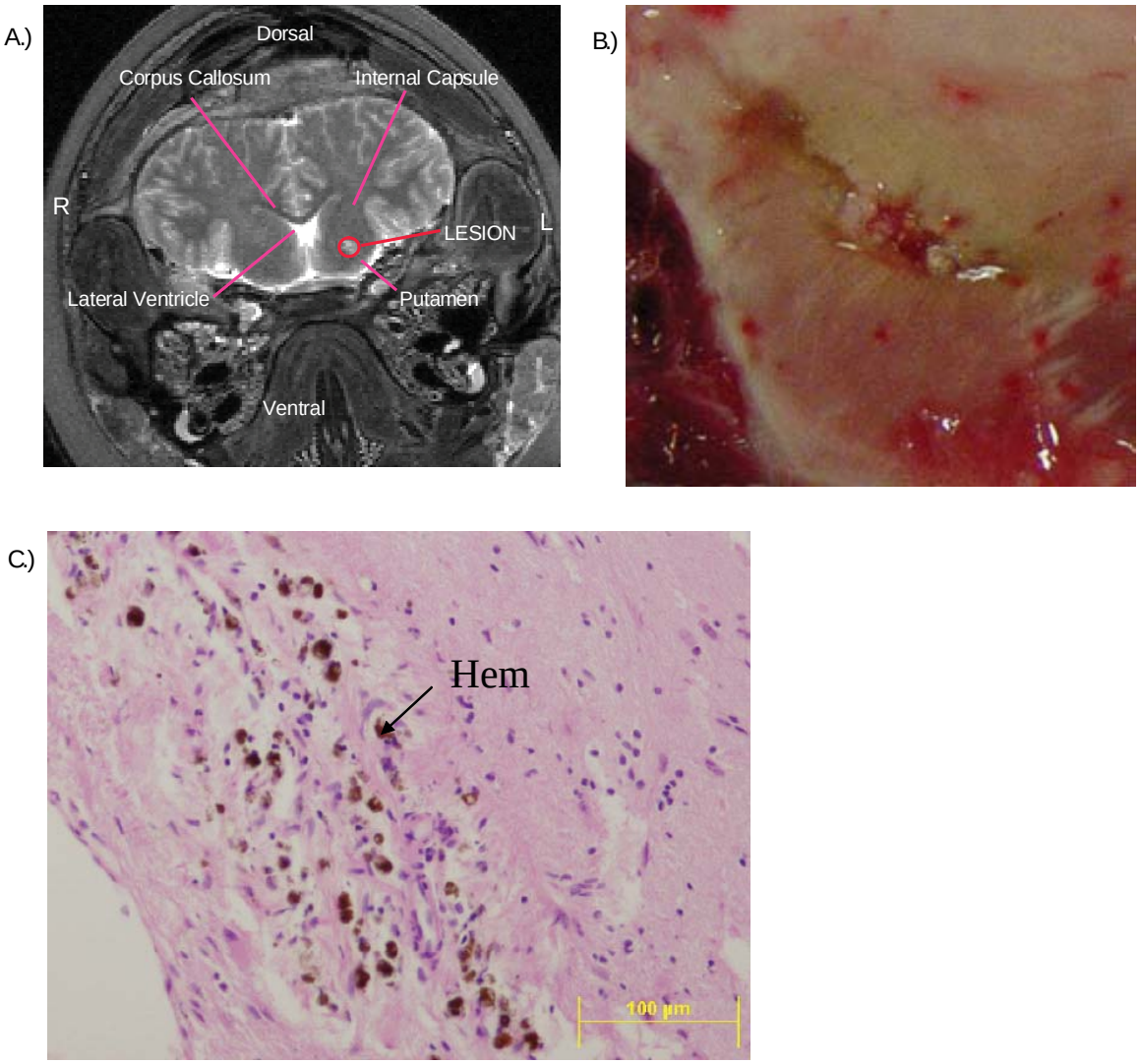


**Figure 2. Brain lesion in CCSN04-191-Dd.** A.) The MR image indicated a small lesion in the region of the putamen and globus pallidus or collectively termed the lentiform nucleus. B) The lesion was revealed during the dissection. C.) Histological analysis revealed irregular tracts of rarefied neuropil, hemosiderin-laden macrophages, and the accumulation of extracelluar hemosiderin (Hem) black-brown pigment. *Dr. David Rotstein (Univ. of Tennessee) performed the histological analysis.*

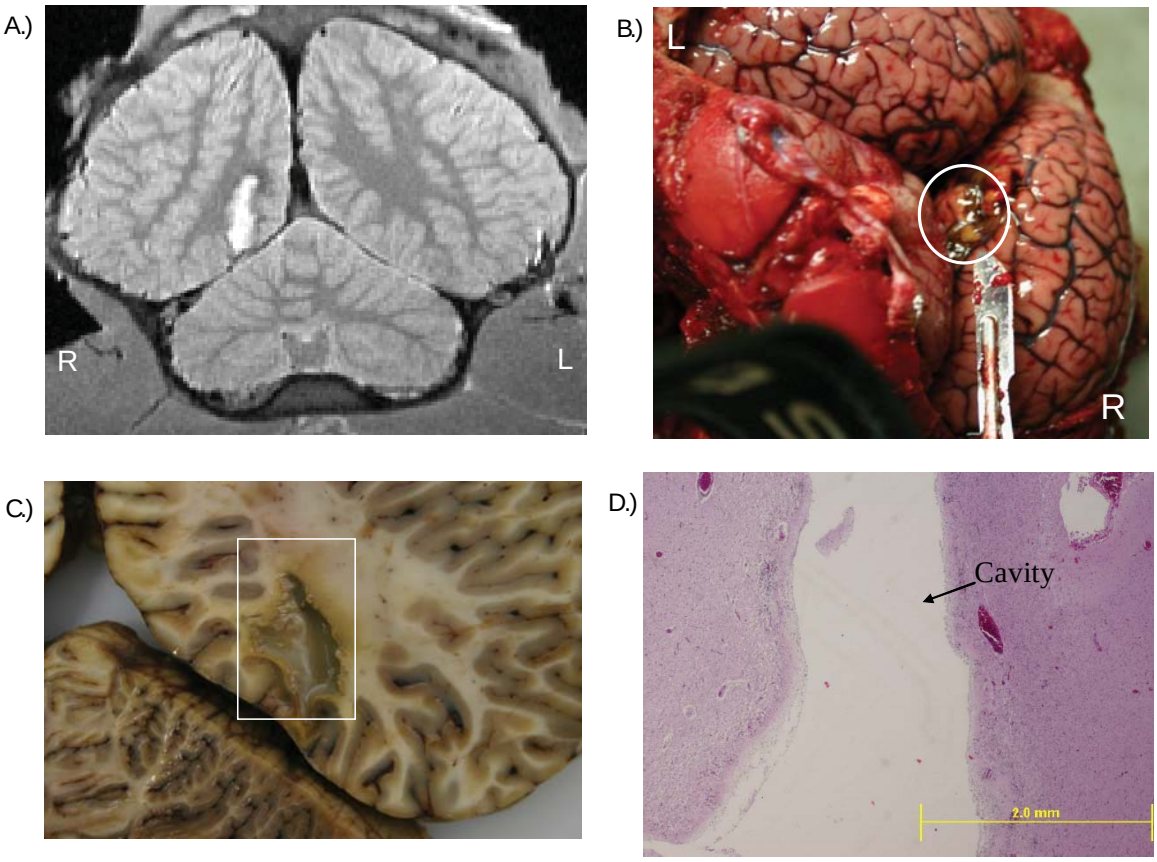


**Figure 3. Brain lesion in CCSN05-038-La.** A.) The MR image indicated a lesion in the right occipital lobe. B) Brain removal revealed pus oozing from the right occipital lobe. C.) The lesion was revealed during the dissection. D.) Histological analysis revealed a 4 cm linear cavity with a central clear core. *Dr. David Rotstein (Univ. of Tennessee) performed the histological analysis.*

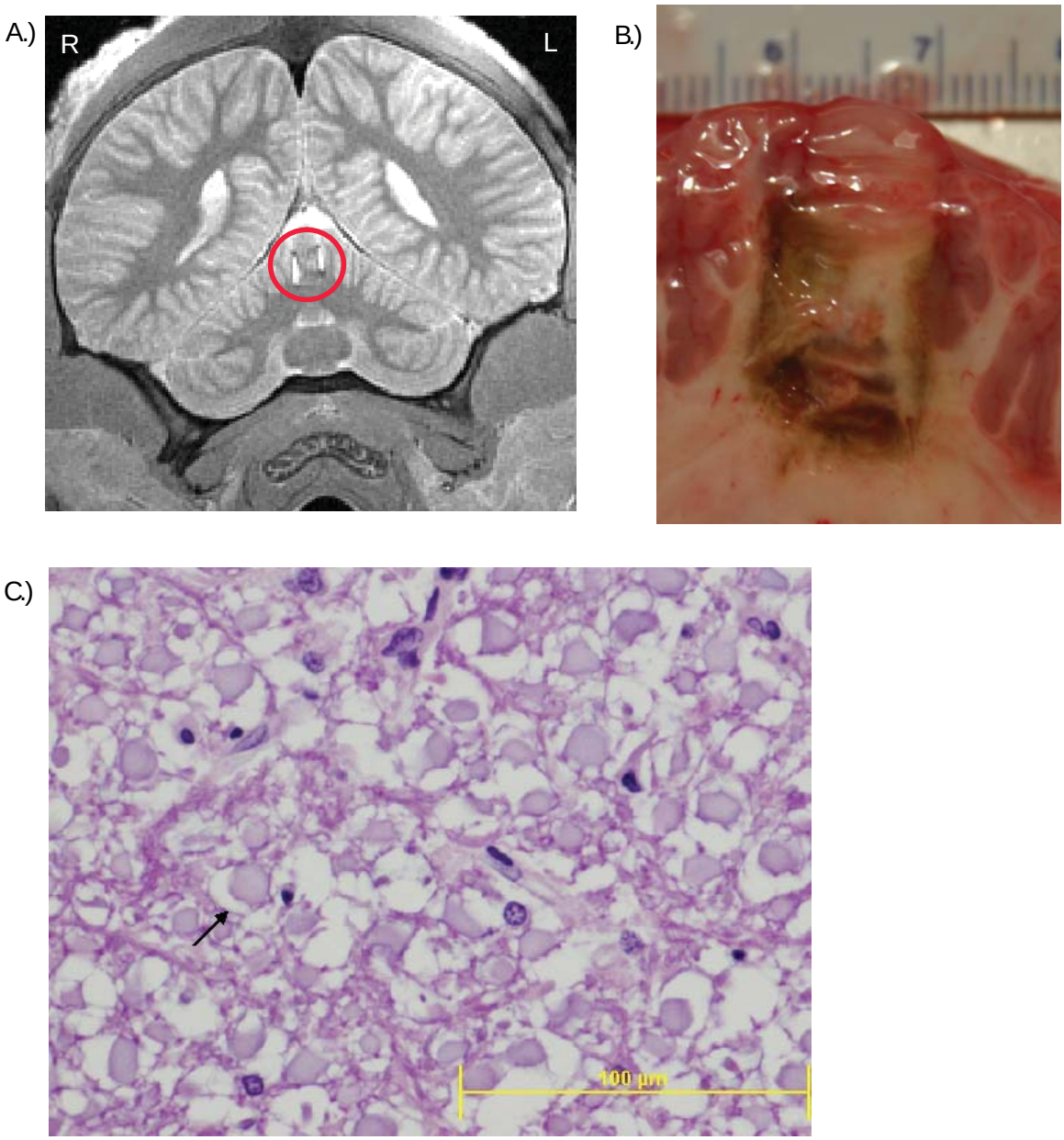


**Figure 4. Brain lesion in CCSN05-232-La.** A.) The MR image indicated bilateral lesions in the vermis. B) The lesion was revealed during the dissection. C.) Histological analysis revealed swelling of myelin sheaths and degeneration of axons. *Dr. David Rotstein (Univ. of Tennessee) performed the histological analysis.*

Table 1. Stranding and Life History Information of Common Dolphins and Atlantic White-sided Dolphins Exhibiting Brain Lesions.

| FIELD ID: | Species | Date of Death | Location | Hours to MRI | Condition Code[1] | Stranding type | Sex | Length (cm) | Weight (kg) |
|---|---|---|---|---|---|---|---|---|---|
| CCSN04-177-Dd | Common dolphin | July 20, 2004 | Elephant Nect Rd, Westport, MA | 4.5 | 1 | single | m | 209 | 91 |
| CCSN04-191-Dd | Common dolphin | September 6, 2004 | Squaw Island, Hyannisport, MA | 31 | 1 | single | f | 207 | 80 |
| CCSN05-038-La | Atlantic white-sided dolphin | February 15, 2005 | Chesequesset Neck, Wellfleet, MA | <24 | 2 | mass | f | 208 | 125 |
| CCSN05-232-La | Atlantic white-sided dolphin | Ocober 4, 2005 | Nauset Beach, Eastham, MA | 11 | 1 | single | f | 185.5 | 77.5 |

[1] A condition code of 1 indicates that the dolphin was euthanized, while a condition code of 2 indicates that the dolphin was found dead but the specimen was in fresh condition (i.e. less than 24 hours had passed since the time of death).

Brain pathologies were found using MR images.

MRIs were completed of the brain intact within the skull and the head attached to the body.

## APPENDIX 2:

## Magnetic Resonance Images and Volumes of the Hippocampus in a California Sea-lion (*Zalophus californianus*) Exhibiting Signs of Domoic Acid Toxicity

Domoic acid (a type of biotoxin produced by some *Pseudo-nitzschia* species and associated with harmful algal blooms) is neurotoxic and has been shown to cause bilateral hippocampal atrophy in California sea lions (*Zalophus californianus*). MR imaging of a live California sea lion (i.e. Shelouba) exhibiting symptoms of domoic acid (DA) toxicity was completed in collaboration with Dr. Frances Gulland from The Marine Mammal Center (TMMC), Sausalito, CA and Dr. Jerome Barakos from the Department of Radiology, University of California, San Francisco, CA. Hippocampus and surrounding fluid structure volumes were determined for Shelouba (Figure 1; Table 1). Future directions will test the hypothesis that live sea lions suffering from DA toxicity exhibit a decrease in hippocampus volumes as measured from MR images.

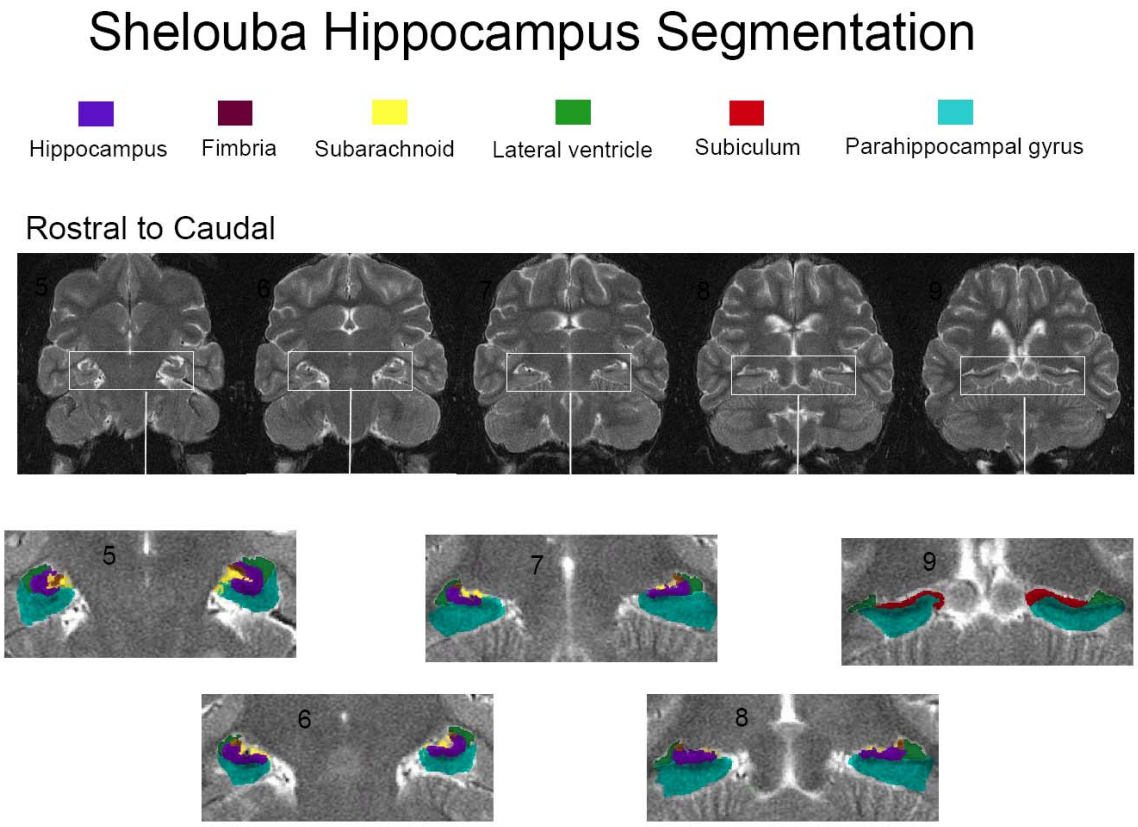


**Figure 1. Label maps of the hippocampus and surrounding fluid structures used to determine the volumes of these brain structures for the California sea lion "Shelouba".**

Table 1. Hippocampus and surrounding fluid structure volumes for the California sea lion “Shelouba”.

| **Brain Region** | **Left Volume (mm3)** | **Right Volume (mm3)** |
|---|---|---|
| **Hippocampus** | **305.5** | **278.4** |
| **Fimbria** | **41.2** | **38.6** |
| **Lateral ventricle** | **211.3** | **154.1** |
| **Parahippocampal gyrus** | **1195.7** | **1156.5** |
| **Subiculum** | **77.4** | **66.3** |
| **Subarachnoid space** | **70.9** | **65.5** |

# APPENDIX 3:

# Exposure of Bottlenose Dolphin (*Tursiops truncatus*) Skin-blubber Biopsies to PCB126: CYP1A1 Response and Identification of Novel Biomarkers

## INTRODUCTION

Planar halogenated aromatic hydrocarbons (PHAHs) are ubiquitous contaminants of the marine environment, and especially coastal areas. PHAHs are known to be highly toxic to vertebrate animals, including laboratory mammals as well as many species of wildlife. However, it is difficult to assess the impact of these compounds in marine mammals and to make causal links between specific contaminants (or other stressors) and effects of toxicological significance in wild populations.

One approach to assessing the impact of PHAHs and other contaminants on marine organisms is through the use of biomarkers. In the context of the bottlenose dolphin health assessment (see Chapters 2 and 3), we combined the use of an established biomarker of PHAH exposure—induction of cytochrome P4501A1 (CYP1A1)—with research to develop novel biomarkers that might be more closely linked to chemical toxicity.

Despite the value of CYP1A1 as a measure of chemical exposure, its value as a biomarker of adverse effect has been hotly debated, because its mechanistic link to PHAH toxicity is uncertain (e.g. see 1, 2). There is a need for new biomarkers of PHAH effects, especially ones that are more directly linked to toxicity. Most toxic effects of PHAH involve altered proliferation or differentiation of cells, which is thought to occur through changes in gene expression caused by activation of the aryl hydrocarbon receptor (AHR) (3). Some of these changes include skin lesions such as hyperkeratosis and squamous cell proliferation. The genes involved in PHAH effects on cell proliferation, if known, would make ideal biomarkers of PHAH effects.

## METHODS

To identify novel PHAH-regulated genes, we designed a series of experiments involving *in vitro* exposure in dolphin skin/blubber biopsies to 3,3',4,4',5-pentachlorobiphenyl (PCB-126) or vehicle, followed by RNA isolation and analysis of differential gene expression by RT-PCR and by subtractive suppressive hybridization (SSH) (4, 5, 6). The results of SSH are pending.

*Biopsy treatment.* Biopsies from seven individual dolphins (all from the Charleston, SC site) were processed for SSH experiments. Immediately after collection, a portion of each biopsy sample was cut manually into six or twelve slices (about 1 mm thick), with each slice spanning the entire biopsy depth. Three slices of each biopsy were incubated with cell culture media containing PCB126 (100 nM final concentration) for 12 or 24hr; the other three slices were incubated with medium containing dimethylsulfoxide (untreated, DMSO, 0.5%) only. For 4 of the 7 biopsy samples, the culture medium did not contain antibiotics. For 3 of the 7 biopsies, incubations were performed both in the presence and absence of an antibiotic mixture (stabilized penicillin, streptomycin, and amphotericin; Sigma A5955; Sigma-Aldrich, St. Louis, MO). Incubations were performed in a tissue culture incubator at 37$^{o}$C and 5% $CO_2$. After the 12 or 24 hr incubation, the untreated and treated tissues slices were rinsed with phosphate buffered saline (PBS), placed in RNAlater (Ambion), and stored at –80$^{o}$C until RNA isolation.

*Identification of* Tursiops *CYP1A1 and Actin.* Total RNA was isolated from all untreated and treated slices using Stat-60 (Tel-Test). The quality of the RNA was confirmed by visualization on ethidium bromide-stained agarose minigels; the quantity was determined by UV absorbance. Total RNA from FB#814 untreated and treated biopsies (without antibiotics) were subjected to RT-PCR using degenerate CYP1A1 and actin primers designed to target conserved regions of mammalian CYP1A1 and actin nucleotide sequences (Table 1). PCR products were cloned into pGEM-T and sequenced in both directions. The sequences of the CYP1A1 and actin RT-PCR products were compared to sequences in GenBank.

## RESULTS AND DISCUSSION

To begin to identify novel PHAH-regulated genes, we exposed dolphin skin/blubber biopsies to PCB-126, isolated RNA, and measured changes in gene expression. *In vitro* exposure of cetacean biopsies to the AHR agonist β-naphthoflavone has been used previously to study the induction of CYP1A1 protein using

immunohistochemical analyses (17). Our intention is to combine *in vitro* PHAH exposure with SSH or similar assays for differential gene expression to identify novel PHAH-regulated genes that might serve as useful biomarkers of PHAH effect in cetaceans.

Seven dolphin biopsy samples (all from the Charleston site) were used in our initial experiments to examine genes induced in response to PHAH exposure (Table 2). For three of the seven biopsy samples, the effect of antibiotics was tested. For two of these three samples, antibiotics stopped microbial growth (Table 2). Thus, we recommend the inclusion of antibiotics for future tissue slice experiments.

Total RNA was isolated from all untreated and treated biopsy samples (Table 3). Our initial goal was to measure the expression of CYP1A1, to verify that the *in vitro* exposure had been effective at activating the AHR and inducing a known AHR-regulated gene. To do this, CYP1A1 (370 bp) and actin (1200 bp) cDNA fragments were amplified by RT-PCR (from FB814), cloned, and sequenced. A comparison of the sequences obtained with those in the GenBank database confirmed the identity of the RT-PCR products. The bottlenose dolphin CYP1A1 amino acid sequence showed a 99% identity to striped dolphin (*Stenella coeruleoalba*) CYP1A1; 89% identity to pig (*Sus crofa*) CYP1A1; 87% identity to the mouse (*Mus musculus*) CYP1A1; and 86% identity to human (*Homo sapiens*) CYP1A1 (Figure 1). The bottlenose dolphin CYP1A1 amino acid sequence showed a 83% identity to human CYP1A2. The slice treated with PCB-126 showed elevated CYP1A1 expression compared to the DMSO-treated slice, while actin expression did not differ with treatment (Figure 2). These results indicate that the *in vitro* biopsy dosing technique was effective in inducing AHR-dependent gene expression.

We plan to follow-up these initial results. We have designed primers for conducting real-time, quantitative RT-PCR analysis of CYP1A1 and actin expression. Using these primers, we will measure the expression of CYP1A1 and actin in all DMSO- and PCB-126-treated slices. The biopsy samples demonstrating the greatest CYP1A1 induction in these assays will be used in SSH (4, 5, 6) to identify novel PHAH-responsive genes.

## REFERENCES


1. Teraoka, H., Dong, W., Tsujimoto, Y., Iwasa, H., Endoh, D., Ueno, N., Stegeman, J. J., Peterson, R. E., and Hiraga, T. (2003) Induction of cytochrome P450 1A is required for circulation failure and edema by 2,3,7,8-tetrachlorodibenzo-p-dioxin in zebrafish. *Biochem Biophys Res Commun* **304**(2)**,** 223-8
2. Carney, S. A., Peterson, R. E., and Heideman, W. (2004) 2,3,7,8-Tetrachlorodibenzo-p-dioxin Activation of the Aryl Hydrocarbon Receptor/Aryl Hydrocarbon Receptor Nuclear Translocator Pathway Causes Developmental Toxicity through a CYP1A-Independent Mechanism in Zebrafish. *Mol Pharmacol* **66**(3)**,** 512-21
3. Poland, A., and Knutson, J. C. (1982) 2,3,7,8-Tetrachlorodibenzo-p-dioxin and related halogenated aromatic hydrocarbons: examination of the mechanism of toxicity. *Annu. Rev. Pharmacol. Toxicol.* **22,** 517-554
8. Hubank, M., and Schatz, D. G. (1994) Identifying differences in mRNA expression by representational difference analysis of cDNA. *Nucleic Acids Res* **22**(25)**,** 5640-8
9. Diatchenko, L., Lau, Y. F., Campbell, A. P., Chenchik, A., Moqadam, F., Huang, B., Lukyanov, S., Lukyanov, K., Gurskaya, N., Sverdlov, E. D., and Siebert, P. D. (1996) Suppression subtractive hybridization: a method for generating differentially regulated or tissue-specific cDNA probes and libraries. *Proc Natl Acad Sci U S A* **93**(12)**,** 6025-30
10. Diatchenko, L., Lukyanov, S., Lau, Y. F., and Siebert, P. D. (1999) Suppression subtractive hybridization: a versatile method for identifying differentially expressed genes. *Methods Enzymol* **303,** 349-80

**Figure 1. Bottlenose dolphin CYP1A1 amino acid sequence and comparison to the striped dolphin (*S. coeruleoalba*), the pig (*S. scrofa*), the house mouse (*M. musculus*), and the human (*H. sapiens*) CYP1A1 amino acid sequences.**

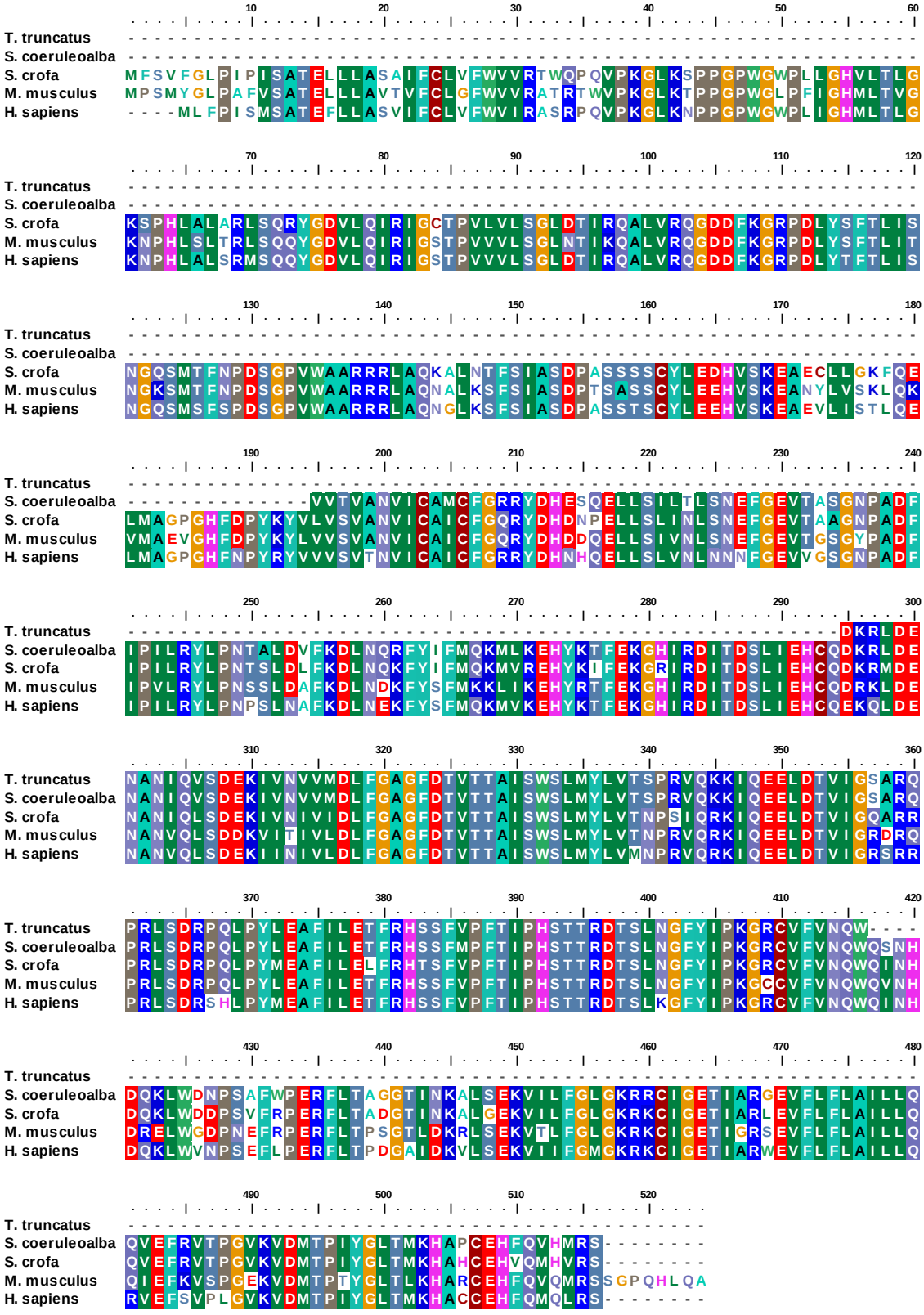
T. truncatus
S. coeruleoalba
S. crofa
M. musculus
H. sapiens

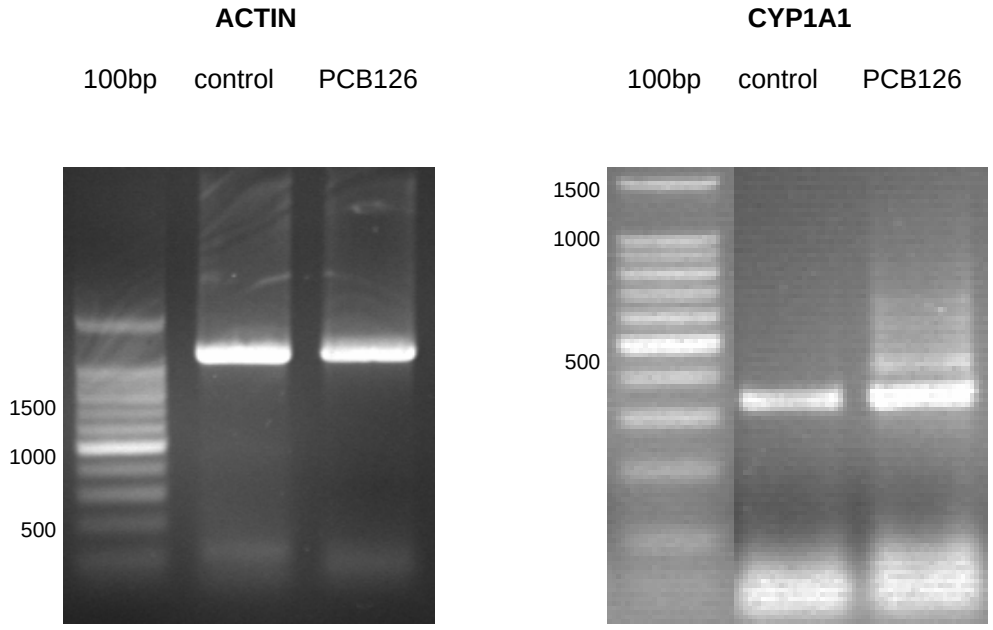


**Figure 2. Control versus PCB126 treated biopsies.** Actin (1200 bp) and CYP1A1 (370 bp) PCR products were obtained from FB814 untreated (control) and treated biopsies (PCB126) (without antibiotics). The slice treated with PCB-126 showed an increase in CYP1A1 expression compared to the untreated slice, while actin expression did not change.

Table 1. Degenerate primer sequences used in RT-PCR to identify CYP1A1 and actin in bottlenose dolphin skin-blubber biopsy samples.

| **Gene** | **Direction** | **Primer Sequence** |
|---|---|---|
| CYP1A1 | Forward | GGAYAAGAGRCTGGACGAGAATGC |
| CYP1A1 | Reverse | GCCACTGGTTYACAAAGACACARC |
| Actin | Forward | GAATTCTGCAGACAACGGYTCSGGYATGTGC |
| Actin | Reverse | CTCGAGGATCCGAAGCAYTTGCGRTGSACRAT |

Table 2. Biopsies processed for SSH experiments. Biopsy samples were cut manually into thin slices (about 1mm thick) spanning the entire biopsy depth. The slices were treated either with cell culture media containing PCB-126 (100 nM) or with medium containing DMSO only (12 or 24 hr; with or without antibiotics).

| Freeze Brand # | Sex | With Antibiotics | Treatment | Media color | Media turbidity | Incubation Time (hr) |
|---|---|---|---|---|---|---|
| 814 | male | no | control | red | clear | 13 |
| 814 | male | no | PCB126 | yellow | cloudy | 13 |
| 814 | male | yes | control | red | clear | 13 |
| 814 | male | yes | PCB126 | red | clear | 13 |
| | | | | | | |
| 801 | female | yes | control | red | clear | 12.5 |
| 801 | female | yes | PCB126 | red | clear | 12.5 |
| | | | | | | |
| 818 | male | no | control | red | clear | 12.5 |
| 818 | male | no | PCB126 | red | clear | 12.5 |
| 818 | male | yes | control | red | clear | 12.5 |
| 818 | male | yes | PCB126 | red | clear | 12.5 |
| | | | | | | |
| 822 | male | yes | control | red | clear | 24 |
| 822 | male | yes | PCB126 | red | clear | 24 |
| | | | | | | |
| 825 | female | yes | control | red | clear | 24 |
| 825 | female | yes | PCB126 | red | clear | 24 |
| | | | | | | |
| 835 | female | yes | control | orange | specs | 24 |
| 835 | female | yes | PCB126 | orange | specs | 24 |
| | | | | | | |
| 839 | female | no | control | yellow | cloudy | 23 |
| 839 | female | no | PCB126 | orange | clear | 23 |
| 839 | female | yes | control | orange | clear | 23 |
| 839 | female | yes | PCB126 | orange | clear | 23 |

Table 3. Total RNA concentrations isolated from all untreated and treated biopsy samples. CA = untreated, with antibiotics; TA = treated, with antibiotics; CNO = untreated, no antibiotics; TNO = treated, no antibiotics.

| RNA extraction date | Sample ID | Total wt (g) | Skin wt (g) | Blubber wt (g) | Total RNA (ug/uL) | Total RNA (ug) | Total RNA yield (ug/mg) |
|---|---|---|---|---|---|---|---|
| 9/23/2003 | FB814CNO | 0.25 | na | na | 0.62 | 12.4 | 0.05 |
| 9/23/2003 | FB814TNO | 0.39 | na | na | 0.35 | 7.0 | 0.02 |
| 6/8/2004 | FB814CA | 0.34 | 0.05 | 0.29 | 0.16 | 3.2 | 0.01 |
| 6/8/2004 | FB814TA | 0.36 | 0.02 | 0.34 | 0.11 | 2.2 | 0.01 |
| | | | | | | | |
| 6/8/2004 | FB801CA | 0.34 | 0.07 | 0.27 | 1.85 | 37.0 | 0.11 |
| 6/8/2004 | FB801TA | 0.31 | 0.04 | 0.27 | 1.26 | 25.1 | 0.08 |
| | | | | | | | |
| 6/10/2004 | FB818CNO | 0.22 | 0.01 | 0.21 | 1.84 | 36.8 | 0.17 |
| 6/10/2004 | FB818TNO | 0.25 | 0.05 | 0.20 | 2.19 | 43.8 | 0.18 |
| 6/8/2004 | FB818CA | 0.22 | 0.06 | 0.16 | 0.71 | 14.2 | 0.06 |
| 6/8/2004 | FB818TA | 0.26 | 0.01 | 0.25 | 0.14 | 2.9 | 0.01 |
| | | | | | | | |
| 6/10/2004 | FB822CA | 0.28 | 0.04 | 0.24 | 2.10 | 41.9 | 0.15 |
| 6/10/2004 | FB822TA | 0.21 | 0.04 | 0.17 | 0.80 | 16.0 | 0.08 |
| | | | | | | | |
| 6/10/2004 | FB825CA | 0.37 | 0.05 | 0.32 | 1.10 | 21.9 | 0.06 |
| 6/10/2004 | FB825TA | 0.46 | 0.06 | 0.40 | 3.28 | 65.6 | 0.14 |
| | | | | | | | |
| 6/14/2004 | FB835CA | 0.69 | 0.09 | 0.60 | 4.82 | 96.4 | 0.14 |
| 6/14/2004 | FB835TA | 0.60 | 0.12 | 0.48 | 5.03 | 100.6 | 0.17 |
| | | | | | | | |
| 6/14/2004 | FB839CNO | 0.26 | 0.05 | 0.21 | 2.47 | 49.4 | 0.19 |
| 6/14/2004 | FB839TNO | 0.24 | 0.06 | 0.18 | 6.04 | 120.8 | 0.50 |
| 6/14/2004 | FB839CA | 0.20 | 0.03 | 0.17 | 1.42 | 28.4 | 0.14 |
| 6/14/2004 | FB839TA | 0.26 | 0.06 | 0.20 | 1.73 | 34.6 | 0.13 |

## APPENDIX 4:

## Type II Iodothyronine Deiodinase (D2) Identification in the Skin-blubber Biopsy of a Bottlenose Dolphin (*Tursiops truncatus*)

The goal of this study was to provide some evidence that type II iodothyronine deiodinase (D2) could be used as a biomarker of effect for marine mammals exposed to thyroid hormone disrupting chemicals such as PCBs, PBDEs, and their hydroxylated metabolites. However, the structural and functional characteristics of D2 in marine mammals are currently unknown.

A 750-bp fragment of a D2 cDNA was identified from a bottlenose dolphin biopsy sample collected from the CHS location in summer 2003 (see Chapters 2 and 3). The cDNA fragment and its deduced amino acid sequence share high identity with other vertebrate D2s (Figure 1). Future directions will obtain the complete D2 bottlenose dolphin sequence. Primers for real-time RT-PCR analysis of D2 expression have been designed based on this sequence. D2 mRNA levels will be measured in a subset of the skin-blubber biopsies previously collected from CHS and IRL locations. The expression of D2 in individual animals will be compared to levels of relevant contaminants (PCBs, PBDEs, and their hydroxylated metabolites). The relationship of D2 expression to other variables such as gender, geographic region, and circulating levels of THs will also be examined.

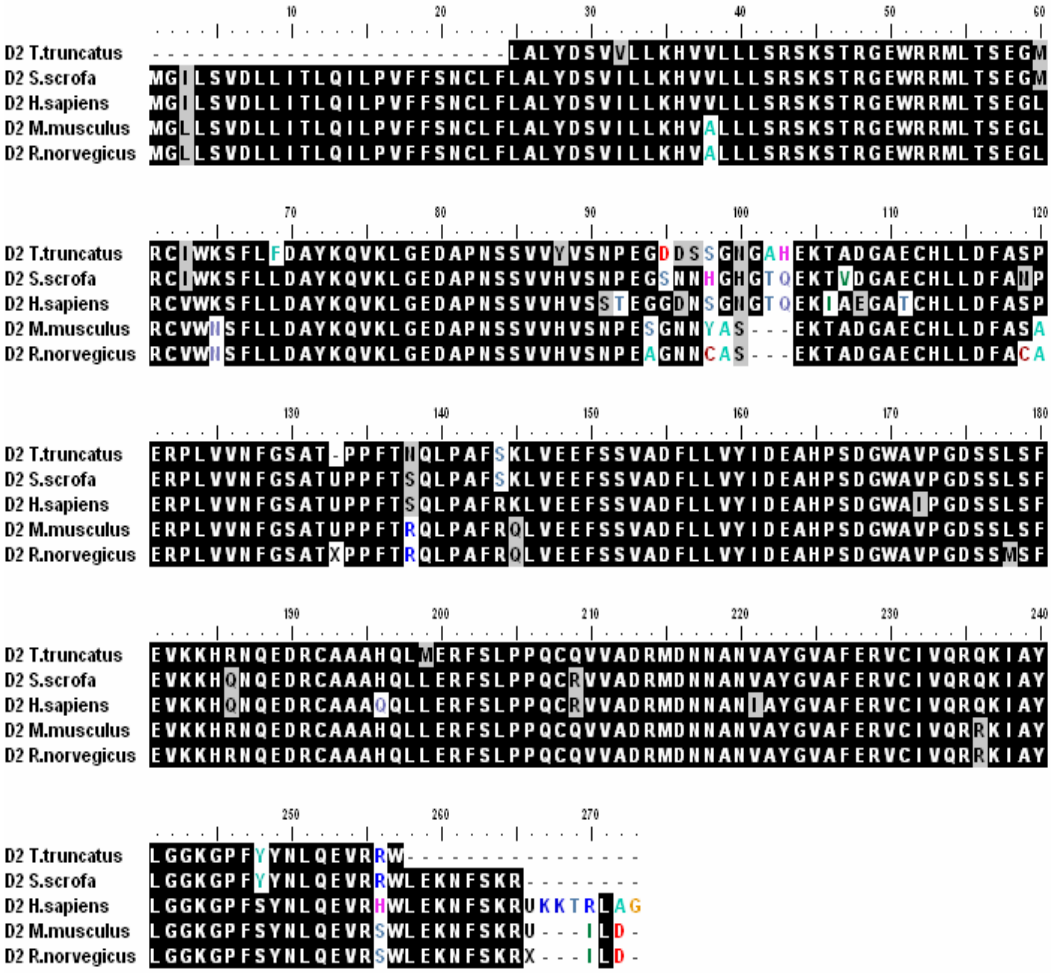


**Figure 1. Bottlenose dolphin Type II 5'-deiodinase (D2) partial amino acid sequence and its comparison to the pig (*S. scrofa*), the human (*H. sapiens*), the house mouse (*M. musculus*), and the rat (*R. norvegicus*) D2 amino acid sequences.**

## APPENDIX 5:

## Identification of Transthyretin (TTR) in the Atlantic White-sided Dolphin (*Lagenorhynchus acutus*)

A characteristic of human and rat transthyretin (TTR) is its ability to bind hydroxylated PCB metabolites and related compounds with higher affinity than the natural ligand, T4. How do marine mammals compare to rats and humans? Do we expect a difference in TTR ligand-binding characteristics? Currently, the structural and functional characteristics of TTR in marine mammals are not known. In fact, efforts to demonstrate TTR in belugas and bottlenose dolphins have proved unsuccessful using methodologies established for other mammals. These unknowns limit our understanding of how halogenated phenolics interact with the thyroid hormone system. The goal of this study was to determine if TTR is expressed in the liver of a Delphinid species (i.e. the Atlantic white-sided dolphin); and if present, to clone, sequence, and compare the partial TTR cDNA with other vertebrate TTR sequences.

Total RNA was isolated from a liver sample using Stat-60 (Tel-Test). The quality of the RNA was confirmed by visualization on ethidium bromide-stained agarose minigels; the quantity was determined by UV absorbance. Samples of total RNA were subjected to RT-PCR using degenerate primers designed to target conserved regions of mammalian TTR nucleotide sequences. PCR products were cloned into pGEM-T and sequenced in both directions. The sequences of the TTR were compared to sequences in GenBank.

Identification of a 280-bp fragment of a TTR cDNA from an Atlantic white-sided dolphin liver sample was identified. The Atlantic white-sided dolphin TTR amino acid sequence showed 84% identity to pig (*S. scrofa*) TTR, 80% identity to human (*H. sapiens*) TTR, 74% identity to mouse (*M. musculus*) TTR, and 75% identity to rat (*R. norvegicus*) TTR (Figure 1). Future directions will obtain the complete TTR Atlantic white-sided dolphin sequence. The cloned TTR will be produced *in vitro* to study its

ligand-binding characteristics, including its affinity for T4, T3, selected PCB and PBDE congeners, and their hydroxylated metabolites (OH-PCBs and OH-PBDEs).

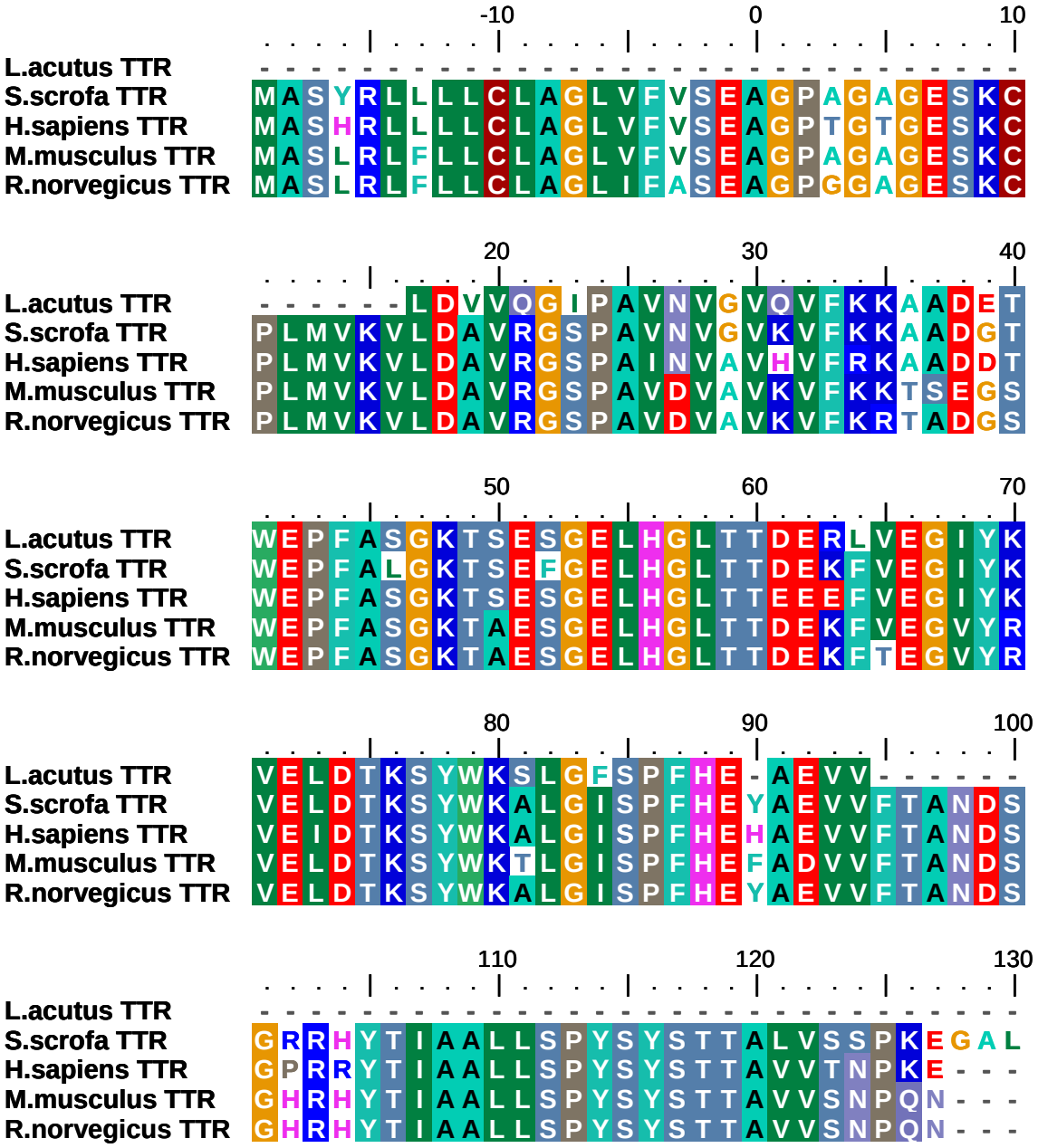


**Figure 1. A comparison of the Atlantic white-sided dolphin TTR to other species.** The Atlantic white-sided dolphin TTR amino acid sequence showed 84% identity to pig (*S. scrofa*) TTR, 80% identity to human (*H. sapiens*) TTR, 74% identity to mouse (*M. musculus*) TTR, and 75% identity to rat (*R. norvegicus*) TTR.

## APPENDIX 6:

## A Comparison of PCBs and PBDEs in Winter Flounder from Cape Cod Bay, Massachusetts

Halogenated aromatic hydrocarbons such as polychlorinated biphenyls (PCBs) and organochlorine pesticides (OCs) are well known contaminants of marine environments. Recent developments have forced a re-evaluation of the relative impact of these and other synthetic compounds on the health of the marine environment. The environmental concentrations of new classes of halogenated pollutants such as the polybrominated diphenyl ethers (PBDEs) are increasing. The overall objective of this research was to provide the first comparative assessment of PCBs and PBDEs in flounder from Cape Cod Bay, MA. Flounder were collected during routine surveys at two stations in Massachusetts Bay (Outfall and Eastern Cape Cod Bay) as part of sampling performed by Dr. Michael Moore. The levels of PCBs, PBDEs, and organochlorine pesticides are compared in Figure 1.

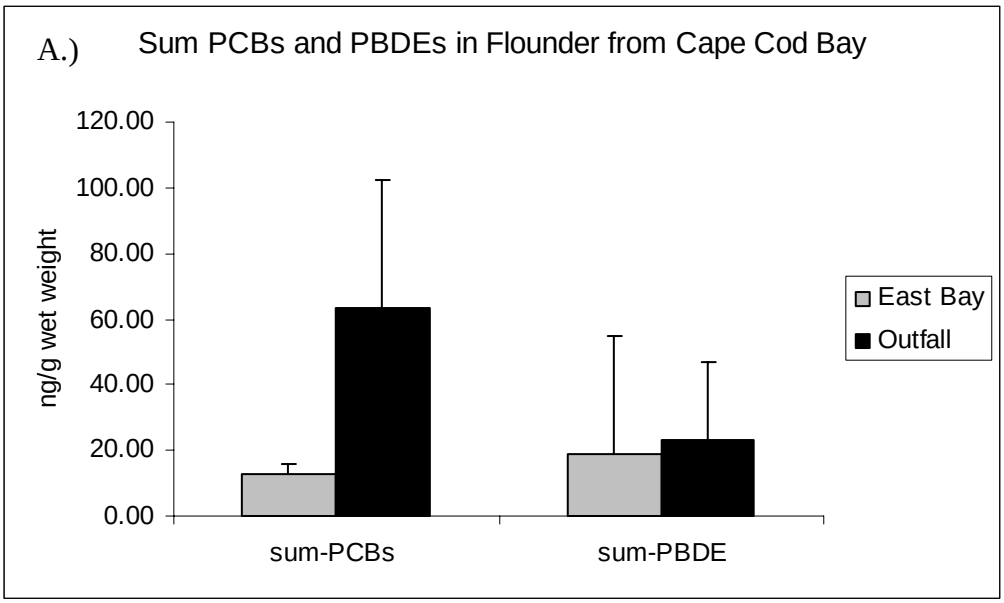


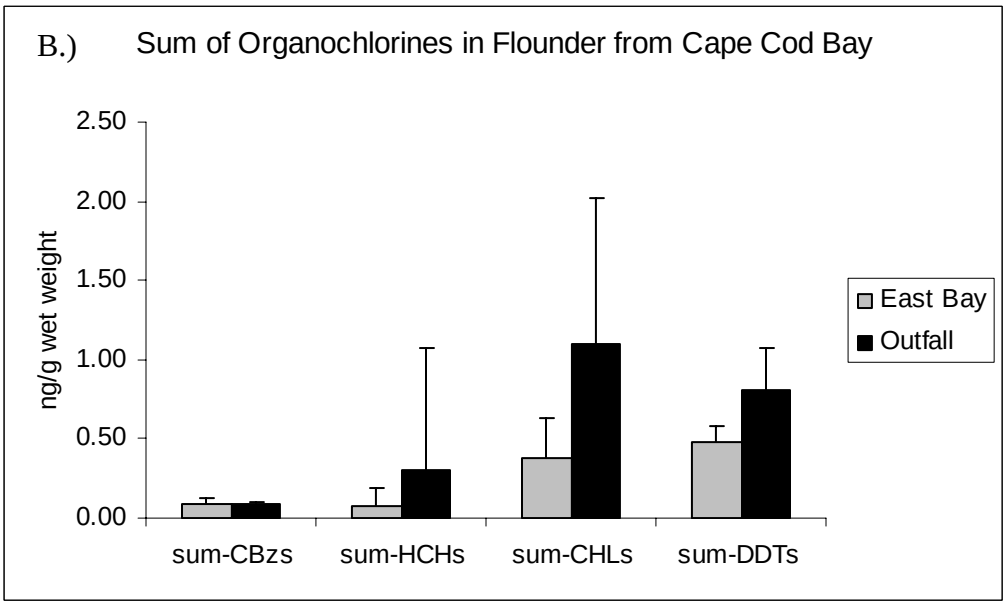


**Figure 1. A comparison of PCBs, PBDEs, and organochlorine pesticides in flounder at the east bay and outfall sites of Cape Cod Bay.**

## APPENDIX 7:

## PCBs, PBDEs, and Hydroxylated Metabolites in Cerebellum Grey Matter of Atlantic White-sided Dolphins (*Lagenorhynchus Acutus*) from the Northwest Atlantic

Cerebellum grey matter samples from CCSN05-037-La, CCSN05-039-La, and CCSN05-040-La (see Table 1, Chapter 4) were analyzed for PCBs, DDTs, $MeSO_2$-PCBs and –DDEs, HO-PCBs, PBDEs and HO-PBDEs, and other halogenated phenolic contaminants. Isolation methodologies involved homogenization, acidification, extraction, chemical partitioning, fractionation and purification. The results are summarized in Figure 1.

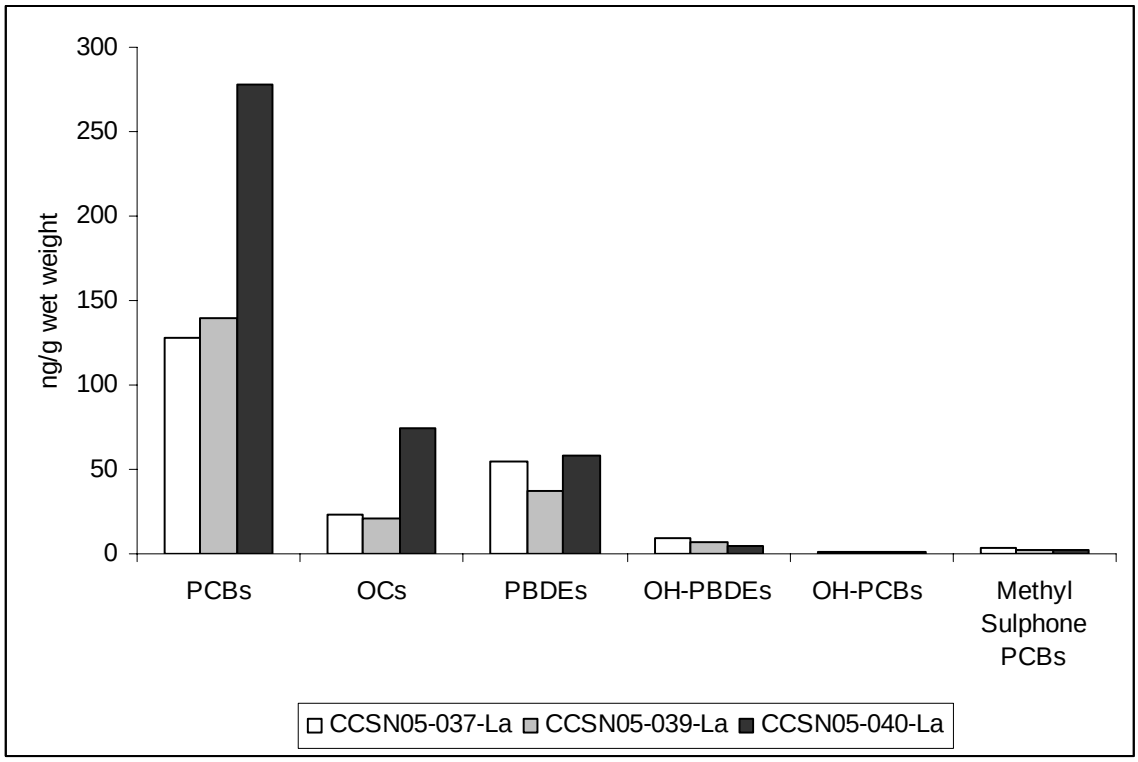


**Figure 1. A comparison of PCBs, organochlorine pesticides (OCs), PBDEs, OH-PBDEs, OH-PCBs, and methyl sulphone PCBs in cerebellum grey matter samples collected from CCSN05-037-La, CCSN05-039-La, and CCSN05-040-La.**